# NON-DONOR LIGANDS IN ORGANOACTINIDE CHEMISTRY

# RIGID NON-DONOR PINCER LIGANDS IN ORGANOACTINIDE CHEMISTRY

By

NICHOLAS R. ANDREYCHUK, H.B.Sc

A Thesis Submitted to the School of Graduate Studies in Partial Fulfillment of the Requirements for the Degree Doctor of Philosophy

McMaster University

© Copyright by Nicholas R. Andreychuk, March 2017.

Ph.D. Thesis
Nicholas R. Andreychuk
Department of Chemistry and Chemical Biology
McMaster University

DOCTOR OF PHILOSOPHY (2017) McMaster University

(CHEMISTRY) Hamilton, Ontario

TITLE: Rigid NON-Donor Pincer Ligands in Organoactinide Chemistry

AUTHOR: Nicholas R. Andreychuk

SUPERVISOR: Prof. David J. H. Emslie

NUMBER OF PAGES: xli, 312

Ph.D. Thesis
Nicholas R. Andreychuk
Department of Chemistry and Chemical Biology
McMaster University

## Abridged Abstract

The coordination- and organometallic chemistry of uranium complexes bearing the non-carbocyclic ancillary ligand $XA_2$ (4,5-bis(2,6-diisopropylanilido)-2,7-di-*tert*-butyl-9,9-dimethylxanthene) has been developed as a major focus of this thesis. A number of air-sensitive actinide chloro complexes and alkyl derivatives featuring reactive An–C bonds were prepared, and investigated using a variety of structural and spectroscopic analytical techniques, including X-ray diffraction, NMR spectroscopy, elemental analysis, and electrochemical methods. The research described in this thesis serves to expand the currently underdeveloped, fundamental chemistry of actinide complexes supported by non-carbocyclic (i.e. non-cyclopentadienyl) ligands. For example, the use of the prototypical xanthene-based ligand $XA_2$ has led to neutral dialkyl uranium(IV) complexes which a) react with alkyl anions to yield anionic trialkyl 'ate' complexes, b) C–H activate neutral pyridines to yield organouranium(IV) species featuring cyclometalated pyridine-based ligands, and c) react with Lewis acids to yield rare examples of cationic monoalkyl uranium(IV) complexes featuring coordinated arene ligands. By altering the nature of the arene solvent/ligand, latent catalytic ethylene polymerization behaviour has also been unlocked in cationic $XA_2$ uranium and thorium complexes, and this development may offer industrial relevance. Additionally, new NON-donor ligand designs featuring bulky terphenyl-based substituents (the "XAT" ligand) as well as 1-adamantyl groups (the "XAd" ligand) have been developed; a family of crystallographically-characterized dipotassium XAT complexes have been prepared which feature unprecedented potassium–alkane interactions, and the XAd ligand has been employed for the development of new organometallic thorium chemistry. The developments described in this thesis contribute to an emerging field and delineate new reactivities and structural motifs, providing important steps forward in organoactinide chemistry.

Ph.D. Thesis
Nicholas R. Andreychuk
Department of Chemistry and Chemical Biology
McMaster University

## Abstract

The coordination- and organometallic chemistry of uranium (III) and (IV) complexes supported by the rigid, dianionic NON-donor pincer ligand $XA_2$ (4,5-bis(2,6-diisopropylanilido)-2,7-di-*tert*-butyl-9,9-dimethylxanthene) has been explored. Transmetalation of the dipotassium precursor $[K_2(dme)_x(XA_2)]$ with $UCl_4$ in dme afforded the salt-occluded tetravalent uranium chloro complex $[(XA_2)UCl_2(\mu\text{-}Cl)\{K(dme)_3\}]$ (**1**). The cyclic voltammogram (CV) of **1** revealed an irreversible reduction peak at $E_{pc} = -2.46$ V vs $FeCp_2^{0/+1}$, and this CV behaviour remained constant after addition of 1 equiv of $Tl[B(C_6F_5)_4]$ to precipitate TlCl, indicating that the redox chemistry of **1** in THF is attributed to $[(XA_2)UCl_2(THF)_x]$ rather than the $[(XA_2)UCl_3]^-$ anion. Chemical reduction with 1.1 equiv of potassium naphthalenide in dme afforded an isolable uranium(III) derivative, $[(XA_2)UCl(dme)]$ (**2**), making **1** and **2** among the first reported diamido actinide(III)/(IV) tandems.

The uranium(IV) trichloro 'ate' complex $[(XA_2)UCl_2(\mu\text{-}Cl)\{K(dme)_3\}]$ (**1**) served as a versatile precursor to various organometallic derivatives; dialkylation with the appropriate RLi or $PhCH_2K$ reagent afforded the base-free bis(hydrocarbyl) complexes $[(XA_2)U(CH_2SiMe_3)_2]$ (**3**), $[(XA_2)U(CH_2{}^tBu)_2]$ (**4**; the first structurally-authenticated neutral uranium neopentyl complex), and $[(XA_2)U(CH_2Ph)_2]$ (**5**). These low-coordinate uranium(IV) dialkyl complexes demonstrate fairly high thermal stability (e.g. complex **3** decomposes over 48 h at 80 °C), and each exhibits fluxional behaviour attributable to a process which exchanges the axial and in-plane alkyl groups in solution; sharp $^1H$ NMR

spectra arising from a species of approximate $C_s$-symmetry were observed at low-temperature for complexes **3**, **4**, and **5**.

Bis((trimethylsilyl)methyl) complex **3** reacted cleanly with 2.2 equiv of $LiCH_2{}^tBu$ in benzene to yield the bis(neopentyl) complex **4**, with $LiCH_2SiMe_3$ as a by-product. Treatment of complex **4** with up to 80 equiv of $LiCH_2SiMe_3$ did not re-form detectable amounts of **3** by $^1H$ NMR spectroscopy; thus, the equilibrium in this reaction must lie far to the side of complex **4**. By contrast, excess $LiCH_2{}^tBu$ (15 equiv) was required to fully convert the thorium analogue $[(XA_2)Th(CH_2SiMe_3)_2]$ (**3-Th**) to $[(XA_2)Th(CH_2{}^tBu)_2]$ (**4-Th**); addition of 2.2 equiv of $LiCH_2{}^tBu$ to **3-Th** yielded an approximate 1:1:3:1 mixture of **4-Th**, mixed alkyl species $[(XA_2)Th(CH_2SiMe_3)(CH_2{}^tBu)]$ (**13-Th**), $LiCH_2SiMe_3$, and $LiCH_2{}^tBu$, respectively. The conversion of complex **3** to **4** likely occurs *via* tris(alkyl) 'ate' intermediates, and while none could be observed spectroscopically during the alkyl metathesis reactions in benzene, such intermediates proved synthetically accessible in ethereal solvents; addition of 1.3 equiv of $LiCH_2SiMe_3$ or 3.3 equiv of MeLi to dialkyl complex **3** in THF afforded the anionic tris(alkyl) 'ate' complexes $[(XA_2)U(CH_2SiMe_3)_3]^-$ (**14**) and $[(XA_2)UMe_3]^-$ (**15**), respectively; by contrast, the addition of 1 equiv of $KCH_2Ph$ to dialkyl complex **3** yielded intractable mixtures. Trimethyl 'ate' complex **15** could also be prepared by reaction of trichloro complex **1** with 3 equiv of MeLi in dme.

Tris(alkyl) anions **14** and **15** are thermally unstable in solution, with significant decomposition observed at room temperature in <1 hr to yield paramagnetic products, and $SiMe_4$ and $CH_4$, respectively. Careful examination of the decomposition of anion **14**

revealed the cyclometalated anion $[(XA_2*)U(CH_2SiMe_3)_2]^-$ (**16**; $XA_2*$ = [4-(NAr)-5-(N{$C_6H_3{}^iPr(CMe_2)$-2,6})-2,7-$^tBu_2$-9,9-$Me_2$(xanthene)]$^{3-}$; Ar = 2,6-$^iPr_2C_6H_3$) as the major product, the result of C–H activation at the methine carbon of an isopropyl group of the $XA_2$ ligand.

No reaction occurred between dialkyl complex **3** and 1 equiv of $PMe_3$, 2,2′-bipyridine (bipy), or quinuclidine (1-azabicyclo[2.2.2]octane) in benzene at 40−45 °C, however, reaction of complex **3** with 2.1 equiv of 4-(dimethylamino)pyridine (DMAP) in *n*-pentane afforded the highly fluxional $[(XA_2)U(CH_2SiMe_3)(\kappa^2\text{-DMAP*})(DMAP)]$ (**17**), a uranium(IV) monoalkyl complex featuring a neutral $\kappa^1$-DMAP ligand and an anionic, cyclometalated $\kappa^2$-*C,N*-DMAP* ligand, where DMAP* is the anion formed upon deprotonating DMAP at the 2-position. A deuterium labeling scheme utilizing DMAP-$d_2$ revealed that complex **17** was formed *via* a σ-bond metathesis mechanism, rather than through an alkylidene intermediate. An analogous product ($[(XA_2)U(CH_2SiMe_3)(\kappa^2\text{-AJ*})(AJ)]$; **18**) was obtained *via* the reaction of dialkyl complex **3** with 9-azajulolidine (AJ), a bulky DMAP derivative featuring a fused tricyclic structure; compound **18** is the first isolated metal complex to feature this bulky pyridine-based ligand.

As with the analogous thorium(IV) species, uranium(IV) dialkyl complex **3** is susceptible to alkyl abstraction in the presence of strong electrophiles; treatment of **3** with one equiv of $[Ph_3C][B(C_6F_5)_4]$ in arene solution afforded the crystallographically-authenticated cationic monoalkyl uranium(IV) complexes $[(XA_2)U(CH_2SiMe_3)(\eta^x\text{-arene})][B(C_6F_5)_4]$ ($\eta^x$-arene = $\eta^6$-$C_6H_6$ (**6**) or $\eta^3$-$C_6H_5Me$ (**7**)). Compounds **6** and **7** are rare examples of cationic uranium complexes bearing σ-bonded hydrocarbyl ligands, and

are the only examples free from external Lewis base coordination. Upon dissolution of cation **6** or **7** in bromobenzene-$d_5$, the uranium-bound proteo-arenes are largely displaced, generating $[(XA_2)U(CH_2SiMe_3)(C_6D_5Br)][B(C_6F_5)_4]$ (**8**) *in situ* as the major product, in which bromobenzene may be π-coordinated or $\kappa^1$-coordinated *via* bromine. However, addition of 100 equiv of the appropriate deuteroarene to $C_6D_5Br$ solutions of cations **6** and **7** shifted the equilibrium in favour of $[(XA_2)U(CH_2SiMe_3)(\eta^6\text{-}C_6D_6)][B(C_6F_5)_4]$ (**6-*d*$_6$**) and $[(XA_2)U(CH_2SiMe_3)(\eta^3\text{-}C_6D_5CD_3)][B(C_6F_5)_4]$ (**7-*d*$_8$**), and $^2$H NMR spectroscopy allowed identification of the $^2$H resonances attributable to coordinated benzene-$d_6$ and toluene-$d_8$ in these cations, respectively. The predominant cationic species in bromobenzene-$d_5$, **8**, demonstrated fairly high thermal stability, with gradual decomposition over the course of 8 h at 80 °C to yield a mixture of unidentified paramagnetic products and $SiMe_4$.

While benzene- and toluene-coordinated $XA_2$ monoalkyl actinide(IV) cations, $[(XA_2)An(CH_2SiMe_3)(\eta^x\text{-arene})][B(C_6F_5)_4]$ (An = U, Th), were inactive as ethylene polymerization catalysts (at temperatures up to 70 °C; 1 atm of ethylene), electronic tuning of the arene ligand led to catalytically active species. Indeed, ethylene polymerization was achieved using fluoroarene-coordinated cations $[(XA_2)U(CH_2SiMe_3)(\eta^3\text{-}C_6H_5F)]^+$ (**10**), $[(XA_2)U(CH_2SiMe_3)(o\text{-}C_6H_4F_2)]^+$ (**12**), and $[(XA_2)Th(CH_2SiMe_3)(\eta^x\text{-}C_6H_5F)]^+$ (**10-Th**) as catalysts; cation **10** is the first structurally-characterized f-element complex bearing a π-coordinated fluoroarene ligand, and **10-Th** is the most active *post-metallocene* actinide ethylene polymerization catalyst known (activity = $5.76 \times 10^4$ g of polyethylene·(mol of Th)$^{-1}$·h$^{-1}$·atm$^{-1}$). Samples of

polyethylene (PE) produced using catalysts **10**, **10-Th**, and **12** were submitted for analysis by gel permeation chromatography (GPC); PE produced using cation **10** or **10-Th** was insoluble in trichlorobenzene at 140 °C, precluding analysis, but the limited solubility of these polymers at elevated temperature suggests they are of high molecular weight. PE formed using the catalyst generated in 1,2-difluorobenzene (cation **12**) was determined to be of moderate molecular weight ($M_w$ of $2.9 \times 10^4$ g·mol$^{-1}$, $M_n$ of $1.1 \times 10^4$ g·mol$^{-1}$, PDI = 2.61).

Structural evolution of the xanthene-based diamido ligand $XA_2$ was also explored. Palladium-catalyzed coupling of the extremely bulky arylamine 2,6-dimestylaniline with 4,5-dibromo-2,7-di-*tert*-butyl-9,9-dimethylxanthene afforded the 2$^{nd}$ generation proligand 4,5-bis(2,6-dimesitylanilino)-2,7-di-*tert*-butyl-9,9-dimethylxanthene, $H_2$[XAT] (**19**). Stirring proligand **19** with excess KH in toluene and layering with hexanes at −30 °C afforded X-ray quality crystals of the dipotassium complex [$K_2$(XAT)(*n*-hexane)]·toluene (**20a**·toluene), which features close approach of a molecule of *n*-hexane to K(1), with a K(1)-C(1S) distance of 3.284(4) Å. Exploration of alternative crystallization conditions afforded several additional dipotassium XAT complexes, [$K_2$(XAT)(*n*-pentane)]·(*n*-pentane) (**20b**·(*n*-pentane)). [$K_2$(XAT)(3-methylpentane)]·3-methylpentane (**20c**·3-methylpentane), [$K_2$(XAT)-(cyclopentane)]·cyclopentane (**20d**·cyclopentane), [$K_2$(XAT)(toluene)]·0.5(toluene) (**20e**·0.5(toluene)), and [$K_2$(XAT){$(Me_3Si)_2O$}$_2$] (**20f**), each featuring an analogous potassium–alkane interaction. Compounds **20a–f** represent the first main-group-metal−alkane complexes to have been observed crystallographically.

Despite numerous attempts at installing the XAT ligand onto thorium and uranium, no new actinide-containing complex could be isolated.

Additionally, palladium-catalyzed coupling of 1-adamantylamine with 4,5-dibromo-2,7-di-*tert*-butyl-9,9-dimethylxanthene afforded the 3rd generation proligand 4,5-bis(1-adamantylamino)-2,7-di-*tert*-butyl-9,9-dimethylxanthene, $H_2$[XAd] (**21**), which upon subsequent deprotonation with 2.5 equiv of $KCH_2Ph$ in dme and addition of [$ThCl_4(dme)_2$] afforded a thorium(IV) chloro derivative [(XAd)$ThCl_4K_2$]·*x*(dme) (**23**·*x*(dme); *x* = 0.5–2). [(XAd)$ThCl_4K_2$]·*x*(dme) served as a suitable precursor to the bis(hydrocarbyl) complexes [(XAd)Th($CH_2SiMe_3)_2$(THF)] (**24**) and [(XAd)Th($\eta^3$-allyl$^{TMS}$)$_2$] (**25**; allyl$^{TMS}$ = 1-($SiMe_3$)$C_3H_4$), prepared by treatment of **23**·*x*(dme) with approximately 2 equiv of $LiCH_2SiMe_3$ or K[1-($SiMe_3$)$C_3H_4$], respectively. Bis(allyl) complex **25** exhibits fairly high thermal stability, withstanding heating at 85 °C for 15 h with minimal decomposition, and up to 155 °C with only <5% decomposition after 10 minutes. Complex **25** also exhibits fluxional behaviour in solution as evidenced by $^1$H NMR spectroscopy; at room temperature, averaging of the geminal *syn* and *anti* protons of the allyl $CH_2$ groups occurred as a consequence of rapid allyl 'flipping', likely *via* a π–σ–π intramolecular conversion. At low temperature (−63 °C), de-coalescence occurred, and the presence of three unique π-coordinated allyl environments is suggestive of two isomers of complex **25**, one of $C_1$ symmetry, and a top-bottom symmetric $C_2$-isomer. The reaction of complex **25** with [$Ph_3C$][$B(C_6F_5)_4$] was carried out in attempt to generate a cationic mono(allyl) derivative for use in ethylene polymerization; however, after stirring the **25**/trityl$^+$ mixture for 1 h under dynamic ethylene, no polyethylene was produced.

## Acknowledgements

First and foremost, I would like to thank my supervisor, Dr. David J. H. Emslie, for the privilege of being a member of his research group, and for training me to be a crafty and conscientious chemist. Your unbridled excitement for chemistry is remarkable, your hardcore-ness is unmatched, and you know how to have a good laugh. You are a true *Doktorvater*, and friend, and I am forever grateful for your guidance and patience. I look forward to talking about ridiculous molecules and having beers together for years to come.

I would like to thank all of my past and present colleagues in the Emslie group, especially Kris Kolpin, Kelly Motolko, Jeff Price, Aathith Vasanthakumar, Katarina Paskaruk, Tara Dickie, Dr. Edwin Wong, Dr. Preeti Chadha, Dr. Todd Whitehorne, Dr. Bala Vidjayacoumar, and Dr. Carlos Cruz. It has been a pleasure to work alongside- and learn from you all. I would also like to extend a special thank you to my friend and colleague Dr. Brad Cowie; we worked our way through this together, and we had a time, with many more to come.

I would also like to thank Dr. Ignacio Vargas-Baca and Dr. Gary Schrobilgen for their guidance and input over the years as members of my Ph.D. committee, I have greatly enjoyed learning from you in our meetings and in the classroom, and I appreciate everything you have done on my behalf. Additionally, I would like to thank Dr. Daniel Leznoff and Dr. Gillian Goward for serving as the external examinder and the examination Chair for my Ph.D. thesis defence, respectively, and Dr. Yurij Mozharivskyj

for serving as a thesis defence committee member. I would like to extend a thank you to the facilities staff as well, including Dr. Hilary Jenkins and Dr. Jim Britten of the McMaster Analytical X-ray Diffraction Facility, Dr. Bob Berno and Dr. Dan Sorensen of the Nuclear Magnetic Resonance Facility, Dr. Steve Kornic for assistance with NMR spectroscopy and elemental analysis, and Dr. Wen Zhou (of Simon Fraser University) and Megan Fair for assistance with elemental analysis; much of this work wouldn't be possible without you. I would also like to extend my appreciation to the office staff of the Department of Chemistry and Chemical Biology.

Additionally, I would like to extend my appreciation to the Government of Ontario, the Department of Chemistry and Chemical Biology and the School of Graduate Studies at McMaster University, and the Natural Sciences and Engineering Research Council of Canada for their generous financial support during my graduate career.

I am forever grateful to my parents, Rob and Donna Andreychuk, for their relentless support; without you none of this would have been possible, literally. I would also like to thank the rest of my family and my outstanding friends, especially Mikey Beach; as a token of my gratitude, none of you will be forced to read this thesis.

Finally, I wish to express my profound gratitude to my darling Danielle Smiley; your love and support are unwavering, even when I am being insufferable. I look forward to our journey together, and to tormenting you for years to come.

# Table of Contents

**Chapter 2 – $XA_2$ Uranium(III) and (IV) Chloro Complexes and Neutral Organometallic $XA_2$ Uranium(IV) Derivatives**



**Chapter 3 – Cationic $XA_2$ Uranium(IV) Monoalkyl Complexes and Ethylene Polymerization**



**Chapter 4 – Reactivity of $XA_2$ Organouranium(IV) Complexes with Small Molecules**

## List of Figures

## List of Schemes

## List of Tables

## List of Compounds

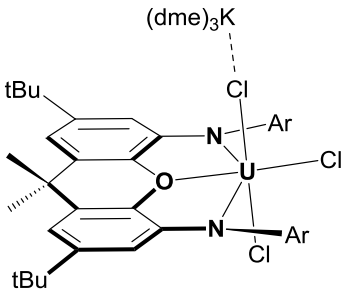


**(1)**

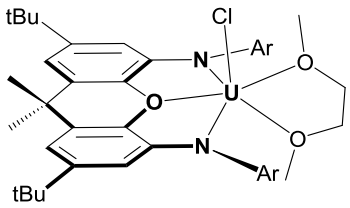


**(2)**

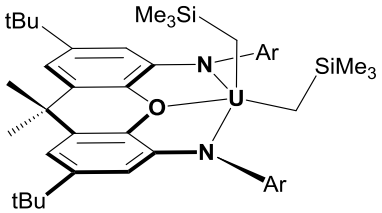


**(3)**

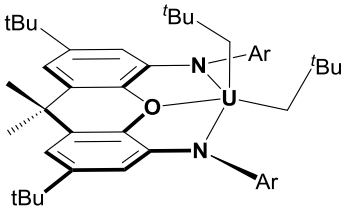


**(4)**

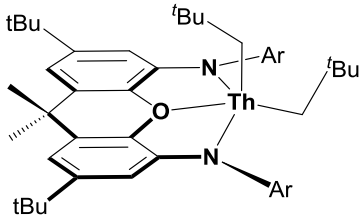


**(4-Th)**

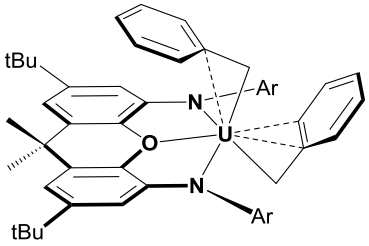


**(5)**

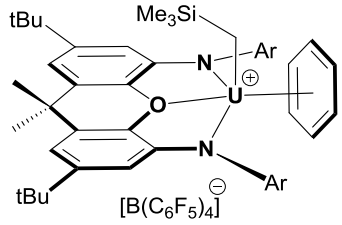


**(6)**

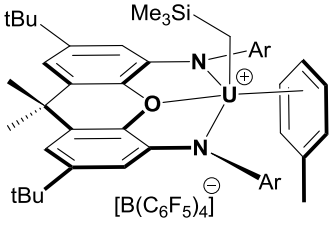


**(7)**

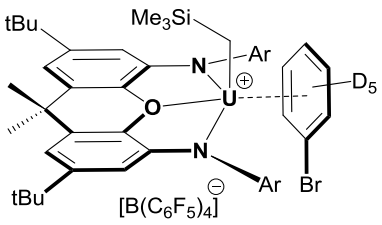


**(8)**

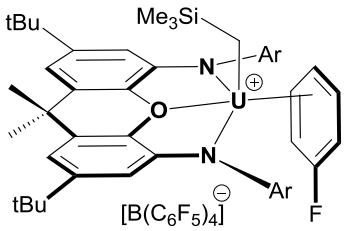


**(10)**

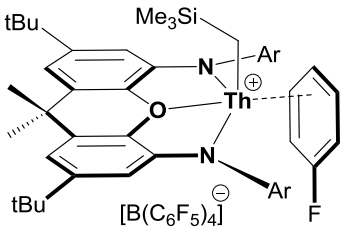


**(10-Th)**

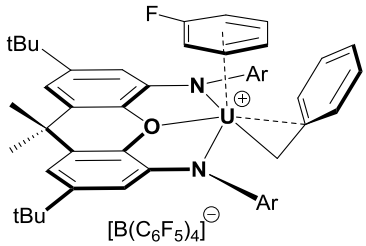


**(11)**

Ar = 2,6-diisopropylphenyl

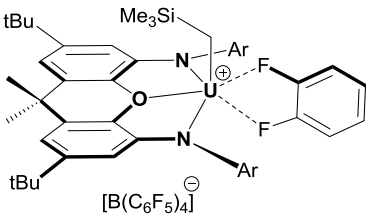


**(12)**

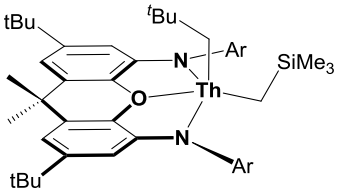


**(13-Th)**

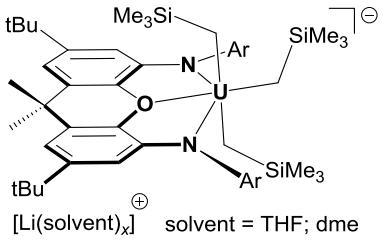


**(14)**

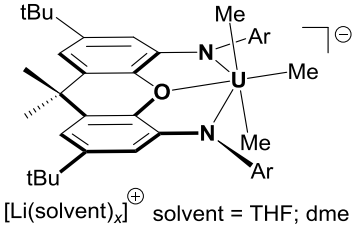


**(15)**

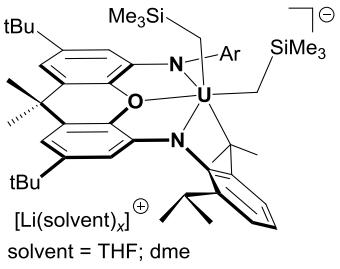


**(16)**

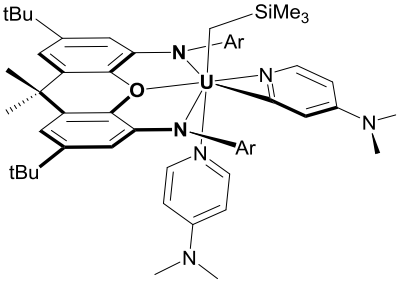


**(17)**

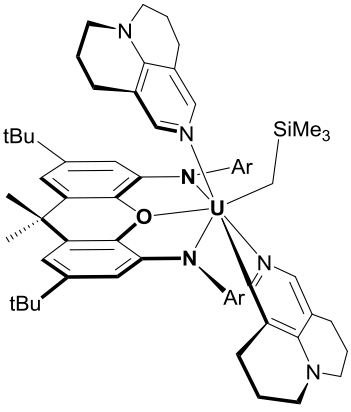


**(18)**

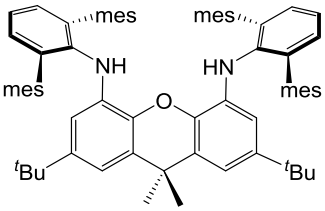


**(19)**

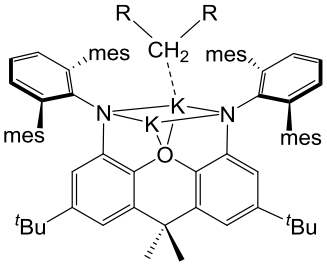


**(20a-f)**

Ar = 2,6-diisopropylphenyl

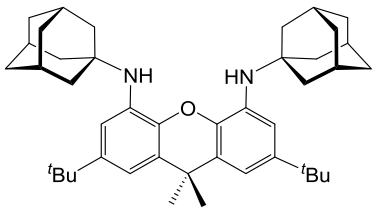


**(21)**

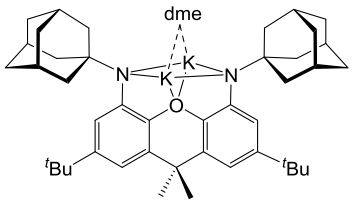


**(22-dme)**

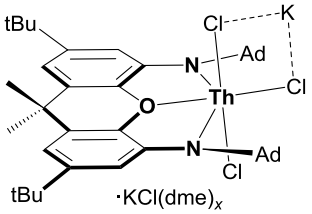


**(23·*x*(dme))**

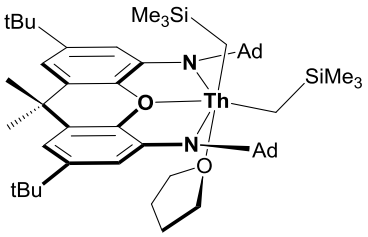


**(24)**

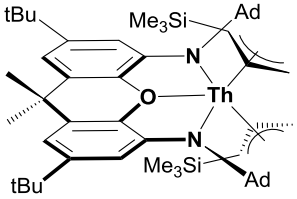


**(25)**

Ad = 1-adamantyl

## List of Abbreviations and Symbols

**General:**

° – degree(s)

**$\eta^x$** – hapticity of a ligand, invoked to describe coordination of a ligand to a metal centre *via* an uninterrupted and contiguous series of *x* atoms.

**$\kappa^x$** – denticity of a ligand, invoked to describe the number, *x*, of donor atoms/groups of a single ligand that bind to a metal centre in a coordination complex.

**$\mu_x$** – invoked when a ligand bridges between *x* atoms

**ADF** – Amsterdam density functional

**AIM** – Atoms in molecules

**alkane elimination** – a reaction involving the installation of a ligand onto a metal, whereby a protic ligand reacts with an organometallic metal precursor complex (in this case a metal alkyl complex) *via* protonolysis, yielding an alkane as a by-product.

**An** – actinide element

**atm** – standard atmosphere

**$[BAr'_4]^-$** – $[B\{3,5\text{-}(CF_3)_2C_6H_3\}_4]^-$

**C** – Celsius

**cent** – centroid

**D** – deuterium

**DFT** – density functional theory

**dme** – 1,2-dimethoxyethane

**ethylene** – ethene

**fold angle** – for allyl ligands, defined as the angle between the $C_3$ allyl plane and the plane passing through the metal atom and the two terminal allyl carbon atoms.

**g** – grams

**h** – hour

**half-sandwich complex** – a class of compounds which feature a single cyclic polyhapto ligand bound to a metal centre.

**hmdso** – hexamethyldisiloxane, $O(SiMe_3)_2$

**homoleptic complex** – a complex where all ligands are identical.

**heteroleptic complex** – a complex featuring at least two unique ligands.

**J** – joule

**K** – Kelvin

**KJ** – kilojoule

**LB** – Lewis base

**ligand bend angle** – for ligands featuring a xanthene backbone, defined as the angle between the planes formed by each aromatic ring of the ligand backbone, where each plane is defined by the six carbon atoms of each aromatic ring within the xanthene backbone.

***m*** – *meta*

**M** – molarity ($mol \cdot L^{-1}$)

**MAO** – methylaluminoxane

**metallocene** – a class of compounds which prototypically feature two cyclopentadienyl ($C_5H_5^-$) anions bound to a metal centre (sometimes referred to as 'sandwich complexes').

**min** – minute

**mL** – millilitre(s)

**MMAO** – modified methylaluminoxane

**mmol** – millimoles

**mol** – moles

***o*** – *ortho*

***p*** – *para*

**PE** – polyethylene

**salt metathesis** – a transmetalation reaction; a reaction involving the installation of a ligand onto a metal, whereby the ligand is transferred from one metal (often an alkali metal) to another (the metal of interest), with concurrent elimination of a salt by-product, typically an alkali metal halide.

**scorpionate ligand** – a class of tridentate ligand which bind the metal in a *fac* disposition; the hydrotris(pyrazolyl)borates are quintessential scorpionates.

**tetraglyme** – tetraethylene glycol dimethylether

**THF** – tetrahydrofuran

**TIBA** – triisobutylaluminum

**tmeda** – *N,N,N′,N′*-tetramethylethane-1,2-diamine

**trityl** – $[Ph_3C]^+$

**tuck-in complex** – an organometallic complex bearing a pentamethylcyclopentadienyl ligand (or variant thereof) wherein a methyl group has been deprotonated and the resulting methylene group binds the metal centre.

**WCA** – weakly-coordinating anion

**Substituents:**

**α-picolyl** – *o*-6-methylpyridyl (*o*-6-$CH_3$-$NC_5H_3$)

**Ad** – 1-adamantyl

**Ar** – aryl

**Cy** – cyclohexyl

**Dipp** – 2,6-diisopropylphenyl (2,6-$^{i}Pr_2$-$C_6H_3$)

**Et** – ethyl

**Fc** – ferrocenyl (ferrocene = $[(C_5H_5)_2Fe]$)

**$^{i}$Bu** – *iso*-butyl

**$^{i}$Pr** – *iso*-propyl

**Me** – methyl

**Mes** – mesityl (2,4,6-trimethylphenyl)

**$^{n}$Bu** – *n*-butyl (*n* = normal)

**neopentyl** – 2,2-dimethylpropyl anion, $\{CH_2C(CH_3)_3\}^-$

**Ph** – phenyl

**pyridyl** – generic pyridine-based substituent

**pz** – pyrazolyl ($C_3N_2H_3$)

**R** – general organic substituent

**$^s$Bu** – *sec*-butyl (*sec* = secondary)

**TBS** – *tert*-butyldimethylsilyl

**TIPS** – triisopropylsilyl

**TMS** – trimethylsilyl

**tosyl (ts)** – *p*-toluenesulfonate, $MeC_6H_4SO_2$

**$^t$Bu** – *tert*-butyl (*tert* = tertiary)

**Tf** – trifyl (trifluoromethylsulfonyl, $SO_2CF_3$)

**Tripp** – 2,4,6-triisopropylphenyl (2,4,6-$^i$Pr$_3$-$C_6H_2$)

**Tol** – tolyl, methylphenyl

**Xyl** – xylyl, 2,6-dimethylphenyl

**Ligands and Compounds:**

**[2.2.2]-cryptand** – 4,7,13,16,21,24-hexaoxa-1,10-diazabicyclo[8.8.1]hexacosane

**12-crown-4** – 1,4,7,10-tetraoxacyclododecane

**18-crown-6 (or 18-C-6)** – 1,4,7,10,13,16-hexaoxacyclooctadecane

**acac** – acetylacetonano $[\{OC(Me)\}_2CH]^-$

**allyl** – $C_3H_5^-$ and derivatives thereof.

**AJ** – 9-azajulolidine ($C_{11}H_{14}N_2$), a pyridonaphthyridine derivative; a 4-(dialkylamino)pyridine in which the 4-amino group is conformationally fixed as a member of two fused rings which are fused to the pyridine ring at the 3,5-positions.

**AJ*** – *o*-9-azajulolidinyl, $(C_{11}H_{13}N_2)^-$

**benzyl** – phenylmethyl ($CH_2Ph$)

**BDPP** – 2,6-bis(2,6-diisopropylanilidomethyl)pyridine

**BDPP*** – $[2,6\text{-}(NC_5H_3)(CH_2NAr)(CH_2N\{C_6H_3{}^{i}Pr(CMe_2)\text{-}2,6\}]^{3-}$; Ar = 2,6-$^{i}Pr_2C_6H_3$

**bipy** – 2,2′-bipyridine

**COT** – cyclooctatetraenide ($\eta^8$-$C_8H_8^{2-}$)

**Cp** – cyclopentadienyl ($\eta^5$-$C_5H_5^-$)

**Cp*** – pentamethylcyclopentadienyl ($\eta^5$-$C_5Me_5^-$)

**Cp′** – $\{\eta^5\text{-}1,2,4\text{-}{}^{t}Bu_3(C_5H_2)\}^-$

**Cp"** – $\{\eta^5\text{-}1,3\text{-}(SiMe_3)_2(C_5H_3)\}^-$

**DMAP** – 4-(dimethylamino)pyridine

**DMAP*** – *o*-4-(dimethylamino)pyridyl (*o*-4-$NMe_2$-$NC_5H_3)^-$

**dmp** – 2,6-dimesitylphenyl

**dmpe** – 1,2-bis(dimethylphosphino)ethane $\{Me_2P(CH_2)_2PMe_2\}$

**DPEPhos** – (oxydi-2,1-phenylene)bis(diphenylphosphine)

**FcNN** – $\{Fc(NSiMe_2R)_2\}^{2-}$; R = $^{t}$Bu, Ph

**hmpa** – hexamethylphosphoramide, $\{(Me_2N)_3PO\}$

**hpp** – the anion of hexahydropyrimidopyrimidine, $(\kappa^2\text{-}C_7H_{12}N_3)^-$, a fused guanidinate ligand (1,3,4,6,7,8-hexahydro-2*H*-pyrimido[1,2-*a*]pyrimidinato)

**ind** – indenyl anion; $C_9H_7^-$

**mesitylene** – 1,3,5-trimethylbenzene

**nacnac** – a generic β-diketiminato ligand, $\{CH(C(R)NR')_2\}^-$

**PNP** – bis[2-(diisopropylphosphino)-4-methylphenyl]amido

**py** – pyridine ($NC_5H_5$)

**salan** – a tetradentate dianionic diamine bis(phenolate) ligand

**SBT** – 2-mercaptobenzothiazolate

**Tp** – hydrotris(pyrazolyl)borate, $\{HB(pz)_3\}^-$

**Tp′** – hydrotris(3,5-dimethyl-1-pyrazolyl)borate, $\{HB(3,5\text{-}Me_2pz)_3\}^-$

**tren$^X$** – $\kappa^4\text{-}\{N(CH_2CH_2NSiR_3)_3\}^{3-}$

**TXA$_2$** – 4,5-bis(2,6-diisopropylanilido)-2,7-di-*tert*-butyl-9,9-dimethylthioxanthene

**XA$_2$** – 4,5-bis(2,6-diisopropylanilido)-2,7-di-*tert*-butyl-9,9-dimethylxanthene

**XA$_2$*** – $[4\text{-}(NAr)\text{-}5\text{-}(N\{C_6H_3{}^i\text{Pr}(CMe_2)\text{-}2,6\})\text{-}2,7\text{-}{}^t\text{Bu}_2\text{-}9,9\text{-}Me_2(\text{xanthene})]^{3-}$; Ar = 2,6-$^i\text{Pr}_2C_6H_3$

**XAd** – 4,5-bis(1-adamantylamido)-2,7-di-*tert*-butyl-9,9-dimethylxanthene

**XAT** – 4,5-bis(2,6-dimesitylanilido)-2,7-di-*tert*-butyl-9,9-dimethylxanthene

**Spectroscopy, Diffraction, and Analytical Techniques:**

**Å** – angstrom

***δ*** – chemical shift (ppm)

**{$^{1}$H}** – proton decoupled

**2D** – two dimensional

**appt.** – apparent

**br** – broad (v. br = very broad)

**COSY** – correlation spectroscopy

**d** – doublet

**DEPT** – distortionless enhancement by polarization transfer

**EXSY** – exchange spectroscopy

**GPC** – gel permeation chromatography

**HMBC** – heteronuclear multiple bond correlation

**HSQC** – heteronuclear single quantum coherence

**Hz** – hertz

***J*** – coupling constant

**m** – multiplet

**MHz** – megahertz

**$^{n}J_{X,Y}$** – coupling constant between nuclei X and Y; n = number of bonds separating each nucleus

**NMR** – nuclear magnetic resonance

**PDI** – polydispersity index

**ppm** – parts per million

**q** – quartet

**s** – singlet

**t** – triplet

**UV** – ultraviolet

Ph.D. Thesis
Nicholas R. Andreychuk
Department of Chemistry and Chemical Biology
McMaster University

## Declaration of Academic Achievement

Dr. B. Vidjayacoumar and Dr. S. Ilango, former postdoctoral fellows in the Emslie group, were responsible for initial syntheses and characterization of chloro complexes $[(XA_2)UCl_2(\mu\text{-}Cl)\{K(dme)_3\}]$ (**1**) and $[(XA_2)UCl(dme)]$ (**2**), and the initial syntheses of organometallic derivatives $[(XA_2)U(CH_2SiMe_3)_2]$ (**3**), $[(XA_2)U(CH_2SiMe_3)(\eta^3\text{-}C_6H_5Me)][B(C_6F_5)_4]$ (**7**), and $[Li(dme)_3][(XA_2)UMe_3]$ (**15**). Prof D. J. H. Emslie was responsible for the cyclic voltammetry of $[(XA_2)UCl_2(\mu\text{-}Cl)\{K(dme)_3\}]$ (**1)** and for the synthesis of $Tl[B(C_6F_5)_4]$. Tara Dickie, a former 4$^{th}$ year undergraduate thesis student in the Emslie group, was responsible for the initial synthesis of $[(XAd)Th(\eta^3\text{-}allyl^{TMS})_2]$ (**25**). Dr. Preeti Chadha, a former postdoctoral fellow in the Emslie group, was responsible for the preparation of $K[1\text{-}(SiMe_3)C_3H_4]$. Dr. Carlos Cruz, a former Ph.D. student in the Emslie group, was responsible for the preparation of $H_2NCH_2C(Ph)_2CH_2CHCH_2$. Dr Steve Kornic and Ms. Meghan Fair (of McMaster University), and Mr. Farzad Haftbaradaran and Dr. Wen Zhou (of Simon Fraser University) were responsible for performing elemental analysis for all samples analyzed using this technique. Dr. Hilary A. Jenkins and Dr. James Britten were responsible for crystal mounting, data acquisition, data processing, and structure solution and refinement for single crystal X-ray diffraction experiments. All other results were obtained by Nicholas R. Andreychuk.

Ph.D. Thesis
Nicholas R. Andreychuk
Department of Chemistry and Chemical Biology
McMaster University

# Chapter 1

# Introduction

## 1.1 – Opening Remarks

Actinides (frequently referred to using the informal chemical symbol 'An') are the group of elements from actinium (element 89) to nobelium (element 102), with lawrencium (element 103) typically considered a group 3 transition metal.[1] Of these elements, only thorium and uranium have substantial natural abundances, similar to those of tantalum, tin, boron and lead in the earth's crust (2–14 ppm).[2] Thorium consists almost exclusively of $^{232}$Th with a half-life of 14.1 billion years. By contrast, natural-abundance uranium consists of a mixture of $^{238}$U ($t_{1/2}$ 4.47 billion years), $^{235}$U (704 million years), and $^{234}$U (246 thousand years), with the latter formed on the decay series from $^{238}$U. Anthropogenic neptunium and plutonium also have several fairly long-lived isotopes, including $^{237}$Np ($t_{1/2}$ 2.14 million years), $^{239}$Pu ($t_{1/2}$ 24.1 thousand years), $^{242}$Pu ($t_{1/2}$ 373 thousand years), and $^{244}$Pu ($t_{1/2}$ 80.8 million years).[2] Chemical studies are most often conducted with $^{237}$Np and $^{239}$Pu, although research with these highly-toxic elements is only possible in highly-regulated facilities, typically government facilities, utilizing specialized equipment (e.g. negative atmosphere gloveboxes) with a variety of measures to guard against, and monitor for, any accidental release.[3] A very small number of organometallic Pa, Am, Cm, Cf and Bk compounds have also been prepared, including $Pa(COT)_2$,[4] $PaCp_4$,[5] and $AnCp_3$ (An = Am,[6] Cm,[7] Cf,[8] Bk[8]). However, the organometallic

chemistry of these synthetic elements has not been more extensively investigated due to a combination of very low availability and high or very high radioactivity (i.e. short or very short half-lives) of all isotopes of these elements.[3]

The vast majority of organoactinide chemistry involves thorium and uranium, but the field is not as well developed as that of organolanthanide chemistry. In addition, while the organometallic chemistry of lanthanide elements has focused more on diamagnetic compounds of trivalent Sc, Y, Lu, La, paramagnetic non-uranium(VI) organometallic chemistry is better developed than diamagnetic thorium(IV) organometallic chemistry, as evidenced by over 300 compounds with U−C bonds in the Cambridge Structural Database at the time of writing (few of these are uranium(VI) complexes), versus less than 120 with Th−C bonds. Greater interest in uranium likely stems from the increased covalency of uranium compounds relative to thorium compounds, including greater participation of the 5f-orbitals in bonding, combined with a rich redox chemistry; uranium provides access to organometallic compounds in oxidation states II–VI,[9] whereas almost all organothorium chemistry involves thorium(IV).[2] The appreciable covalency of uranium compounds is apparent from the volatility of $UF_6$, $U(NMe_2)_4$ and $U(BH_4)_4$, the accessibility of higher oxidation states, and may also be responsible for the increased solubility of most uranium organometallic compounds versus thorium analogues in nonpolar solvents such as hexane.[10]

The covalency of most uranium−ligand bonds is believed to be significantly lower than that in related transition metal complexes (groups 4−11), but is generally far greater than that in trivalent rare earth complexes, and so uranium is uniquely positioned as a

high natural abundance f-element with certain properties in common with lanthanides (large size and electropositivity) and certain properties more in common with mid-transition metals (appreciable covalency and a rich redox chemistry), combined with unique availability of the f-orbitals for participation in bonding (due to greater radial extension of early actinide 5f orbitals vs lanthanide 4f orbitals). Less readily accessible Np and Pu, and to a lesser extent Pa and Am, share many of these properties, whereas the late actinide elements (Cm–No) are more lanthanide-like, generally forming highly ionic compounds, with one primary oxidation state and a second less-common oxidation state; as with the lanthanide elements, the last member of the actinide series, nobelium, has the most readily accessible divalent oxidation state, with an $f^{14}$ configuration.[2]

The ionic radii for Th(IV) and U(IV) are 0.94 and 0.89 Å respectively (for a coordination number of 6),[11] which is smaller than that of early trivalent lanthanide ions such as La(III) (1.03 Å), but is comparable with later members of the lanthanide series and yttrium (e.g. 0.96, 0.90 and 0.87 Å for Sm(III), Y(III) and Yb(III), respectively), and is significantly larger than that of the group 4 transition metals Ti, Zr and Hf (0.61–0.72 Å). By contrast, the ionic radius of U(III) is 1.03 Å, which is nearly identical to that of lanthanum(III). The ionic radii of U(V) and U(VI) are 0.76 and 0.73 Å, respectively, which are significantly larger than those of Ta(V) (0.64 Å) and W(VI) (0.60 Å). The Pauling electronegativities of Th and U are 1.3 and 1.4 respectively, which are on par with those of Sc, Y and Lu (1.4, 1.2 and 1.3, respectively).[2]

## 1.2 – Anhydrous Actinide Halide Starting Materials

The availability of suitable anhydrous actinide starting materials, halide species in particular, has played a critical role in the development of organometallic actinide chemistry. However, none of these compounds are commercially available, and as such, synthetic routes to common anhydrous halide compounds are outlined herein, with a focus on compounds with demonstrated or potential utility as starting materials for the preparation of organometallic derivatives. Base-free and diethylether-, dme- (dme = 1,2-dimethoxyethane), THF-, or 1,4-dioxane-coordinated compounds are of the most general utility, since more strongly-donating nitrogen-based ligands are not easily displaced, and nitriles and pyridines are incompatible with many strong nucleophiles.

The most common halide starting materials in organothorium chemistry are $ThCl_4$ and square antiprismatic $[ThCl_4(dme)_2]$. $ThCl_4$ has not been commercially available for many years, but can be prepared by passing $N_2$ containing $CCl_4$ vapours over $ThO_2$ at 750 °C.[12] However, $[ThCl_4(dme)_2]$ is a more common choice since it can be accessed using standard wet-chemistry techniques; $[Th(NO_3)_4(H_2O)_x]$ ($x = 4-6$) is boiled in concentrated HCl until $NO_2$ evolution has ceased, and the solvent is then removed under reduced pressure to afford $[ThCl_4(H_2O)_x]$; reduced pressure is required because hydrated thorium(IV) chloride decomposes to a mixed hydroxide-chloride species between 100 and 160 °C.[13] The resulting colourless complex $[ThCl_4(H_2O)_4]$ is converted to square antiprismatic $[ThCl_4(dme)_2]$ either by: (a) stirring in $SOCl_2$ to remove $H_2O$, yielding $[ThCl_4(OSCl_2)]$,[14] followed by Soxhlett extraction in dme,[15] or (b) reaction with excess

$Me_3SiCl$ in dme.[16] $[ThCl_4(H_2O)_4]$ can also be refluxed in 1,4-dioxane with excess $Me_3SiCl$ and anhydrous $HCl/OEt_2$ to form $[ThCl_4(1,4\text{-dioxane})_2]$, and reaction of this product with THF yielded $[ThCl_4(THF)_{3.5}]$.[16] Furthermore, $[ThCl_4(dme)_2]$ can be converted to $[ThX_4(dme)_2]$ (X = Br or I) by treatment with $Me_3SiX$.[16,17]

In organouranium(IV) and (III) chemistry, the most common halide starting materials are $UCl_4$ and $[UI_3(OR_2)_x]$. By contrast, simple uranium(V) and (VI) halide complexes such as $UCl_5$ and $UF_6$ are rarely used as entry points to high valent uranium chemistry, since they are highly oxidizing, and $UCl_5$ is also prone to disproportionation.[2] Instead, higher oxidation state complexes are often accessed by initial ligand attachment to uranium(III) or (IV) and subsequent chemical oxidation, or alternatively, uranyl precursors such as $[\{UO_2Cl_2(THF)_2\}_2]$ are employed.[18]

Forest-green uranium tetrachloride can be prepared by passing $CCl_4$ vapours over $UO_2$ in a tube furnace at 400 °C,[19] or, by cautious slow addition of solid $UO_3$ to hexachloropropene at 190 °C,[20] the latter route being more suitable for application in a typical synthetic laboratory.[§] Analogous syntheses of $UCl_4$ starting from $U_3O_8$, $[UO_2Cl_2]\cdot xH_2O$ or $[UO_2(NO_3)_2]\cdot 6(H_2O)$ were also recently reported.[21] Additionally, reaction of $UCl_4$ with $Me_3SiI$ in diethylether or acetonitrile afforded $[UI_4(OEt_2)_2]$[22] and $[UI_4(NCMe)_4]$,[23] respectively; these uranium(IV) tetraiodo complexes are stable at room temperature, in contrast to base-free $UI_4$ which eliminates $I_2$ to form $UI_3$.[24] $[UI_4(OEt_2)_2]$

[§] For the synthesis of $UCl_4$ from $UO_3$ with hexachloropropene, it is recommended to add $UO_3$ via a solid addition funnel placed at the top of a reflux condenser, and the use of silicone grease rather than hydrocarbon-based H-grease is required in order to obtain a forest green product.

has also been prepared by reaction of $UH_3$[22] or uranium turnings[25] with 2 equiv of $I_2$ in $OEt_2$, although the reaction with $UH_3$ has been reported to proceed more cleanly than that with uranium metal.[22] Reaction of $UH_3$ with 4 equiv of AgBr, AgCl, $CuCl_2$ or AgOTf in dme also yields $[UX_4(dme)_2]$ (X = Br, Cl or OTf).[22]

Base-free $UI_3$ can be prepared via solvent-free reactions between uranium turnings and $HgI_2$ (1.5 equiv)[26] or $I_2$ (1.5 equiv) at high temperature,[27] or more conveniently *via* the reaction of uranium turnings with 1.5 equiv of $I_2$ in diethylether.[25] Alternatively, $[UX_3(THF)_4]$ (X = I or Br), $[UI_3(dme)_2]$ or $[UI_3(pyridine)_4]$ can be prepared *via* the reactions of amalgamated uranium turnings with 1.5 equiv of $I_2$ or $Br_2$ in the appropriate donor solvent, although it has been noted that the THF-coordinated compounds are prone to decomposition involving THF ring-opening.[28] However, uranium turnings are not readily accessible to many research groups, so the recent synthesis of "$[UCl_3(pyridine)_4]$" from $UCl_4$, by reduction with Mg turnings in 1,4-dioxane (100 °C) followed by reaction with pyridine, provides an alternative pathway into low-valent uranium chemistry.[29] This compound is a well-defined uranium(III) chloro compound, in contrast to $[UCl_3(THF)_x]$ ($x$ = 1−2), which is prepared from $UCl_4$ and excess NaH in THF.[30]

### 1.3 – Homoleptic Acyclic Hydrocarbyl Compounds and their Lewis Base Adducts

#### 1.3.1 – Homoleptic Actinide Alkyl Complexes

Simple, homoleptic actinide alkyl complexes have been desirable targets for more than 70 years, with early interest stemming from the need for thermally-stable and volatile compounds for use in isotope separation (especially uranium enrichment) during

the Manhattan project.[31] However, isolation of such neutral polyalkyl actinide species proved untenable at the time as a consequence of limited thermal stability, likely due to insufficient electronic saturation at the metal centre.[32] Beyond nuclear applications, homoleptic polyalkyl actinide complexes remain highly sought after due to the potential for their utility as soluble- and reactive precursors akin to the versatile lanthanide trialkyl species $[Ln(CH_2R)_3(THF)_x]$ (R = $SiMe_3$ or Ph), which enjoy widespread application.[33]

While isolation of neutral homoleptic polyalkyl actinide species remained a challenge, the Marks group was able to isolate stable actinide(IV) 'ate' complexes of the form $[Li(OR_2)_4]_2[UR_6]$ ($OR_2$ = THF, $Et_2O$; R = $CH_3$, $C_6H_5$, $CH_2SiMe_3$)[34] and $[Li(tmeda)]_3[Th(CH_3)_7]$ (tmeda = *N,N,N′,N′*-tetramethylethane-1,2-diamine),[35] which boast significantly improved thermal stability as a result of increased- electronic saturation and steric protection. More recently, the groups of Ephritikhine and Hayton have re-visited this approach, resulting in the isolation of a number of new anionic poly(hydrocarbyl) actinide(IV) 'ate' complexes, including $[Li_2(py)_3][U(Fc)_3]$ (Fc = 1,1′-ferrocenediyl),[36] $[Li(dme)_3][U(CH_2SiMe_3)_5]$, $[Li(THF)_4][U(CH_2{}^tBu)_5]$, $[Li(tmeda)]_2[UMe_6]$, $\{[K(THF)]_3[K(THF)_2][U(CH_2Ph)_6]_2\}_x$,[37] $[Li(THF)_4][Th(CH_2{}^tBu)_5]$ (**c** in Figure 1.1), $[Li(dme)_2][Th(CH_2SiMe_3)_5]$, $[K(THF)]_2[Th(CH_2Ph)_6]$ (**e** in Figure 1.1),[38] $[Li(dme)_3]_2[ThPh_6]$, and $[Li(THF)(12\text{-crown-4})]_2[ThPh_6]$.[39]

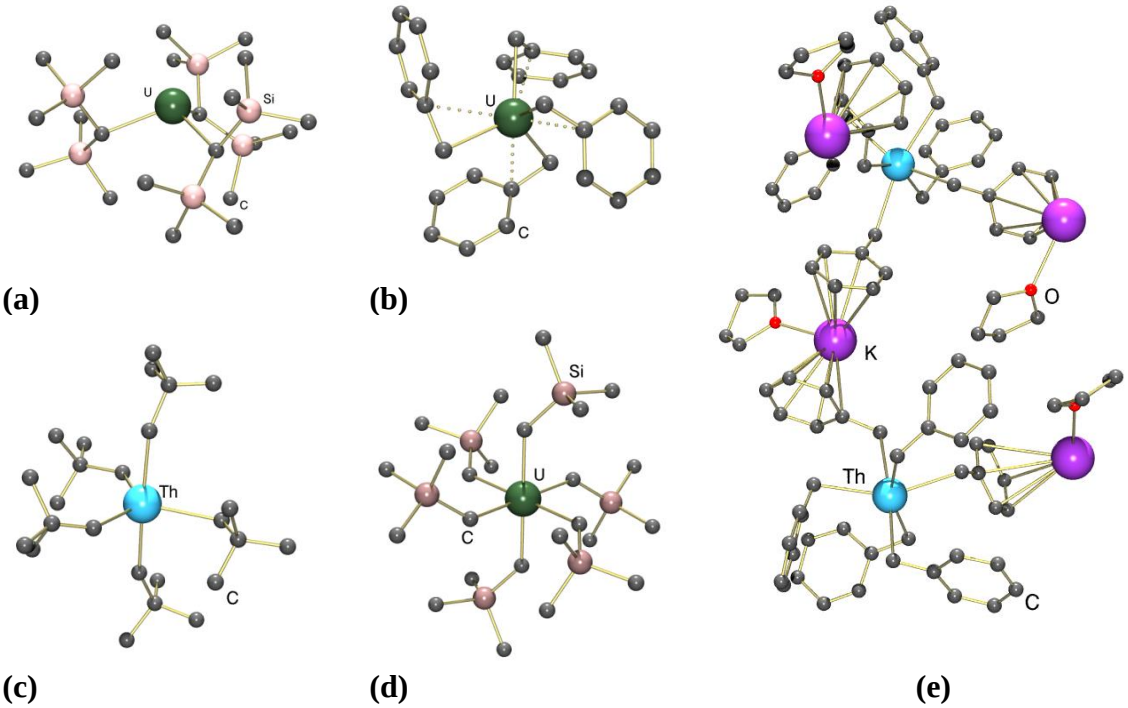


**Figure 1.1 –** X-ray crystal structures of (a) $[U\{CH(SiMe_3)_2\}_3]$ bearing 3 alkyl groups, (b) $[U(CH_2Ph)_4]$ bearing 4 benzyl groups, (c) the anionic portion of $[Li(THF)_4][Th(CH_2{}^tBu)_5]$ featuring 5-coordinate thorium, (d) the anionic portion of $[Li(THF)_4][U(CH_2SiMe_3)_6]$ featuring 6-coordinate uranium, and (e) $[K(THF)]_2[Th(CH_2Ph)_6]$.

Despite early challenges, a small number of neutral polyalkyl actinide complexes have been reported. The thorium(IV) tetraalkyl complex "$[Th(CH_2SiMe_3)_4(dme)_x]$",[40] formed from the reaction between $[ThCl_4(dme)_2]$ and 4 equiv of $LiCH_2SiMe_3$, has been proposed based on its alkane elimination reactions with protonated ligand precursors (*vide infra*), but the tetrakis((trimethylsilyl)methyl)thorium(IV) species was not isolated. Along the same vein, tetrabenzylthorium(IV) is reportedly accessible by the reaction of benzyllithium with $ThCl_4$, but characterization of this species was limited to IR spectroscopy,[41] and a structurally-authenticated sample of $[Th(CH_2Ph)_4]$ remains elusive.

However, by utilizing methyl-substituted benzyl ligands, Marks and co-workers were able to isolate the yellow tetrabenzyl derivative [Th($CH_2C_6H_3Me_2$-3,5)$_4$] from the reaction between $ThCl_4$ and $LiCH_2C_6H_3Me_2$-3,5 in THF.[42] Although this species also lacks structural-authentication, it has been characterized *via* $^1$H NMR spectroscopy and elemental analysis. Similarly, [U($CH_2Ph$)$_4$($MgCl_2$)] was reported as a finely-crystalline red-brown product from the reaction of [$UCl_4$(THF)$_3$] with Mg($CH_2Ph$)$_2$, but this species was only characterized by elemental analysis.[43]

More recently, Bart and co-workers reported the synthesis of a family of tetrabenzyluranium(IV) compounds, [U($CH_2$Ar)$_4$] (Ar = Ph (**b** in Figure 1.1), $C_6H_4$Me-*p*, $C_6H_3Me_2$-*m*, $C_6H_4{}^i$Pr-*p*, $C_6H_4{}^t$Bu-*p*, $C_6H_4(NMe_2)$-*p*, $C_6H_4$(SMe)-*p*, $C_6H_4$(OMe)-*p*, $C_6H_4$(OMe)-*o*, 2-pyridinyl), *via* the reaction of $UCl_4$ with 4 equiv of $KCH_2$Ar in THF, and all but the *p*-$NMe_2$ and *p*-SMe derivatives are stable in the solid state at room temperature.[44] The benzyl groups in these complexes are polyhapto coordinated with short U–$C_{ipso}$ distances in the solid state, except in the latter two compounds where uranium–heteroatom coordination is observed.[44] Along similar lines, reaction of [$ThCl_4$(dme)$_2$] with excess Li[$C_6H_4(CH_2NMe_2)$-*o*] in cold THF afforded the homoleptic aryl complex, [Th{$C_6H_4(CH_2NMe_2)$-*o*}$_4$], which is stabilized by thorium–amine interactions.[45]

Interestingly, Hayton and co-workers did not observe analogous reactivity when Li[$C_6H_4(CH_2NMe_2)$-*o*] was introduced to $UCl_4$; instead, a mixture of uranium(IV) aryl/benzyne complexes ([LiU{$C_6H_4(CH_2NMe_2)$-*o*}$_3${2,3-$C_6H_3(CH_2NMe_2)$}] and [Li(THF)$_2$][$LiUCl_2${$C_6H_4(CH_2NMe_2)$-*o*}$_2${2,3-$C_6H_3(CH_2NMe_2)$}]) was obtained.[45] Use of

the related α-amine-substituted benzyl ligand $\{CH(NMe_2)Ph\}^-$ by Walensky and co-workers also revealed divergent reactivities for thorium and uranium. The reaction of $[ThCl_4(dme)_2]$ with 4 equiv of $KCH(NMe_2)Ph$ provided $[Th\{\kappa^4\text{-}CH(NMe_2)Ph\}_2\{\kappa^5\text{-}(CH_2)MeNC(H)Ph\}]$, in which two of the amine-substituted benzyl ligands are $\kappa^4$-$NC_3$-coordinated, and an *N*-methyl group of the third benzyl substituent has been deprotonated to yield a dianionic ligand.[46] By contrast, reaction of $[UI_3(THF)_4]$ *or* $UCl_4$ with $KCH(NMe_2)Ph$ (3 or 4 equiv, respectively) afforded the uranium(III) product $[U\{CH(NMe_2)Ph\}_3]$, in which each amine-substituted benzyl ligand is $\kappa^4$-$NC_3$-coordinated.

While neutral, base-free tetraalkyl actinide(IV) complexes remain a synthetic challenge in general, related diphosphine-stabilized tetraalkyl compounds are readily accessible. Indeed, reaction of the diphosphine chloro precursors $[(dmpe)_2AnCl_4]$ (An = Th, U) with four equiv of methyllithium[47] or benzyllithium[48] afforded $[(dmpe)_xAnR_4]$ (R = $CH_3$, $x$ = 2; R = $CH_2Ph$, $x$ = 1). These species were characterized by elemental analysis, X-ray diffraction (in the case of the methyl derivative), and *via* reactions with phenol, which provided the corresponding $[(dmpe)An(OPh)_4]$ complexes. The related mixed methyl/benzyl derivative, $[(dmpe)An(CH_2Ph)_3Me]$, was obtained by reaction of $[(dmpe)_2AnCl_4]$ with 3 equiv of $PhCH_2Li$ and 1 equiv of MeLi.[48]

Based on their alkane elimination reactions with protonated ligand precursors (*vide infra*), the *in-situ*-generated uranium(III) trialkyl complexes, $[U(CH_2R)_3(THF)_x]$ (R = Ph, $SiMe_3$ or $CMe_3$),[49] have been proposed. However, the only isolated homoleptic trialkyluranium(III) complex is royal blue $[U\{CH(SiMe_3)_2\}_3]$ (**a** in Figure 1.1) prepared

by Sattelberger and co-workers *via* the reaction of $[U(OC_6H_3{}^tBu_2\text{-}2,6)_3]$ with 3 equiv of $LiCH(SiMe_3)_2$ in hexanes. By contrast, the reaction of $[UCl_3(THF)_x]$ with 3 equiv of $LiCH(SiMe_3)_2$ in THF afforded green $[Li(THF)_3][UCl\{CH(SiMe_3)_2\}_3]$; an 'ate' complex resulting from LiCl salt-occlusion. In the solid state, room temperature-stable $[U\{CH(SiMe_3)_2\}_3]$ is trigonal pyramidal with C–U–C angles of 108°;[50] this was initially attributed to γ-agostic U–H–C interactions on the more open face of the molecule, but based on computational studies on $[Ln\{CH(SiMe_3)_2\}_3]$ (Ln = La and Sm), pyramidalization may well be a consequence of U–(β-C–Si) interactions.[51] Rather intriguingly, Zwick and co-workers reported that the yellow-brown homoleptic trialkylplutonium(III) complex $[Pu\{CH(SiMe_3)_2\}_3]$ could be prepared *via* the reaction of $[Pu(OAr)_3]$ (Ar = 2,6-$^tBu_2C_6H_3$) with 3 equiv of $LiCH(SiMe_3)_2$ in hexane, and the corresponding neptunium(III) species $[Np\{CH(SiMe_3)_2\}_3]$ was also accessible using $[NpI_3(THF)_4]$ as a precursor, though characterization of these transuranium complexes was limited to IR spectroscopy.[52]

High-valent homoleptic alkyl compounds are particularly rare. Addition of excess LiR to $[U_2(OEt)_{10}]$ in 1,4-dioxane was reported by Wilkinson and co-workers to yield 8-coordinate uranium(V) complexes, $[Li(dioxane)]_3[UR_8]$ (R = Me, $CH_2SiMe_3$, $CH_2{}^tBu$), but these compounds have not been structurally characterized.[32] In 2011, Hayton and co-workers reported the first well-characterized U(V) alkyl complex, octahedral $[Li(THF)_4][U(CH_2SiMe_3)_6]$ (**d** in Figure 1.1), via the reaction of $[Li(dme)_3][U(CH_2SiMe_3)_5]$ with half an equiv of $I_2$, followed by rapid addition of $LiCH_2SiMe_3$. Cyclic voltammetry of $[Li(THF)_4][U(CH_2SiMe_3)_6]$ revealed a reversible

$U^{V/VI}$ wave at –1.22 V vs $[FeCp_2]^{0/+1}$ in THF, and reaction with $[U(O^tBu)_6]$ ($U^{V/VI}$ $E_{1/2}$ = –1.12 V) afforded $[U(CH_2SiMe_3)_6]$ and $[Li(THF)_4][U(O^tBu)_6]$. However, isolation of $[U(CH_2SiMe_3)_6]$ was precluded by high solubility combined with rapid decomposition above –25 °C.[53,54] Hayton and co-workers also recently isolated and structurally characterized the uranium(VI) alkyl complex $[Li(dme)_{1.5}]_2[UO_2(CH_2SiMe_3)_4]$;[54] a dianionic relative of the thermally unstable neutral uranyl $[UO_2(R)_2(THF)_x]$ (R = Me, Et, $CH{=}CH_2$, $^i$Pr, $^n$Bu, $^t$Bu, Ph) complexes generated *in-situ* in the early 1980s by Seyam and co-workers.[55]

### 1.3.2 – Homoleptic Actinide Allyl Complexes

Anionic allyl ligands are known to adopt various coordination modes; they may be $\eta^1$-coordinated (like alkyl ligands), or they may be $\eta^3$-coordinated *via* a π-system with 2 filled MOs (with 0 and 1 node) and 1 empty MO (with 2 nodes), depending on the requirements of the metal centre. This flexible bonding situation bears some resemblance to the variable hapticity of benzyl ligands, although the extent of delocalization is greater in $\eta^3$-allyl complexes than $\eta^3$-benzyl complexes. Although allyl ligands are frequently employed in transition metal systems, they are comparatively underutilized in actinide chemistry.

The prototypical thorium(IV) tetra(allyl) complex $[Th(C_3H_5)_4]$ was first mentioned by Wilke in 1966,[56] and published by Marks in 1992.[42] This complex was prepared by reaction of $[ThCl_4(THF)_3]$ with $(C_3H_5)MgBr$, and suffers from relatively poor

thermal stability, decomposing at temperatures above 0 °C. Homoleptic uranium(IV) allyl analogues, $[U(C_3H_5)_4]$ and $[U(C_3H_4Me\text{-}2)_4]$ were prepared similarly *via* reactions of $UCl_4$ with $(C_3H_4R)MgBr$ (R = H or Me) at –30 °C,[57] and as in the case of thorium, both complexes are thermally unstable, decomposing above –20 °C.[58]

Hanusa and co-workers later developed homoleptic tetra(allyl) complexes which feature mono- and di-substituted (trimethylsilyl)allyl ligands, $[\{1\text{-}(SiMe_3)C_3H_4\}_4Th]$ and $[\{1,3\text{-}(SiMe_3)_2C_3H_3\}_4Th]$.[59] These complexes were prepared by transmetalation of $[ThBr_4(THF)_4]$ with $K[1\text{-}(SiMe_3)C_3H_4]$ and $K[1,3\text{-}(SiMe_3)_2C_3H_3]$, respectively, in THF at −78 °C, and as a result of incorporating bulky silyl groups, these species are remarkably thermally robust, decomposing only at temperatures of 90 and 124 °C, respectively.

## 1.4 – Ligand Attachment Protocols for the Synthesis of Heteroleptic Actinide Complexes

The vast majority of organoactinide species are of heteroleptic composition, typically adhering to the common paradigm wherein complexes bear supportive ancillary ligand(s) accompanied by additional co-ligands. In this section, attachment protocols that afford access to such species are described, with an emphasis on commonly utilized methodology.

### 1.4.1 – Salt Metathesis

Ancillary ligand attachment in actinide chemistry is frequently achieved by transmetalative salt metathesis, typically utilizing an appropriate alkali metal or thallium(I) reagent in combination with an actinide halide or triflate. In a minority of cases, especially in donor solvents, this results in halide products containing occluded alkali metal halide salts. However, such species can still serve as precursors for further derivatization, and often yield salt-free products upon substitution of the remaining halide anions with bulkier and more electron donating organometallic ligands (Scheme 1.1).[60,61] In fact, 'ate' complexes may in some cases offer synthetic benefits. For example, Evans and co-workers have reported substantial differences in reactivity between anionic [$^{n}$Bu$_4$N][Cp$^{*}_2$UCl$_3$] and neutral [Cp$^{*}_2$UCl$_2$]; the former reacted in minutes, rather than hours or days, with 1 equiv of KL (L = hpp (1,3,4,6,7,8-hexahydro-2H-pyrimido(1,2-a)-pyrimidine) or NC$_4$Me$_4$) to afford [Cp$^{*}_2$UCl(L)], and reaction of [$^{n}$Bu$_4$N][Cp$^{*}_2$UCl$_3$] with 3 equiv of K(hpp) afforded [Cp$^{*}$U(hpp)$_3$] (via KCl, [$^{n}$Bu$_4$N]Cl and KCp$^{*}$ elimination), which was not observed as a product in the reaction of neutral [Cp$^{*}_2$UCl$_2$] with 3 equivalents of K(hpp).[62]

Problems have in some cases been encountered using alkyllithium reagents in combination with actinide iodide precursors; for example, Bart and co-workers reported that reaction of [Tp′UI$_2$(THF)$_2$] (Tp′ = {HB(3,5-Me$_2$pz)$_3$}$^{-}$) with 2 equiv of LiCH$_2$SiMe$_3$ in THF yielded [Li(THF)$_4$][Tp′UI$_3$] in over 60% yield, and the same triiodide 'ate' complex was formed in reactions of [Tp′$_2$UI] with LiCH$_2$SiMe$_3$ or MeLi. However, alkylsodium reagents (NaR; R = CH$_2$SiMe$_3$, Me or $^{n}$Bu) proved to be much more

effective in the latter reaction, cleanly yielding the desired [Tp′$_2$UR] compounds and poorly soluble NaI as a non-interfering byproduct.[63]

**Scheme 1.1 –** Ancillary ligand attachment by salt metathesis, illustrating solvent-dependent 'ate' complex formation, and subsequent derivatization to yield a salt-free dialkyl complex (Dipp = 2,6-diisopropylphenyl).[60]

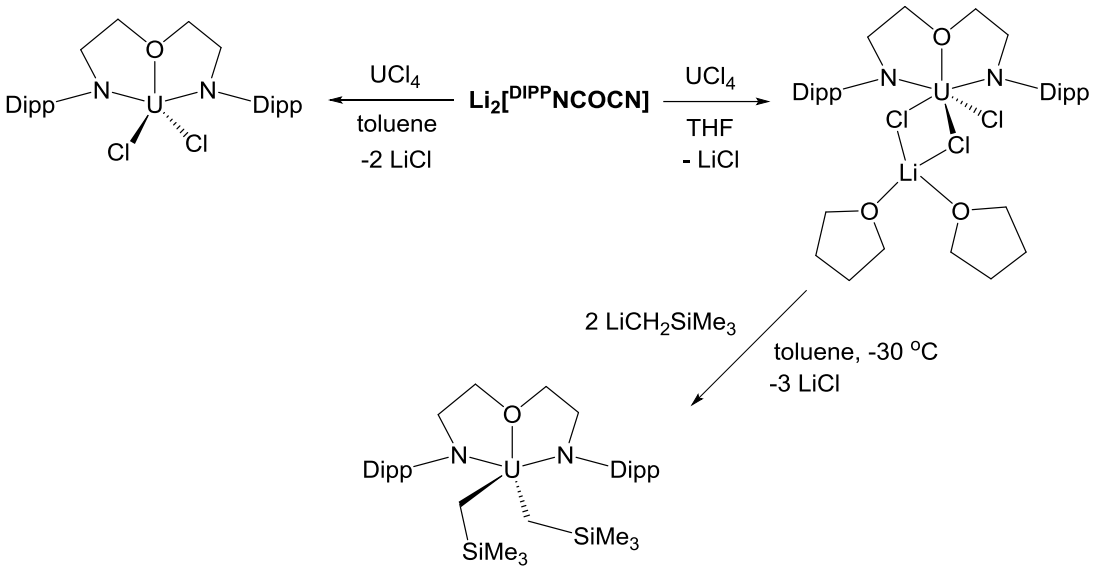

Magnesium reagents (e.g. $Mg(C_5H_2{}^tBu_3\text{-}1,2,4)_2$, $[Mg(CH_2CR{=}CRCH_2)(THF)_2]$, $MgMe_2$, [Cp*MgCl], or MeMgBr) have also been utilized to install organometallic ligands, although in rare cases this has resulted in competing ancillary ligand transfer to magnesium,[64,65] or halide exchange reactivity,[66,67] rather than the expected salt metathesis (Scheme 1.2); halide exchange presumably occurs via Grignard adducts similar to that in Figure 1.2.[64]

**Scheme 1.2 –** Reactions between actinide halide precursors and Grignard reagents that do not yield the expected alkylated products: **(a)** Transfer of a dianionic NON-donor ligand (4,5-bis(2,6-diisopropylanilido)-2,7-di-*tert*-butyl-9,9-dimethylxanthene; $XA_2$) from thorium to magnesium,[64] and **(b)** Halide exchange converting $[\{(^{t\text{Bu}}NON)UCl(\mu\text{-}Cl)\}_2]$ ($^{t\text{Bu}}NON = \{O(SiMe_2N{}^tBu)_2\}^{2-}$) to a mixed chloride/bromide analogue.[67]

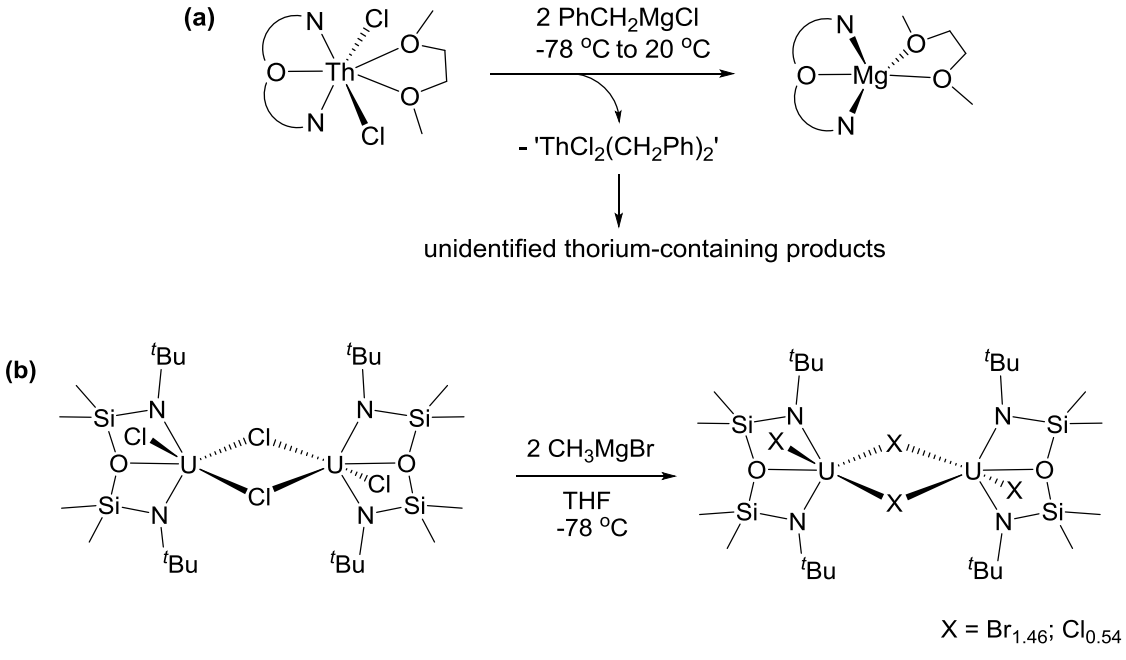

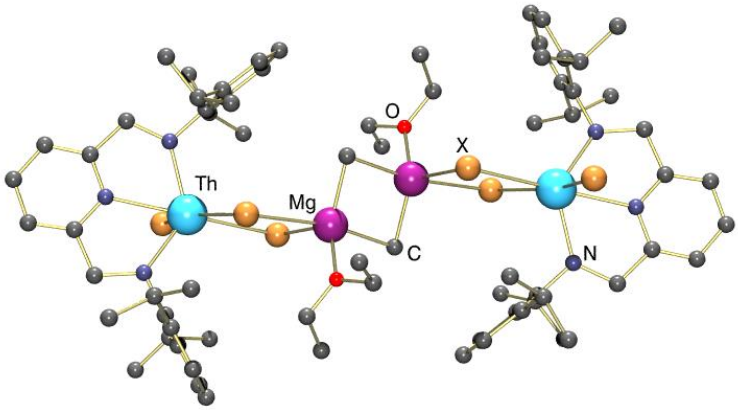


**Figure 1.2 –** X-ray crystal structure of [{(BDPP)ThX(μ-X)$_2$Mg(OEt$_2$)(μ-Me)}$_2$] (X = Br$_{0.73–0.87}$/Cl$_{0.13–0.27}$; BDPP = 2,6-bis(2,6-diisopropylanilidomethyl)pyridine).[64]

Actinide borohydride and tetraarylborate species can also be utilized as salt metathesis precursors, eliminating MBH$_3$R or MBAr$_4$ salts (M = alkali-metal) rather than an alkali-metal halide. For example, the reaction of [Cp*****$_2$U{(μ-Ph)$_2$BPh$_2$}] with KX (X = Cp***** or NC$_4$Me$_4$) in non-coordinating solvents is synthetically valuable as a means to access base-free [Cp*****$_2$UX].[68,69] Along similar lines, actinide alkoxide or aryloxide compounds have also be utilized as alternative salt metathesis precursors, eliminating LiOR salts rather than a lithium halide. For example, [U(CH(SiMe$_3$)$_2$)$_3$] was prepared by reaction of [U(OC$_6$H$_3$$^t$Bu$_2$-2,6)$_3$] with 3 equiv of LiCH(SiMe$_3$)$_2$,[70] Furthermore, in very sterically hindered complexes such as [UCp*****$_3$] and [Cp*****$_2$U(μ-η$^6$:η$^6$-C$_6$H$_6$)UCp*****$_2$], the Cp***** ligands become unusually vulnerable to replacement by less sterically hindered κ$^1$- or κ$^2$-coordinating anions such as {N(SiMe$_3$)$_2$}$^-$, {CH(SiMe$_3$)$_2$}$^-$, (OAr)$^-$ (Ar = C$_6$H$_2$($^t$Bu-*o*)$_2$(Me-*p*)), and {MeC(N$^i$Pr)$_2$}$^-$.[71,72]

### 1.4.2 – Alkane Elimination

Alkane elimination is a frequently employed ligand attachment protocol in the chemistry of the lanthanides, facilitated by the ready accessibility of trialkyl [Ln(CH$_2$R)$_3$(THF)$_x$] (R = SiMe$_3$ or Ph) starting materials.[33] However, this approach has rarely been employed to install multidentate ligands on actinide metals, partly due to the low thermal stability of homoleptic (trimethylsilyl)methyl thorium and uranium compounds, and only recent availability of well-defined homoleptic benzyl uranium complexes.[44] Notable examples of alkane elimination from a homoleptic alkyl actinide precursor include the reactions of (a) H$_2$[XA$_2$] and H$_2$[BDPP] (XA$_2$ = 4,5-bis(2,6-diisopropylanilido)-2,7-di-tert-butyl-9,9-dimethylxanthene; BDPP = 2,6-bis(2,6-diisopropylanilidomethyl)pyridine) with *in-situ* generated "[Th(CH$_2$SiMe$_3$)$_4$(dme)$_x$]" (prepared by reaction of [ThCl$_4$(dme)$_2$] with 4 equiv of LiCH$_2$SiMe$_3$ at 0 °C) reported by Emslie and co-workers,[40] (b) H$_2$[BDPP] or H$_2$[FcNN] (FcNN = {Fe($\eta^5$-C$_5$H$_4$NSiR$_3$)$_2$}$^{2-}$; R = $^t$Bu, Ph) with *in-situ* generated "[U(CH$_2$R)$_3$(THF)$_x$]" (R = Ph, SiMe$_3$, $^t$Bu; prepared by reaction of [UI$_3$(THF)$_3$] with 3 equiv of various MCH$_2$R (R = Ph, SiMe$_3$ or $^t$Bu; M = Li or K) reagents) reported by Diaconescu and co-workers,[49] (c) the reaction of thermally unstable [U(C$_3$H$_5$)$_4$] with two equivalents of $^t$BuOH at –20 °C to afford [($^t$BuO)$_2$U(C$_3$H$_5$)$_2$],[58] and reaction of [U{CH(NMe$_2$)Ph}$_3$] with 3 equiv of H[S$_2$C(C$_6$H$_3$Mes$_2$-2,6)] in THF to produce [U{S$_2$C(C$_6$H$_3$Mes$_2$-2,6)}$_4$(THF)].[46] By comparison, alkane elimination from non-homoleptic precursors such as [Cp*****AnMe$_2$] and [Cp′$_2$AnMe$_2$] (Cp′ = {$\eta^5$-1,2,4-$^t$Bu$_3$(C$_5$H$_2$)}$^-$) in combination with protic reagents such as terminal alkynes,[73] primary or secondary amines,[74] and phosphines,[75] alcohols,[76] and

thiols[77] is common. Alkane or alkylsilane elimination is also a common strategy for the synthesis of heteroleptic actinide hydride complexes via σ-bond metathesis between a heteroleptic alkyl complex and $H_2$ or a hydrosilane (most commonly $PhSiH_3$).[78-80]

### 1.4.3 – Less Common Ligand Attachment Protocols

In addition to the ubiquitous salt-metathesis and alkane elimination methodologies, a number of less common approaches to ligand installation onto actinide metals have also been reported. These approaches include[§] trialkyltin halide elimination,[81] $H_2$ elimination from a hydride precursor,[82] amine elimination from an amido precursor,[83] insertion chemistry,[69] reductive elimination chemistry,[44] and sterically-induced reduction (SIR) reactivity developed primarily by the Evans group.[71] However, further discussion of these- and other less common methodologies is beyond the scope of this thesis.

## 1.5 – Carbocyclic Organoactinide Complexes

Ancillary ligands are responsible for providing the metal centre with sufficient electronic saturation and steric protection to ensure thermal stability, often with the additional desirable consequence of rendering the complex monomeric and soluble. Furthermore, the diverse steric- and electronic profiles afforded by ancillary ligands are highly influential on the reactivity observed for their respective coordination- and organometallic complexes, and as such, their construction has become the fulcrum for the rational design of functional compounds and catalysts. To date, the vast majority of

[§] The reference accompanying each type of ligand attachment protocol serves as a single example of the respective methodology.

organoactinide complexes bear carbocyclic ancillaries, a family of annular π-ligands which are constituted of contiguous carbon atoms[¶]. These include cyclopentadienyl ($C_5R_5^-$) and related indenyl ($ind^-$) and fluorenyl anions, cyclooctatetraenide ($C_8R_8^{2-}$) and pentalene dianions, carboranes, arenes, and the cycloheptatrienyl trianion (Figure 1.3).

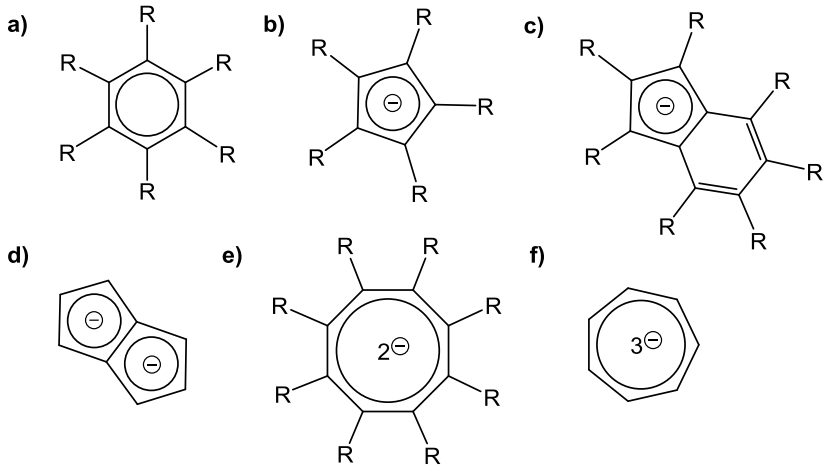


**Figure 1.3** – Selected carbocyclic ligands in actinide chemistry: (**a**) arenes, (**b**) cyclopentadienyl anions, (**c**) indenyl anions, (**d**) pentalene dianions, (**e**) cyclooctatetraenide dianions, and (**f**) the cycloheptatrienyl trianion.

Having been under development for more than 60 years, carbocyclic actinide chemistry is rich in breadth and includes an extensive catalogue of systems based on the cyclopentadienyl family of ancillary ligands, which have been discussed thoroughly in this context in many reviews and books.[84] While a comprehensive audit of carbocyclic actinide chemistry is beyond the scope of this thesis, in this section, organometallic actinide(IV) complexes bearing the ubiquitous cyclopentadienyl and cyclooctatetraenide ancillary ligands will be broadly surveyed, with bis(cyclopentadienyl) species warranting

[¶] Heteroatoms are occasionally present in carbocyclic ligands.

additional focus given the similarities between $(Cp^{X}_{2})^{2-}$ ligand sets and the dianionic diamido(ether) pincer ligands that are the primary focus of the research in this thesis. Discussion will focus primarily on tetravalent actinide systems, though compounds in differing oxidation states are highlighted occasionally.

### 1.5.1 – Actinide(IV) Cyclopentadienyl Complexes

The vast majority of carbocyclic actinide species are supported by cyclopentadienyl ligands ($C_5R_5^-$; denoted $Cp^X$), unsurprising given the extensive breadth of analogous transition metal and lanthanide cyclopentadienyl derivatives. Among the most commonly employed cyclopentadienyl anions in organoactinide chemistry are $C_5H_5$ (Cp), $C_5H_4Me$ ($Cp^{Me}$), $C_5H_4(SiMe_3)$ ($Cp^{TMS}$), 1,3-$(SiMe_3)_2C_5H_3$ (Cp''), 1,2,4-$(SiMe_3)_3C_5H_2$ ($Cp^{'''}$), 1,3-$(^tBu)_2C_5H_3$ ($Cp^{t2}$), 1,2,4-$(^tBu)_3C_5H_2$ (Cp′), $C_5HMe_4$ ($Cp^{Me4}$) and $C_5Me_5$ (Cp*****), and these ligands are capable of binding the actinide in an $\eta^1$-, $\eta^3$- or $\eta^5$-coordination mode, with $\eta^5$-coordination being observed almost exclusively in actinide chemistry (although lower hapticities are more favorable for related indenyl anions).[3] The remarkable uptake of the cyclopentadienyl ligand system by the organometallic actinide community is likely due to the stability this system provides its coordination- and organometallic complexes, as well as the impressive versatility it affords. Indeed, Cp derivatives are readily accessible and easily tuned, and a diverse array of mono-, bis-, tris-, and tetrakis(cyclopentadienyl) actinide complexes can be prepared, with representative tetravalent examples of each of these types of complexes described in the following sections.

### 1.5.1.1 – $Cp^{X}_{4}An$, $Cp^{X}_{3}AnR$, and $Cp^{X}AnR_{3}$ Complexes

Although the electronically- and sterically saturated tetrakis(cyclopentadienyl)actinide(IV) complexes offer few opportunities for further derivatization, their conception and development represents an important keystone in early organoactinide chemistry. Complexes of the form $[Cp_4An]$ (An = Th,[85] U (**c** in Figure 1.4),[86] Pa,[87] Np[88]) were prepared by reaction of the respective tetrachloro precursors $MCl_4$ (M = Th, U or Np) with 4 equiv of KCp, or by reaction of $PaCl_4$ with 2 equiv of $BeCp_2$, which has proven to be a highly useful reagent for preparing transplutonium cyclopentadienyl complexes.[89] The cyclopentadienyl ligands were found to coordinate *via* an $\eta^5$-bonding mode and to adopt a pseudo-tetrahedral arrangement around the actinide centre in each of these complexes, as determined using powder- and single crystal X-ray diffraction, and IR spectroscopy. This contrasts the bonding situation in group 4 transition metal analogues, which adopt $[(\eta^5\text{-}Cp)_2M(\eta^1\text{-}Cp)_2]$ (M = Ti (**a** in Figure 1.4) or Hf)[90] and $[(\eta^5\text{-}Cp)_3Zr(\eta^1\text{-}Cp)]$ (**b** in Figure 1.4) structures[91] in the solid state and in solution. A closely related thorium(IV) complex featuring four indenyl ($C_9H_7^-$) ligands, $[Th(ind)_4]$ (**d** in Figure 1.4), has also been prepared by reaction of $K(C_9H_7)$ with $ThCl_4$ in THF,[92] but while compositionally analogous to $[Cp_4Th]$, each indenyl ring in this species adopts an $\eta^3$-coordination mode as a consequence of the increased steric pressure exerted by the extended ring system of the indenyl ligands.

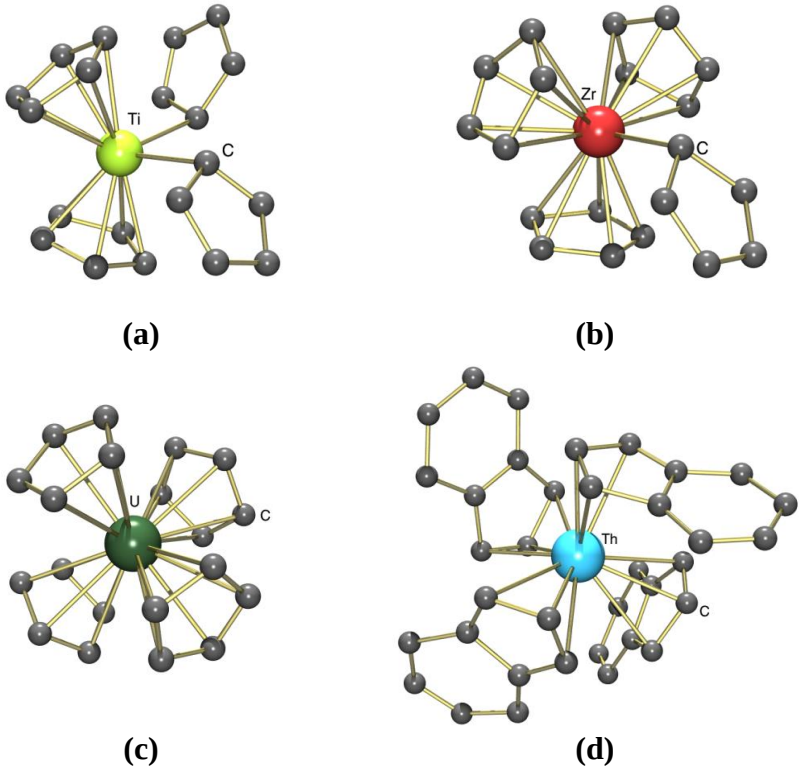


**Figure 1.4 –** X-ray crystal structures of (**a**) [$TiCp_4$], (**b**) [$ZrCp_4$], (**c**) [$UCp_4$], and (**d**) [$Th(ind)_4$] illustrating the effects of steric and electronic influences on π-ligand hapticity.

Conceptually, by replacing one of the cyclopentadienyl ancillary ligands with a reactive co-ligand, the resulting tris(cyclopentadienyl)actinide(IV) motif, of the form [$Cp_3AnX$], affords an opportunity for derivatization and subsequent reactivity that is lacking in the tetrakis(cyclopentadienyl) species. Wilkinson and co-workers' early report[93] outlining the preparation of [$Cp_3UCl$] by treatment of $UCl_4$ with 3 equiv of NaCp initiated the development of tris(cyclopentadienyl) organoactinide chemistry, as [$Cp_3UCl$] is readily alkylated to afford complexes of the form [$Cp_3UR$] (R = Me, $^{n}$Bu, $CH_2{}^{t}$Bu, $^{i}$Pr, $^{t}$Bu) by treatment with LiR or RMgX reagents.[94] Indeed, the tris(cyclopentadienyl) scheme has proven highly suitable as a platform for the support of a diverse array of

actinide(IV) species, as evidenced by over 130 compounds featuring the $(Cp^{X}_{3})^{3-}$ and $(ind^{X}_{3})^{3-}$ ligand sets in the Cambridge Structural Database at the time of writing. The versatility of $[Cp_3AnX]$ halide and hydrocarbyl complexes is additionally evident by the broad array of derivatives accessible *via* transmetalation, protonation, or σ-bond metathesis routes, including allyl, aryl, vinyl, and alkynyl,[94-96] hydrido,[97] borohydride,[98,99] aluminohydride,[100] silyl, germyl, stannyl,[101] amido and alkoxide,[102,103] phosphido,[103] thiolate[98], and tetrakis(cyclopentadienyl) species.[95,104] However, actinide(IV) species bearing only one reactive co-ligand are not especially relevant to the research described in this thesis, limiting the need for a comprehensive discussion of tris(cyclopentadienyl) actinide chemistry.

Beyond tetrakis- and tris(cyclopentadienyl)actinide(IV) systems, at the other end of the coordinative-saturation spectrum are the relatively low-coordinate mono(cyclopentadienyl) 'half-sandwich' species of the form $[Cp^{X}AnX_3L_x]$ (L = neutral donor ligand or occluded alkali-metal salt). Half-sandwich actinide(IV) complexes bearing the unsubstituted cyclopentadienyl ligand suffer from poor steric protection and insufficient electronic saturation, and are fairly uncommon as a consequence (i.e. only 12 mono(cyclopentadienyl) actinide complexes can be found in the Cambridge Structural Database at the time of writing). The stability of such complexes can be improved by saturating the coordination sphere through the formation of 'ate' complexes (e.g. in $[CpUCl_3(THF)(\mu\text{-}Cl)\{Li(THF)_3\}]$),[105] or the use of neutral Lewis bases (e.g. phosphine oxide ligands in $[CpNpCl_3(OPPh_2Me)_2]$).[106]

While the mono(cyclopentadienyl) motif is limiting, organometallic derivatives can be accessed by utilizing the pentamethyl-substituted cyclopentadienyl ligand, Cp*****. Indeed, tris(hydrocarbyl) complexes of the form [Cp*****$AnR_3$] (An = U, R = $C_3H_5$, 2-methylallyl (**a** in Figure 1.5), $CH_2Ph$; An = Th, R = $CH_2Ph$, $CH_2{}^tBu$, $C_3H_5$, *o*-$C_6H_4NMe_2$) can be prepared by treatment of [Cp*****$_3AnCl_3L_2$] (L = THF, $OEt_2$, 1,4-dioxane) with the appropriate LiR or RMgX reagent.[20,107-109] Each benzyl ligand of [Cp*****$U(CH_2Ph)_3$] (**b** in Figure 1.5) adopts a multi-hapto binding mode, as evidenced by acute U−$CH_2$−$C_{ipso}$ angles and relatively short U−$C_{ipso}$ contacts, likely a consequence of the limited electronic saturation provided by the single Cp***** ancillary.[20] Additionally, reaction of [Cp*****$ThBr_3(THF)_x$] with one equivalent of KOAr (Ar = 2,6-$^tBu_2C_6H_3$) afforded [Cp*****$ThBr_2$(OAr)(THF)], which was alkylated using $Me_3SiCH_2MgCl$ to form [Cp*****$Th(CH_2SiMe_3)_2$(OAr)] (**c** in Figure 1.5), and subsequent reaction with $H_2$ provided [Cp*****$Th(\mu\text{-}H)_2(OAr)]_3$.[110] Uranium(III) mono(cyclopentadienyl) species are also rare; the notable alkyl complex [{Cp*****$U\{CH(SiMe_3)_2\}\}_2(\mu\text{-}\eta^6\text{:}\eta^6\text{-}C_6H_6)$] features a doubly-reduced bridging $(C_6H_6)^{2-}$ ligand that provides significant electronic saturation to the low-coordinate "[Cp*****$U\{CH(SiMe_3)_2\}]^+$" fragment.[72]

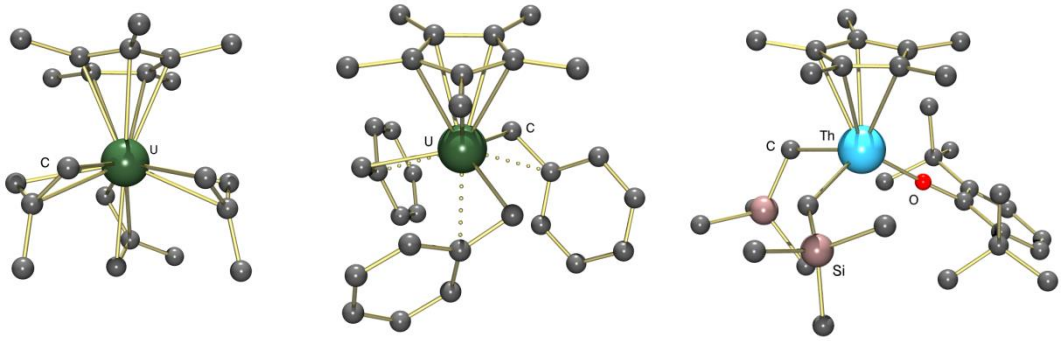


**(a)** **(b)** **(c)**

**Figure 1.5** – X-ray crystal structures of (**a**) [Cp*****U(2-methylallyl)$_3$],[108] (**b**) [Cp*****U(CH$_2$Ph)$_3$],[20] and (**c**) [Cp*****Th(CH$_2$SiMe$_3$)$_2$(OAr)] (Ar = 2,6-$^t$Bu$_2$C$_6$H$_3$).[110]

### 1.5.1.2 – $Cp^X_2AnR_2$ Complexes

The bis(cyclopentadienyl) platform has played a particularly important role in the development of organoactinide chemistry, as complexes supported by the $(Cp^X_2)^{2-}$ ligand set are closely analogous to the broad family of transition metal metallocene species.[111] Additionally, bis(cyclopentadienyl)actinide(IV) chemistry bears particular relevance to the research presented in this thesis, as tetravalent species of the form $[Cp^X_2AnR_2]$ feature two reactive co-ligands, a motif that is reflected in the bis(hydrocarbyl) actinide(IV) complexes presented in Chapters 2–5.

As with unsubstituted mono(cyclopentadienyl) actinide species, complexes supported by the unsubstituted $(Cp_2)^{2-}$ ligand system suffer from poor steric protection, rendering such species susceptible to ligand redistribution reactions.[112] Indeed, only two actinide hydrocarbyl derivatives bearing the unsubstituted $(Cp_2)^{2-}$ ligand set have been

crystallographically-characterized, [$Cp_2ThMe_2$(dmpe)] and [$Cp_2Th(CH_2Ph)_2$(dmpe)], and in each case, Lewis base coordination appears necessary to stabilize the metallocene-type species.[113] By contrast, utilizing substituted cyclopentadienyl ligands has led to a diverse array of pseudo-tetrahedral complexes of the form [$Cp^X_2AnX_2$] that boast dramatically improved thermal stability and advantageous solubility- and crystallinity profiles.[78,79] Indeed, at the time of writing, over 530 "[$Cp^X_2An$]" species could be found in the Cambridge Structural Database, illustrating the propriety of the $(Cp^X_2)^{2-}$ ligand set for the support of tetravalent actinides. The sterically bulky cyclopentadienyl anions Cp*****, Cp′ (1,2,4-($^t$Bu)$_3C_5H_2$), Cp" (1,3-($SiMe_3$)$_2C_5H_3$), and $Cp^{t2}$ (1,3-($^t$Bu)$_2C_5H_3$) have proven the most versatile, facilitating access to organometallic derivatives of the form [$Cp^X_2AnR_2$] (e.g. **b** in Figure 1.6), typically by reaction of the respective dichloride precursors, [$Cp^X_2AnCl_2$], with RLi, RMgX, or $KCH_2Ph$ reagents.[78,79,114,115,116,117]

Although $(Cp^X_2)^{2-}$ ligand sets have proven highly suitable for the support of organoactinide complexes, Marks and co-workers noted that while necessary, the bulky substituents of such anions resulted in sterically-congested actinide coordination spheres, possibly limiting the reactivity accessible to such species.[118] The ring-bridged chelating cyclopentadienyl ligand $\{Me_2Si(C_5Me_4)_2\}^{2-}$ was thus developed in attempt to access sterically-open but sufficiently protected actinide species, and organometallic derivatives of the form [$\{Me_2Si(C_5Me_4)_2\}AnR_2$] (An = Th, R = $CH_2SiMe_3$, $CH_2$$^t$Bu, $C_6H_5$, $^n$Bu, $CH_2Ph$; An = U, R = Me, $CH_2Ph$) are readily accessible *via* alkylation of the dichloride precursors with the appropriate RLi or RMgX reagent.[118,119] Through use of the *ansa*-metallocene actinide platform, enhanced catalytic activity has been observed for the

dimerization of terminal alkynes, hydrosilylation, and 1-hexene hydrogenation (relative to unlinked actinide metallocene systems).[118,120]

By design, *ansa*-metallocene complexes of the form [{$Me_2Si(C_5Me_4)_2$}$AnX_2$] feature a 'pulling-back' of the bis(cyclopentadienyl) coordination geometry. For example, the Cent–Th–Cent (Cent = ring centroid) angle in [{$Me_2Si(C_5Me_4)_2$}$Th(CH_2SiMe_3)_2$] (118.4°; **a** in Figure 1.6) is significantly contracted relative to the comparable angle in the analogous unlinked complex [Cp*****$_2$$Th(CH_2SiMe_3)_2$] (134.9°).[109] Additionally, related {($^t$BuN)$SiMe_2(C_5Me_4)$}$^{2-}$ ligands have been utilized to generate sterically open "constrained-geometry" catalysts (CGCs) such as [{($^t$BuN)$SiMe_2(C_5Me_4)$}$An(NMe_2)_2$] for intramolecular alkene hydroamination[121] and alkyne hydroalkoxylation.[122] At the other end of the spectrum of Cp–An–Cp angles, linear actinide metallocenes were accessed by coordination of a dicationic [Cp*****$_2$U]$^{2+}$ core to five neutral or anionic donor atoms; example complexes include dicationic [Cp*****$_2$$U(NCMe)_5$][$BPh_4$]$_2$ (**c** in Figure 1.6) and [Cp*****$_2$$U(phen)(NCMe)_3$][$BPh_4$]$_2$ (phen = 1,10-phenanthroline),[123] and trianionic [$NEt_4$]$_3$[Cp*****$_2$$U(CN)_5$].[124]

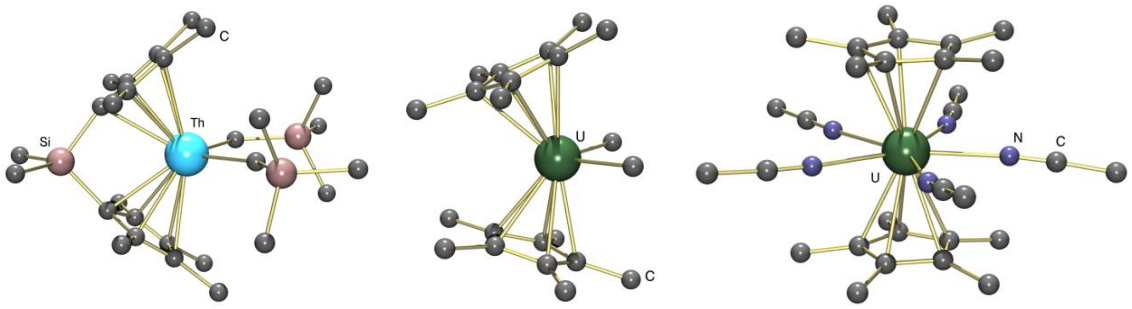


**(a)** **(b)** **(c)**

**Figure 1.6 –** X-ray crystal structures illustrating the differences in Cent–An–Cent (Cent = cyclopentadienyl ring centroid) angles in (**a**) [{$Me_2Si(C_5Me_4)_2$}$Th(CH_2SiMe_3)_2$],[118] (**b**) [$Cp^*_2UMe_2$][125] and (**c**) the dicationic portion of [$Cp^*_2U(NCMe)_5$][$BPh_4$]$_2$.[123]

Selected reactivity of alkyl[78] and allyl[114] actinide metallocene complexes is highlighted in Scheme 1.3, including insertion reactions with $CO_2$ and $CN^tBu$,[114,126] insertion of CO followed by rearrangement (due to significant contributions from both acyl An–C(=O)R and carbene An–O–C–R resonance structures),[127] reversible benzene elimination from the diphenyl complex to generate a benzyne complex which can be trapped with diphenylacetylene,[79] unusual cyclometalation rather than oxygen-atom transfer reactivity with pyridine-*N*-oxide,[128] cyclometalation reactions leading to metallacyclobutane products which are particularly capable of σ-bond metathesis with the C−H bonds in substrates including methane, $SiMe_4$, $SnMe_4$ and $PMe_3$,[129] double cyclometalation of [{$C_5Me_4(SiMe_3)$}$_2UMe_2$] to form a double 'tuck-in' complex,[126] reaction of dialkyl complexes with $H_2$ or $PhSiH_3$ to form dimetallic tetrahydride species (in equilibrium with a uranium(III) hydride species for An = U),[78,79,80] and reaction of [$Cp^*_2UMe_2$] with the aminoborane $H_2BN(SiMe_3)_2$ (2 or 4 equiv) to form [$Cp^*_2UMe${$H_3BN(SiMe_3)_2$}] and [$Cp^*_2U${$H_3BN(SiMe_3)_2$}$_2$], respectively.[130]

**Scheme 1.3 –** Synthesis and selected reactions of alkyl, allyl and aryl actinide metallocene complexes bearing Cp***** and $Cp^{TMS}$ ($C_5Me_4(SiMe_3)$) ancillary ligands.

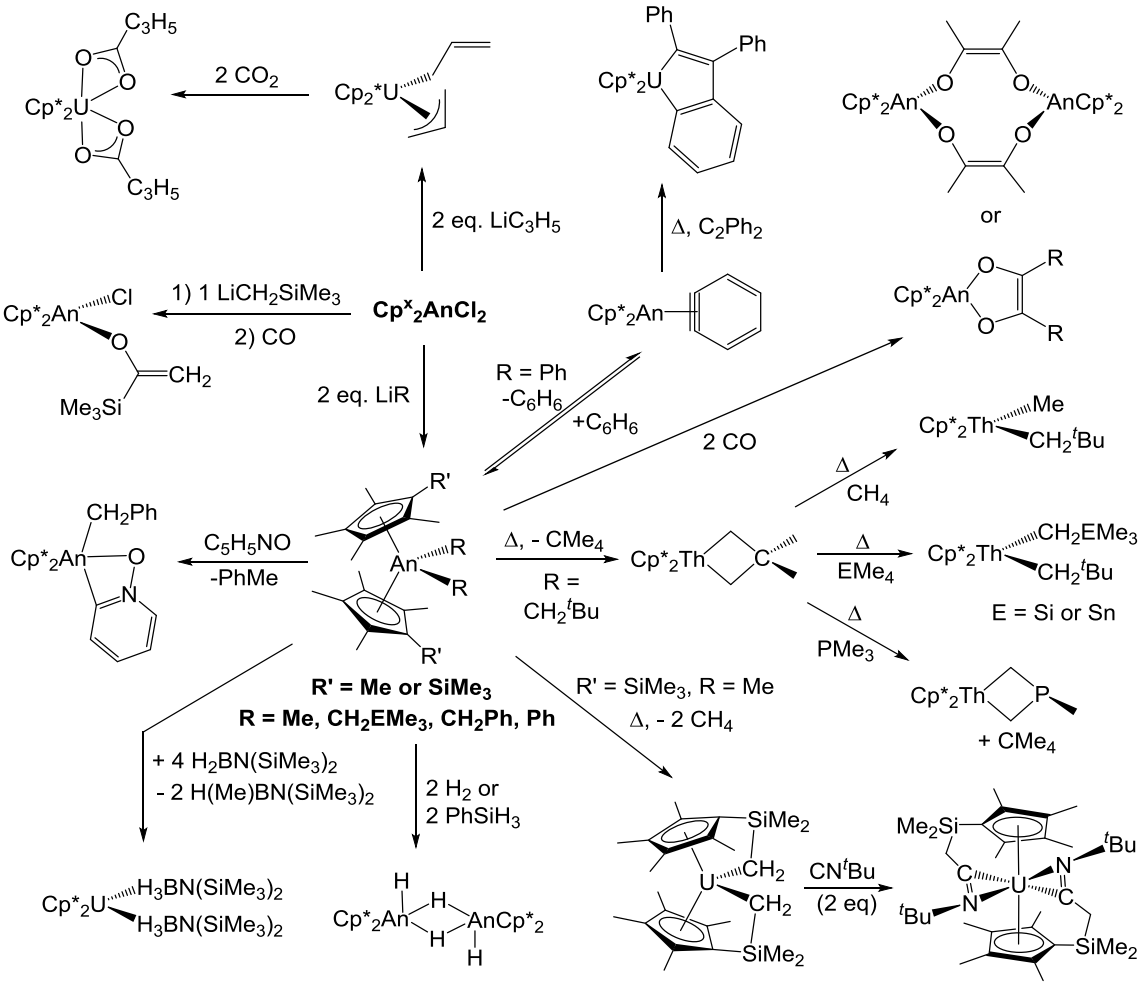

### 1.5.2 – Actinide Cyclooctatetraenide Complexes

Alongside cyclopentadienyl ligands and derivatives thereof, the cyclooctatetraenide family of ancillaries (*i.e.* $C_8R_8^{2-}$; denoted $^{X}$COT) have also been widely utilized as supporting ligands in organoactinide chemistry. Pyrophoric green bis(cyclooctatetraenide)uranium(IV), [U($\eta^8$-COT)$_2$], was prepared in 1968 by the reaction of $UCl_4$ with $K_2$[COT] by Streitwieser and Müller-Westerhoff,[131] and the $D_{8h}$ solid-state structure was published in 1969 by Raymond and Zalkin.[132] [U(COT)$_2$] is thermally robust, subliming at 180 °C (0.03 mm Hg), and hydrolyzes only very slowly in water at neutral pH. It is named uranocene to highlight its similarity to ferrocene, as a sandwich complex featuring planar aromatic π-ligands (10π vs 6π in Cp derivatives), and the bonding in uranocene has been the subject of numerous experimental and theoretical investigations.[133] Isostructural yellow [Th(COT)$_2$],[134] yellowish [Pa(COT)$_2$],[4] and red [An(COT)$_2$] (An = Np and Pu)[135] were also subsequently prepared from $AnCl_4$ (An = Th, Pa, Np) or [$NEt_4$][$PuCl_6$] with $K_2$[COT], or by reaction of finely divided pyrophoric thorium or plutonium metal powder (prepared by actinide hydride thermolysis) with cyclooctatetraene.[136]

*Ansa*-actinidocenes have been prepared with an –$SiMe_2(CH_2)_nSiMe_2$– (*n* = 1[137] or 2)[138] bridge between the two cyclooctatetraenide rings, and in the structurally characterized (*n* = 2) complexes, the An–C bond lengths are analogous to those in unsubstituted [An(COT)$_2$] complexes and the Cent–An–Cent (Cent = ring centroid) angles of 178° (U) and 177° (Th) are only slightly distorted. As with the corresponding cyclopentadienyl actinide chemistry, systems featuring substituted cyclooctatetraenide

ligands have also been developed for thorium and uranium, with most recent studies focusing on the 1,4-$(SiMe_3)_2C_8H_6$ ($^{TMS2}$COT),[139] 1,3,6-$(SiMe_3)_3C_8H_5$ ($^{TMS3}$COT),[140] 1,4-$(Si^iPr_3)_2C_8H_6$ ($^{TIPS2}$COT),[141] and 1,4-$(Si^tBuMe_2)_2C_8H_6$ ($^{TBS2}$COT)[12] dianions. The extremely bulky 1,4-$(SiPh_3)_2C_8H_6$ ($^{BIG}$COT) ligand was also introduced to uranium leading to a unique bent uranocene, [($^{BIG}$COT)$_2$U], with a Cent–U–Cent angle of 169°.[142] The vast majority of disubstituted COT ligands are 1,4-substituted due to straightforward synthesis, but nevertheless, [U($^{1,5\text{-}t\text{Bu2}}$COT)$_2$] was prepared from 1,5-di-*tert*-butylcyclooctatetraene ($^{1,5\text{-}t\text{Bu2}}$COT), which was synthesized in 10 steps with an 11 % overall yield.[143] Actinide complexes of mono- and tetrasubstituted cyclooctatetraenide ligands (e.g. $^{t\text{Bu}}$COT and $^{1,3,5,7\text{-Me4}}$COT) have also been reported, as have actinide complexes of fused-ring derivatives such as 1,2-$(CH_2)_3C_8H_6$.[144]

Beyond bis(cyclooctatetraenide) complexes, a host of mono(cyclooctatetraenide) actinide complexes have been reported. These complexes include actinide(III), (IV) and (V) compounds, such as [(COT)U(hmpa)$_3$][BPh$_4$]$_n$ ($n$ = 1 and 2; hmpa = {$(Me_2N)_3PO$}),[145] [(COT)AnCl$_2$(THF)$_2$] (An = Th or U)[146] and [(COT)U$(NEt_2)_3]^{x-}$ ($x$ = 1 and 0).[147] However, organometallic derivatives are largely confined to the IV oxidation state, and include [(COT)U$(NEt_2)${$CH(SiMe_3)_2$}],[148] [(COT)U$(CH_2R)_2$(hmpa)$_x$] (R = $SiMe_3$ or Ph), and [Li(THF)$_3$][(COT)U$(CH_2SiMe_3)_3$].[149]

Mixed $^{X}$COT/L (L = monoanionic ligand) systems are also known, including $^{X}$COT/Cp***** thorium[150] and uranium[151] derivatives. The Evans group has played the major role in the development of COT/Cp***** chemistry, including the synthesis of [(COT)(Cp*****)UR] (R = Me, Et, $CH_2{}^tBu$, $CH(SiMe_3)_2$, and Ph) derivatives,[152,153] the 'tuck-

in' complexes [(COT)($C_5Me_4CH_2$)U(THF)$_x$] ($x$ = 0 and 1), which undergo insertion reactions with unsaturated substrates such as $^t$BuNC and C(N$^i$Pr)$_2$,[153] and bimetallic [{(COT)(Cp*****)U}$_2$(μ-η$^3$:η$^3$-COT)], which readily eliminates COT and reacts as a source of "[(COT)(Cp*****)U]" in the presence of oxidizing substrates such as phenazine and PhEEPh (E = S, Se or Te).[154] More sterically-hindered- and crystalline [($^{TIPS2}$COT)(Cp*****)UR] (R = H, Me (**a** in Figure 1.7), $CH_2SiMe_3$, $CH_2Ph$ and $CH(SiMe_3)_2$) derivatives, and the 'tuck-in' complexes [($^{TIPS2}$COT)($C_5Me_4CH_2$)U(THF)$_x$] {$x$ = 0 (**b** in Figure 1.7) and 1} have also been prepared by Cloke et al.,[155] as have the thorium complexes [($^{TIPS2}$COT)(Cp*****)Th($CH_2Ph$)], [{($^{TIPS2}$COT)(Cp*****)ThH}$_n$] ($n$ = 1 or 2), and [{($^{TIPS2}$COT)($C_5Me_4CH_2$)Th}$_2$].[156]

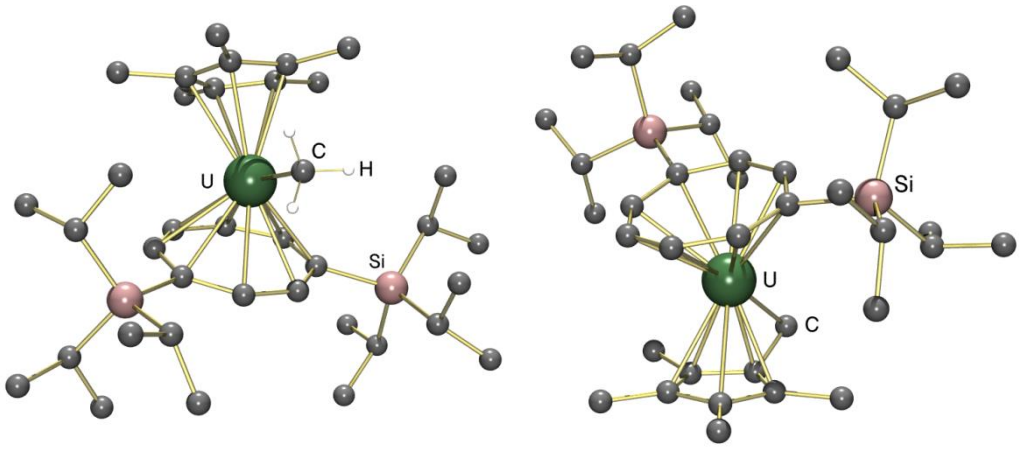


**(a)** **(b)**

**Figure 1.7 –** X-ray crystal structures of (**a**) [($^{TIPS2}$COT)(Cp*****)UMe] and 'tuck-in' complex (**b**) [($^{TIPS2}$COT)($C_5Me_4CH_2$)U].[155]

Additionally, Cloke and co-workers have employed the $^{(SiR3)2}$COT/Cp$^X$ ligand set to great advantage in the development of low-valent uranium chemistry and small

molecule activation. For example, reaction of [($^{TIPS2}$COT)(Cp**)U(THF)] with excess CO yielded exclusively the deltate ($C_3O_3^{2-}$) complex, [{($^{TIPS2}$COT)(Cp**)U}$_2$(μ-κ$^1$:κ$^2$-$C_3O_3$)],[141] as a result of reductive CO trimerization. By contrast, the marginally less sterically hindered Cp$^{Me4}$ analogue reacted with excess CO to form only the squarate ($C_4O_4^{2-}$) complex, [{($^{TIPS2}$COT)(Cp$^{Me4}$)U}$_2$(μ-κ$^2$:κ$^2$-$C_4O_4$)].[157] However, given the breadth of developments in this area, a more complete discussion of cyclooctatetraenide actinide systems is beyond the scope of this thesis.

### 1.6 – Neutral and Anionic Non-Carbocyclic Actinide Hydrocarbyl Complexes

In contrast to actinide alkyl complexes of carbocyclic supporting ligands, non-carbocyclic actinide hydrocarbyl complexes are significantly less well-developed. Prior to 2006, this field was dominated by bulky monodentate amido,[158,159] alkoxide,[58,160,161] and aryloxide[162,163] ligands, as well as amidinate,[164] tris(pyrazolyl)borate (Tp$^X$)[165] and triamidoamine (tren$^X$; {N(CH$_2$CH$_2$NR)$_3$}$^{3-}$)[166] ligands pioneered by Edelmann, Marquez/Santos/Takats, and Scott, respectively (Figure 1.8). Subsequently, the organoactinide chemistry of Tp$^X$, tren$^X$, and bis(iminophosphorane)methanediide (BIPM$^X$; {C(PPh$_2$NR)$_2$}$^{2-}$) ligands has been extended by the groups of Bart[63,167,168,169] and Liddle,[170-173] respectively, and new ligand designs have been implemented by the Leznoff,[60,67,174-176] Emslie,[40,64,177-180] Diaconescu,[49,181,182,183] Bart,[44,184] and Maria/Mazzanti[185] groups (Figure 1.9).

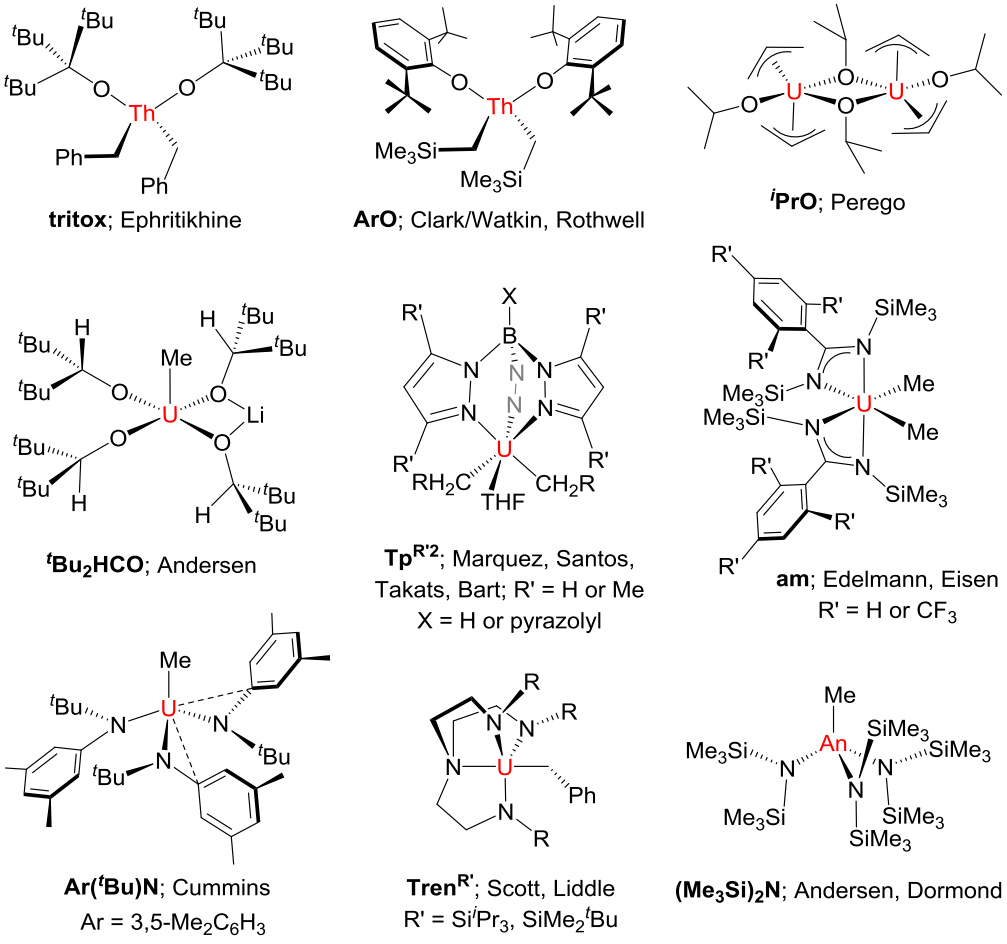


**Figure 1.8 –** Complexes featuring non-cyclopentadienyl supporting ligands applied in actinide hydrocarbyl chemistry prior to 2006 (An = Th or U; R is typically H, $SiMe_3$, $^t$Bu or Ph). Authors are those who have contributed to organoactinide chemistry, at any time, using each ligand framework.

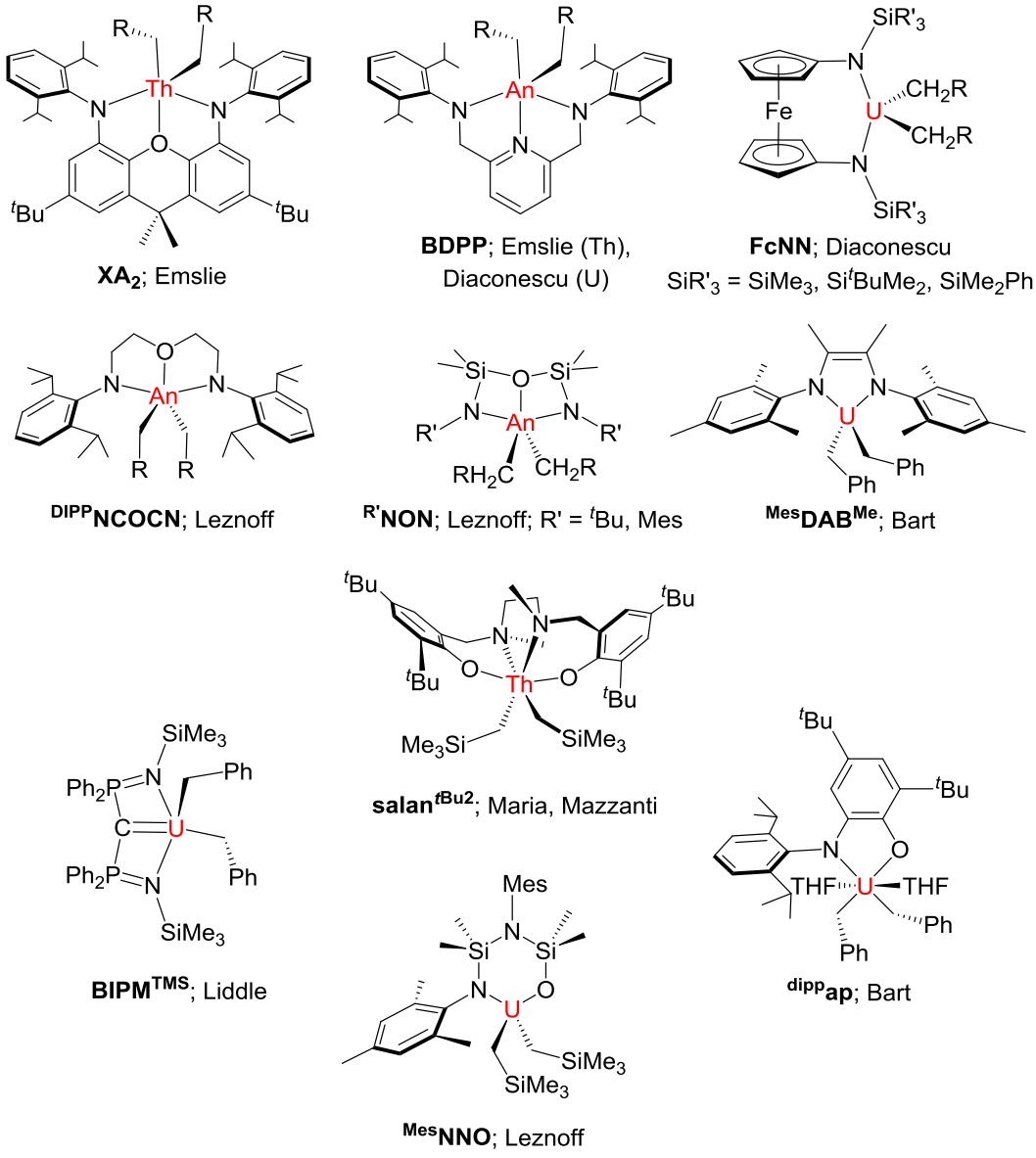


**Figure 1.9** – Complexes featuring non-cyclopentadienyl ancillary ligands deployed in actinide hydrocarbyl chemistry after 2006 (An = Th or U; R is typically H, $SiMe_3$, $^t$Bu or Ph). Authors are those who have contributed to organoactinide chemistry using each ligand framework.

Most non-carbocyclic organoactinide complexes were synthesized by salt metathesis using an RLi, RNa, $PhCH_2K$, or RMgBr reagent and an appropriate actinide halide precursor. However, $[\{U(allyl)_2(O^iPr)_2\}_2]$ was prepared by reaction of thermally unstable $[U(allyl)_4]$ with 2 equiv of $^i$PrOH, and related reactions with $^t$BuOH and EtOH were also described.[58] Along similar lines, $[(XA_2)Th(CH_2SiMe_3)_2]$, $[(BDPP)An(CH_2SiMe_3)_2]$ (An = Th, U), and $[(FcNN)U(CH_2R)_2]$ (R = Ph, $SiMe_3$, $^t$Bu) could be prepared by reaction of *in-situ*-generated polyalkyl actinide precursors with the appropriate proteo-ligand $H_2[L]$ (L = $XA_2$, BDPP, FcNN), presumably *via* alkane elimination (*vide supra*, Section 1.4.2).[40,49]

At present, many of the successfully employed ligand designs in actinide chemistry are based on the chelating diamido motif, which offers numerous desirable characteristics. Significant advantages of diamido ligand systems include: (a) bidentate coordination of hard, strongly π-donating amido donors, which are highly partial to actinide binding, (b) modular, economical, and straight-forward syntheses leading to ancillaries with appropriately sized binding pockets, (c) facile electronic- and steric tuning through variation of the amido substituents, and (d) access to tetravalent actinide species which feature two reactive co-ligands, a design scheme which mirrors that of the prominent bis(cyclopentadienyl) motif in complexes of the form $[Cp^X_2AnR_2]$.[186] Unique among the various diamido-based designs is the xanthene-based NON-donor ligand $XA_2$ developed by Emslie and co-workers[40,64,177,179,180,187]. In contrast to more flexible systems, the $XA_2$ platform boasts rigid construction, which has contributed to the high thermal-stability observed for various organothorium(IV) derivatives, including base-free

hydrocarbyl complexes (Figure 1.10), the first non-carbocyclic actinide alkyl cations, and a rare thorium dication (*vide infra*, Section 1.7.1).

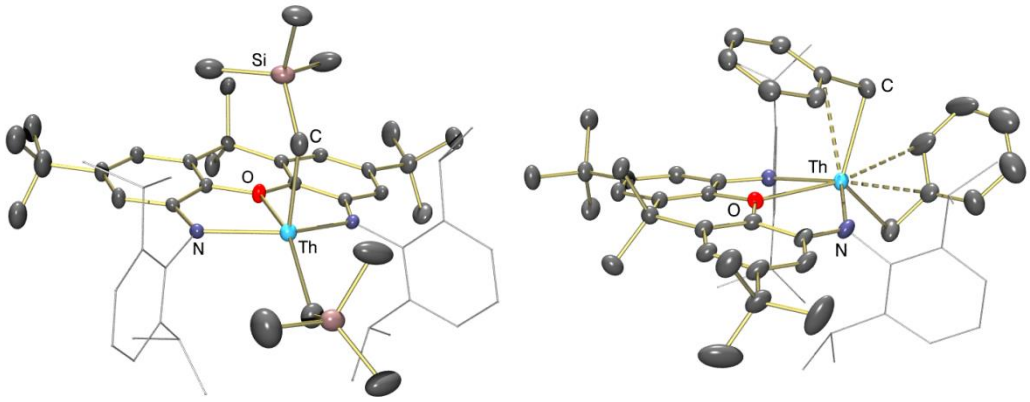


**(a)** **(b)**

**Figure 1.10 –** X-ray crystal structures of (**a**) [$(XA_2)Th(CH_2SiMe_3)_2$] and (**b**) [$(XA_2)Th(CH_2Ph)_2$], highlighting the rigid design of the $XA_2$ ancillary.[40,180]

A number of additional diamido ligand systems (depicted in Figure 1.11) developed by the groups of Cloke,[188] Emslie,[187] Leznoff,[175] Bart,[189] Ephritikhine,[190] and Gambarotta[15,191] have been employed primarily for the preparation of various actinide coordination compounds. Installation of these ancillaries is typically accomplished *via* salt metathesis of the respective $M_2[L]$ (M = Li or K) precursor with the appropriate actinide(IV) halide starting material. However, the $^{TMS}$NN ligand in [($^{TMS}$NN)UI{$N(SiMe_3)_2$}] was formed *in-situ via* oxidative C–C coupling when the bis(metallacycle) 'ate' precursor [Na{$(Me_3Si)_2N$}U{$\kappa^2$*CN*-$CH_2SiMe_2NSiMe_3$}$_2$] was treated with one equiv of $I_2$.[190]

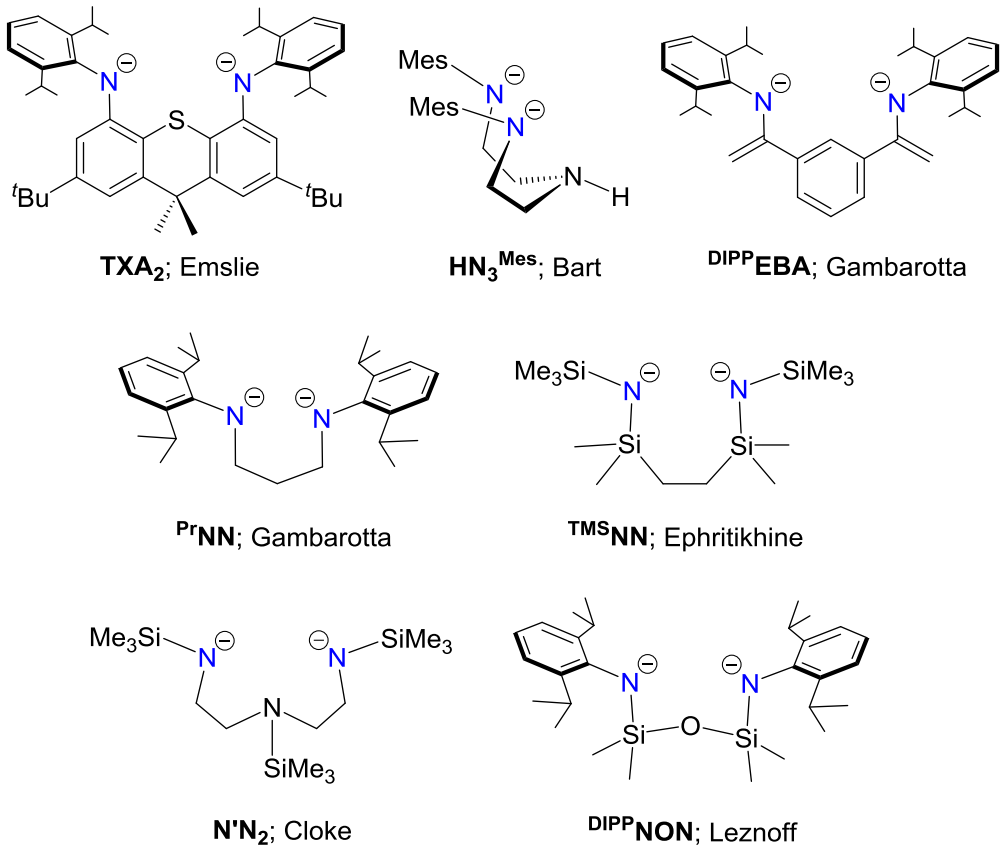


**Figure 1.11** – Diamido ligands employed primarily for the support of actinide coordination complexes. Authors are those who have contributed to actinide chemistry using each ligand framework.

Although the majority of actinide coordination compounds supported by the aforementioned diamido ancillaries are simple halide-, cyano-, Lewis base-stabilized- and bis-ligand complexes, interesting reactivity has been occasionally observed. For example, attempted reduction of the thorium(IV) bis-ligand 'ate' complex $[(^{Pr}NN)_2ThCl]^-$ with K(naphthalenide) resulted in C–H activation of an isopropyl methyl substituent, yielding the cyclometalated 'ate' complex $[(^{Pr}NN)Th(^{Pr}NN^*)]^-$ ($^{Pr}NN^*$ = $\kappa^3$*NNC*-{(Dipp)N(CH$_2$)$_3$N(2-$^i$Pr-6-CH(Me)(CH$_2$)-C$_6$H$_3$)}$^{3-}$).[15] Additionally, Bart's diamidoamine

chloro complex [($HN_3^{Mes}$)U(Cp**)Cl] was not amenable to alkylation with $^{n}$BuLi; instead, deprotonation of the pendant amine proceeded, yielding the salt-occluded triamido complex [($N_3^{Mes}$)U(Cp**)(μ-Cl){Li(THF)$_2$}].[189] A range of bis(pyrrolyl) ligands[192,193] have also been utilized to develop the chemistry of thorium and uranium, however, discussion of such species is beyond the scope of this thesis.

Beyond traditional routes, ancillary ligand installation in organoactinide chemistry has also been achieved through redox reactivity. In particular, [($^{Mes}$DAB$^{Me}$)U(CH$_2$Ph)$_2$] and [($^{dipp}$ap)U(CH$_2$Ph)$_2$(THF)$_2$] were prepared by Bart and co-workers *via* reaction of [U(CH$_2$Ph)$_4$] with a neutral redox-active α-diimine ($^{Mes}$DAB$^{Me}$)[44] or iminoquinone ($^{dipp}$ap)[184] ligand. In the former case, this reaction occurs via a concerted reductive elimination mechanism, since reaction with a 1:1 mixture of [U(CH$_2$C$_6$H$_5$)$_4$] and [U(CD$_2$C$_6$D$_5$)$_4$] yielded only $C_{14}H_{14}$ and $C_{14}D_{14}$. In the latter case, reaction of the iminoquinone with a 1:1 mixture of [U(CH$_2$C$_6$H$_5$)$_4$] and [U(CD$_2$C$_6$D$_5$)$_4$] generated 50 % of $C_{14}H_7D_7$, supporting a radical mechanism involving homolytic cleavage. This reaction was hypothesized to take place by initial coordination of the iminoquinone ligand with concurrent benzyl radical extrusion to yield a uranium(IV) iminosemiquinone intermediate, [LU(CH$_2$Ph)$_3$], followed by ejection of a second benzyl radical to form the 2-amidophenoxide product, [LU(CH$_2$Ph)$_2$(THF)$_2$] (L = $^{dipp}$ap; Scheme 1.4). The proposed [LU(CH$_2$Ph)$_3$] iminosemiquinone intermediate is considered to be viable based on the accessibility of [LUI$_3$(THF)$_2$]; an iminosemiquinone complex of uranium(IV) which reacts with 3 equiv of KCH$_2$Ph to form the same [LU(CH$_2$Ph)$_2$(THF)$_2$] product (Scheme 1.4).

**Scheme 1.4 –** Benzyl radical extrusion reactions to generate [($^{dipp}$ap)U($CH_2Ph$)$_2$(THF)$_2$].

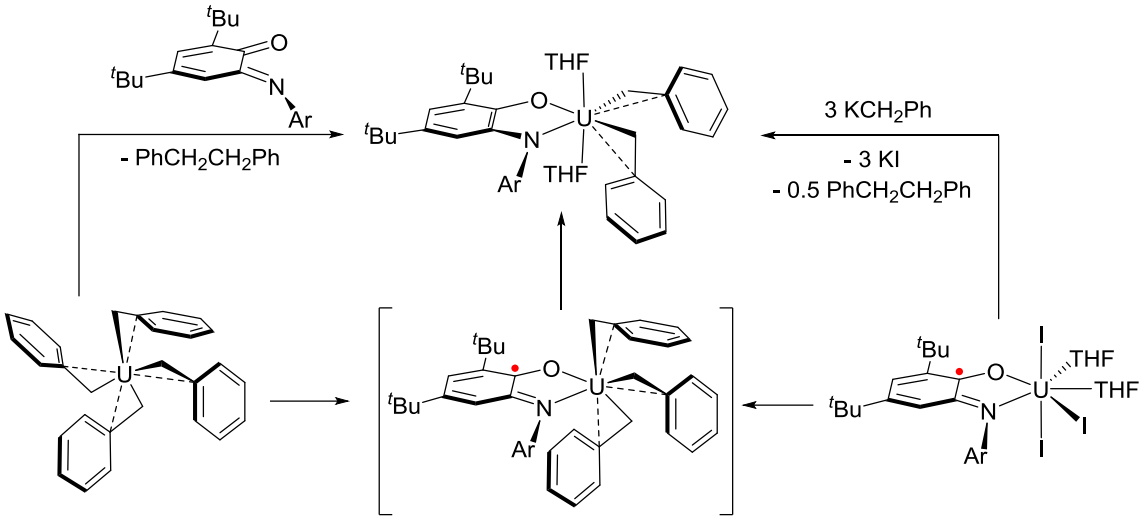


Significant differences in the chemistry of thorium and uranium analogues are often observed in non-carbocyclic organoactinide chemistry; a prime example of such divergent reactivity is highlighted by the reactions of [(tren$^{TIPS}$)AnI] (TIPS = Si$^i$Pr$_3$) with $KCH_2Ph$ reported by Liddle and co-workers (Scheme 1.5).[171] In the case of thorium, this reaction yields [(tren$^{TIPS}$)Th($CH_2Ph$)], which undergoes cyclometalation upon heating to 80 °C to afford [(tren$^{TIPS\text{-}H}$)Th] (tren$^{TIPS\text{-}H}$ = $\kappa^5N_4C$-{N($CH_2CH_2NSi^iPr_3$)$_2$$CH_2CH_2NSi^iPr_2CH(Me)CH_2$}$^{4-}$). By contrast, the reaction of [(tren$^{TIPS}$)UI] with $KCH_2Ph$ proceeds directly to [(tren$^{TIPS\text{-}H}$)U] and a benzyl intermediate was not observed, even when the reaction was monitored at –80 °C. This reactivity difference was shown computationally to derive from stabilization of the σ-bond metathesis transition state in the uranium complex by 5f-orbital participation in the interatom interactions.[171]

**Scheme 1.5 –** Cyclometalation of the thorium(IV) and uranium(IV) [(tren$^{TIPS}$)An(CH$_2$Ph)] complexes.[171]

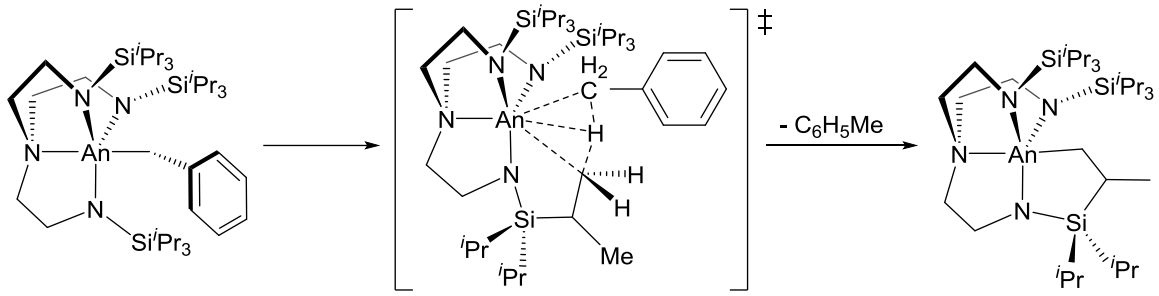


Rapid cyclometalation was also observed by Liddle and co-workers in the reaction of less sterically-encumbered [(tren$^{TMS}$)UI(THF)] (TMS = SiMe$_3$) with KCH$_2$Ph, but in this case, a dimetallic 'tuck-in' 'tuck-over' complex, [U$_2$(tren$^{TMS-2H}$)(tren$^{TMS}$)] was formed, containing one doubly-cyclometalated ligand (tren$^{TMS-2H}$) and one intact tren$^{TMS}$ ligand.[172] Furthermore, subsequent reaction with [Et$_3$NH][BPh$_4$] in THF did not yield [(tren$^{TMS}$)U(THF)$_x$][BPh$_4$], but instead resulted in double de-arylation of the BPh$_4$ anion to afford a product containing an NR-SiMe$_2$-CH-BPh$_2$ linkage (Scheme 1.6).[172]

**Scheme 1.6 –** Reaction of [(tren$^{TMS}$)UI(THF)] (TMS = $SiMe_3$) with $KCH_2Ph$ to form dimetallic [$U_2$(tren$^{TMS-2H}$)(tren$^{TMS}$)] containing one doubly-cyclometalated tren$^{TMS-2H}$ ligand and one intact tren$^{TMS}$ ligand, and subsequent reaction with [$Et_3NH$][$BPh_4$].

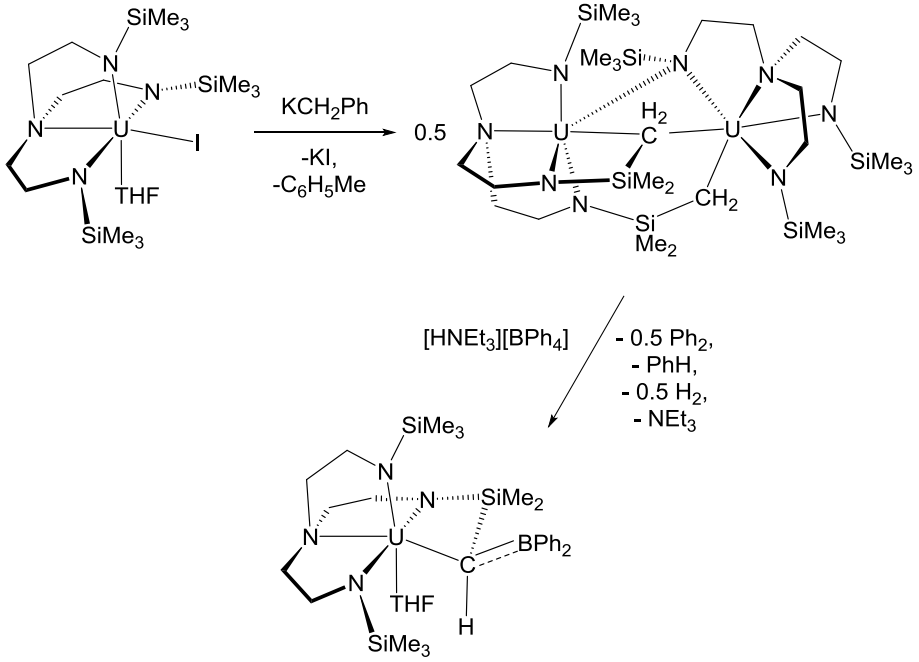


Many other reactions of non-carbocyclic actinide alkyl complexes involve σ-bond metathesis (e.g. with $H_2$, terminal alkynes, pyridines, acetone, amines, alcohols and thiols) or 1,2–insertion (e.g. with $CO_2$, ketones or azides). However, in the chemistry of uranium, especially uranium(III), redox reactions with azides and related oxidants must also be considered. For example, reaction of Bart and co-workers' scorpionate complex [Tp′U($CH_2Ph$)$_2$(THF)] with 1 equiv of $MesN_3$ afforded the uranium(IV) product [Tp′U(=NMes)($CH_2Ph$)(THF)] and 0.5 $PhCH_2CH_2Ph$, while reaction with a second equiv of $MesN_3$ generated the insertion product, [Tp′U(=NMes)($MesN_3CH_2Ph$)(THF)] (Scheme 1.7).[168]

**Scheme 1.7 –** Stepwise reaction of [Tp′U($CH_2Ph$)$_2$(THF)] with 2 equiv of $MesN_3$.

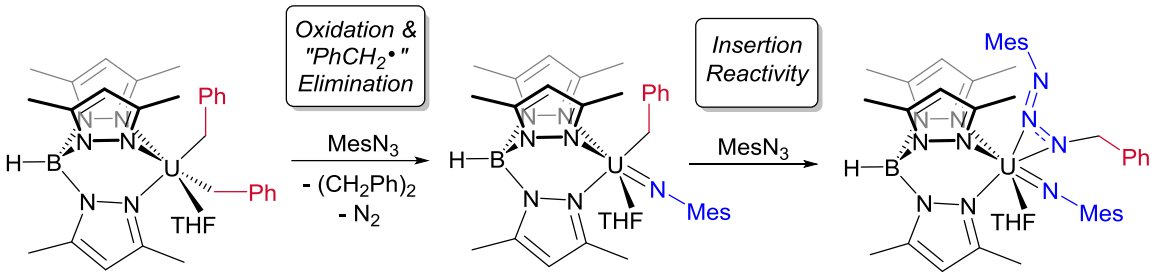


A further area of non-carbocyclic organoactinide chemistry which has been explored fairly extensively is the reactivity of [(FcNN)U($CH_2Ph$)$_2$] with heterocycles including pyridine, 2-picoline *N*-methylimidazole, *N*-methylbenzimidazole, benzoxazole, benzothiazole, and quinoline by Diaconescu and co-workers.[181,194] These reactions gave rise to a range of products in good yields, in several cases *via* multistep mechanisms involving alkyl transfer, C–C coupling, double C–H bond activation, and/or ring opening (Scheme 1.8).[181,194]

**Scheme 1.8 –** Reactions of [(FcNN)U($CH_2Ph$)$_2$] with: (a) pyridine or 2-picoline followed by benzoxazole or benzothiazole, (b) *N*-methylimidazole (3 equiv) followed by heating, (c) *N*-methylbenzimidazole (3 equiv), and (d) *N*-methylbenzimidazole (1 equiv) followed by benzoxazole or quinoline.

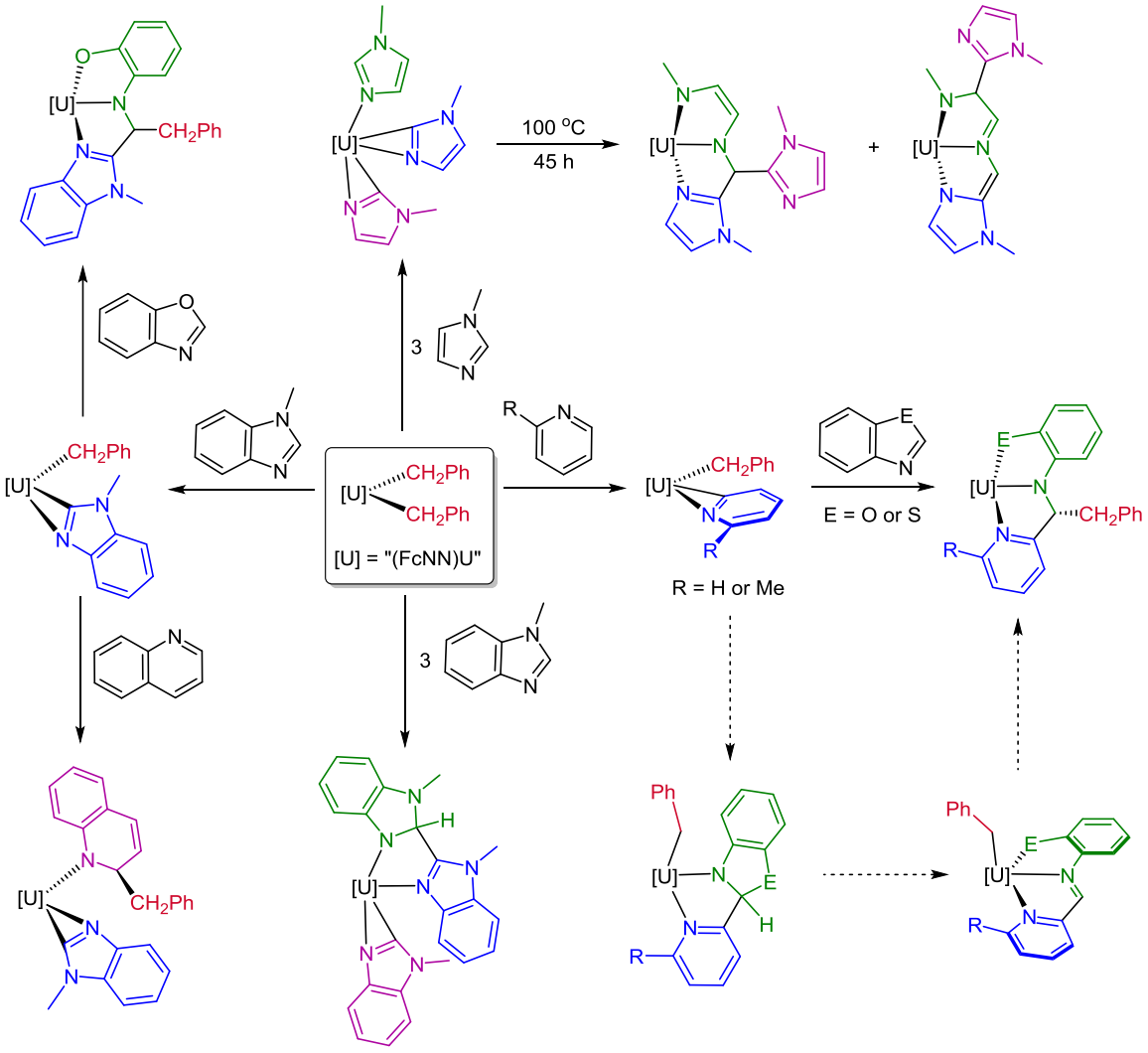

## 1.7 – Cationic Actinide Alkyl and Related Complexes, and Ethylene Polymerization

### 1.7.1 – Cationic Actinide Alkyl and Related Complexes

Cationic group 4 transition metal alkyl complexes are widely employed as olefin polymerization catalysts, and f-element alkyl cations are also of interest for this purpose. However, for the actinide elements, cationic alkyl species are rare. In cyclopentadienyl chemistry, the only base-free and mononuclear examples of actinide alkyl cations were reported by Marks and co-workers, and are of the form $[Cp^*_2ThR][A]$ (R = Me,[195-201] $CH_2SiMe_3$,[198] $CH_2Ph$,[199] allyl[195] and H[198]; [A] = weakly-coordinating borate anion such as $[BPh_4]^-$, $[B(C_6F_5)_4]^-$, or $[MeB(C_{12}F_9)_3]^-$, or a carborane-based anion $[M(B_9C_2H_{11})_2]^{x-}$ (M = Co, $x$ = 1; M = Fe, $x$ = 2) (Figure 1.12). Cationic alkyl complexes featuring specifically engineered counter-anions are of interest due to the ability of the anion to strongly influence polymerization activity, thermal stability, and polymer characteristics through interactions with the cationic metal centre, and to modify solubility and crystallinity.[201]

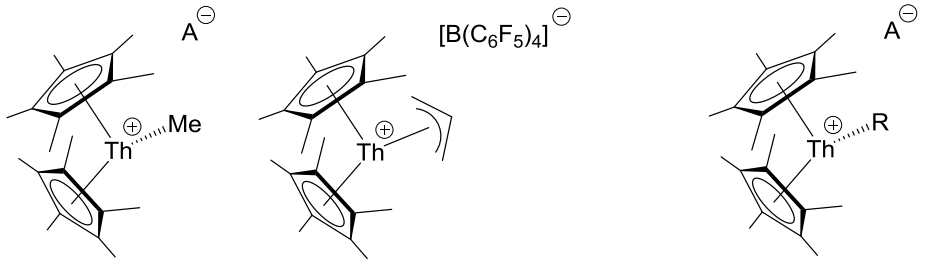


A = $MeB(C_{12}F_9)_3$, $BPh_4$, $B(C_6F_5)_4$, $B(C_6F_4TBS)_4$, $B(C_6F_4TIPS)_4$, $[^tBuCH_2CH\{B(C_6F_5)_2\}_2H]$, $[Co(B_9C_2H_{11})_2]$, 0.5 $[Fe(B_9C_2H_{11})_2]$

R = $CH_2SiMe_3$, A = $[Co(B_9C_2H_{11})_2]$
R = H, A = $[Co(B_9C_2H_{11})_2]$
R = $CH_2Ph$, A = $B(C_6F_5)_4$

**Figure 1.12 –** Base-free cyclopentadienyl actinide alkyl cations.

A number of non-cyclopentadienyl alkyl cations have also been reported by Emslie and co-workers.[179,180] Reaction of neutral $[(XA_2)Th(CH_2SiMe_3)_2]$ or $[(XA_2)Th(CH_2Ph)_2]$ with $[Ph_3C][B(C_6F_5)_4]$ ($XA_2$ = dianionic NON-donor ligand 4,5-bis(2,6-diisopropylanilido)-2,7-di-*tert*-butyl-9,9-dimethylxanthene) in benzene or toluene at room temperature yielded $[(XA_2)Th(CH_2SiMe_3)(\eta^6\text{-}C_6H_5R)][B(C_6F_5)_4]$ (R = H or Me) and $[(XA_2)Th(\eta^2\text{-}CH_2Ph)(\eta^6\text{-}C_6H_5Me)][B(C_6F_5)_4]$, respectively; rare examples of arene solvent-separated ion-pairs (Scheme 1.9). In $[(XA_2)Th(CH_2SiMe_3)(\eta^6\text{-}C_6H_6)]^+$, the arene is $\eta^6$-coordinated in the solid state (Th–$C_{arene}$ (ave.) = 3.26 Å; Figure 1.13), whereas in $[(XA_2)Th(CH_2Ph)(\eta^6\text{-}C_6H_5Me)]^+$, two Th–$C_{arene}$ distances are similar to those in the benzene complex (3.21, 3.28 Å), two are shorter (3.06, 3.09 Å), and two are longer (3.37, 3.44 Å) (Figure 1.13). For $[(XA_2)Th(CH_2SiMe_3)(\eta^x\text{-}C_6H_5Me)]^+$, bromobenzene-$d_5$ does not displace toluene from the metal centre to any observable extent, and coordinated- and free toluene only undergo slow exchange on the NMR timescale at room temperature.[179]

The reactions of $[(XA_2)Th(CH_2SiMe_3)_2]$ and $[(XA_2)Th(CH_2Ph)_2]$ with sub-stoichiometric amounts of $[Ph_3C][B(C_6F_5)_4]$ provided no evidence for dinuclear monocation formation. By contrast, reaction of $[(BDPP)Th(CH_2Ph)_2]$ (BDPP = 2,6-bis(2,6-diisopropylanilidomethyl)pyridine) with 0.5 equiv of $[Ph_3C][B(C_6F_5)_4]$ precipitated an insoluble oil containing the dinuclear cation, $[(BDPP)Th(\eta^2\text{-}CH_2Ph)(\mu\text{-}\eta^1{:}\eta^6\text{-}CH_2Ph)Th(\eta^1\text{-}CH_2Ph)(BDPP)][B(C_6F_5)_4]$ in which a benzyl group adopts a previously unknown $\mu\text{-}\eta^1{:}\eta^6$-bridging mode.[179] This compound is effectively composed of a "$[(BDPP)Th(CH_2Ph)]^+$" cation that is π-coordinated (Th–$C_{arene}$ (ave.) = 3.13 Å) to the

phenyl ring of a benzyl group provided by the dibenzyl starting material (Scheme 1.9; Figure 1.13).

Reaction of $[(XA_2)Th(CH_2Ph)_2]$ with $B(C_6F_5)_3$ afforded $[(XA_2)Th(\eta^1\text{-}CH_2Ph)][\eta^6\text{-}PhCH_2B(C_6F_5)_3]$ in which the benzylborate anion is $\eta^6$-coordinated to the metal centre, and addition of a second equiv of $B(C_6F_5)_3$ afforded dicationic $[(XA_2)Th][\eta^6\text{-}PhCH_2B(C_6F_5)_3]_2$ (Th–$C_{arene}$ (ave.) = 3.06-3.07 Å), in which both benzylborate anions are $\eta^6$-coordinated (Scheme 1.9; Figure 1.13).[180] The metal centre in all of the above $XA_2$ and BDPP complexes is π-coordinated, either to neutral arene solvent, a benzyl group in $[(BDPP)Th(CH_2Ph)_2]$, or a benzyl group in a $[PhCH_2B(C_6F_5)_3]$ anion, highlighting a pronounced tendency for these systems to engage in arene π-coordination.

**Scheme 1.9 –** Synthesis of non-cyclopentadienyl actinide alkyl cations free from external ether or amine Lewis base coordination.

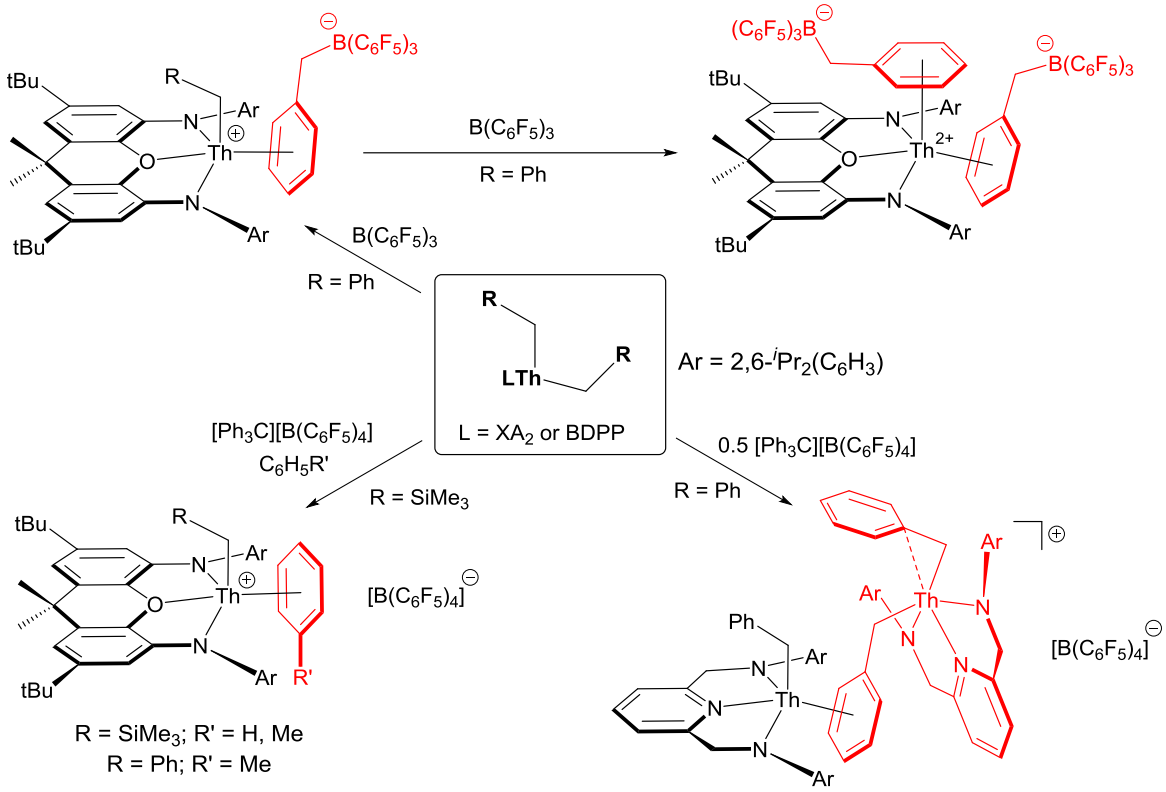

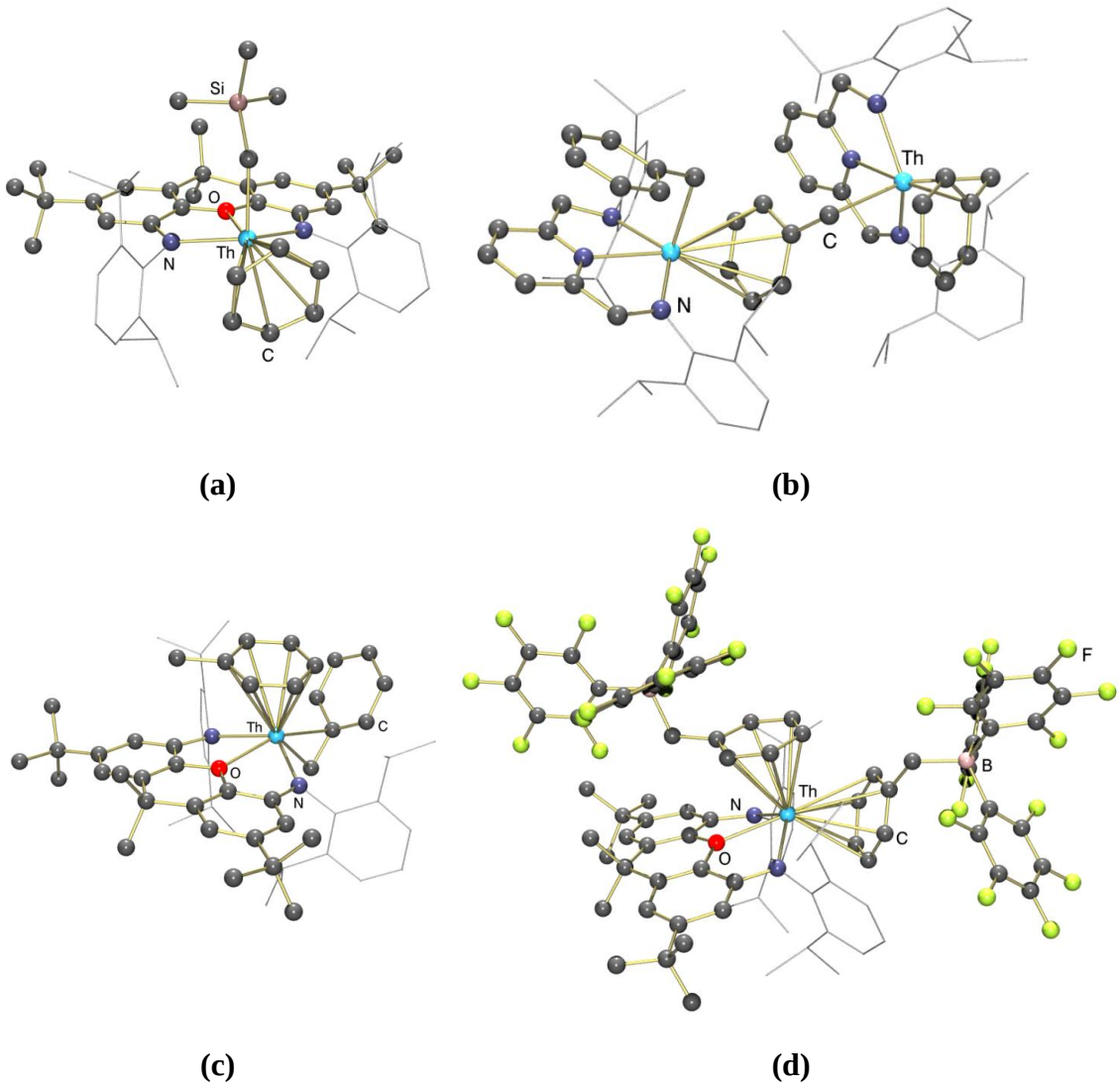


**Figure 1.13** – X-ray crystal structures of the cationic portions of (**a**) $[(XA_2)Th(CH_2SiMe_3)(\eta^6\text{-}C_6H_6)][B(C_6F_5)_4]$, (**b**) $[(BDPP)Th(CH_2Ph)(\mu\text{-}\eta^1\text{:}\eta^6\text{-}CH_2Ph)Th(CH_2Ph)(BDPP)][B(C_6F_5)_4]$, (**c**) $[(XA_2)Th(CH_2Ph)(\eta^6\text{-}C_6H_5Me)][B(C_6F_5)_4]$, and (**d**) $[(XA_2)Th][\eta^6\text{-}PhCH_2B(C_6F_5)_3]_2$.

Lewis base-stabilized actinide alkyl cations are also known, including $[Cp^*_2ThMe(L)_x]^+$ (L = THF, $NMe_3$, or $NEt_3$; $x$ = 1–2),[197,200] $[Cp^*_2UMe(THF)][MeBPh_3]$,[202] and $[(FcNN)U(CH_2Ph)(OEt_2)][BPh_4]$[183] (Figure 1.14).

Additionally, Marks and co-workers reported that the dimetallic species [{Cp*$_2$ThMe}$_2$(μ-Me)][B(C$_6$F$_5$)$_4$] (a contact ion-pair featuring a neutral dimethyl precursor coordinated to a cationic [Cp*$_2$ThMe]$^+$ fragment *via* a bridging methyl group) exists in equilibrium with neutral [Cp*$_2$ThMe$_2$] and cationic [Cp*$_2$ThMe][B(C$_6$F$_5$)$_4$] in solution.[195,199] This dimetallic complex bears similarity to the 'pseudo-cationic' uranium alkyl species [Cp*$_2$UMe(μ-Me){Al$_3$Me$_6$(μ$_3$-CH$_2$)(μ$_2$-CH$_3$)}] reported by Evans and co-workers,[203] which may be viewed as a contact ion-pair comprised of a trimetallic organoaluminum anion and a cationic [Cp*$_2$UMe]$^+$ fragment.

Beyond alkyl species, actinide aryl and alkynyl cations are also known, including [Cp*$_2$Th(κ$^2$-*CN*-C$_6$H$_4$CH$_2$NMe$_2$-*o*)][BPh$_4$], accessed *via* protonation of the aryl/methyl precursor [Cp*$_2$ThMe(κ$^2$-*CN*-C$_6$H$_4$CH$_2$NMe$_2$-*o*)] with [Et$_3$NH][BPh$_4$],[200] and Eisen's [(Et$_2$N)$_2$U(η$^1$-C$_2$$^t$Bu)(η$^2$-HC$_2$$^t$Bu)][BPh$_4$], which was generated *in-situ via* the reaction between [(Et$_2$N)$_3$U][BPh$_4$] and two equiv of *tert*-butylacetylene (Figure 1.14).[204] In addition, actinide borohydride cations have been reported by the groups of Ephritikhine, Arnold, and Love; the cyclooctatetraenide cation [(COT)U(BH$_4$)(THF)$_2$][BPh$_4$] was accessed *via* protonolysis of [(COT)U(BH$_4$)$_2$(THF)] with [Et$_3$NH][BPh$_4$],[205] and [(η$^5$:κ$^1$-C$_5$Me$_4$-*o*-pyridyl)$_2$U(BH$_4$)][BPh$_4$] was generated from [(η$^5$:κ$^1$-C$_5$Me$_4$-*o*-pyridyl)U(BH$_4$)$_2$] through analogous reactivity (Figure 1.14).[206] By contrast, [(calix)U(BH$_4$)][B(C$_6$F$_5$)$_4$] was prepared by oxidation of the uranium(III) borohydride complex, [(calix)U(BH$_4$)] (calix = *trans*-calix[2]benzene[2]pyrrolyl), with [CPh$_3$][B(C$_6$F$_5$)$_4$], and this reactivity resulted in a change in calix coordination mode, from κ$^1$*N*-coordination of the pyrrolyl anions and η$^6$-coordination of the arenes (U–C$_{arene}$ (ave.) = 2.94 Å) in the uranium(III) precursor, to η$^5$-

coordination of the pyrrolyl anions and $\eta^1$-coordination of the arenes in the uranium(IV) cation (U–$C_{ipso}$ = 2.74 Å).[193]

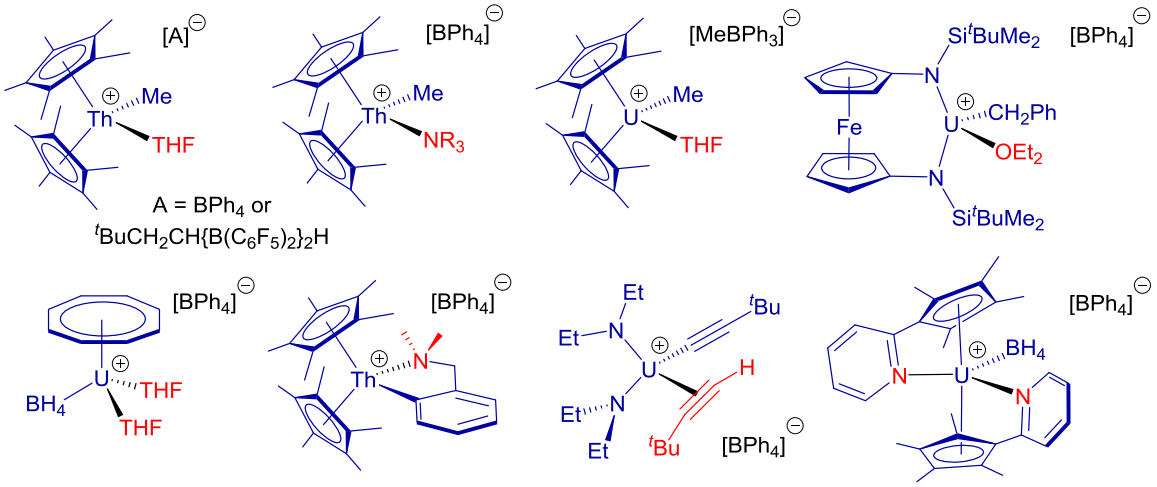


**Figure 1.14 –** Actinide alkyl cations stabilized by Lewis base coordination, and actinide alkynyl or borohydride cations.

### 1.7.2 – Actinide-Catalyzed Ethylene Polymerization

Despite considerable academic and potential industrial interest, ethylene insertion-polymerization catalysis remains an underdeveloped capability of actinides. Early efforts by Marks and co-workers revealed that [Cp*$_2$UCl] is a potent catalyst for ethylene polymerization,[207] and although further details were not disclosed, the group later rigorously explored the use of cationic thorium(IV) metallocene species of the form [Cp*$_2$ThMe][A] (A = weakly-coordinating anion) as well-defined single-site catalysts for the polymerization of ethylene.[197,199,200] While [Cp*$_2$ThMe][BPh$_4$] was found to be a fairly active catalyst (activity = 1.1 × $10^3$ g of polyethylene·(mol of Th)$^{-1}$·h$^{-1}$·atm$^{-1}$),

thorough anion-engineering efforts of Marks and co-workers led to catalysts of remarkably improved activity. By replacing the tetraphenylborate anion with polyfluorinated $[B(C_6F_5)_4]^-$ and $[^tBuCH_2CH\{B(C_6F_5)_2\}_2H]^-$ anions, the authors were able to reduce cation–anion interactions, affording the metallocene greater cationic character. The resulting species $[Cp^*_2ThMe][B(C_6F_5)_4]$ and $[Cp^*_2ThMe][^tBuCH_2CH\{B(C_6F_5)_2\}_2H]$ demonstrate impressive ethylene polymerization activities of $3.6 \times 10^6$ and $5.8 \times 10^6$ $g\cdot(mol\ of\ Th)^{-1}\cdot h^{-1}\cdot atm^{-1}$, respectively, three orders of magnitude more active than the original complex.[197] Marks and co-workers have additionally developed highly active heterogeneous olefin polymerization systems based on bis(metallocene) organoactinide complexes such as $[Cp^*_2AnMe_2]$ (An = Th, U) adsorbed onto porous metal oxides (e.g. partially dehydroxylated (PDA) or dehydroxylated (DA) γ-alumina), or $MgCl_2$.[208,209]

Given the lucrative nature of polymer science, numerous actinide-based systems that catalyze olefin polymerization have been patented; Marks and co-workers have developed ethylene polymerization technology utilizing cationic derivatives of the dimethyl precursors $[\{Me_2Si(ind)_2\}AnMe_2]$ and $[Cp^*_2AnMe_2]$ (An = Th or U),[210] and the Dow Chemical Company has developed actinide-based polymerization systems utilizing mixtures of the bis(metallocene) precursors $[Cp^*_2AnX_2]$ and $[Cp^*AnX_3]$ (An = Th, U; X = Cl, Me or $CH_2SiMe_3$) with various activating agents (e.g. MAO).[211]

Beyond the bis(metallocene) design, Clark and co-workers have explored the use of the low-coordinate half-sandwich species $[Cp^*Th(OAr)(CH_2SiMe_3)_2]$ (Ar = 2,6-$^tBu_2C_6H_3$) as a precursor for generating catalytically-active cationic derivatives.[110] Indeed, *in-situ* generated $[Cp^*Th(OAr)(CH_2SiMe_3)][B(C_6F_5)_4]$ serves as a fairly active

ethylene polymerization catalyst (activity = $3.46 \times 10^4$ g·(mol of Th)$^{-1}$·h$^{-1}$·atm$^{-1}$); the authors attributed the relatively modest catalytic activity of their cation to substantial π-donation to the thorium centre by the aryloxide ligand. Furthermore, Evans and co-workers reported that [Cp*$_3$U] also polymerizes ethylene, but additional details were not provided.[212]

By contrast, investigations of *post-metallocene* systems, complexes supported by non-carbocyclic ancillary ligands, that function as ethylene polymerization catalysts are rare, but in recent years exploration of this area has begun in earnest.

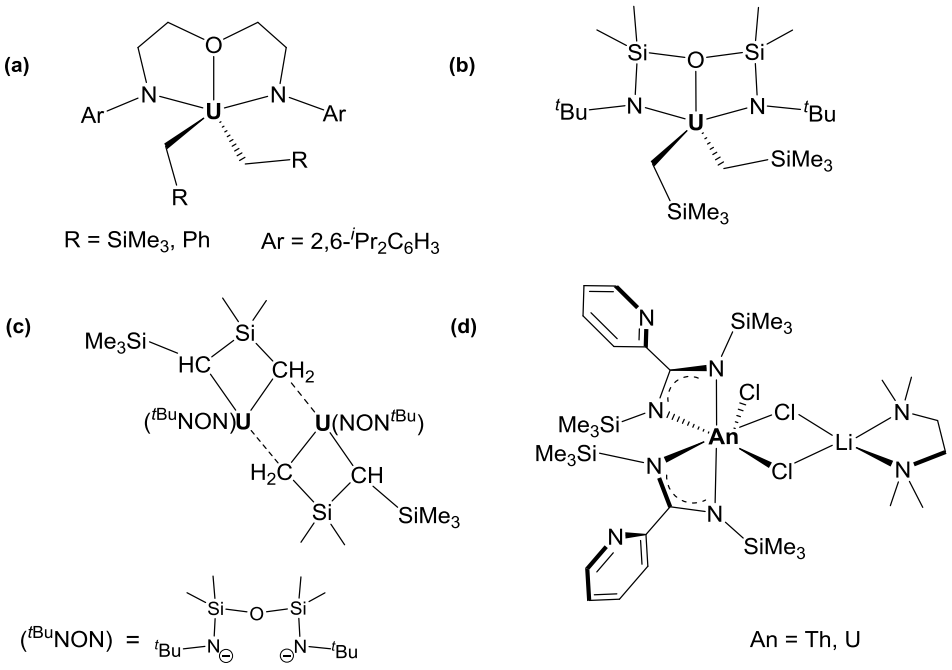


**Figure 1.15** – Post-metallocene actinide catalysts and procatalysts for ethylene polymerization. (**a**) [($^{DIPP}$NCOCN)U(CH$_2$R)$_2$] ($^{DIPP}$NCOCN = κ$^3$-{(ArNCH$_2$CH$_2$)$_2$O}$^{2-}$, Ar = 2,6-$^i$Pr$_2$C$_6$H$_3$; R = SiMe$_3$, Ph), (**b**) [($^{t\text{Bu}}$NON)U(CH$_2$SiMe$_3$)$_2$], (**c**) [($^{t\text{Bu}}$NON)U{CH(SiMe$_3$)(SiMe$_2$CH$_2$)}]$_2$ ($^{t\text{Bu}}$NON = {($^t$BuNSiMe$_2$)$_2$O}$^{2-}$), and (**d**) [(2-

pyridylamidinate)$_2$AnCl(μ-Cl)$_2$Li(tmeda)] (2-pyridylamidinate = {(Me$_3$SiN)$_2$C(2-py)}; An = Th, U).

Leznoff and co-workers reported a variety of neutral uranium(IV) dialkyl complexes[174] [($^{DIPP}$NCOCN)U(CH$_2$R)$_2$] ($^{DIPP}$NCOCN = κ$^3$-{(ArNCH$_2$CH$_2$)$_2$O}$^{2-}$, Ar = 2,6-$^i$Pr$_2$C$_6$H$_3$; R = SiMe$_3$, Ph), [($^{t\text{Bu}}$NON)U(CH$_2$SiMe$_3$)$_2$], and dimeric [($^{t\text{Bu}}$NON)U{CH(SiMe$_3$)(SiMe$_2$CH$_2$)}]$_2$ ($^{t\text{Bu}}$NON = {($^t$BuNSiMe$_2$)$_2$O}) (**a**–**c** in Figure 1.15), supported by flexible diamido pincer-type ligands that demonstrate modest ethylene polymerization activities (2.4 ×10$^1$ – 5.6 × 10$^2$ g·(mol of U)$^{-1}$·h$^{-1}$·atm$^{-1}$) in hexane solution. The authors noted a surprisingly substantial decrease in activity upon addition of activating agents such as B(C$_6$F$_5$)$_3$, Et$_2$AlCl, and modified methylaluminoxane (MMAO) (activities limited to <10$^2$ g·(mol of U)$^{-1}$·h$^{-1}$·atm$^{-1}$), and attributed the behaviour to tris(perfluorophenyl)alkylborate- or toluene solvent coordination to the presumably cationic species generated *in-situ*, but no cations were isolated or characterized spectroscopically.

More recently, Eisen and co-workers reported bis(amidinate) actinide(IV) chloro complexes of the form [(2-pyridylamidinate)$_2$AnCl(μ-Cl)$_2$Li(tmeda)] (2-pyridylamidinate = {(Me$_3$SiN)$_2$C(2-py)}; An = Th, U) (**d** in Figure 1.15),[213] that serve as precursors to ethylene polymerization catalysts. While solutions containing the thorium(IV) or uranium(IV) bis(amidinate) procatalyst and methylalumoxane (MAO) as an activator produced polyethylene with varying efficacy (activities ranging from 1.1 × 10$^2$ to 9.5 × 10$^3$ g·(mol of An)$^{-1}$·h$^{-1}$·atm$^{-1}$), the authors were able to significantly boost the activity by utilizing a mixture of [Ph$_3$C][B(C$_6$F$_5$)$_4$] and triisobutylaluminum (TIBA), reaching up to

$1.02 \times 10^4$ g of polyethylene·(mol of U)$^{-1}$·h$^{-1}$·atm$^{-1}$). However, the active cationic species were not isolated or investigated spectroscopically.

## 1.8 – Thesis Goals

Previously, research in the Emslie group demonstrated that the xanthene-based NON-donor ligand $XA_2$ is suitable for the support of thermally robust and highly reactive organothorium(IV) species, including cationic monoalkyl derivatives. However, persistent arene π-coordination rendered these thorium(IV) alkyl cations catalytically-inactive toward olefin polymerization, and furthermore, since thorium is largely confined to the tetravalent state, the opportunity to explore actinide redox chemistry is inherently restricted. The goals of this thesis were to: a) probe the ability of the $XA_2$ ligand to stabilize uranium in various oxidation states, b) prepare $XA_2$ uranium(IV) hydrocarbyl complexes and explore their reactivity profiles, c) generate cationic organouranium(IV) derivatives and investigate their catalytic activity for ethylene polymerization, and d) develop new sterically-modified $XA_2$ ligand analogues in order to probe the effect of ligand modifications on the structures and reactivity of thorium and/or uranium derivatives.

# Chapter 2

## $XA_2$ Uranium(III) and (IV) Chloro Complexes and Neutral Organometallic $XA_2$ Uranium(IV) Derivatives

Adapted from: Vidjayacoumar, B., Ilango, S., Ray, M. J., Chu, T., Kolpin, K. B., Andreychuk, N. R., Cruz, C. A., Emslie, D. J. H., Jenkins, H. A., and Britten, J. F. *Dalton Trans.*, **2012**, ***41***, 8175–8189 with permission from the Royal Society of Chemistry.

Adapted with permission from: Andreychuk, N. R., Ilango, S., Vidjayacoumar, B., Emslie, D. J. H., and Jenkins, H. A. *Organometallics* **2013**, *32*, 1466–1474 Copyright 2013 American Chemical Society.

### 2.1 – Introduction and Ligand Synthesis

Given the successful application of the rigid, dianionic NON-donor ligand $XA_2$ (4,5-bis(2,6-diisopropylanilido)-2,7-di-*tert*-butyl-9,9-dimethylxanthene) for the synthesis of both thermally robust and highly reactive thorium(IV) complexes,[40,179,180] we became interested in the synthesis of uranium complexes supported by this bis(amido)ether pincer-type ligand. (Figure 2.1).

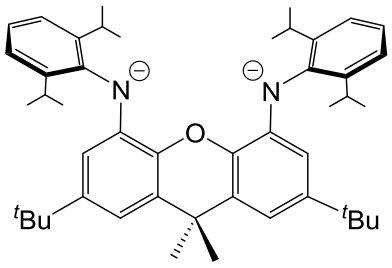


**Figure 2.1** – Structure of the $XA_2$ dianionic pincer-type ligand.

The NON-donor proligand, $H_2[XA_2]$, was synthesized by Hartwig–Buchwald coupling of 4,5-dibromo-2,7-di-*tert*-butyl-9,9-dimethylxanthene with 2,6-diisopropylaniline, and was obtained as a white crystalline solid upon recrystallization from ethanol/toluene (10:1) in 91% yield following the established procedure.[40,214] While 4,5-dibromo-2,7-di-*tert*-butyl-9,9-dimethylxanthene is commercially available, it can be more economically obtained *in-house* from xanthone on a 50 g scale *via* a protocol[§] modified from the original procedure[215] (Scheme 2.1).

**Scheme 2.1** – Synthesis of proligand $H_2[XA_2]$.

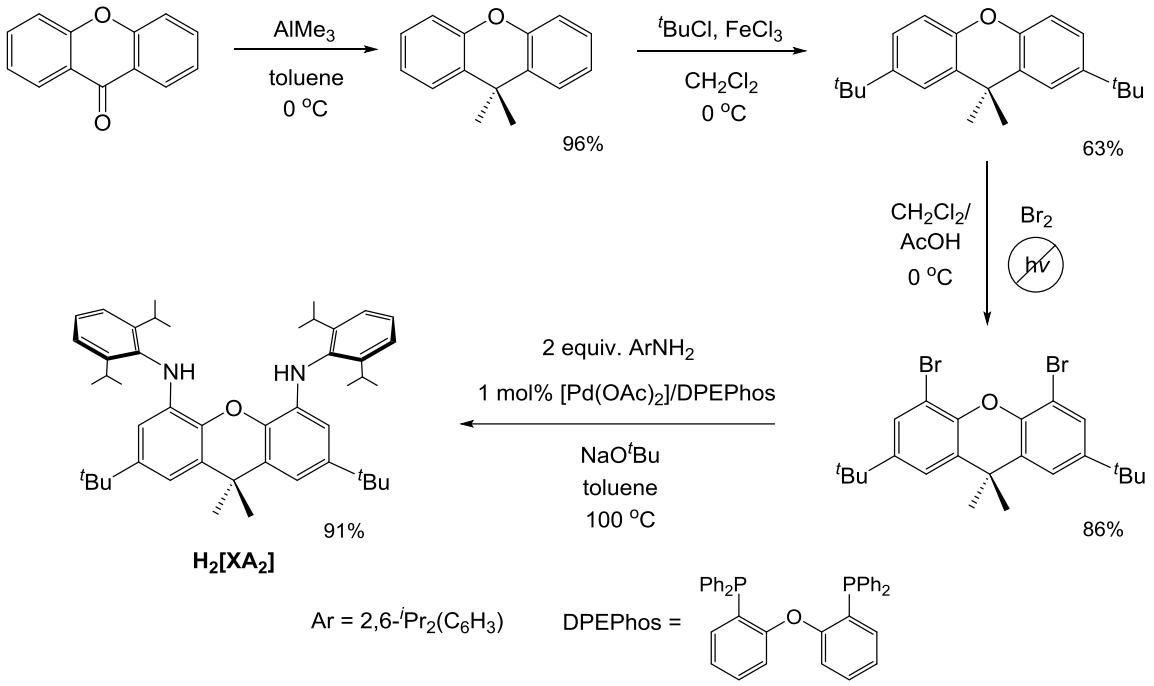


[§] 4,5-dibromo-2,7-di-*tert*-butyl-9,9-dimethylxanthene was prepared *via* a modified route developed *in-house*; $Br_2$ (4 equiv) was added drop-wise to a $CH_2Cl_2$/AcOH (180 mL total; 1:1) solution of 2,7-di-*tert*-butyl-9,9-dimethylxanthene (10 g) at 0 °C under $N_{2\,(g)}$ in the absence of light. The mixture stirred for 24 h, followed by aqueous workup and recrystallization from hot hexanes (1L).

Although $H_2[XA_2]$ is dried *in vacuo* at 85 °C for 24 h, the proligand was also subsequently treated with excess NaH to remove all traces of moisture and ethanol prior to use, given the high oxophilicity of the early actinides. Stirring proligand $H_2[XA_2]$ with excess KH in 1,2-dimethoxyethane (dme) at room temperature for 5 hours followed by filtration to remove unreacted KH, and evaporation to dryness afforded the base-stabilized bis(potassium) salt $[K_2(dme)_2(XA_2)]$ as an off-white solid in 81% yield.[40] However, $[K_2(dme)_x(XA_2)]$ was most conveniently generated and used *in situ*.

## 2.2 – $XA_2$ Uranium(IV) Chloro Complex

Reaction of *in-situ* generated $[K_2(dme)_x(XA_2)]$ with $UCl_4$ at room temperature afforded the tetravalent uranium complex $[(XA_2)UCl_2(\mu\text{-}Cl)\{K(dme)_3\}]$ (**1**), which was obtained as an orange solid in 75% yield upon crystallization from dme/hexanes at −30 °C (Scheme 2.2). Complex **1** was characterized by $^1H$ NMR spectroscopy, X-ray crystallography, elemental analysis, and cyclic voltammetry.[187]

**Scheme 2.2** – Synthesis of $XA_2$ uranium(IV) complex $[(XA_2)UCl_2(\mu\text{-}Cl)\{K(dme)_3\}]$ (**1**).

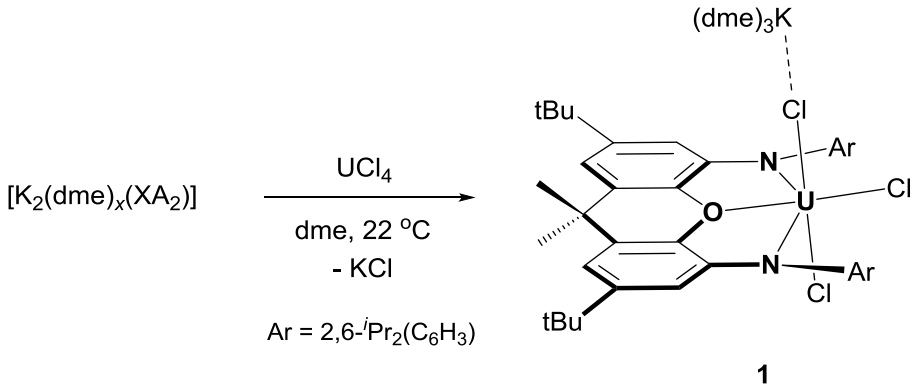


**1**

Alkali metal salt-occluded trichloro complex **1** is stable for months in the solid-state at −30 °C, and while highly soluble in ethereal solvents (*i.e.* THF, dme), **1** exhibits only partial solubility in aromatic solvents (*i.e.* benzene, toluene) and is insoluble in saturated hydrocarbons (*i.e.* hexanes, *n*-pentane). The room-temperature $^{1}$H NMR spectrum of **1** in THF-$d_8$ revealed nine paramagnetically shifted resonances located between +17 and −20 ppm, indicative of $C_{2v}$ symmetry; for example, a single C*H*Me$_2$ signal was observed at 16.08 ppm representing four protons.[§] Addition of Tl[B(C$_6$F$_5$)$_4$] to a solution of **1** in THF-$d_8$ resulted in immediate precipitation of a white solid (presumably TlCl) with no significant change in the $^{1}$H NMR spectrum, indicating that the $C_{2v}$ symmetry of **1** in THF is due to [K(THF)$_x$]Cl dissociation to form [(XA$_2$)UCl$_2$(THF)], with both chloro ligands in axial positions (cf. [(XA$_2$)ThCl$_2$(dme)]).[40]

[§] The $^{1}$H NMR spectrum of [(XA$_2$)UCl$_2$(μ-Cl){K(dme)$_3$}] (**1**) in C$_6$D$_6$ was also consistent with $C_{2v}$ symmetry.

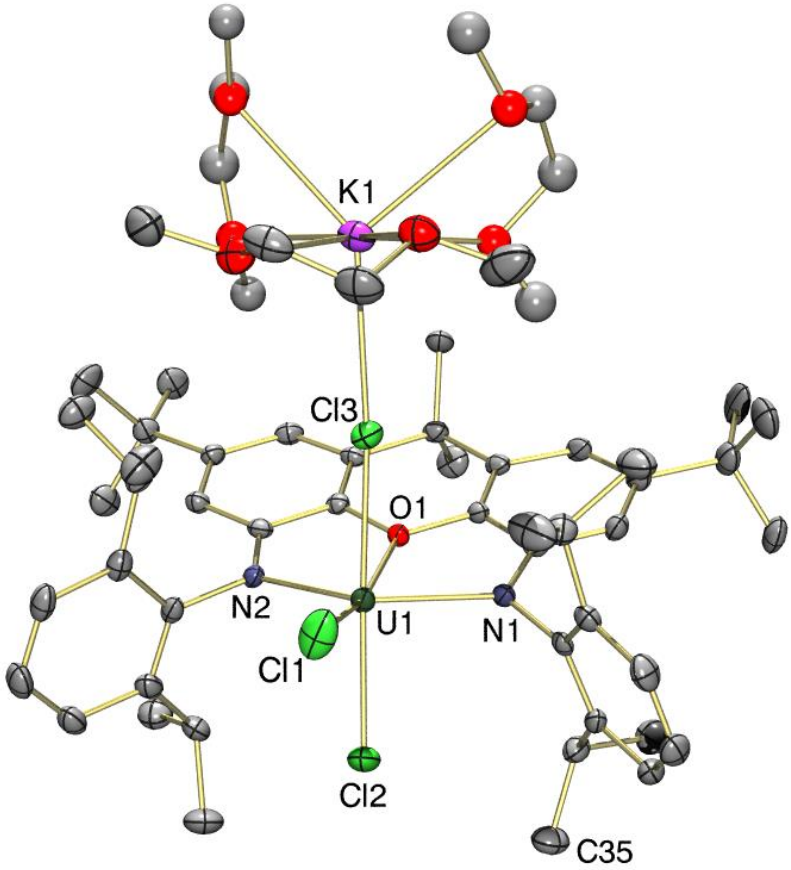


**Figure 2.2** – X-ray crystal structure of [(XA$_2$)UCl$_2$(μ-Cl){K(dme)$_3$}]·dme (**1**·dme), with thermal ellipsoids at 50% probability. Hydrogen atoms and dme lattice solvent are omitted for clarity. Two dme ligands are disordered and so were refined isotropically, and only one of the two orientations of each disordered dme ligand is shown.

In the solid state (Figure 2.2; Table 2.1), complex **1** is an approximately $C_s$-symmetric, six coordinate 'ate' complex with a K(dme)$_3^+$ counterion coordinated to Cl(3) (the K–Cl distance is 3.151(2) Å). The five anionic donors (N(1), N(2), and Cl(1)−Cl(3)) adopt a distorted trigonal-bipyramidal arrangement around the metal centre, with N(1)−U−N(2), N(1)−U−Cl(1), N(2)−U−Cl(1), and Cl(2)−U−Cl(3) angles of 129.1(1), 116.2(1), 114.6(1), and 177.07(6)°, respectively, and the neutral diarylether donor is

coordinated between the two amido groups roughly in the equatorial plane of the trigonal bipyramid. The N/$Cl_{eq}$/N-plane of the trigonal bipyramid in trichloro complex **1** is tilted relative to the plane of the $XA_2$ ligand, indicated by the relatively expanded 21.7° angle between the N/O/N- and N/Cl(1)/N-planes. The xanthene backbone of the meridionally-coordinated $\kappa^3$-$XA_2$ ligand is exceptionally planar (the angle between the two aryl rings of the xanthene backbone is 1.2°), and the uranium ion is located 0.344 Å above the NON-plane.

X-ray crystal structures containing M–(μ-Cl)–$K(dme)_3$ linkages have not previously been reported, although comparable K–Cl distances are observed in [{$\kappa^2$-$CH_2$(4-Me-6-$^t$Bu-$C_6H_2O$-2)$_2$}$_2$Th($\kappa^1$-dme)(μ-Cl)K(dme)$_2$] (3.127(2) Å),[216] [$Cp_3$Ho(μ-Cl)K(18-C-6)] (3.131 and 3.151 Å),[217] and [{$\kappa^3$-$C_6R_3O(CH_2C_6R_4O$-2)-2,6}Ta(μ-Cl)$_2$K(dme)$_2$}$_2$($OCH_2CH_2O$)] [3.166(3) and 3.196(3) Å].[218] As a result of $K(dme)_3^+$ coordination in **1**, U–Cl(3) is elongated to 2.672(1) Å, relative to U–Cl(1) and U–Cl(2) (2.619(1) and 2.597(1) Å, respectively). Longer U–Cl distances of 2.707(5), 2.700(5) Å (bridging) and 2.648(5) Å (terminal) were observed in related [($^{DIPP}$NCOCN)UCl(μ-Cl)$_2$Li(THF)$_2$] ($^{DIPP}$NCOCN = $\kappa^3$-{$(ArNCH_2CH_2)_2O$}$^{2-}$, Ar = 2,6-$^i$Pr$_2$$C_6H_3$),[60] perhaps due to closer approach of the amido donors in the latter more flexible NON-donor ligand; U–$N_{avg}$ is 2.19 Å vs. 2.30 Å in **1**. However, a wide range of U(IV)–$NR_2$ bond distances have been reported, for example 2.18(2)–2.19(2) Å in [($^{tBu}$NON)UI(μ-I)$_2$Li(THF)$_2$] ($^{tBu}$NON = $\kappa^3$-{$O(SiMe_2N^tBu)_2$}$^{2-}$),[60] 2.21(2)–2.35(2) Å in [$U(NPh_2)_4$],[219] 2.23(1) Å in [($\kappa^3$-Tp′)$UCl_2(NPh_2)$] (Tp′ = HB(3,5-$Me_2$pz)$_3$),[220] 2.29(1) Å in [$Cp_3U(NPh_2)$],[221] and 2.343(7)

and 2.411(3) Å in [(PNP)$UCl_3$(L)] (PNP = bis{2-(diisopropylphosphino)-4-methylphenyl}amido; L = THF or $OPPh_3$).[222]

The U–O distance in **1** is 2.465(3) Å, which is quite similar to the U–O dialkylether bond of 2.43(1) Å in [($^{DIPP}$NCOCN)UCl(μ-Cl)$_2$Li(THF)$_2$] (Ar = 2,6-$^{i}Pr_2C_6H_3$).[60] Electronically more comparable uranium diarylether complexes have not been structurally characterized, but U–OArMe distances in simple halide or acetylacetonate uranium(IV) complexes of *O*-dimethylated *para-tert*-butylcalix[4]arene are significantly longer at 2.60 to 2.64 Å.[223] The short U–O distance in **1** is likely a consequence of the rigidity of the xanthene backbone; for comparison, Th–$O_{diarylether}$ distances of 2.526(2)–2.535(4) Å were observed in related [($XA_2$)Th($CH_2R)_2$] (R = $SiMe_3$ (**3-Th**) and Ph (**5-Th**); *vide infra*) complexes.[40,180] These Th–O distances are comparable with the U–O distance in **1**, after taking into consideration the greater ionic radius of thorium(IV) relative to uranium(IV) (0.94 vs. 0.89 Å).[11]

**Table 2.1** – Selected bond lengths (Å) and angles (deg) for complexes **1** and **2**.

| Compound | **1** | **2** |
|---|---|---|
| U−$O_{xanthene}$ | 2.465(3) | 2.523(6) |
| U−N | 2.297(4), 2.306(4) | 2.340(8), 2.364(8) |
| U−Cl(1) *in-plane* | 2.619(1) | 2.689(3) (*apical*) |
| U−Cl(2) *apical* | 2.597(1) | n/a |
| U−Cl(3) *bridging* | 2.672(1) | n/a |
| U−$O_{dme}$ | n/a | 2.580(6), 2.655(7) |
| K−Cl | 3.151(2) | n/a |
| K−$O_{dme}$ | 2.55(1) – 3.10(1) | n/a |
| U···[NON plane] | 0.344 | 0.964 |
| Ligand Bend Angle[a] | 1.2° | 20.9° |

| | | |
|---|---|---|
| N(1)···N(2) | 4.16 | 4.03 |

[a] Ligand Bend Angle = The angle between the planes formed by each aromatic ring of the ligand backbone, where each plane is defined by the six carbon atoms of each aromatic ring within the xanthene backbone.

The cyclic voltammogram (CV) of **1** in THF/$[NBu_4][B(C_6F_5)_4]$[224] showed an irreversible reduction peak at $E_{pc}$ = −2.46 V vs $FeCp_2^{0/+1}$ ($\nu$ = 200 mV·s$^{-1}$) which gave rise to a product wave with $E_{1/2}$ = −1.83 V. The irreversibility of the primary redox process is likely due to rapid chloride loss from the uranium(III) redox product, although rapid reaction of the uranium(III) redox product with the $[NBu_4][B(C_6F_5)_4]$ base electrolyte (present in 100 fold excess) cannot be ruled out.[§] In keeping with the $^1$H NMR spectrum of **1** after treatment with $Tl[B(C_6F_5)_4]$ (*vide supra*), the CV of **1** was essentially unchanged after addition of 1 equiv of $Tl[B(C_6F_5)_4]$ to precipitate TlCl.[¶] The redox chemistry of **1** in THF is therefore attributed to $[(XA_2)UCl_2(THF)_x]$ rather than the $[(XA_2)UCl_3]^-$ anion, and this neutral uranium(IV) dichloride species appears to be reduced at a more negative potential than $[Cp^*_2UCl_2]$ ($Cp^* = C_5Me_5^-$) ($E_{1/2}$ = −1.85 V vs $FeCp_2^{0/+1}$) or $[(PNP)_2UCl_2]$ (PNP = bis{2-(diisopropylphosphino)-4-methylphenyl}amido) ($E_{1/2}$ = −2.19 V vs $FeCp_2^{0/+1}$).[222,225]

[§] We were unable to obtain a cyclic voltammogram for uranium(III) complex $[(XA_2)UCl(dme)]$ (**2**), perhaps due to rapid reaction with the 100-fold excess of $[NBu_4][B(C_6F_5)_4]$ base electrolyte.

[¶] The CV of complex **1** was also unchanged after addition of 10 equivalents of $[NBu_4]Cl$.

### 2.3 – $XA_2$ Uranium(III) Chloro Complex

Reaction of **1** with 1.1 equiv of potassium naphthalenide in dme, followed by centrifugation and crystallization from toluene/hexanes at −30 °C afforded the reduced uranium(III) complex [($XA_2$)UCl(dme)]·toluene (**2**·toluene) as an extremely air-sensitive dark green crystalline solid in 60% yield (Scheme 2.3).

**Scheme 2.3** – Synthesis of [($XA_2$)UCl(dme)] (**2**) *via* one-electron reduction of complex **1**.

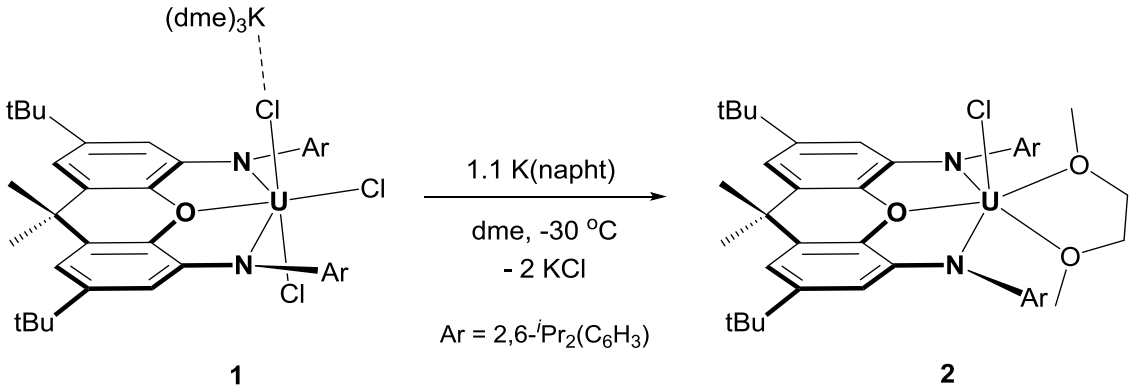


In the solid-state, uranium(III) complex **2**·4.5(toluene) adopts a distorted six-coordinate geometry, with a chloride ligand occupying an apical position and a dme molecule $\kappa^2$-coordinated to uranium roughly in the plane of the meridionally-bound $\kappa^3$-$XA_2$ ligand (Figure 2.3; Table 2.1). Unlike the uranium(IV) $XA_2$ precursor, **1**, complex **2** is free from occluded alkali metal salt, and features a xanthene backbone that is bent considerably away from planarity (the angle between the two aromatic rings of the xanthene backbone is 20.9° vs. 1.2° in **1**). The dme ligand in **2** is asymmetrically bound, with U–O distances of 2.580(6) and 2.655(7) Å, presumably due to a combination of steric crowding at the metal centre and weak U–$O_{dme}$ binding. Significant asymmetry in

dme binding was also reported for the seven-coordinate thorium(IV) complex [($XA_2$)$ThCl_2$(dme)] (Th–$O_{dme}$ = 2.673(8) and 2.728(8) Å)[40] and the uranium(III) calix[4]tetrapyrrole complex [(dme)U(μ-L)K(dme)] (L = {$CH_2(C_4H_2N)$}$_4$; $C_4H_2N$ = 2,5-disubstituted pyrrolide anion; U–O = 2.63(1) and 2.69(1) Å).[226]

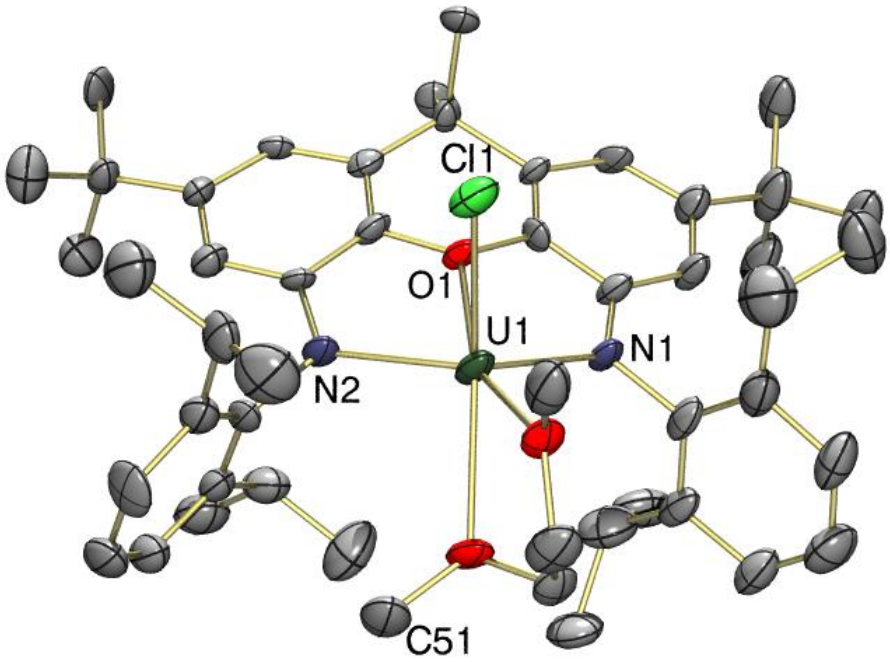


**Figure 2.3** – X-ray crystal structure of [($XA_2$)UCl(dme)]·4.5(toluene) (**2**·4.5(toluene)), with thermal ellipsoids at 40% probability. Hydrogen atoms and toluene solvent are omitted for clarity.

All uranium–$XA_2$ ligand bond lengths in **2** are 0.04–0.06 Å longer than those in complex **1**, consistent with the increased ionic radius of uranium(III) relative to uranium(IV) (for a coordination number of six: $U^{4+}$ = 0.89 Å and $U^{3+}$ = 1.03 Å).[11] At 2.689(3) Å, the U–Cl bond in **2** is also significantly longer than the U–$Cl_{terminal}$ bonds in **1** (2.597(1), 2.619(1) Å). Uranium–ligand bond elongation has previously been observed

for the uranium(III) compound in other uranium(III)/(IV) pairs, including $[Cp^{*}_{2}U(CN)_{3}]^{n-}$ ($n$ = 1 and 2),[124] $[(\kappa^2\text{-dmpe})U(BH_4)_4]$ and $[(\kappa^2\text{-dmpe})_2U(BH_4)_3]$,[227] and $[U(\kappa^2\text{-SBT})_4]$ and $[U(\kappa^2\text{-SBT})_4(py)]^-$ (SBT = 2-mercaptobenzothiazolate).[228] However, bond elongation in the $BH_4$ and SBT examples may be due to an increase in coordination number in the uranium(III) complex, and a significant dependence of uranium–ligand bond lengths on metal oxidation state is not always observed. For example, U–$PR_3$ and U–$NAr_2$ bonds in tri- and tetravalent uranium complexes of the PNP monoanion (PNP = bis{2-(diisopropylphosphino)-4-methylphenyl}amido) were largely unaffected by changes in oxidation state.[222] All 16 resonances in the $^1$H NMR spectrum of **2** in $C_6D_6$ are localized between +10 to −10 ppm, and confirm that the approximate $C_s$ symmetry of the solid state structure is maintained in solution. For example two C*H*$Me_2$ signals were observed at 1.68 and −2.17 ppm, coupled to four CH*Me*$_2$ signals at 0.26, −0.92, −2.04 and −8.69 ppm.

In addition to the NON-donor $XA_2$ ligand, members of the Emslie group also pursued uranium complexes of the previously unreported NSN-donor analogue $TXA_2$, which features a thioxanthene backbone supporting 2,6-diisopropylanilido donors. A salt-occluded uranium(IV) complex bearing the $\kappa^3$-coordinated $TXA_2$ ligand $[Li(dme)_3][(TXA_2)UCl_3]$ was accessible, and reduction with potassium naphthalenide yielded the uranium(III) species $[(TXA_2)UCl(dme)(\mu\text{-}Cl)Li(dme)_2]$. A computational study was carried out to explore the bonding in the related $XA_2$ and $TXA_2$ uranium chloro complexes, and ADF and AIM calculations point to significantly greater covalency in U–$SAr_2$ versus U–$OAr_2$ bonding in these complexes.[187] However, $TXA_2$ complexes of

uranium(IV) and uranium(III) are significantly less thermally stable than the corresponding $XA_2$-supported species, and while organometallic derivatives proved accessible in solution, their considerable solubility precluded isolation. Further, attempts to access cationic derivatives of the dialkyl complexes $[(TXA_2)U(CH_2SiMe_2R)_2]$ (R = Me; Ph) (generated *in-situ*) resulted in complex mixtures of products as evinced by $^1H$ and $^{19}F$ NMR spectroscopy, and further exploration of $TXA_2$ uranium complexes was not pursued as a result.

### 2.4 – $XA_2$ Uranium(IV) Bis((trimethylsilyl)methyl) Complex

Reaction of $[(XA_2)UCl_2(\mu\text{-}Cl)\{K(dme)_3\}]$ (**1**) with 2.1 equiv of $LiCH_2SiMe_3$ afforded neutral, base-free $[(XA_2)U(CH_2SiMe_3)_2]$ (**3**; Scheme 2.4), which was obtained as red-orange crystals in 78% yield after crystallization from *n*-pentane at −30 °C.[177] Bis((trimethylsilyl)methyl) complex **3** is highly soluble in ethereal- and aromatic solvents, as well as saturated hydrocarbons.

**Scheme 2.4** – Synthesis of $[(XA_2)U(CH_2SiMe_3)_2]$ (**3**).

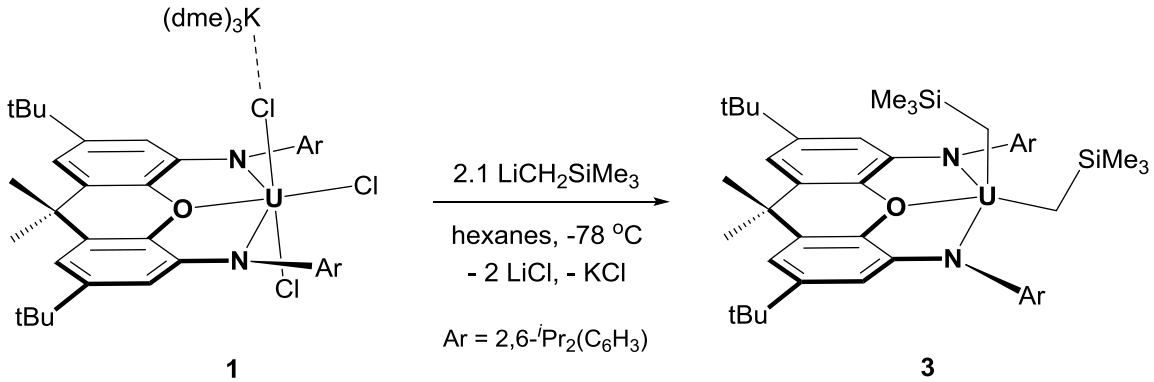

The room-temperature $^{1}$H NMR spectrum of **3** in $C_6D_6$ or toluene-$d_8$ (spectrum **a**) in Figure 2.4) shows only four resonances: those for the *tert*-butyl groups, the *para* positions of the 2,6-diisopropylphenyl rings, and the C*H*$^{1,8}$ and C*H*$^{3,6}$ positions of the xanthene backbone. These signals are unaffected by the top−bottom symmetry of the molecule, since they lie in the plane of the xanthene backbone of the ligand. All other resonances are broadened into the baseline due to a fluxional process which exchanges the axial and in-plane $CH_2SiMe_3$ groups. However, at low temperature, a full complement of $^{1}$H NMR signals was observed, ranging from +180 to −225 ppm at −60 °C (spectrum **b**) in Figure 2.4), indicative of $C_s$ symmetry. Most notably, the extremely broad resonances assigned to the UC*H*$_2$SiMe$_3$ α-protons (178.2, −222.3 ppm) experience significant shifts to both higher- and lower-frequencies, and are located approximately 400 ppm apart. Such significant chemical shifts arising from the α-protons of uranium alkyl complexes have been frequently observed,[229] and the magnitude of the shift is generally attributed to the close proximity of the α-protons to the paramagnetic uranium centre.

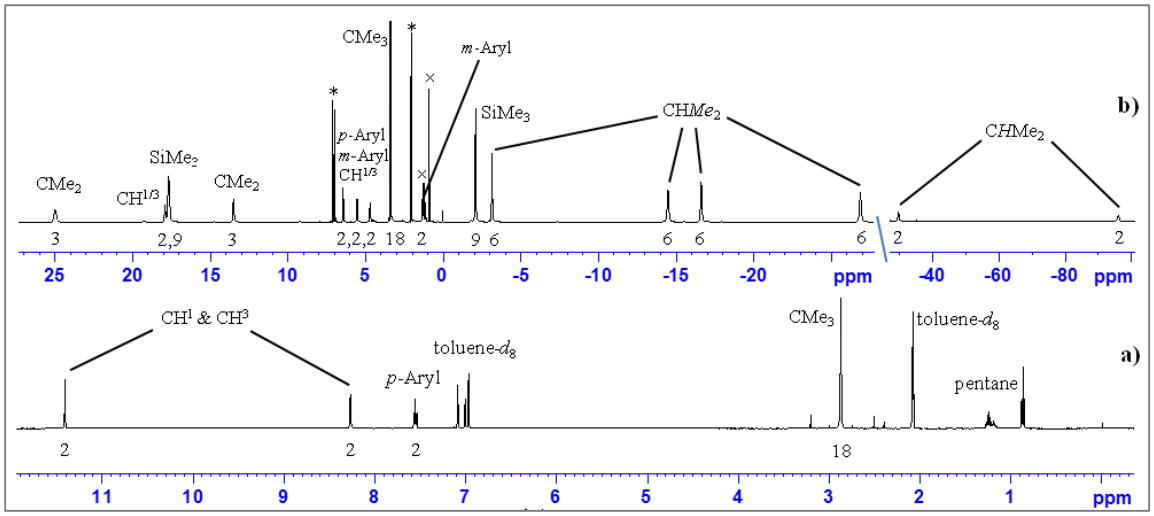


**Figure 2.4** – Selected regions of the $^{1}$H NMR spectra of [(XA$_2$)U(CH$_2$SiMe$_3$)$_2$] (**3**) in toluene-$d_8$ (500 MHz): (a) at room temperature; (b) at −60 °C. * denotes toluene-$d_8$ and × denotes *n*-pentane. Numbers below the baseline indicate the integration of each peak. Signals for U−C*H*$_2$ protons, which are located at very high (>100 ppm) and very low (<−100 ppm) frequencies in spectrum (b) are not shown. The CMe$_3$ peaks are truncated in both spectra.

The X-ray crystal structure of **3**·2(*n*-hexane) (Figure 2.5; Table 2.2) has two independent but structurally analogous five-coordinate molecules in the unit cell, each with one CH$_2$SiMe$_3$ group in an apical position and one located approximately in the plane of the ancillary ligand backbone. The four anionic donors adopt a distorted-tetrahedral arrangement with N(1)−U−N(2), C(48)−U−C(52), and N−U−C angles of 123.7(2)−124.0(2), 103.2(2)−105.0(2), and 101.0(2)−112.5(2)°, respectively. The neutral oxygen donor is located 0.92 and 0.95 Å out of the NUN plane in the direction of the axial alkyl group, and the complex has approximate $C_s$ symmetry, consistent with the low-temperature $^{1}$H NMR spectra.

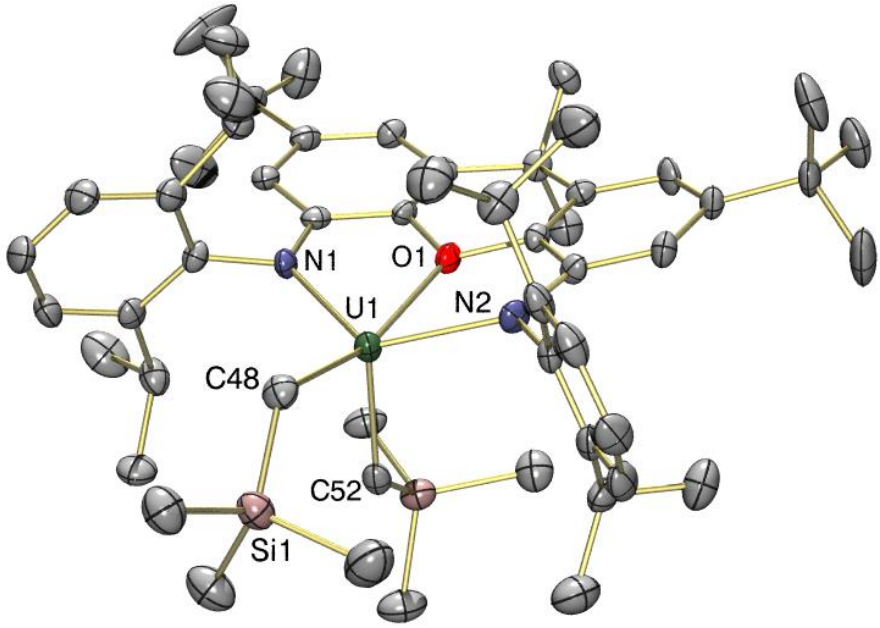


**Figure 2.5** – X-ray crystal structure of $[(XA_2)U(CH_2SiMe_3)_2]\cdot 2(n\text{-hexane})$ (**3**·2(*n*-hexane)), with thermal ellipsoids at 30% probability (collected at 173 K). Only one of the two independent molecules in the unit cell is shown. Hydrogen atoms and hexane solvent are omitted for clarity. Ar–*C*$HMe_2$ atoms numbered clockwise from the top left of the figure: C(30), C(45), C(42), C(33).

**Table 2.2** – Selected bond lengths (Å) and angles (deg) for complexes **3**, **4**, and **3-Th** (for comparison).

| Compound | **3** | **3-Th** | **4** |
|---|---|---|---|
| An−O | 2.484(5), 2.504(4) | 2.535(4) | 2.528(5), 2.529(5) |
| An−N | 2.261(5), 2.262(5), 2.272(5), 2.280(5) | 2.291(4), 2.312(4) | 2.260(6), 2.272(6), 2.279(5), 2.289(6) |
| An−$C_{apical}$ | 2.368(7), 2.380(7) | 2.467(6) | 2.386(8), 2.396(7) |
| An−$C_{in\text{-}plane}$ | 2.418(7), 2.393(7) | 2.484(6) | 2.409(7), 2.417(7) |
| An−$CH_2$−E[a] | 128.2(3), 130.4(3), 130.5(4), 130.8(3) | 126.8(3), 127.6(3) | 134.3(5), 134.4(5), 130.3(5), 130.3(5) |
| Ligand Bend Angle[b] | 17.5, 18.8° | 9.0° | 34.3, 33.3° |
| C−An−C | 103.2(2), 105.0(2) | 111.9(2) | 105.1(2), 106.6(3) |

| | | | |
|---|---|---|---|
| N−An−N | 123.7(2), 124.0(2) | 123.8(2) | 120.8(2), 120.9(2) |
| N−An−$C_{apical}$ | 101.0(2), 101.6(2), 103.2(2), 103.3(2) | 100.6(3), 100.8(2) | 103.6(2), 105.5(2), 105.8(2), 108.5(2) |
| N−An−$C_{in\ plane}$ | 108.1(2), 110.8(2), 111.7(2), 112.5(2) | 109.1(2), 109.7(2) | 107.6(2), 108.3(2), 109.2(2), 109.8(2) |
| N−An−O | 63.9(2), 64.0(2), 64.2(2), 64.4(2) | 62.9(1), 63.0(1) | 64.4(2), 64.5(2), 64.7(2), 65.1(2) |
| O−An−$C_{apical}$ | 94.8(2), 95.0(2) | 98.1(2) | 92.2(2), 95.0(2) |
| An···(N/O/N-plane) | 0.64, 0.65 | 0.48 | 0.84, 0.87 |
| O···(N/An/N-plane) | 0.91. 0.95 | 0.66 | 1.23, 1.30 |
| N(1)···N(2) | 4.00, 4.02 | 4.06 | 3.95, 3.96 |
| C(30)···C(45)[c] | 4.63, 4.86 | 5.00 | 4.16, 4.22 |
| C(42)···C(33)[c] | 7.63, 7.70 | 7.51 | 8.01, 8.07 |

[a] For **3** and **3-Th**, E = Si, for **4**, E = C. [b] Ligand Bend Angle = the angle between the two aromatic rings of the xanthene ligand backbone. [c] Or analogous distance in **3-Th**.

The U−C distances of 2.368(7)−2.418(7) Å are comparable with those observed in Leznoff's [($^{DIPP}$NCOCN)U($CH_2SiMe_3$)$_2$] ($^{DIPP}$NCOCN = $\kappa^3$-{(ArN$CH_2CH_2$)$_2$O}$^{2-}$, Ar = 2,6-$^i$Pr$_2$C$_6$H$_3$; U−C = 2.40(2) and 2.44(2) Å),[60] one of two other crystallographically characterized neutral uranium(IV) (trimethylsilyl)methyl complexes, but are shorter than that of Cloke's mixed sandwich complex [($^{TIPS2}$COT)(Cp*****)U($CH_2SiMe_3$)] ($^{TIPS2}$COT = {1,4-(Si$^i$Pr$_3$)$_2$C$_8$H$_6$}$^{2-}$; U−C = 2.464(4) Å),[155] and those of Hayton's homoleptic 'ate' complex [Li$_{14}$(O$^t$Bu)$_{12}$Cl][U($CH_2SiMe_3$)$_5$] (U−C = 2.445(6)−2.485(6) Å).[37] The U−C−Si angles of 128.2(3)−130.8(3)° are in line with previously reported values (125.7(3)−130.6(3)°),[§] and the U−N distances are unremarkable.[187] However, as

[§] The U−C−Si angle in Cloke's mixed sandwich complex [(COT$^{TIPS2}$)(Cp*****)U($CH_2SiMe_3$)] is considerably expanded (147.5(2)°), likely due to significant steric crowding at the metal centre; see: Higgins, J. A.; Cloke, F. G. N.; Roe, S. M. *Organometallics* **2013,** *32*, 5244.

previously discussed in the context of [($XA_2$)$UCl_2$(μ-Cl){K(dme)$_3$}] (**1**), [($XA_2$)UCl(dme)] (**2**),[187] and [($XA_2$)Th($CH_2SiMe_3$)$_2$] (**3-Th**),[40] the An−$O_{xant}$ distances in $XA_2$ actinide complexes (2.484(5) and 2.504(4) Å in **3**) are invariably shorter than might be expected for actinide−diarylether linkages, presumably due to steric constraints imposed by the rigid ligand framework.

The geometry of **3** is analogous to that of the thorium analogue, [($XA_2$)Th($CH_2SiMe_3$)$_2$] (**3-Th**),[40] although the An−C, An−N, and An−O distances in **3** are slightly shorter (Table 2.2), consistent with the smaller size of uranium (the six-coordinate ionic radii for $U^{4+}$ and $Th^{4+}$ are 0.89 and 0.94 Å, respectively).[11] In addition, the xanthene backbone in **3** deviates further from planarity (the angles between the two aryl rings of the xanthene backbone are 17.5 and 18.8° for **3** vs 9.0° for **3-Th**), and uranium is positioned further from the NON donor plane (0.64 and 0.65 Å for **3** vs 0.48 Å for **3-Th**). However, the N(1)···N(2) distance in **3** is only slightly shorter than that in the thorium analogue (4.00 and 4.02 Å in **3** vs 4.06 Å in **3-Th**), and the extent to which the 2,6-diisopropylphenyl groups are rotated away from the axial alkyl group are similar in **3** and **3-Th** (C(42)···C(33) = 7.63 and 7.70 Å and C(30)···C(45) = 4.63 and 4.86 Å in **3**; the corresponding distances in **3-Th** are 7.51 and 5.00 Å).

## 2.5 – $XA_2$ Uranium(IV) Bis(neopentyl) Complex

Analogous to the synthesis of bis((trimethylsilyl)methyl) complex **3**, reaction of $[(XA_2)UCl_2(\mu\text{-}Cl)\{K(dme)_3\}]$ (**1**) with 2.1 equiv of $LiCH_2{}^tBu$ afforded the highly soluble bis(neopentyl) complex $[(XA_2)U(CH_2{}^tBu)_2]$ (**4**; Scheme 2.5), which was obtained as dark red crystals in 69% yield upon crystallization from *n*-pentane or hexanes at −30 °C.[177]

**Scheme 2.5** – Synthesis of $[(XA_2)U(CH_2{}^tBu)_2]$ (**4**).

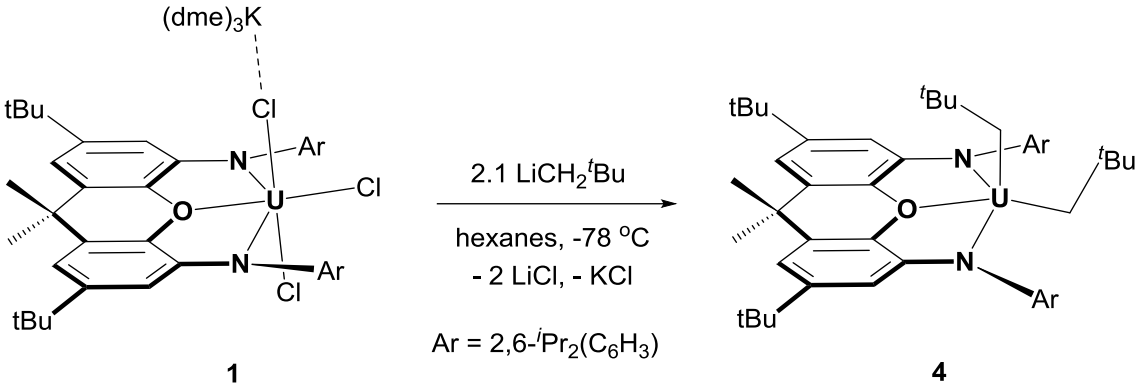


Many of the resonances in the room-temperature $^1H$ NMR spectrum of **4** in toluene-$d_8$ are extremely broad, indicative of a fluxional process which exchanges the axial and in-plane alkyl groups, but as for complex **3**, a sharp spectrum consistent with $C_s$ symmetry was observed at low temperature (Figure 2.6; −50 °C), with extremely broad resonances assigned to the $UCH_2{}^tBu$ α-protons arising at 223.3 and −221.5 ppm.

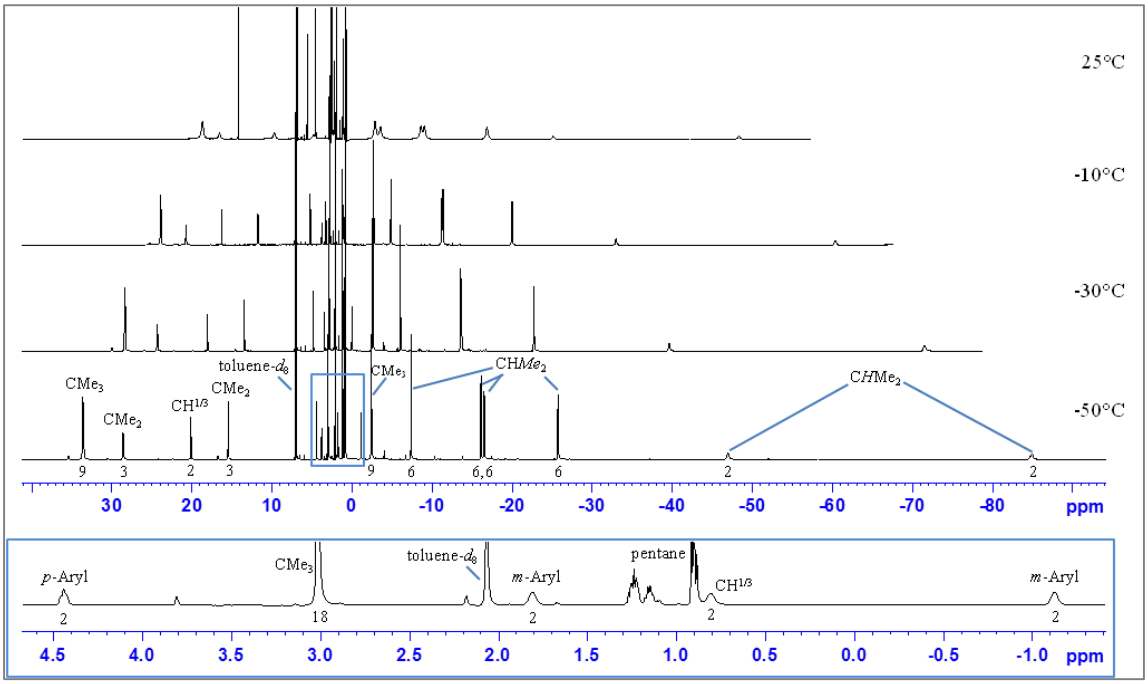


**Figure 2.6** – Selected regions of the $^{1}$H NMR spectra of [(XA$_2$)U(CH$_2$$^t$Bu)$_2$] (**4**) in toluene-$d_8$ at temperatures ranging from 25 to −50 °C (500 MHz). Numbers below the baseline indicate the integration of each peak. Signals for U−C*H*$_2$ protons, which are located at very high (>100 ppm) and very low (<−100 ppm) frequencies, are not shown. The inset at the bottom shows a portion of the −50 °C spectrum.

The solid-state geometry of complex **4** (Figure 2.7 and Table 2.2) is analogous to that of **3**, and as with **3**, there are two independent but structurally analogous molecules in the unit cell. The U−C and U−N distances are comparable with those in **3**, despite the increased basicity of CH$_2$$^t$Bu groups relative to CH$_2$SiMe$_3$ groups,[230] and the U−O distances are only marginally longer than those in **3**. However, due to the increased steric presence of the neopentyl anion, uranium is located further from the NON donor plane in complex **4** (0.84 and 0.87 Å vs 0.64 and 0.65 Å in **3**), and the neutral oxygen donor is located further from the NUN plane (1.23 and 1.30 Å vs 0.91 and 0.95 Å in **3**). In

addition, the ligand backbone deviates further from planarity (the angles between the aromatic rings in the xanthene backbone are 33.3 and 34.3° versus 17.5 and 18.8° in **3**), and the 2,6-diisopropylphenyl groups are more strongly rotated away from the axial alkyl group so as to minimize unfavorable steric interactions: C(33)···C(42) = 8.01 and 8.07 Å and C(30)···C(45) = 4.16 and 4.22 Å (cf. C(33)···C(42) = 7.63 and 7.70 Å and C(30)···C(45) = 4.63 and 4.86 Å in **3**).

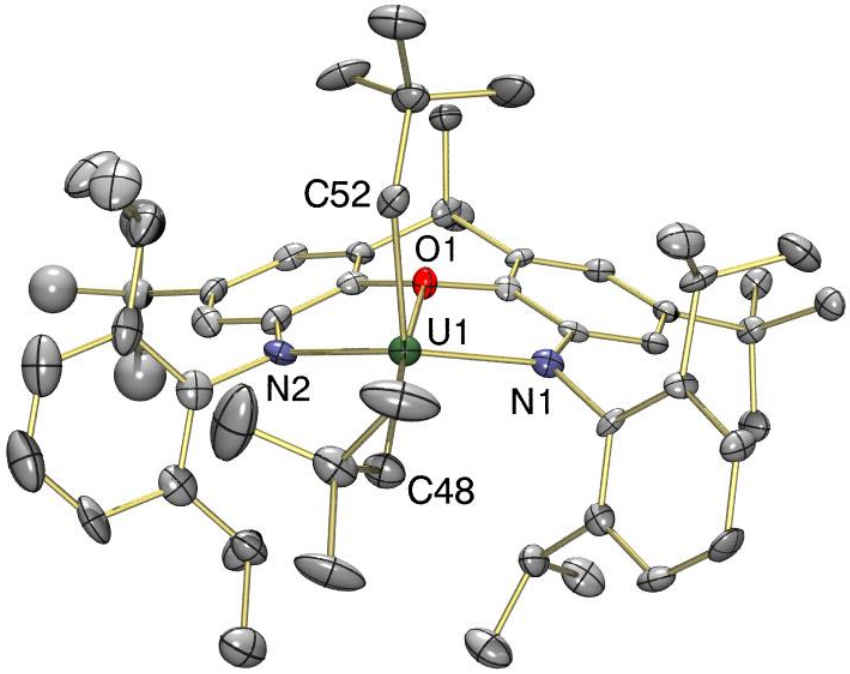


**Figure 2.7** – X-ray crystal structure of [(XA$_2$)U(CH$_2$$^t$Bu)$_2$]·(*n*-hexane) (**4**·(*n*-hexane)), with thermal ellipsoids at 50% probability (collected at 100 K). Only one of the two independent molecules in the unit cell is shown. Hydrogen atoms and hexane solvent are omitted for clarity. One *tert*-butyl group is disordered and so was refined isotropically, and only one of the two orientations of the disordered *tert*-butyl group is shown. Ar–*C*HMe$_2$ atoms numbered clockwise from the top left of the figure: C(42), C(33), C(30), C(45).

The U−C distances in **4** (2.386(8)−2.417(7) Å) are relatively shorter than those of Hayton's homoleptic neopentyl 'ate' complex $[Li(THF)_4][U(CH_2{}^tBu)_5]$ (U−C = 2.47(1)−2.51(1) Å),[37] which are likely elongated as a consequence of steric pressure, increased electronic saturation relative to **4**, and the fact that $[U(CH_2{}^tBu)_5]^-$ bears a net negative charge. The U−$CH_2$−C angles in **4** (130.3(5)−134.4(5)°) also fall within the range reported by Hayton and co-workers for $[Li(THF)_4][U(CH_2{}^tBu)_5]$ (U−$CH_2$−C = 126.3(7)−149(1)°), however, the authors noted that the considerably expanded latter angle was anomalous and possibly an artifact of the neopentyl disorder.[37] To our knowledge, $[(XA_2)U(CH_2{}^tBu)_2]$ (**4**) is the only crystallographically characterized neutral uranium neopentyl complex.

The U−$CH_2$−E angles of 128.2(3)−134.4(5)° in complexes **3** (E = Si) and **4** (E = C) are considerably expanded relative to the ideal 109.5° angle, which suggests that the alkyl groups may be engaged in α-agostic C−H−U interactions. This bonding consideration was previously observed for the related thorium complex $[(XA_2)Th(CH_2SiMe_3)_2]$ (**3-Th**) (Th−$CH_2$−Si = 126.8(3)−127.6(3)°), and in **3-Th** the α-agostic interactions were confirmed by small $^1J_{^{13}C,^1H}$ coupling constants for the Th$CH_2$ groups.[40] However, in paramagnetic **3** and **4**, $^1J_{^{13}C,^1H}$ coupling constants could not be measured, and therefore, it is not possible to draw any definite conclusions from the expanded U−$CH_2$−E angles.

The noteworthy paucity of structurally-authenticated uranium neopentyl complexes may be a consequence of the considerable basicity of the bulky neopentyl anion, which often promotes unexpected reactivity or yields short-lived uranium

neopentyl species prone to activation/metalation. For instance, Kiplinger and co-workers were unable to access the desired bis(neopentyl) derivative of [{CpCo{P(O)(OEt)$_2$}$_3$}$_2$UCl$_2$]; instead, reaction with neopentyllithium resulted in nucleophilic attack of the cyclopentadienyl groups of each Kläui ligand ([CpCo{P(O)(OEt)$_2$}$_3$]$^-$), yielding [{($\eta^4$-C$_5$H$_5$(CH$_2$$^t$Bu))Co{P(O)(OEt)$_2$}$_3$}$_2$U].[231] Evans and co-workers reported several isolable uranium(IV) hydrocarbyl complexes of the form [Cp*****$_2$UR(hpp)] (hpp$^-$ = 1,3,4,6,7,8-hexahydro-2*H*-pyrimido[1,2-*a*]pyrimidinato; R = Me, Et, C≡CPh, Ph),[232] but a neopentyl derivative proved inaccessible. Reaction of the chloro precursor [Cp*****$_2$UCl(hpp)] with neopentyllithium yielded the metalated 'tuck-in' complex [(Cp*****)($\eta^5$:$\eta^1$-C$_5$Me$_4$CH$_2$)U(hpp)], the result of activating a C−H bond of a Cp*****-methyl group, among other unidentified products, possibly *via* [Cp*****$_2$U(CH$_2$$^t$Bu)(hpp)] as an intermediate.[232] The stability of bis(neopentyl) complex **4** is thus a testament to the suitability of XA$_2$ to serve as a chemically-robust ancillary ligand, as it has demonstrated the ability to stabilize reactive uranium alkyl species that are otherwise inaccessible.

Dialkyl complexes **3** and **4** are thermally stable for days at room temperature in aromatic solvents. However, over the course of several days at 45 °C, **3** and **4** were converted to a mixture of unidentified paramagnetic products with concomitant evolution of SiMe$_4$ or CMe$_4$, respectively. Upon further heating at 60−80 °C for 24−48 h, **3** and **4** were fully decomposed to give spectra dominated by SiMe$_4$ or CMe$_4$ (at this point, $^1$H NMR signals attributable to diamagnetic or paramagnetic XA$_2$ ligand-containing products were low in intensity). We have previously reported similar behavior for the decomposition of [(XA$_2$)Th(CH$_2$SiMe$_3$)$_2$] (**3-Th**) at 90 °C.[40]

## 2.6 – $XA_2$ Uranium(IV) Dibenzyl Complex

Reaction of the versatile trichloro precursor [$(XA_2)UCl_2(\mu\text{-}Cl)\{K(dme)_3\}$] (**1**) with 2 equiv of benzylpotassium at −94 °C afforded base-free [$(XA_2)U(CH_2Ph)_2$] (**5**), which was obtained as a black microcrystalline solid in 74% yield upon crystallization from *n*-pentane at −30 °C (Scheme 2.6). Although noticeably less soluble than the bis((trimethylsilyl)methyl) analogue **3**, dibenzyl complex **5** is saturated hydrocarbon-soluble, and stable in arene solution for weeks at room temperature.

**Scheme 2.6** – Synthesis of neutral dibenzyl complex [$(XA_2)U(CH_2Ph)_2$] (**5**).

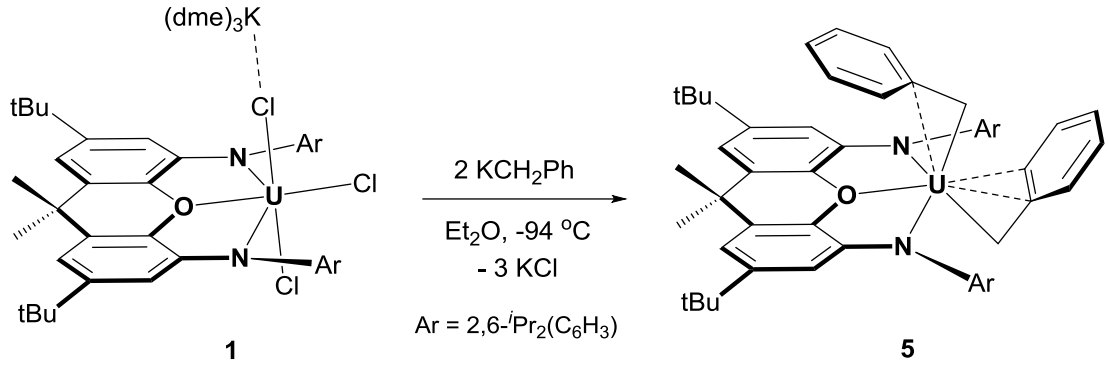


The room-temperature $^1$H NMR spectrum of complex **5** in toluene-$d_8$ consists of twenty two paramagnetically shifted resonances ranging from +101 to −63 ppm. The resonances are broadened, indicative of a fluxional process which slowly exchanges the two benzyl groups, much like we have observed previously for the bis(neopentyl) complex [$(XA_2)U(CH_2{}^tBu)_2$] (**4**).[177] Cooling to −11 °C resulted in a sharpening of the twenty two resonances, though both the room- and low-temperature $^1$H NMR spectra of dibenzyl complex **5** feature the full complement of signals representative of a top-bottom

asymmetric species of approximate $C_s$ symmetry in solution. Most notably, extremely broad resonances assigned to the UC$H_2$Ph protons (100.92, 61.75 ppm at 298 K) are shifted to higher frequency by more than 20 ppm upon cooling (124.45, 82.22 ppm at 262 K).

The X-ray crystal structure of **5**·THF (Figure 2.8; Table 2.3) revealed an approximately $C_s$-symmetric complex consistent with the $^1$H NMR spectral assignment, with one benzyl ligand located approximately in the plane of the $XA_2$ ligand, and the other occupying an apical site. If we view each benzyl ligand as the occupant of a single coordination site, uranium is five-coordinate. The four anionic donors (N(1), N(2), C(48), and C(55)) adopt a distorted-tetrahedral arrangement around the metal centre with N(1)−U−N(2), C(48)−U−C(55), and N−U−C angles of 127.76(9), 121.6(1), 98.2(1)–108.35(9)°, respectively, with the neutral oxygen donor located 0.46 Å out of the NUN plane in the direction of the apical benzyl ligand, capping an edge of the aforementioned tetrahedron. Unsurprisingly, **5** is qualitatively isostructural with Emslie's previously reported thorium(IV) dibenzyl complex [$(XA_2)$Th$(CH_2Ph)_2$], **5-Th**,[180] but generally features shorter actinide–ligand bond distances than those of the thorium analogue due to the smaller ionic radius of uranium(IV) versus thorium(IV) (0.89 vs 0.94 Å).[11]

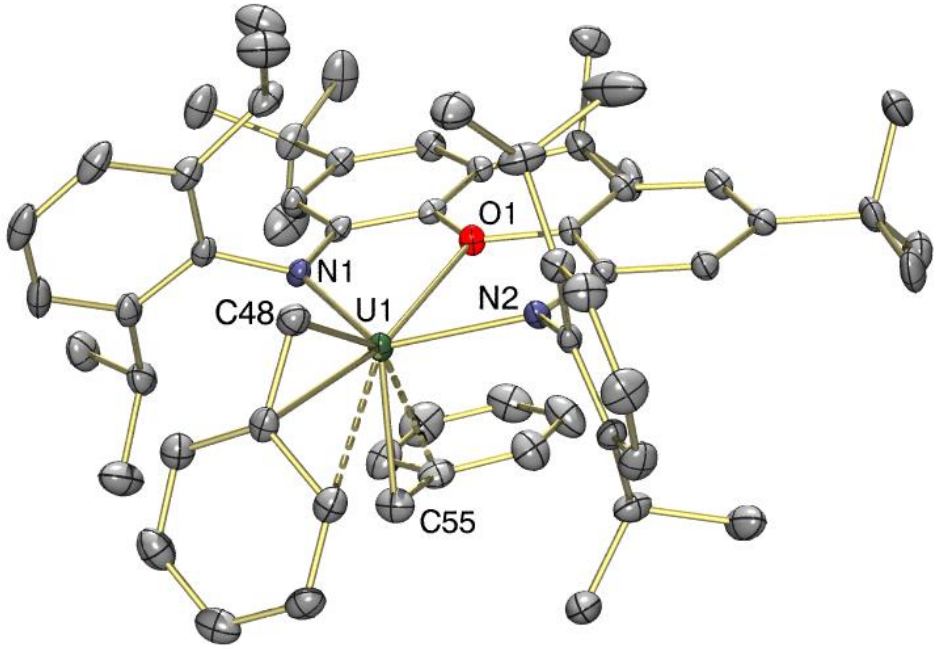


**Figure 2.8** – X-ray crystal structure of $[(XA_2)U(CH_2Ph)_2]\cdot(THF)$ (**5**·THF), with thermal ellipsoids at 50% probability. Hydrogen atoms and THF lattice solvent molecule are omitted for clarity.

**Table 2.3** – Selected bond lengths (Å) and angles (deg) for complexes **5**, **5-Th** and **3** (for comparison).

| Compound | **5** | **5-Th** | **3** |
|---|---|---|---|
| An−O | 2.477(2) | 2.5194(19), 2.5263(17) | 2.484(5), 2.504(4) |
| An−N | 2.270(2), 2.301(2) | 2.318(2), 2.332(2), 2.331(2), 2.339(3) | 2.261(5), 2.262(5), 2.272(5), 2.280(5) |
| An−$CH_2$ *in plane* | 2.462(3) | 2.517(3), 2.545(3) | 2.393(7), 2.418(7) |
| An−$C_{ipso\ in\ plane}$ | 2.751(3) | 2.826(3), 2.851(3) | n/a |
| An−$C_{ortho\ in\ plane}$ | 3.220(3), 3.367(3) | 3.191(3), 3.510(3), 3.126(4), 3.647(4) | n/a |
| An−$CH_2$ *apical* | 2.451(4) | 2.503(3), 2.531(3) | 2.368(7), 2.380(7) |

| | | | |
|---|---|---|---|
| An−$C_{ipso\ apical}$ | 3.036(3) | 3.402(3), 3.058(3) | n/a |
| An−$C_{ortho\ apical}$ | 3.550(4), 3.817(4) | 3.922, 4.359, 3.392, 3.927 | n/a |
| Ligand Bend Angle[a] | 4.0° | 12.2, 18.6° | 17.5, 18.8° |
| An−$CH_2$−E[b] $_{in\ plane}$ | 85.2(2) | 85.6(2), 87.5(2) | 130.5(4), 130.8(3) |
| An−$CH_2$−E[b] $_{apical}$ | 98.1(2) | 96.1(2), 115.1(2) | 128.2(3), 130.4(3) |
| O···(N/An/N-plane) | 0.46 | 0.86, 0.87 | 0.91. 0.95 |
| An···(N/O/N-plane) | 0.31 | 0.62, 0.63 | 0.64, 0.65 |
| N(1)···N(2) | 4.11 | 4.09, 4.11 | 4.00, 4.02 |

[a] Ligand Bend Angle = the angle between the two aromatic rings of the xanthene ligand backbone. [b] For **5** and **5-Th**, E = $C_{ipso}$, for **3**, E = Si.

The U−O (2.477(2) Å) and U−N (2.270(2), 2.301(2) Å) bond distances of **5** are quite typical, in good agreement with those observed for the closely related bis((trimethylsilyl)methyl) complex **3**, and with those of Leznoff's dibenzyl complex [($^{DIPP}$NCOCN)U($CH_2Ph)_2$] ($^{DIPP}$NCOCN = $\kappa^3$-{($ArNCH_2CH_2)_2O$}$^{2-}$, Ar = 2,6-$^i$Pr$_2$C$_6$H$_3$; U−O = 2.485(8) Å, U−N = 2.20(1), 2.22(1) Å),[174] which bears a flexible tridentate bis(amido)ether ligand with a donor-set analogous to that of our rigid $XA_2$ ancillary. The U−$CH_2$ bond distances in **5** (2.451(4), 2.462(3) Å) are also unremarkable, falling within the range typical of U−$C_{benzyl}$ single bonds (cf. 2.446(7)−2.477(7) Å in Bart's homoleptic tetrabenzyl complex [U($CH_2Ph)_4$],[44] and 2.48(1)-2.54(1) Å in Leznoff's [($^{DIPP}$NCOCN)U($CH_2Ph)_2$]). The xanthene backbone in **5** is considerably planar (the angle between the two aryl rings of the xanthene backbone is 4.0°), much more so than that of closely related **5-Th** (12.2° and 18.6° for the two molecules in the unit cell), or the related bis((trimethylsilyl)methyl) complex **3**. This may be a consequence of the multi-

hapto coordination of the benzyl ligands of **5**, which brings steric bulk closer to the coordination sphere of the metal.

As observed in **5-Th**,[180] the in-plane benzyl ligand of **5** adopts a multi-hapto bonding mode intermediate between $\eta^2$- and $\eta^3$-coordintion as evidenced by the considerably acute U−C(48)−C(49) angle of 85.2(2)°, and relatively short U−$C_{ipso}$ and U−$C_{ortho}$ distances of 2.751(3) and 3.220(3) Å, respectively. The in-plane benzyl group of Leznoff's [($^{DIPP}$NCOCN)U($CH_2Ph)_2$] complex also features a severely acute U−C−C angle (80.8(8)°) and relatively short U−$C_{ipso}$ distance (2.72(2) Å), and the authors similarly concluded that multi-hapto bonding was in effect.[174] Also like that of **5-Th**, the apical benzyl ligand of **5** adopts a bonding mode approaching $\eta^2$-coordination, featuring a relatively acute U−C(55)−C(56) angle (98.1(2)°) and relatively short U−$C_{ipso}$ distance (3.036(3) Å).

It remains a challenge to definitively assign hapticity in actinide benzyl complexes. For example, Bart's homoleptic tetrabenzyl complex [U($CH_2Ph)_4$] and diphosphine derivative [(dmpe)U($CH_2Ph)_4$] (dmpe = 1,2-bis(dimethylphosphino)ethane) feature a wide variety of U–C–C angles (82.7(4)–116.2(5)°) and some considerably long U–$C_{ortho}$ contact distances (U–$C_{ortho}$ contact = 3.171–4.253 Å).[44] Utilizing the Δ and Δ′ metrical parameters,[48] Bart and co-workers concluded that each benzyl ligand of [U($CH_2Ph)_4$] and [(dmpe)U($CH_2Ph)_4$] adopts an $\eta^4$-coordination mode.[44] Conversely, Leznoff and co-workers concluded that the apical benzyl ligand of [($^{DIPP}$NCOCN)U($CH_2Ph)_2$] adopts an $\eta^1$-coordination mode,[174] yet the U–C–C angle (116.6(10)°) and U–$C_{ortho}$ contact distance (4.014 Å) fall into the range reported by Bart.

Other structurally-characterized, neutral uranium(IV) dibenzyl complexes include Diaconescu's 1,1′-diamidoferrocene species [(FcNN)U($CH_2Ph)_2$] (FcNN = $\{Fc(NSiMe_2R)_2\}^{2-}$; R = $^t$Bu, Ph),[183,233] and [(BDPP)U($CH_2Ph)_2$] (BDPP = 2,6-bis(2,6-diisopropylanilidomethyl)pyridine),[49] Kiplinger's bis(metallocene) [Cp*$_2$U($CH_2Ph)_2$],[125] Bart's scorpionate [(Tp′)U($CH_2Ph)_2${OC($Ph)_2CH_2Ph$}] (Tp′ = $\kappa^3$-{$HB(3,5\text{-}Me_2pz)_3$}$^-$),[168] and amido(phenolate) complex [($^{dipp}$ap)U($CH_2Ph)_2(THF)_2$] ({$^{dipp}$ap}$^{2-}$ = 4,6-di-*tert*-butyl-2-[(2,6-diisopropylphenyl)amido]phenolate),[184] and Liddle's bis(iminophosphorane)methanediide complex [($BIPM^{TMS}$)U($CH_2Ph)_2$] ($BIPM^{TMS}$ = $\kappa^3$-{$C(PPh_2NSiMe_3)_2$}$^{2-}$).[173] Additionally, Hayton and co-workers reported the noteworthy homoleptic hexabenzyl 'ate' species {[K(THF)]$_3$[K(THF)$_2$][U($CH_2Ph)_6$]$_2$}$_x$.[37]

**Table 2.4** – Crystallographic data collection and refinement parameters for complexes **1**, **2**, and **3**.

| Structure | **1**·dme | **2**·4.5(toluene) | **3**·2(*n*-hexane) |
|---|---|---|---|
| Formula | $C_{59}H_{92}Cl_3KN_2O_7U$ | $C_{82.50}H_{108}ClN_2O_3U$ | $C_{134}H_{224}N_2O_2Si_2U$ |
| Formula wt | 1324.83 | 1449.19 | 2427.39 |
| *T* (K) | 173(2) | 100(2) | 173(2) |
| Cryst. Syst. | Orthorhombic | Monoclinic | Triclinic |
| Space Group | *P*2(1)2(1)2(1) | *P*2(1)/*c* | *P*–1 |
| *a* (Å) | 11.4562(16) | 14.402(2) | 12.3983(16) |
| *b* (Å) | 22.380(3) | 15.964(2) | 19.246(3) |
| *c* (Å) | 25.144(3) | 29.638(5) | 26.498(4) |
| α [deg] | 90 | 90 | 82.016(4) |
| β [deg] | 90 | 94.854(3) | 79.396(4) |
| γ [deg] | 90 | 90 | 88.571(2) |
| Volume [Å$^3$] | 6446.7(15) | 6789.8(17) | 6154.8(14) |
| *Z* | 4 | 4 | 2 |

| | | | |
|---|---|---|---|
| Density (calcd;Mg/m$^3$) | 1.365 | 1.418 | 1.310 |
| μ (mm$^{-1}$) | 2.754 | 2.482 | 2.697 |
| *F*(000) | 2712 | 3000 | 2540 |
| Crystal Size (mm$^3$) | 0.50×0.08× 0.04 | 0.354×0.177×0.101 | 0.30×0.20×0.04 |
| θ Range for Collection [deg] | 1.82–30.54 | 1.38–25.00 | 2.07–25.00 |
| No. of reflns. Collected | 151566 | 63693 | 64632 |
| No. of Indep. Reflns. | 19639 | 11944 | 21560 |
| Completeness to θ Max (%) | 99.5 | 99.9 | 99.5 |
| Absorption Correction | Numerical | Numerical | Numerical |
| Max and Min Transmission | 0.8978, 0.3397 | 0.7892, 0.4767 | 0.8998, 0.4983 |
| Data / Parameters | 19639 / 646 | 11944 / 584 | 21560 / 1126 |
| GOF on $F^2$ | 1.012 | 1.059 | 0.964 |
| Final $R_1$ [$I > 2\sigma(I)$] | R1 = 0.0453<br>wR2 = 0.0856 | R1 = 0.0781<br>wR2 = 0.1973 | R1 = 0.0499<br>wR2 = 0.1063 |
| *R* indices (all data) | R1 = 0.0783<br>wR2 = 0.0972 | R1 = 0.1248<br>wR2 = 0.2135 | R1 = 0.0824<br>wR2 = 0.1162 |

**Table 2.5** – Crystallographic data collection and refinement parameters for complexes **4** and **5**.

| Structure | **4**·(*n*-hexane) | **5**·THF |
|---|---|---|
| Formula | $C_{63.50}H_{84}N_2OU$ | $C_{65}H_{84}N_2O_2U$ |
| Formula wt | 1129.36 | 1163.37 |
| *T* (K) | 100(2) | 100(2) |
| Cryst. Syst. | Monoclinic | Triclinic |
| Space Group | *P*2(1)/*c* | *P*–1 |
| *a* (Å) | 31.383(16) | 11.5747(8) |
| *b* (Å) | 9.827(5) | 12.7230(8) |
| *c* (Å) | 38.880(20) | 20.5456(14) |
| α [deg] | 90 | 80.8830(10) |
| β [deg] | 102.716(11) | 79.2670(10) |

| | | |
|---|---|---|
| γ [deg] | 90 | 84.4930(10) |
| Volume [Å$^3$] | 11697(10) | 2928.3(3) |
| *Z* | 8 | 2 |
| Density (calcd; Mg/m$^3$) | 1.283 | 1.319 |
| μ (mm$^{-1}$) | 2.815 | 2.814 |
| *F*(000) | 4632 | 1192 |
| Crystal Size (mm$^3$) | 0.38×0.17×0.10 | 0.294×0.193×0.066 |
| θ Range for Collection [deg] | 1.13–25.00 | 1.795– 33.218 |
| No. of reflns. Collected | 117765 | 50599 |
| No. of Indep. Reflns. | 20610 | 21180 |
| Completeness to θ Max (%) | 100.0 | 99.5 |
| Absorption Correction | Numerical | Numerical |
| Max and Min Transmission | 0.7661, 0.4143 | 0.8693, 0.5263 |
| Data / Parameters | 20610 / 1130 | 21180 / 639 |
| GOF on $F^2$ | 0.959 | 1.018 |
| Final $R_1$ [$I > 2\sigma(I)$] | R1 = 0.0528 wR2 = 0.1168 | R1 = 0.0425 wR2 = 0.0876 |
| *R* indices (all data) | R1 = 0.0980 wR2 = 0.1317 | R1 = 0.0647 wR2 = 0.0953 |

# Chapter 3

## Cationic $XA_2$ Uranium(IV) Monoalkyl Complexes and Ethylene Polymerization

### 3.1 – Introduction

Previously, Emslie and co-workers reported a variety of neutral, base-free thorium(IV) dialkyl complexes supported by the xanthene-based tridentate pincer ligand $XA_2$ (4,5-bis(2,6-diisopropylanilido)-2,7-di-*tert*-butyl-9,9-dimethylxanthene) and McConville's pyridine-based BDPP ligand (2,6-bis(2,6-diisopropylanilidomethyl)pyridine).[40,179,180] Reaction of the thorium(IV) dialkyls with $B(C_6F_5)_3$ and $[Ph_3C][B(C_6F_5)_4]$ provided access to the first non-cyclopentadienyl thorium alkyl cations (*vide supra*, Section 1.7.1),[179,180] with the ultimate goal of deploying such reactive species toward the insertion-polymerization of olefins. These complex tandems are listed in Table 3.1.

**Table 3.1** – Pairs of neutral and cationic Th(IV) derivatives reported by the Emslie group.

| Neutral Precursor | Cationic/Dicationic Derivative |
|---|---|
| $[(XA_2)Th(CH_2SiMe_3)_2]$ (**3-Th**) | $[(XA_2)Th(CH_2SiMe_3)(\eta^x\text{-arene})][B(C_6F_5)_4]$ $\eta^x$-arene = $\eta^6$-$C_6H_6$ (**6-Th**), $\eta^3$-$C_6H_5Me$ (**7-Th**) |
| $[(XA_2)Th(CH_2Ph)_2]$ (**5-Th**) | $[(XA_2)Th(CH_2Ph)(\eta^6\text{-}C_6H_5Me)][B(C_6F_5)_4]$ (**9-Th**) $[(XA_2)Th(CH_2Ph)][PhCH_2B(C_6F_5)_3]$ $[(XA_2)Th][PhCH_2B(C_6F_5)_3]_2$ |
| $[(BDPP)Th(CH_2Ph)_2]$ | $[(BDPP)Th(CH_2Ph)(\mu\text{-}\eta^1\text{:}\eta^6\text{-}CH_2Ph)Th(CH_2Ph)(BDPP)][B(C_6F_5)_4]$ |

The presence of a facially-bound arene provided by the solvent, the benzyl moiety of the benzylborate counterion, or remaining neutral dialkyl precursor complex ([(BDPP)Th($CH_2Ph)_2$]) was quickly established as a persistent structural motif in Emslie's cationic thorium(IV) complexes, and although fundamentally intriguing, this behaviour remains a barrier to the goal of developing highly active olefin polymerization catalysts. In attempt to circumvent this issue, the prototypical $XA_2$ ligand was installed on uranium(IV), which has an ionic radius approximately 0.05 Å smaller than its thorium(IV) congener.[11] We envisioned that the shorter uranium–element bonds in a cationic $XA_2$ monoalkyl uranium fragment would result in a tighter coordination environment, and perhaps serve to disfavor the undesirable arene coordination. Herein we describe the synthesis, structures, solution behaviour, and ethylene polymerization activity of cationic monoalkyl $XA_2$ uranium(IV) complexes, which despite our best efforts also demonstrate a proclivity for incorporating π-coordinated arenes into the coordination sphere.

### 3.2 – Cationic $XA_2$ Uranium(IV) Monoalkyl Complexes Bearing Proteo-Arenes

Cationic monoalkyl uranium complexes $[(XA_2)U(CH_2SiMe_3)(\eta^x\text{-arene})][B(C_6F_5)_4]$ ($\eta^x$-arene = $\eta^6$-$C_6H_6$ (**6**); $\eta^3$-$C_6H_5Me$ (**7**)) were accessed by treatment of the uranium(IV) dialkyl complex $[(XA_2)U(CH_2SiMe_3)_2]$ (**3**)[177] with one equiv of $[Ph_3C][B(C_6F_5)_4]$ in arene solution to effect abstraction of a single (trimethylsilyl)methyl ligand (Scheme 3.1).

**Scheme 3.1** – Synthesis of monoalkyl uranium(IV) cations **6** and **7**.

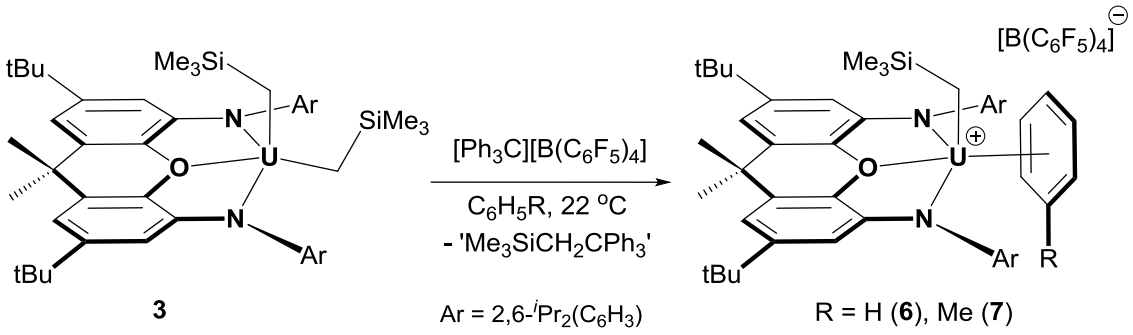


Unlike the analogous thorium(IV) monoalkyl cations, $[(XA_2)Th(CH_2SiMe_3)(\eta^x\text{-arene})][B(C_6F_5)_4]$ ($\eta^x$-arene = $\eta^6$-$C_6H_6$ (**6-Th**); $\eta^3$-$C_6H_5Me$ (**7-Th**)),[179] which precipitated as oils from benzene and toluene, cationic uranium(IV) species **6** and **7** exhibit improved solubility in proteo-arenes, a trend congruent with the general solubility behaviour of the neutral precursors $[(XA_2)U(CH_2SiMe_3)_2]$ (**3**) and $[(XA_2)Th(CH_2SiMe_3)_2]$ (**3-Th**). The increased solubility of uranium complexes in nonpolar solvents relative to closely-related thorium-containing species is common,[234] and may be ascribed to increased covalency in the uranium system.[10] Layering solutions of **6** in benzene and **7** in toluene with hexanes

and cooling to −30 °C resulted in precipitation of **6**·2(benzene) and **7**·2(toluene) as deep-brown crystalline solids in 72% and 81% yield, respectively.

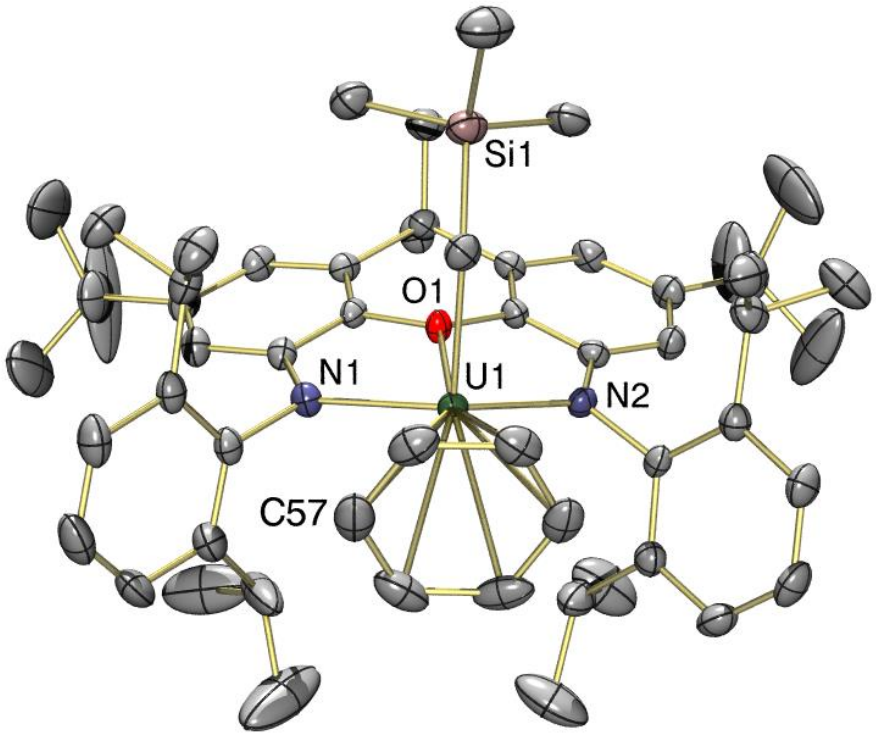


**Figure 3.1** – X-ray crystal structure of $[(XA_2)U(CH_2SiMe_3)(\eta^6\text{-}C_6H_6)][B(C_6F_5)_4]\cdot 2(\text{benzene})$ (**6**·2(benzene)), with thermal ellipsoids at 50% probability. Hydrogen atoms, the borate anion, and two non-coordinated benzene solvent molecules are omitted for clarity. Ar–*C*HMe$_2$ atoms numbered clockwise from the top left of the figure: C(42), C(33), C(45), C(30).

In the solid state, **6** exists as a solvent-separated ion pair consisting of a uranium(IV) monoalkyl cation stabilized by π-coordination of an $\eta^6$-benzene ligand originating from the solvent, and a distal tetrakis(pentafluorophenyl)borate anion, with two non-coordinated benzene solvent molecules incorporated into the lattice (Figure 3.1

and Table 3.2). Cation **6** has approximate $C_s$ symmetry (with the plane of symmetry bisecting two C–C bonds of coordinated benzene) and structurally resembles the neutral dialkyl precursor $[(XA_2)U(CH_2SiMe_3)_2]$ (**3**), but with the equatorial (trimethylsilyl)methyl ligand replaced by an $\eta^6$-coordinated benzene ring. The U−$C_{arene}$ distances range from 3.099(3) to 3.249(3) Å, and the U−centroid distance is 2.86 Å. If the arene in **6** is viewed as the occupant of a single coordination site, uranium adopts a pseudo square-pyramidal geometry with the (trimethylsilyl)methyl ligand bound in the apical position. This structure is qualitatively identical to that of $[(XA_2)Th(CH_2SiMe_3)(\eta^6\text{-}C_6H_6)][B(C_6F_5)_4]$ (**6-Th**), but with shorter actinide–ligand bond distances (Table 3.2) due to the smaller ionic radius of uranium(IV) versus thorium(IV) (0.89 vs 0.94 Å).[11] Additionally, the ligand backbone is less planar in **6** in order to accommodate a shorter N(1)···N(2) distance, and the O–U–$C_{apical}$ angle is more acute (87.26(8) vs 91.3(1)°), reflecting increased steric hindrance around the smaller actinide metal.

**Table 3.2** – Selected bond lengths (Å) and angles (deg) for cations **6** and **7** (vs. **6-Th** and **3** for comparison).

| Compound | **6** | **6-Th** | **7** | **3** |
|---|---|---|---|---|
| An−O | 2.441(2) | 2.496(5) | 2.417(9) | 2.484(5), 2.504(4) |
| An−N | 2.224(2), 2.236(2) | 2.278(3), 2.288(3) | 2.21(1), 2.22(1) | 2.261(5), 2.262(5), 2.272(5), 2.280(5) |
| An−$C_{alkyl}$ | 2.365(3) | 2.434(5) | 2.36(2) | 2.368(7), 2.380(7), 2.418(7), 2.393(7) |
| An−$C_{arene}$ | 3.099(3)−3.249(3) | 3.18−3.31 | 3.05(2)−3.78(2) | n/a |
| An−Centroid[a] | 2.86 | 2.95 | 3.14 | n/a |

| | | | | |
|---|---|---|---|---|
| Ligand Bend Angle[b] | 18.9° | 8.7° | 5.9° | 17.5, 18.8° |
| O−An−$C_{apical}$ | 87.26(8) | 91.3(1) | 88.8(4) | 94.8(2), 95.0(2) |
| An−C−Si | 133.7(2) | 131.0(2) | 136.8(7) | 128.2(3), 130.4(3), 130.5(4), 130.8(3) |
| N(1)···N(2) | 3.94 | 4.04 | 3.98 | 4.00, 4.02 |
| C(42)···C(33)[c] | 7.82 | 7.38 | 7.32 | 7.63, 7.70 |
| C(45)···C(30)[c] | 4.53 | 5.37 | 5.29 | 4.63, 4.86 |

[a] Centroid = centroid of the coordinated arene ring. [b] Ligand Bend Angle = the angle between the planes formed by each aromatic ring of the ligand backbone, where each plane is defined by the six carbon atoms of each aromatic ring within the xanthene backbone. [c] Or analogous distance in **3-Th**.

Structurally-authenticated cationic uranium complexes bearing σ-bonded hydrocarbyl ligands are limited to Evans' bis(metallocene) [Cp*$_2$UMe(THF)][MeBPh$_3$] (U−$C_{Me}$ = 2.39(1) Å),[235] and Diaconsecu's 1,1′-diamidoferrocene species [(FcNN)U(CH$_2$Ph)(OEt$_2$)][BPh$_4$] (FcNN = {Fe(C$_5$H$_4$NSi$^t$BuMe$_2$)$_2$}$^{2-}$; U−$C_{benzyl}$ = 2.48(1) Å)[183] (**a** and **b** in Figure 3.2).

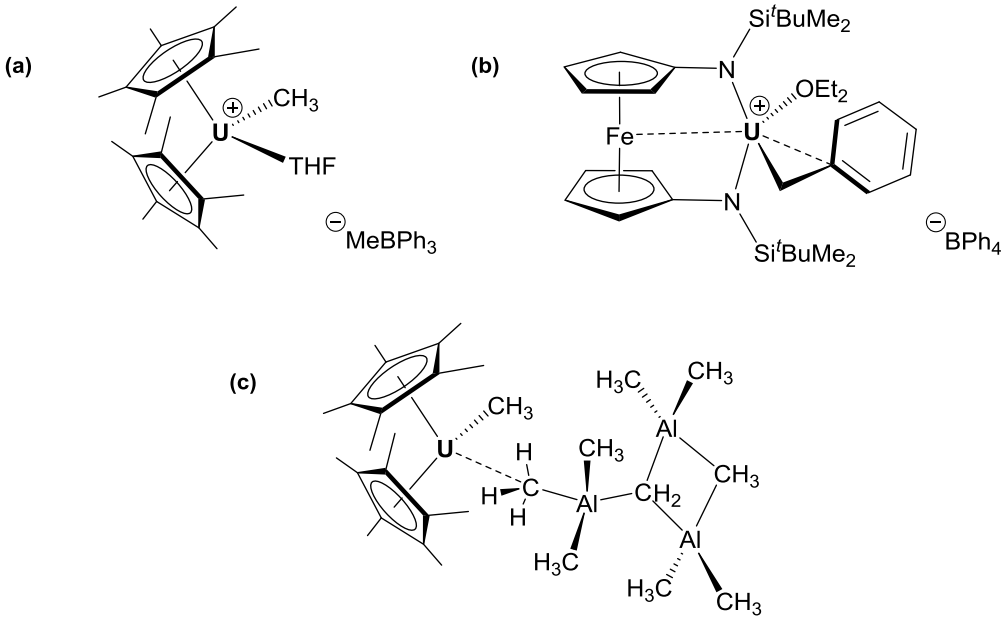

**Figure 3.2** – Cationic monoalkyl uranium complexes (**a**) [Cp*$_2$UMe(THF)][MeBPh$_3$] and (**b**) [(FcNN)U(CH$_2$Ph)(OEt$_2$)][BPh$_4$], and contact ion-pair (**c**) [Cp*$_2$UMe(μ-Me){Al$_3$Me$_6$(μ$_3$-CH$_2$)(μ$_2$-CH$_3$)}] (*vide infra*).

The U−C$_{alkyl}$ bond distance in **6** (2.365(3) Å) is comparable to the analogous U−C distance in Evans' bis(metallocene) complex [Cp*$_2$UMe(THF)][MeBPh$_3$]; although the metallocene species features a coordinated external Lewis base (U−O$_{THF}$ = 2.419(8) Å), cation **6** similarly features coordination of a diarylether donor, in this case provided by the XA$_2$ ligand, which is bound through a comparable U−O distance (U−O$_{xanthene}$ = 2.441(2) Å). Interestingly, neutral dialkyl **3** also features comparable U−C bond distances relative to that of Evan's [Cp*$_2$UMe(THF)]$^+$ cation (U−C = 2.368(7)−2.418(7) Å in **3**), which is likely a consequence of increased steric congestion- and electronic saturation in Evans' 18-electron bis(metallocene) cation relative to the formally 12-electron dialkyl [(XA$_2$)U(CH$_2$SiMe$_3$)$_2$] (**3**). In the case of Diaconescu's diamidoferrocene cation [(FcNN)U(CH$_2$Ph)(OEt$_2$)][BPh$_4$], the nature of the hydrocarbyl ligand is primarily responsible for the significantly longer U−C bond distance (2.48(1) Å) relative to that of **6**, as U−C$_{benzyl}$ bond distances are generally elongated relative to U−C$_{aliphatic}$ bonds. For example, the U−C$_{benzyl}$ bond distances of 2.451(4) and 2.462(3) Å in [(XA$_2$)U(CH$_2$Ph)$_2$] (**5**), and 2.467(5) and 2.489(5) Å in [Cp*$_2$U(CH$_2$Ph)$_2$][125] are significantly longer than the respective U−C$_{alkyl}$ bonds in bis((trimethylsilyl)methyl) complex **3** (U−C = 2.368(7)−2.418(7) Å) and dimethyl [Cp*$_2$UMe$_2$] (U−C$_{Me}$ = 2.414(7), 2.424(7) Å).[125] As an additional point, while the U−C$_{benzyl}$ bond of cationic [(FcNN)U(CH$_2$Ph)(OEt$_2$)]$^+$ (U−C = 2.48(1) Å) is only modestly contracted relative to those of the neutral dibenzyl

precursor [(FcNN)U($CH_2Ph)_2$] (U−C = 2.483(4), 2.515(4) Å),[233] most notably, the hapticity of the benzyl ligand is more pronounced in the cationic derivative. This reinforced benzyl π-coordination appears to be the most prominent structural consequence of rendering dibenzyl actinide complexes cationic by means of abstracting a benzyl ligand, rather than significant An−C bond contraction.[179]

Evans and co-workers also reported the 'pseudo-cationic' uranium alkyl species [Cp*****$_2$UMe(μ-Me){$Al_3Me_6$(μ$_3$-$CH_2$)(μ$_2$-$CH_3$)}],[203] the product of the reaction between neutral dimethyl [Cp*****$_2$$UMe_2$] and excess $AlMe_3$, which may be viewed as a contact ion-pair featuring a trimetallic organoaluminum anion {$Al_3Me_6$(μ$_3$-$CH_2$)(μ$_2$-$CH_3$)$_2$}$^-$ coordinated to a cationic [Cp*****$_2$UMe]$^+$ fragment *via* one of the bridging methyl groups (**c** in Figure 3.2, *vide supra*). The U−C bond distance in cation **6** (2.365(3) Å) is marginally shorter than the terminal U−$C_{Me}$ bond distance (2.395(6) Å) of the contact ion-pair, likely a consequence of increased steric hindrance- and electronic saturation in the bis(metallocene) complex relative to **6**, in large part due to coordination of the organoaluminum anion.

The U–$C_{alkyl}$ distances in cationic **6** and neutral **3** are very similar, despite the increased electrophilicity of **6**, most likely due to additional steric pressure from the coordinated arene in **6**. Suggestive of such a steric effect, the apical (trimethylsilyl)methyl ligand in **6** is bent towards the plane of the xanthene backbone with an acute O−U−$C_{apical}$ angle of 87.26(8)°, compared to O−U−$C_{apical}$ angles of 94.8(2)° and 95.0(2)° in the two crystallographically independent molecules in the unit cell of **3**. Additionally, the U(1)−C(48)−Si(1) angle of 133.7(2)° in **6** is considerably expanded relative to the ideal

109.5° angle, which strongly suggests that the alkyl group is engaged in α-agostic C−H−U interactions[60,162], a bonding consideration that was observed crystallographically for cationic **6-Th** (Th−C−Si = 131.0(2)°), neutral **3-Th** (Th−C−Si = 126.8(3)-127.6(3)°), and **3** (U−C−Si = 128.2(3)-130.8(3)°), as well as spectroscopically for **3-Th**, **6-Th** and **7-Th**.

Likely due to increased electrophilicity of the cationic U centre, the $XA_2$ ligand is bound to cation **6** through shortened U−N and U−O bonds compared to those of the neutral dialkyl precursor, with U−N distances of 2.224(2) and 2.236(2) Å (cf. 2.261(5) −2.280(5) Å in neutral **3**) and a U−O distance of 2.441(2) Å (cf. 2.484(5)−2.504(4) Å in neutral **3**). Although the donor atoms of $XA_2$ are drawn closer to the U centre in **6**, the xanthene backbone is bent to a similar extent as that in neutral dialkyl **3**, with an angle between the two aryl rings of the backbone of 18.9° (cf. 17.5-18.8° in neutral **3**).

Single crystal X-ray diffraction on **7**·toluene revealed a similar solvent-separated ion pair (Figure 3.3; Table 3.2) with approximate $C_s$ symmetry, pseudo square-pyramidal geometry (if the arene is viewed as the occupant of a single coordination site), and an axially-positioned (trimethylsilyl)methyl ligand. However, coordinated toluene in **7** is rotated approximately 30° relative to coordinated benzene in cation **6**, so that the $C_{ipso}$−$C_{methyl}$ bond of toluene lies approximately in the plane of symmetry for the molecule, presumably to minimize unfavourable steric interactions with the flanking 2,6-diisopropylphenyl groups. Furthermore, toluene in **7** is much less symmetrically bound than benzene in **6**, as demonstrated by the relatively shorter U−$C_{para}$ (3.05(2) Å) and U−$C_{meta}$ (3.36(2) Å and 3.13(2) Å) bonds, and relatively longer U−$C_{ortho}$ (3.47(2) and

3.70(2) Å) and U−$C_{ipso}$ (3.78(2) Å) distances, leading to an expanded U−centroid distance of 3.14 Å, and a hapticity between $\eta^3$ and $\eta^4$.

The U−N (2.21(1) and 2.22(1) Å), U−O (2.417(9) Å) and U−$C_{alkyl}$ (2.36(2) Å) bond lengths, and the U(1)−C(48)−Si(1) (136.8(7)°) and O−U−$C_{alkyl}$ (88.8(4)°) angles in **7** are very similar to those in benzene-coordinated **6**, suggesting that although toluene is a superior donor, the steric inability of the bulkier arene to achieve an $\eta^6$-coordination mode limits the electron density it can provide the metal centre, resulting in a similarly electrophilic cation. However, in contrast to the bent xanthene backbone (18.9°) of cation **6**, the angle between the two aryl rings of the ligand backbone of **7** is considerably more acute (5.9°), likely to accommodate the bulky methyl substituent of the toluene ligand in **7**. The relatively planar backbone in **7** allows for the two isopropyl groups protecting the apical site *trans* to the (trimethylsilyl)methyl ligand to be significantly farther apart than those of cation **6**; the shortest of the two $Me_2HC\cdots CHMe_2$ distances (C(45)···C(30)) in **7** is 5.29 Å vs. 4.53 Å in **6**, which affords less steric hindrance to the methyl substituent of toluene.

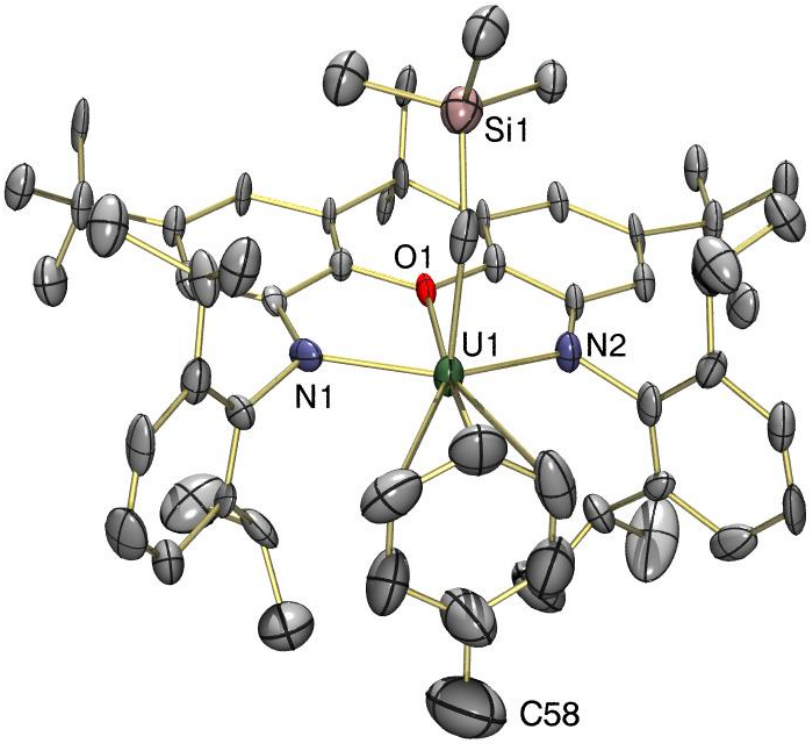


**Figure 3.3** – X-ray crystal structure of $[(XA_2)U(CH_2SiMe_3)(\eta^3\text{-}C_6H_5Me)][B(C_6F_5)_4]\cdot$toluene (**7**·toluene), with thermal ellipsoids at 50% probability. Hydrogen atoms, the borate anion and a non-coordinated toluene solvent molecule are omitted for clarity. Ar–*C*H$Me_2$ atoms numbered clockwise from the top left of the figure: C(42), C(33), C(45), C(30).

Other structurally characterized uranium(IV) complexes featuring intermolecular[236] interactions with a neutral arene are limited to Cotton's hexamethylbenzene species, dimetallic $[\{(\eta^6\text{-}C_6Me_6)UCl_2\}_2(\mu\text{-}Cl)_3][AlCl_4]$, and trimetallic $[\{(\eta^6\text{-}C_6Me_6)UCl_2(\mu\text{-}Cl)_3\}_2(UCl_2)]$, with U−$C_{mean}$ bond distances of 2.92 and 2.94 Å, and U−Centroid (average) distances of 2.55 and 2.58 Å, respectively.[237] The U−$C_{arene}$ bond distances in cations **6** and **7** are significantly longer than those reported by Cotton, likely due to the decreased donor ability of toluene and benzene relative to

hexamethylbenzene, and the flanking 2,6-diisopropylphenyl groups in the $XA_2$ complexes, which limit the approach of the coordinated arene to uranium. The thorium analogue of **7**, **7-Th**, was not structurally characterized. However, Emslie and co-workers previously reported toluene-coordinated $[(XA_2)Th(CH_2Ph)(\eta^6\text{-}C_6H_5Me)][B(C_6F_5)_4]$ (**9-Th**; Figure 3.4), which features a multi-hapto π-coordinated benzyl group in place of a (trimethylsilyl)methyl group, and in this cation, the arene occupies an axial rather than an equatorial position, and the Th–$C_{toluene}$ distances span a narrower range (3.063(5) to 3.435(6) Å) than those in **7**, leading to a substantially shorter An–centroid distance of 2.94 Å.[179]

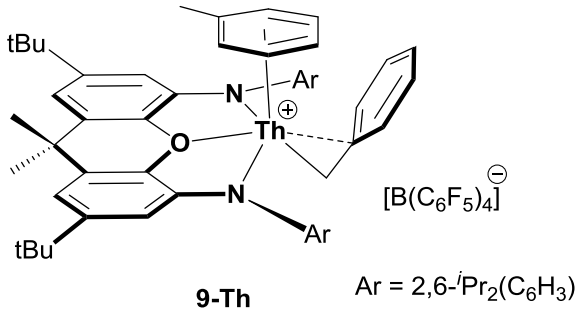


**Figure 3.4** – Previously reported $[(XA_2)Th(CH_2Ph)(\eta^6\text{-}C_6H_5Me)][B(C_6F_5)_4]$ (**9-Th**).

Once isolated in crystalline form, cations **6** and **7** suffer from very poor solubility in either benzene or toluene, and as such, $^1$H NMR spectra were recorded in bromobenzene-$d_5$, in which both cations dissolve readily. Unexpectedly, the major signals in the room-temperature $^1$H NMR spectra of **6** and **7** are effectively identical, consisting of sixteen paramagnetically shifted and broadened signals ranging from +80 to −41 ppm. This collection of resonances is evincive of a top-bottom asymmetric $XA_2$-uranium(IV)

monoalkyl fragment of approximate $C_s$ symmetry in solution, consistent with the solid-state structures of both cations. However, the presence of approximately three equivalents of free proteo-benzene (from **6**) or proteo-toluene (from **7**) in solution suggests that the uranium-bound proteo-arenes are largely liberated upon dissolution in $C_6D_5Br$, generating $[(XA_2)U(CH_2SiMe_3)(C_6D_5Br)][B(C_6F_5)_4]$ (**8**; Scheme 3.2) *in situ* as the major product, in which bromobenzene may be π-coordinated or $\kappa^1$-coordinated via bromine; *vide infra*.[§]

**Scheme 3.2** – Generation of $C_6D_5Br$-coordinated cation **8** *in situ* ($[B(C_6F_5)_4]^-$ anions are omitted, and although bromobenzene is depicted as π-coordinated, $\kappa^1$-coordination *via* bromine cannot be ruled out).

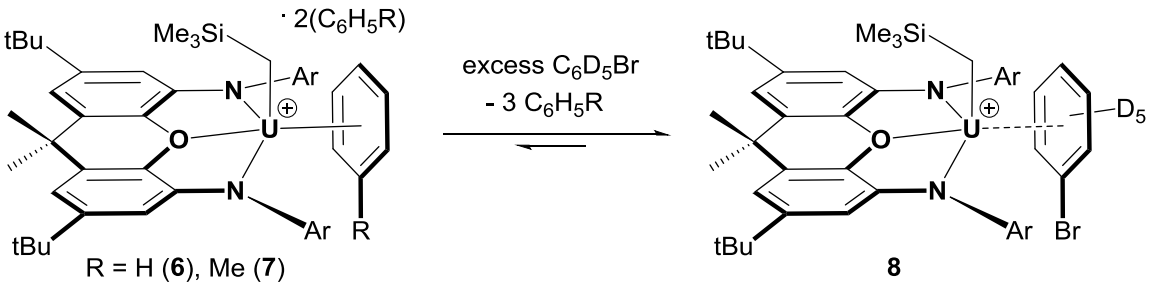


Given the poor donor ability of bromobenzene, a sample of **8**, prepared by dissolution of benzene-coordinated **6** in $C_6D_5Br$, was spiked with 100 equivalents of benzene-$d_6$. This yielded 16 new major resonances that are slightly shifted relative to

[§] Although facial, multi-hapto $C_6D_5Br$ coordination is believed predominant, a broad, low-intensity (<10%) resonance at 5.50 ppm present in the $^1H$ NMR spectrum of bromobenzene-bound cation **8** is speculatively assigned to the C*Me*$_3$ groups of the $\kappa^1$-halogen-coordinated isomer, $[(XA_2)U(CH_2SiMe_3)(\kappa^1\text{-}BrC_6D_5)][B(C_6F_5)_4]$. The resonance is present if cation **8** is derived from either the toluene- or benzene-bound cation in solution, and is entirely washed out upon addition of benzene-$d_6$/toluene-$d_8$.

those for **8**, ranging from +80 to −40 ppm, indicating that the equilibrium has been driven nearly entirely towards $[(XA_2)U(CH_2SiMe_3)(\eta^6\text{-}C_6D_6)][B(C_6F_5)_4]$ (**6-*d*$_6$**), consistent with the superior donor ability of benzene relative to bromobenzene.

The $^1$H NMR signal for coordinated benzene in **6** was located at −29.43 ppm by addition of excess proteo benzene to a solution of **6** in $C_6D_5Br$. This assignment was validated by independently synthesizing and isolating the deuterobenzene-coordinated cation, **6-*d*$_6$**, which gave rise to a lone $^2$H NMR resonance at −29.8 ppm in a $C_6H_5Br$ solution spiked with 5 additional equiv of $C_6D_6$. Furthermore, this $^2$H NMR signal was completely eliminated upon subsequent addition of 100 equiv of proteo-benzene (Figure 3.5).

As described above for cation **6**, **8** is the dominant product in the $^1$H NMR spectrum once toluene-coordinated **7** is dissolved in $C_6D_5Br$. However, these signals are accompanied by an additional collection of signals that are in most cases highly similar to those of **8**, but with significantly less intensity (~20%). These signals were identified as belonging to $[(XA_2)U(CH_2SiMe_3)(\eta^3\text{-}C_6H_5Me)][B(C_6F_5)_4]$ (**7**) by addition of 100 equiv of toluene-$d_8$ to the $C_6D_5Br$ solution, resulting in an increase in the intensity of these signals (excluding those for coordinated $C_6H_5CH_3$) to give 16 unique resonances ranging from +79 to −38 ppm, with concomitant loss of signals due to **8**. The binding preferences of the "$[(XA_2)U(CH_2SiMe_3)]^+$" cation can be deduced to follow the order: toluene ≈ benzene >> bromobenzene, in line with the donor abilities of the arenes.[238]

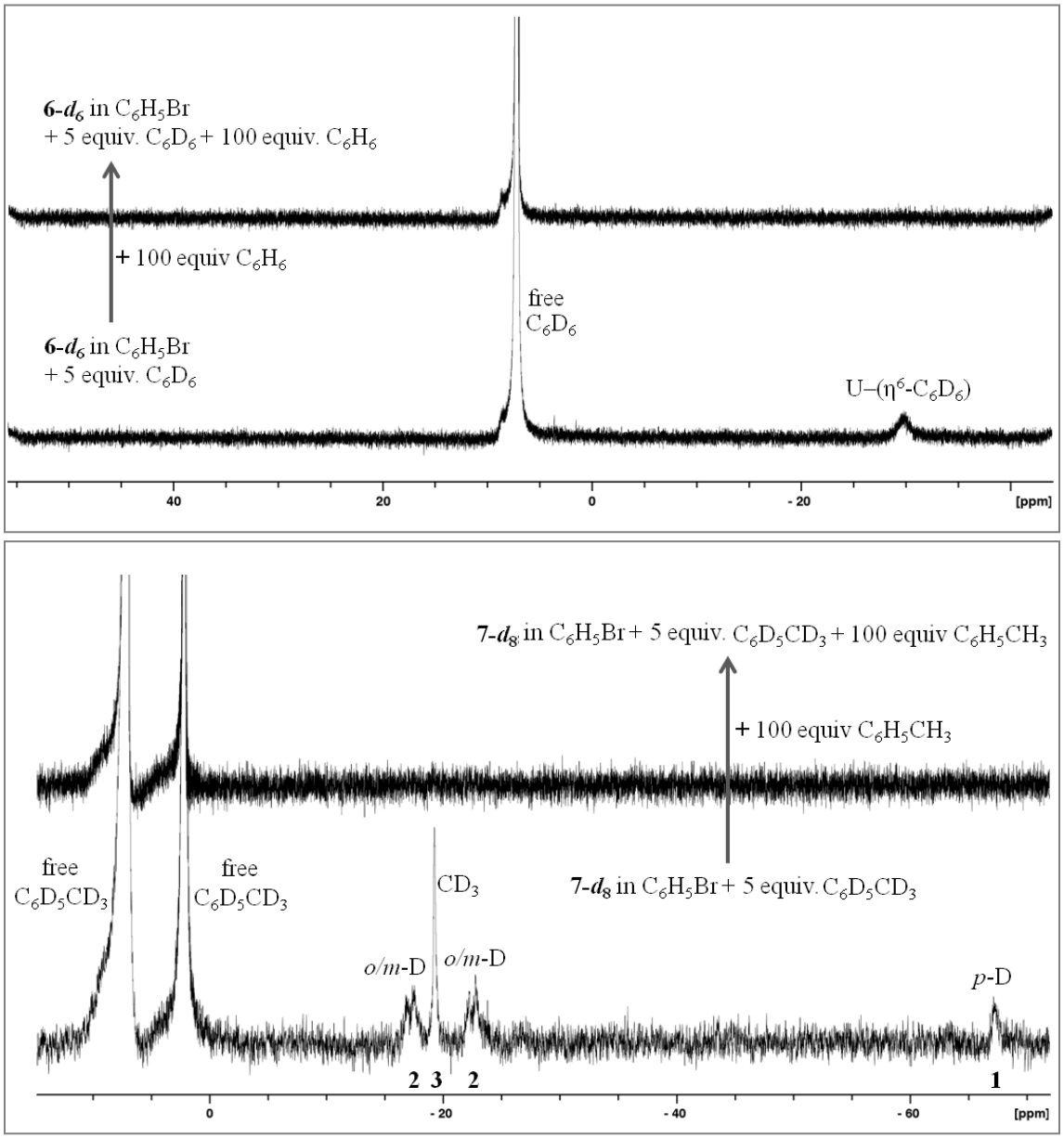


**Figure 3.5 –** $^2$H NMR spectra showing displacement of coordinated $C_6D_6$ in **6-*d*$_6$** by addition of excess $C_6H_6$ (top), and displacement of coordinated $C_6D_5CD_3$ in **7-*d*$_8$** by addition of excess $C_6H_5Me$ (bottom). Numbers below the baseline indicate the relative integrations of each signal.

To identify the resonances arising from the coordinated toluene ligand of cation **7**, the deuterotoluene-coordinated cation, **7-*d*$_8$**, was isolated and subjected to $^2$H NMR spectroscopy. Four deuterium resonances at −17.4, −19.2, −22.7, and −67.1 ppm were observed in the $^2$H NMR spectrum of **7-*d*$_8$** in $C_6H_5Br$ solution spiked with 5 equiv of toluene-$d_8$, arising from the four chemically unique environments of the coordinated $C_6D_5CD_3$ ligand. These resonances exhibit the appropriate relative integrations of 2:3:2:1, respectively, and correlate very well to four previously unassigned low-intensity resonances in the $^1$H NMR spectrum of **7** in pure $C_6D_5Br$.[§] Introduction of 100 equiv of proteo-toluene resulted in displacement of the bound $C_6D_5CD_3$ ligands in solution, entirely eliminating the deuterium resonances for coordinated $C_6D_5CD_3$ in the $^2$H NMR spectrum of **7** (Figure 3.5).

The identity of the coordinated arene appears to have only a minimal effect on the $^1$H NMR spectral signature of cationic **6-*d*$_6$**, **7-*d*$_8$** and **8**, suggesting that the arenes in all three complexes are π-coordinated in solution; for bromobenzene-coordinated **8**, a hapticity similar or less than that in the toluene-coordinated cation **7** may be anticipated due to the presence of the bulky bromine substituent, and reduced donor ability of bromobenzene. Although $\kappa^1$-coordination of haloarenes via the halogen is more typical[239], Piers and Hayes *et al.* demonstrated that bromobenzene is capable of facial multi-hapto coordination to cationic $d^0$ metal centres bearing hydrocarbyl ligands, as observed in the

[§] The four $^1$H NMR resonances assigned to coordinated $C_6H_5CH_3$ of cation **7** were observed at −17.05, −19.20, −22.63, and −67.53 ppm.

scandium(III) β-diketiminate complex [(nacnac)Sc(Me)($\eta^6$-$C_6H_5Br$)][$B(C_6F_5)_4$] (nacnac = {$CH(CMeNAr)_2$}$^-$, Ar = 2,6-$^i$Pr$_2$C$_6$H$_3$)[238,240] (Figure 3.6).

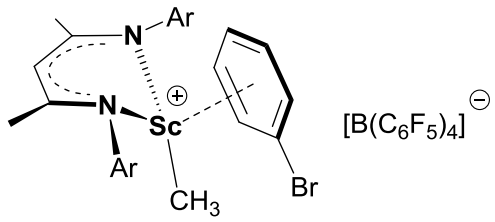


**Figure 3.6** – Piers and co-workers' Scandium(III) bromobenzene complex [(nacnac)Sc(Me)($\eta^6$-$C_6H_5Br$)][$B(C_6F_5)_4$].

$^1$H NMR spectroscopic observation of uranium-coordinated $C_6X_6$ and $C_6X_5CX_3$ (X = H or D) in the presence of excess of $C_6X_6$ and $C_6X_5CX_3$, respectively, demonstrates that degenerate exchange between free and coordinated benzene or toluene is slow on the NMR timescale at room temperature. This behaviour mirrors that of Emslie's [$(XA_2)Th(CH_2SiMe_3)(\eta^x$-$C_6H_5Me)$][$B(C_6F_5)_4$] (**7-Th**) in $C_6D_5Br$ in the presence of 6 equiv of free toluene, for which well-separated $^1$H and $^{13}$C NMR resonances were observed for free and coordinated toluene, with corresponding exchange cross peaks in the 2D EXSY NMR spectrum. However, for **7-Th** in $C_6D_5Br$ at the same concentration, no signals due to a bromobenzene-coordinated cation were observed, indicating that the equilibrium between a toluene- and a bromobenzene-coordinated cation lies substantially further towards the former in the case of thorium than uranium.[§]

[§] For the benzene-coordinated thorium alkyl cation **6-Th**, overlap between the resonances for coordinated benzene and $XA_2$, "$Ph_3CCH_2SiMe_3$", $Ph_3CH$, and $CPh_3^+$ signals prevented detailed analysis; see: Cruz, C. A.; Emslie, D. J. H.; Robertson, C. M.; Harrington, L. E.; Jenkins, H. A.; Britten, J. F. *Organometallics* **2009**, *28*, 1891.

In bromobenzene-$d_5$ solutions of **6** and **7**, the predominant cationic species, bromobenzene-bound **8**, is thermally stable for weeks at room temperature, and can tolerate heating at 60 °C for at least one hour with minimal decomposition. However, further heating at 80 °C resulted in gradual decomposition over the course of 8 hours, yielding a mixture of unidentified paramagnetic products and $SiMe_4$ as the predominant by-product. The thermal stability profile of cation **8** is remarkably similar to that of its neutral dialkyl precursor **3**, which slowly decomposes at 80 °C over the course of ~ 24 hours. The high thermal integrity of **8** in solution likely stems from the judiciously positioned steric bulk of the rigid $XA_2$ ligand combined with increased coordinative saturation through bromobenzene coordination, as cationic derivatives tend to suffer from deteriorated thermal stability relative to their neutral precursors.[241]

Complexes **6** and **7** join a collection of considerably rare cationic d- and f-element alkyl species featuring intermolecular interactions with neutral arenes. This small group includes Baird's $[Cp^*M(Me)_2(\eta^6\text{-arene})][MeB(C_6F_5)_3]$ (M = Ti, Zr, Hf; $\eta^6$-arene = $C_6H_6$, $C_6H_5Me$, $C_9H_{12}$, styrene, *m*-xylene, *p*-xylene, anisole),[242] Hursthouse's $[Cp''MR_2(C_6H_5Me)][RB(C_6F_5)_3]$ (Cp" = 1,3-bis(trimethylsilyl)cyclopentadienyl; M = Zr, R = Me; M = Hf, R = Me, Et),[243] McConville's bis(amido) complexes $[\{CH_2(CH_2NAr)_2\}Ti(Me)(C_6H_5Me)][MeB(C_6F_5)_3]$ (Ar = 2,6-$^i$Pr$_2$C$_6$H$_3$; 2,6-Me$_2$C$_6$H$_3$),[244,245] Marks' 'tuck-in' complex $[\{Me_2Si(\eta^5,\eta^1\text{-}C_5Me_3CH_2)(^t BuN)\}Ti(C_6H_5Me)][B(C_6F_5)_4]$,[246] Schrock's dimeric cyclometalated complex $[\{(MesNCH_2CH_2)NMe(CH_2CH_2)N(\eta^1\text{-Mes})\}Zr]_2[B(C_6F_5)_4]_2$,[247] Piers' β-diketiminato complexes $[(nacnac)Sc(Me)(\eta^6\text{-arene})][B(C_6F_5)_4]$ (nacnac = $CH(CMeNAr)_2$,

Ar = 2,6-$^{i}$Pr$_2$C$_6$H$_3$; $\eta^6$-arene = $C_6H_6$, $C_6H_5Me$, 1,3,5-$Me_3C_6H_3$, $C_6H_5Br$),[238,240] and [(nacnac)YR($\eta^6$-$C_6H_5NMe_2$)][B($C_6F_5$)$_4$] (R = $CH_3$; $CH_2SiMe_2Ph$),[248] and Emslie's thorium(IV) $XA_2$ complexes [($XA_2$)Th($CH_2SiMe_3$)($\eta^x$-$C_6H_5R$)][B($C_6F_5$)$_4$] (R = H (**6-Th**) or Me (**7-Th**)) and [($XA_2$)Th($CH_2Ph$)($\eta^6$-$C_6H_5Me$)][B($C_6F_5$)$_4$] (**9-Th**).[179]

The scarcity of isolated cationic σ-bound hydrocarbyl complexes featuring coordinated neutral arenes may be a consequence of low thermal stability, or the requirement to eliminate or sterically block all molecules of superior donor ability, including donor solvents (e.g. $OEt_2$ or THF), donating reaction byproducts (e.g. $NMe_2Ph$ formed when [$HNMe_2Ph$][B($C_6F_5$)$_4$] is used for alkyl abstraction; **a** in Figure 3.7),[249] remaining neutral polyalkyl precursor complex (e.g. [($\eta^5$-$C_5H_3Me_2$-1,2)$_2$$ZrMe_2$] or [(BDPP)Th($CH_2Ph$)$_2$] which react with the mono(hydrocarbyl) cation to afford a dimetallic monocation; **b-c** in Figure 3.7),[179,201] and cation–anion interactions that can lead to contact ion-pairs such as [($XA_2$)Th($CH_2Ph$)][$PhCH_2B(C_6F_5)_3$],[179] [(nacnac)Sc($CH_2SiMe_2CH_2SiMe_3$)][$MeB(C_6F_5)_3$],[250] and [$Cp^{TMS}$Sc{$CH_2$($C_6H_4$-*o*)$NMe_2$}][B($C_6F_5$)$_4$][251] ($Cp^{TMS}$ = {($SiMe_3$)$C_5Me_4$)}$^-$) (**d-f** in Figure 3.7).

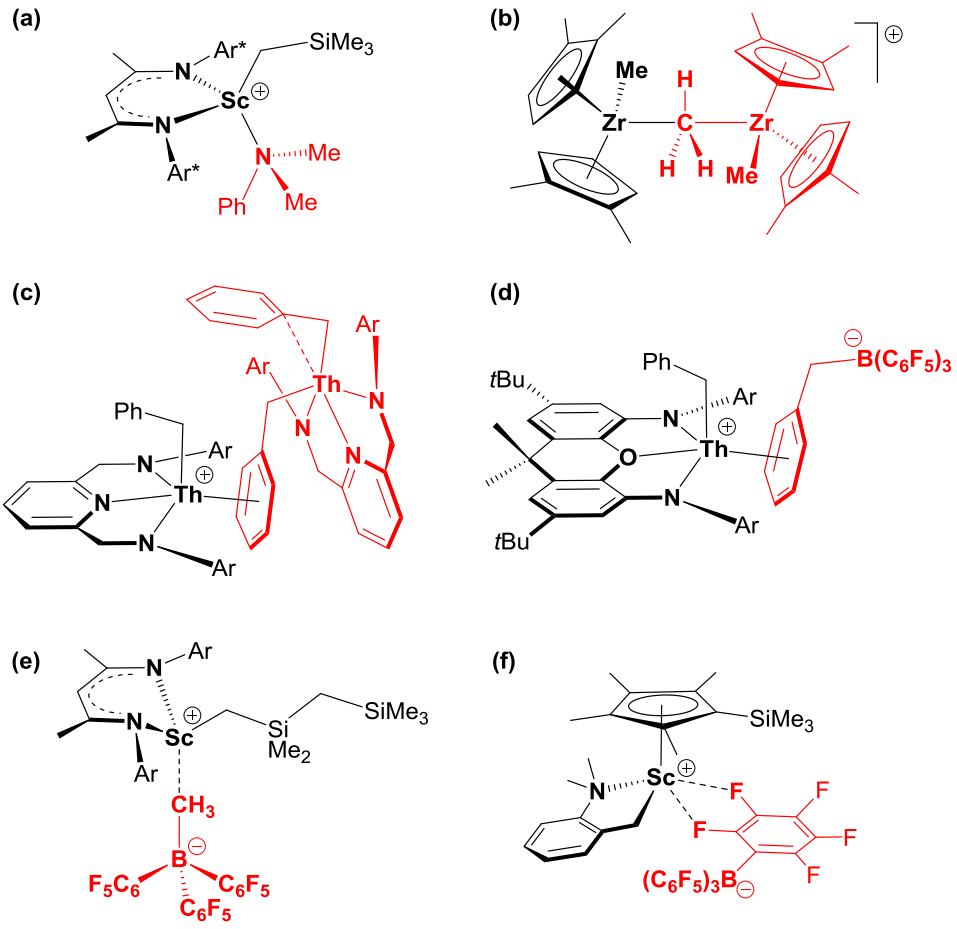


**Figure 3.7** – Cationic metal alkyl complexes coordinated to a) *N*,*N*-dimethylaniline, b) and c) a neutral bis(hydrocarbyl) precursor molecule, and (d-f) a weakly coordinating $RB(C_6F_5)_3$ anion: (**a**) $[(nacnac^*)Sc(CH_2SiMe_3)(NMe_2Ph)][B(C_6F_5)_4]$ (nacnac* = $\{CH(CMeNAr^*)_2\}^-$; Ar* = 3,5-bis(2,4,6-triisopropylphenyl)phenyl), (**b**) $[\{(\eta^5\text{-}C_5H_3Me_2\text{-}1,2)_2ZrMe\}_2(\mu\text{-}Me)][MeB(C_{12}F_9)_3]$ ($C_{12}F_9$ = 2-perfluorobiphenyl), (**c**) $[(BDPP)Th(\eta^2\text{-}CH_2Ph)(\mu\text{-}\eta^1\text{:}\eta^6\text{-}CH_2Ph)Th(\eta^1\text{-}CH_2Ph)(BDPP)][B(C_6F_5)_4]$ (BDPP = 2,6-bis(2,6-diisopropylanilidomethyl)pyridine), (**d**) $[(XA_2)Th(CH_2Ph)][PhCH_2B(C_6F_5)_3]$, (**e**) $[(nacnac)Sc(CH_2SiMe_2CH_2SiMe_3)][MeB(C_6F_5)_3]$ (nacnac = $\{CH(CMeNAr)_2\}^-$; Ar = 2,6-diisopropylphenyl), and (**f**) $[Cp^{TMS}Sc\{CH_2(C_6H_4\text{-}o)NMe_2\}][B(C_6F_5)_4]$.

### 3.3 – Cationic $XA_2$ Uranium(IV) Monoalkyl Fluorobenzene Complexes and Ethylene Polymerization

In generating cationic derivatives of neutral dialkyl **3**, our goal was to access an electrophilic, low-coordinate uranium(IV) species toward application in ethylene insertion-polymerization catalysis, which remains an underdeveloped capability of actinides. To date, the majority of molecular actinide systems capable of catalyzing olefin polymerization are supported by metallocene (and *ansa*-metallocene) ancillary ligand systems, such as [Cp*****$_2$ThMe][A] (A = weakly-coordinating anion, often a tetra(aryl)borate), largely developed by Marks and co-workers.[110,197,199,200,207,209,210-212] However, reports of post-metallocene systems (complexes supported by non-carbocyclic ancillary ligands) that function as ethylene polymerization catalysts have recently emerged. Leznoff and co-workers reported a variety of neutral uranium(IV) dialkyl complexes[174] [($^{DIPP}$NCOCN)U($CH_2R)_2$] ($^{DIPP}$NCOCN = $\kappa^3$-{($ArNCH_2CH_2)_2O\}^{2-}$, Ar = 2,6-$^i$Pr$_2$C$_6$H$_3$; R = SiMe$_3$, Ph), [($^{tBu}$NON)U($CH_2SiMe_3)_2$], and dimeric [($^{tBu}$NON)U{CH($SiMe_3$)($SiMe_2CH_2$)}]$_2$ ($^{tBu}$NON = $\kappa^3$-{($^t$BuNSiMe$_2)_2O\}^{2-}$) supported by flexible diamido pincer-type ligands that demonstrate modest[252] ethylene polymerization activities ($2.4 \times 10^1 – 5.6 \times 10^2$ g·(mol of U)$^{-1}$·h$^{-1}$·atm$^{-1}$) in hexane solution. Additionally, Eisen and co-workers recently reported that the bis(amidinate) actinide(IV) chloro complexes [(2-pyridylamidinate)$_2$AnCl(μ-Cl)$_2$Li(tmeda)] (2-pyridylamidinate = {($Me_3SiN)_2$C(2-py)}; An = Th, U)[213] can be utilized as precursors to ethylene polymerization catalysts. Activation of the chloro precursors with mixtures of co-catalysts such methylalumoxane (MAO) produced polyethylene with varying efficacy (activities

ranging from $1.1 \times 10^2$ to $1.02 \times 10^4$ g·(mol of An)$^{-1}$·h$^{-1}$·atm$^{-1}$). However, the active, presumably cationic species were not isolated or investigated spectroscopically in either study.

Although these early reports demonstrate the viability of post-metallocene actinide systems in homogeneous ethylene polymerization catalysis, non-carbocyclic actinide species have failed to prove superior to Marks' metallocene complexes, which remain the state-of-the-art in actinide olefin polymerization catalysis. Furthermore, Marks' [Cp*****$_2$ThMe][A] systems remain at least an order-of-magnitude less active than the analogous group 4 transition metal metallocene species (e.g. the activitiy of [Cp*****$_2$ThMe][B(C$_6$F$_4$TBS)$_4$] (TBS = *tert*-butyldimethylsilyl) is $9.2 \times 10^5$ g of polyethylene·(mol of Th)$^{-1}$·h$^{-1}$·atm$^{-1}$) vs. $1.1 \times 10^7$ g·(mol of Zr)$^{-1}$·h$^{-1}$·atm$^{-1}$) for [Cp*****$_2$ZrMe][B(C$_6$F$_4$TBS)$_4$]).[195] However, numerous group 4 transition metal systems supported by non-carbocyclic ancillary ligands have been developed that boast polymerization activities that rival their metallocene counterparts. Gibson and co-workers reported chelating bis(silylamido) complexes of zirconium(IV) which serve as potent ethylene polymerization catalysts upon activation by MAO.[253] A mixture of [(κ$^2$-ArNSiMe$_2$CH$_2$CH$_2$SiMe$_2$NAr)Zr(NMe$_2$)$_2$] (Ar = 2,6-Me$_2$C$_6$H$_3$) and excess MAO in toluene solution was highly productive, demonstrating an activity > $1.0 \times 10^6$ g of polyethylene ·(mol of Zr)$^{-1}$·h$^{-1}$·atm$^{-1}$. In many cases, the development and utilization of non-carbocyclic '*designer ligands*' affords access to considerably low-coordinate and catalytically active metal species (e.g. cationic [(κ$^2$-ArNSiMe$_2$CH$_2$CH$_2$SiMe$_2$NAr)Zr(NMe$_2$)]$^+$ is formally a 6-electron complex vs. 14-

electron $[Cp^*_2ZrMe]^+$), a consideration that warrants further attention in the design of actinide catalysts.

By design, low-coordinate organometallic $XA_2$-uranium(IV) derivatives exhibit bulk features that mirror those of catalytically-active metallocene species, such as $[Cp^*_2ThMe]^+$, which feature robust, unreactive ancillary ligand systems and at least one reactive metal-carbon linkage. Additionally, neutral dialkyl **3** bears resemblance to Leznoff's catalytically active dialkyl complex $[(^{DIPP}NCOCN)U(CH_2SiMe_3)_2]$ (Ar = 2,6-$^iPr_2C_6H_3$)[174] which is supported by a flexible tridentate bis(amido)ether ligand that is analogous to our rigid $XA_2$ ancillary. These design considerations decisively suggest that **3** and derivatives thereof should be capable of catalyzing the insertion-polymerization of ethylene. Toward that objective, 1 millimolar solutions of neutral dialkyl **3** in hexane, and cations **6** and **7** in benzene and toluene, respectively, were exposed to ethylene (1 atm, 20–70 °C). However, in all cases, no polyethylene had been produced after 30 minutes. This behaviour mirrors that of Emslie's previously reported, structurally-analogous cationic thorium(IV) complexes **6-Th** and **7-Th**,[§] which also failed to polymerize ethylene at 1 atm (20–100 °C) in either benzene or toluene solution, likely due to an inability of ethylene to compete with arene solvent for coordination of the cationic actinide centre to initiate and sustain insertion-polymerization. The suppression of polymerization activity due to arene coordination has been previously observed by

[§] Emslie's previously reported complexes **9-Th**, zwitterionic benzylborate-coordinated $[(XA_2)Th(CH_2Ph)][PhCH_2B(C_6F_5)_3]$, and dibenzyl-precursor-coordinated dimer $[(BDPP)Th(CH_2Ph)(\mu\text{-}\eta^1\text{:}\eta^6\text{-}CH_2Ph)Th(CH_2Ph)(BDPP)][B(C_6F_5)_4]$ also failed to polymerize ethylene at 1 atm (20 – 100 °C) in either benzene or toluene solution.

McConville *et al.*,[245] who noted a significant reduction in the 1-hexene polymerization activity of [{$CH_2(CH_2NAr)_2$}$TiMe_2$]/$B(C_6F_5)_3$ (Ar = 2,6-$^i$Pr$_2C_6H_3$; 2,6-$Me_2C_6H_3$) in the presence of small amounts of toluene. The authors hypothesized that competitive binding of toluene to titanium was responsible for the greatly reduced polymerization activities, citing species of the form [{$CH_2(CH_2NAr)_2$}Ti(Me)($C_6H_5Me$)]$^+$. Attempts to carry out alkyl abstraction on **3** in hexane solution to avoid the inclusion of arenes altogether yielded intractable material, and that avenue was not pursued further.

Coordination of arenes to cationic $XA_2$-thorium(IV) and uranium(IV) monoalkyl complexes is a persistent and unavoidable outcome, therefore, in an attempt to render the cationic [($XA_2$)U($CH_2SiMe_3$)($\eta^x$-arene)]$^+$ fragment catalytically active, we sought to weaken the donor ability of the coordinated arene. Piers and co-workers have observed that while the cationic mesitylene-bound scandium(III) complex [(nacnac)Sc(Me)($\eta^6$-1,3,5-$Me_3C_6H_3$)][$B(C_6F_5)_4$] (nacnac = {CH(CMeNAr)$_2$}$^-$, Ar = 2,6-$^i$Pr$_2C_6H_3$, mesitylene = 1,3,5-$Me_3C_6H_3$) demonstrates negligible catalytic activity in toluene, it is an active ethylene polymerization catalyst in more weakly-donating bromobenzene.[240] In that vein, toluene-bound cation **7** was dissolved in $C_6H_5Br$ to generate bromobenzene-bound cation **8** *in-situ*, and the 1 millimolar solution was subsequently exposed to ethylene (1 atm, 20 °C), but after 30 minutes no polyethylene was produced. As we have observed that the proteo-arene ligands of cations **6** and **7** are nearly fully liberated upon dissolution in $C_6H_5Br$ to yield the bromobenzene-bound complex **8**, it appears that ethylene cannot compete with bromobenzene for the active site, and the potential catalytic activity is asphyxiated as a consequence.

In an additional attempt to limit the interaction between the arene ligand and the uranium centre, we conducted the alkyl abstraction of **3** in mesitylene solution (Scheme 3.3). Compared to the π-coordinated toluene ligand of cation **7**, we hypothesized that the additional methyl groups of mesitylene would result in unfavourable interactions between the arene ligand and the steric bulk surrounding the coordination sphere, hindering the approach of the arene as a consequence. Upon addition of one equiv of $[Ph_3C][B(C_6F_5)_4]$ to a mesitylene solution of dialkyl **3**, the mixture became deep brown and an oily, brownish-black solid precipitated which was insoluble in additional mesitylene. Despite numerous attempts at isolating a crystalline product, only intractable material was obtained. Nevertheless, the oily mesitylene suspension was exposed to ethylene (1 atm, 20 °C, 30 min) but unsurprisingly, no polyethylene was detected.

**Scheme 3.3** – Attempted synthesis of the proposed mesitylene-containing monoalkyl uranium(IV) cation.

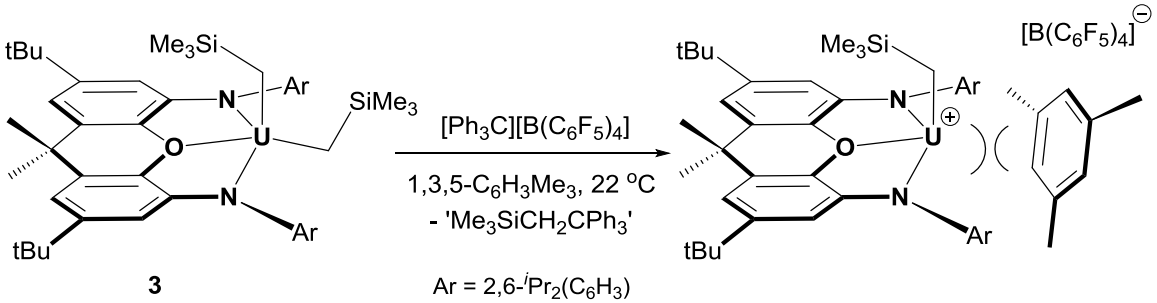


To implant the cationic "$[(XA_2)U(CH_2SiMe_3)]^+$" fragment into an even less coordinatively supportive environment, we conducted alkyl abstraction reactions with **3** in fluoroarene solutions. Upon addition of one equiv of $[Ph_3C][B(C_6F_5)_4]$ to a

fluorobenzene solution of dialkyl **3**, the red solution immediately became deep brown, indicative of cation formation, yielding fluorobenzene-bound $[(XA_2)U(CH_2SiMe_3)(\eta^3\text{-}C_6H_5F)][B(C_6F_5)_4]$ (**10**; Scheme 3.4).

**Scheme 3.4** – Synthesis of monoalkyl uranium(IV) cation **10**.

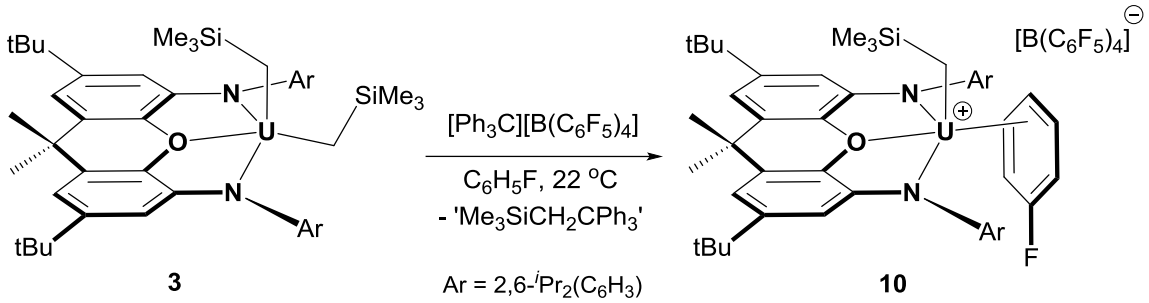


While neutral dialkyl **3** is considerably less soluble in fluoroarenes than in proteo-arenes or ethereal solvents, cationic **10** is highly soluble in fluorobenzene (and 1,2-difluorobenzene, *vide infra*), perhaps unsurprising given the high solubility of cationic $XA_2$-uranium(IV) species in bromobenzene. Layering a concentrated solution of **10** in fluorobenzene with *n*-pentane and cooling to −30 °C resulted in precipitation of **10** as a deep-brown microcrystalline solid in 91% yield. The $^1$H NMR spectrum of cation **10** in $C_6D_5Br$ is relatively uninformative; given the relative strength of arene donor abilities, **10** is converted entirely to bromobenzene-bound cation **8** in solution, with clear indication of one equivalent of free fluorobenzene, and no additional resonances attributable to the original fluorobenzene-containing complex. $^{19}F\{^1H\}$ NMR spectroscopy of **10** in $C_6D_5Br$ is equally inconsequential, revealing resonances attributable to both free fluorobenzene and those of the tetrakis(pentafluorophenyl)borate counteranion, with no additional resonance attributable to coordinated $C_6H_5F$.

Single crystals of **10**·fluorobenzene were grown from fluorobenzene/*n*-pentane at −30 °C; X-ray diffraction revealed a familiar arene solvent-separated ion pair comprised of an approximately $C_s$-symmetric, approximately square-pyramidal uranium(IV) cation (if the arene is viewed as the occupant of a single coordination site) with an axially-positioned (trimethylsilyl)methyl ligand, and a distal tetrakis(perfluorophenyl)borate anion. (Figure 3.8; Table 3.3). Most intriguingly, the fluorobenzene ligand in **10** is π-coordinated to the uranium(IV) cation, and to our knowledge, **10** represents the first crystallographically-characterized f-element complex bearing a π-coordinated fluoroarene ligand. As expected, the $C_{ipso}$−F bond length in **10** (1.357(7) Å) is significantly shorter than the $C_{ipso}$–$C_{methyl}$ distance in **7** (1.46(3) Å), and falls within the range of $C_{ipso}$−F bond distances observed in other crystallographically-characterized π-coordinated fluorobenzene complexes (1.292(3)–1.381(8) Å).[254,255]

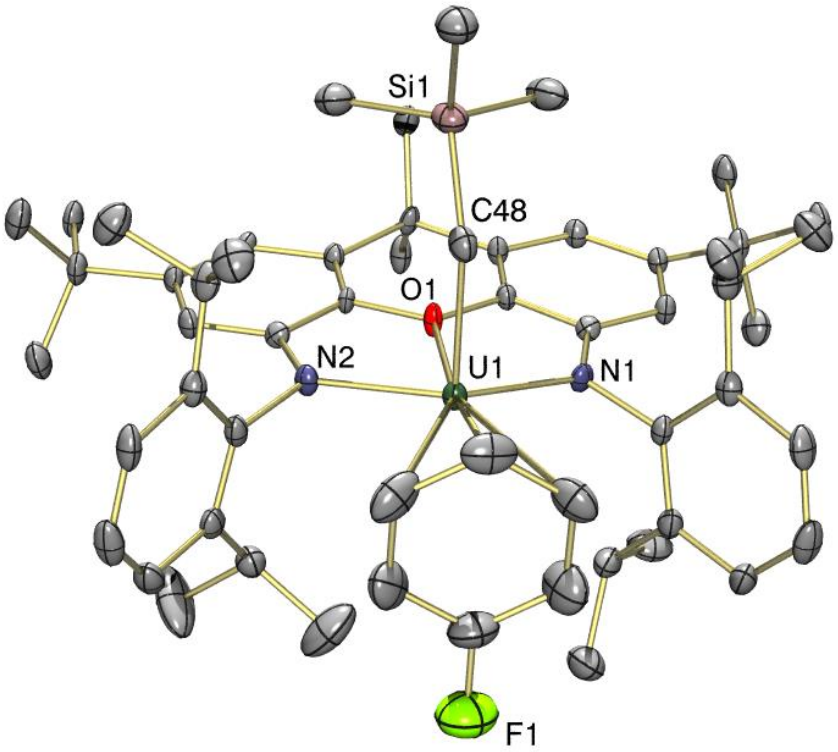


**Figure 3.8** – X-ray crystal structure of $[(XA_2)U(CH_2SiMe_3)(\eta^3\text{-}C_6H_5F)][B(C_6F_5)_4]\cdot$fluorobenzene (**10**·fluorobenzene), with thermal ellipsoids at 50% probability. Hydrogen atoms, the borate anion, and non-coordinated fluorobenzene lattice solvent molecule are omitted for clarity. Ar–*C*H$Me_2$ atoms numbered clockwise from the top left of the figure: C(42), C(33), C(30), C(45).

Structurally, fluorobenzene-bound cation **10** bears resemblance to toluene-bound cation **7**, with U−N and U−$C_{alkyl}$ bond distances in close agreement (Table 3.3), a relatively planar xanthene backbone, and an arene ligand that is limited to sub-$\eta^6$-coordination as a consequence of monosubstitution. The fluorobenzene ligand in **10** is bound so that the C–F bond lies approximately in the plane of symmetry of the molecule, presumably to minimize unfavourable steric interactions with the flanking 2,6-

diisopropylphenyl groups. However, the F-substituent of the fluorobenzene ligand in **10** is significantly smaller than the methyl group of coordinated-toluene in **7** (van der Waals radii: F = 1.47 Å; $CH_3$ group as a whole = 2.0 Å).[256] As a result, the fluorine substituent is able to more intimately approach the sterically congested apical region protected by two isopropyl groups of the $XA_2$ ligand, allowing the fluorobenzene ring to approach the NON-plane in a more perpendicular fashion than toluene (the angle between the plane of the coordinated arene and the NON-plane is 83.4° in **10** and 77.6° in **7**). This results in a slightly longer U−$C_{para}$ distance in **10** (3.129(5) Å vs. 3.05(2) Å in **7**), but allows for a relatively shorter U−Centroid distance (3.08 Å vs. 3.14 Å in **7**) as a consequence of shorter U−$C_{ortho}$ and U−$C_{ipso}$ distances, and a hapticity between $\eta^3$ and $\eta^4$.

**Table 3.3** – Selected bond lengths (Å) and angles (deg) for $XA_2$ cation **10** (vs. **7**).

| Compound | **10** | **7** |
|---|---|---|
| U−O | 2.431(3) | 2.417(9) |
| U−N | 2.215(3), 2.218(3) | 2.21(1), 2.22(1) |
| U−$C_{alkyl}$ | 2.350(4) | 2.36(2) |
| U−$C_{para\ arene}$ | 3.129(5) | 3.05(2) |
| U−$C_{meta\ arene}$ | 3.217(6), 3.299(5) | 3.13(2), 3.36(2) |
| U−$C_{ortho\ arene}$ | 3.437(5), 3.529(5) | 3.47(2), 3.70(2) |
| U−$C_{ipso\ arene}$ | 3.598(6) | 3.78(2) |
| U−Centroid[a] | 3.08 | 3.14 |
| Ligand Bend Angle[b] | 7.2° | 5.9° |
| O−U−$C_{alkyl}$ | 89.6(1)° | 88.8(4)° |
| U−C−Si | 134.8(2) ° | 136.8(7)° |
| $C_{ipso}$−R[c] | 1.357(7) | 1.46(3) |
| N(1)···N(2) | 3.98 | 3.98 |
| C(42)···C(33) | 7.26 | 7.32 |

| | | |
|---|---|---|
| C(30)···C(45) | 5.25 | 5.29 |
| U···R[c] | 4.53 | 4.88 |

[a] Centroid = Centroid of the coordinated arene ring.[b] Ligand Bend Angle = the angle between the two aromatic rings of the xanthene ligand backbone.[c] For cation **10**, R = F; for **7**, R = $CH_3$.

Structurally-characterized complexes featuring coordinated neutral fluoroarene ligands are surprisingly uncommon (selected examples are depicted in Figures 3.9 and 3.10), possibly a consequence of facile fluoroarene-displacement given the limited donor ability of the electron-deficient π-system and the fluorine substituent. Electron-rich transition metals with formal $d^6$ and $d^8$ electronic configurations represent the majority of reported complexes bearing π-coordinated fluoroarene ligands (e.g. **a**–**c** in Figure 3.9),[254,257] but this coordination mode has also been observed in zwitterionic post-transition metal species (**d**),[258] as well as cationic main-group complexes (**e**)[259] where back-donation is unlikely to contribute strongly to the overall stability of the metal-arene interaction.

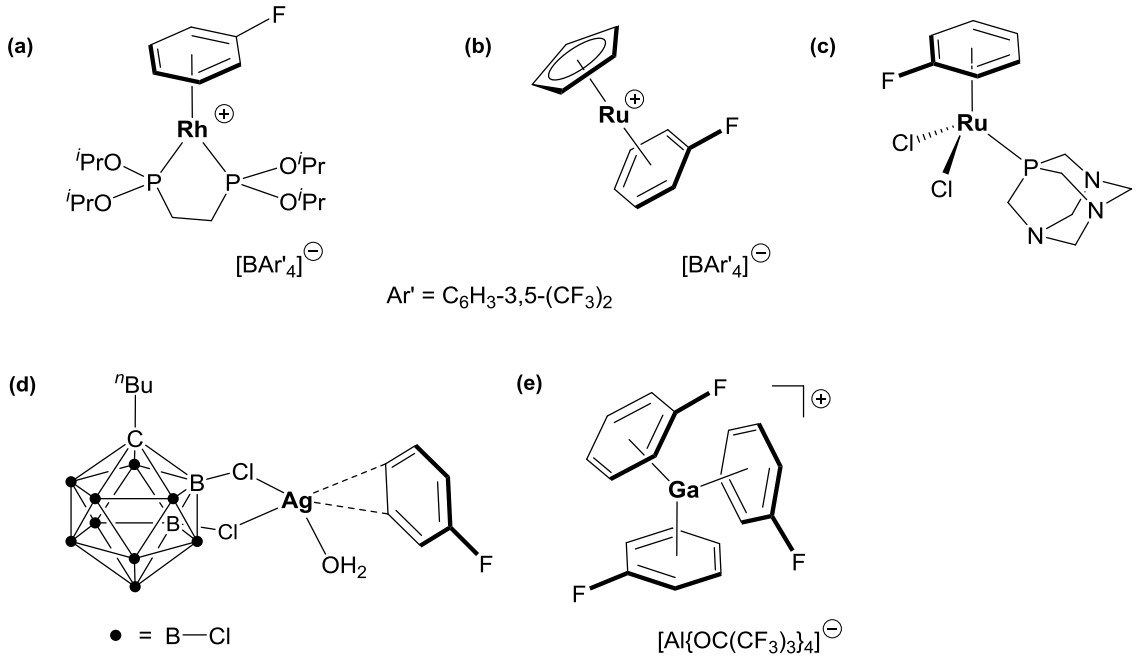


**Figure 3.9** – Selected examples of isolated fluorobenzene complexes. (a) [($\eta^6$-$C_6H_5F$)Rh{($^i$PrO)$_2$PCH$_2$CH$_2$P(O$^i$Pr)$_2$}][BAr′$_4$] (Ar′ = 3,5-(CF$_3$)$_2$C$_6$H$_3$), (b) [CpRu($\eta^6$-$C_6H_5F$)][BAr′$_4$], (c) [($\eta^6$-$C_6H_5F$)RuCl$_2$(pta)] (pta = 1,3,5-triaza-7-phosphaadamantane), (d) [($\eta^2$-$C_6H_5F$)Ag(H$_2$O)][$^n$BuCB$_{11}$Cl$_{11}$], and (e) [($\eta^6$-$C_6H_5F$)$_3$Ga][Al{OC(CF$_3$)$_3$}$_4$].

By contrast, fluoroarenes coordinated to electrophilic early transition metals tend to adopt a $\kappa^1$-*F* coordination mode (e.g. **a–c** in Figure 3.10).[239,260,261] However, Schaverien and co-workers reported a zwitterionic lanthanum alkyl complex[262] (**d** in Figure 3.10) supported by a tetraarylborato ligand [B(*p*-C$_6$H$_4$F)$_4$]$^-$ that is possibly π-coordinated. Characterization of the isolated lanthanum complex is limited to selected $^1$H NMR resonances, not including those for the tetraarylborato ligand, from which little can be gleaned regarding the coordination-mode of the [B(*p*-C$_6$H$_4$F)$_4$]$^-$ ligand. However, a structurally authenticated niobium(I) species [{(*p*-C$_6$H$_4$F)$_2$B($\eta^6$-*p*-C$_6$H$_4$F)$_2$}Nb(C$_2$Me$_2$)]

featuring the $[B(p\text{-}C_6H_4F)_4]^-$ ligand adopting the proposed coordination mode ($\eta^6$-coordination of two fluoroaryl rings) is known.[263]

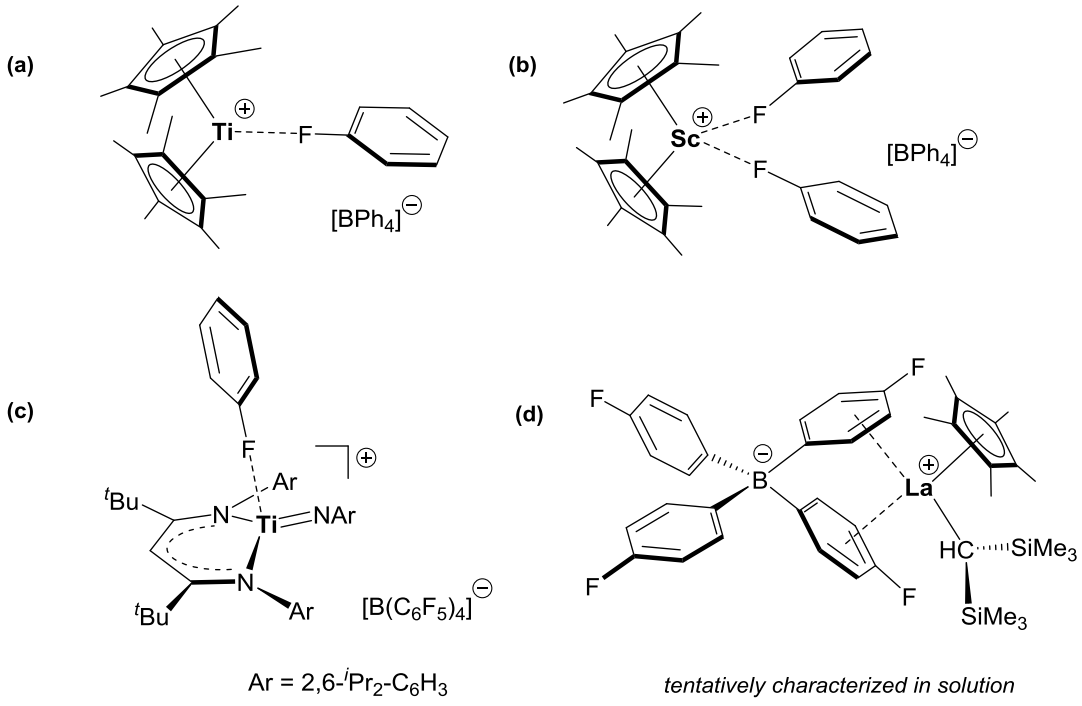


**Figure 3.10** – Selected fluoroarene complexes of electrophilic metals. (a) $[Cp^*_2Ti(\kappa^1\text{-}FC_6H_5)][BPh_4]$, (b) $[Cp^*_2Sc(\kappa^1\text{-}FC_6H_5)_2][BPh_4]$, (c) $[(nacnac)Ti{=}NAr(\kappa^1\text{-}FC_6H_5)][B(C_6F_5)_4]$ (nacnac = $\{CH(C(^tBu)NAr)_2\}^-$; Ar = 2,6-diisopropylphenyl), and (d) $[Cp^*La\{CH(SiMe_3)_2\}\{(\eta^x\text{-}p\text{-}C_6H_4F)_2B(p\text{-}C_6H_4F)_2\}]$.

In the absence of relatively strongly donating arenes such as benzene or toluene, the cationic uranium fragment "$[(XA_2)U(CH_2SiMe_3)]^+$" is expected to exhibit increased electrophilicity, perhaps unlocking latent ethylene polymerization activity. Indeed, upon exposure of a 1 millimolar fluorobenzene solution of cation **10** to ethylene (1 atm, 20 °C), turbidity was observed, and upon quenching with acidified methanol after 30 minutes, 0.032 g of white, solid polyethylene was obtained. This outcome appends an activity of

$1.28 \times 10^4$ g·mol$^{-1}$·h$^{-1}$·atm$^{-1}$ to cation **10**, confirming that the $XA_2$-uranium(IV) system can in fact serve as a platform for ethylene polymerization catalysis (Table 3.4). However, increasing the reaction time to 3 h resulted in a decrease of activity to $3.7 \times 10^3$ g of polyethylene·(mol of U)$^{-1}$·h$^{-1}$·atm$^{-1}$ for **10**, suggestive of either limited catalytic robustness, or increased solution viscosity and catalyst ensnarement in precipitated polyethylene. More consistent with the latter explanation, conducting the reaction at elevated temperature (70 °C) resulted in a 3-fold increase in activity ($3.92 \times 10^4$ g of polyethylene·(mol of U)$^{-1}$·h$^{-1}$·atm$^{-1}$) (Table 3.5). To our knowledge, cation **10** represents the most active uranium ethylene polymerization catalyst supported by a non-carbocyclic ancillary ligand.

Having unearthed catalytic behaviour in fluorobenzene-bound **10**, we broadened our investigation of the $[(XA_2)U(CH_2R)(\eta^x\text{-}C_6H_5F)]^+$ family of cations by attempting to access a cationic derivative of the dibenzyl complex $[(XA_2)U(CH_2Ph)_2]$ (**5**). In fluorobenzene solution, neutral **5** was treated with one equiv of $[Ph_3C][B(C_6F_5)_4]$ to effect abstraction of a single benzyl ligand, as this reagent has been previously utilized successfully to abstract a benzyl group from the analogous thorium(IV) dibenzyl species **5-Th**, yielding the desired cationic monobenzyl species $[(XA_2)Th(CH_2Ph)(\eta^6\text{-}C_6H_5Me)][B(C_6F_5)_4]$ (**9-Th)** under mild conditions.[179] Immediately upon addition, the black-green fluorobenzene solution of **5** became a familiar yellow-brown colour, suggestive of cation formation; the *in-situ* generated cationic species is presumably $[(XA_2)U(CH_2Ph)(\eta^x\text{-}C_6H_5F)][B(C_6F_5)_4]$ (**11**) (Scheme 3.5), with a structure analogous to the toluene-bound thorium(IV) cation **9-Th**.

**Scheme 3.5** – *In-situ* generation of proposed monobenzyl uranium(IV) cation **11**.

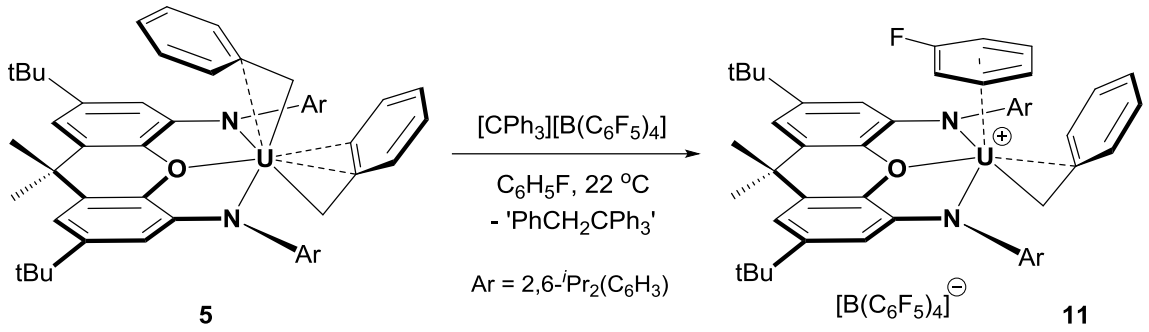


The fluorobenzene solution of *in-situ*-generated cation **11** (1 millimolar) was exposed to ethylene (1 atm, 20–70 °C), but unfortunately, no polyethylene had been produced after 30 minutes. We attribute this catalytic inactivity to the stability imparted to the cationic "$[(XA_2)U(\eta^x\text{-}CH_2Ph)]^+$" fragment by the multi-hapto π-coordination of the lone benzyl ligand. This bonding arrangement was previously observed in **9-Th**,[179] which exhibits a highly acute Th−C−C angle of 83.3(2)°, and short Th–$C_{ortho}$ contacts (3.192(4), 3.293(5) Å) typical of multi-hapto π-coordination, and was also evident in Diaconescu's cationic benzyl complex $[(FcNN)U(CH_2Ph)(OEt_2)][BPh_4]$ (U−C−C = 86.0(7)°).[183]

**Table 3.4 –** Room Temperature Ethylene Polymerization Results.

| Catalyst[a] | Solvent | Yield of PE (g) | Activity[b] |
|---|---|---|---|
| $[(XA_2)U(CH_2SiMe_3)_2]$ (**3**) | hexane | 0 | 0 |
| $[(XA_2)U(CH_2SiMe_3)(\eta^6\text{-}C_6H_6)]^+$ (**6**) | $C_6H_6$ | 0 | 0 |
| $[(XA_2)U(CH_2SiMe_3)(\eta^3\text{-}C_6H_5Me)]^+$ (**7**) | $C_6H_5Me$ | 0 | 0 |
| $[(XA_2)U(CH_2SiMe_3)(1,3,5\text{-}Me_3C_6H_3)]^+$ | $C_9H_{12}$ | 0 | 0 |
| $[(XA_2)U(CH_2SiMe_3)(\eta^x\text{-}C_6H_5Br)]^+$ (**8**)[c] | $C_6H_5Br$ | 0 | 0 |
| $[(XA_2)U(CH_2SiMe_3)(\eta^3\text{-}C_6H_5F)]^+$ (**10**) | $C_6H_5F$ | 0.032 | 12800 |
| $[(XA_2)U(CH_2Ph)(\eta^x\text{-}C_6H_5F)]^+$ (**11**) | $C_6H_5F$ | 0 | 0 |

| | | | |
|---|---|---|---|
| $[(XA_2)U(CH_2SiMe_3)(o\text{-}C_6H_4F_2)]^+$ (**12**) | $o\text{-}C_6H_4F_2$ | 0.028 | 11200 |
| $[(XA_2)U(CH_2SiMe_3)(m\text{-}C_6H_4F_2)]^+$ | $m\text{-}C_6H_4F_2$ | 0 | 0 |
| $[(XA_2)U(CH_2SiMe_3)(C_6F_6)]^+$ | $C_6F_6$ | 0 | 0 |
| $[(XA_2)Th(CH_2SiMe_3)(\eta^x\text{-}C_6H_5F)]^+$ (**10-Th**) | $C_6H_5F$ | 0.042 | 16800 |

[a] Conditions: 0.005 mmol of catalyst (< 10 mg), 5 mL of solvent, 1 atm of ethylene, 20 °C, 30 min. [b] Activities are measured in $g\cdot(mol\ of\ An)^{-1}\cdot h^{-1}\cdot atm^{-1}$. For cationic species, $[B(C_6F_5)_4]^-$ is the counteranion. [c] Bromobenzene-bound complex **4** was generated *in-situ* by dissolving toluene-bound complex **3** in $C_6H_5Br$.

**Table 3.5 –** High Temperature (70 °C) Ethylene Polymerization Results.

| Catalyst[a] | Solvent | Yield of PE (g) | Activity[b] |
|---|---|---|---|
| $[(XA_2)U(CH_2SiMe_3)(\eta^6\text{-}C_6H_6)]^+$ (**6**) | $C_6H_6$ | 0 | 0 |
| $[(XA_2)U(CH_2SiMe_3)(\eta^3\text{-}C_6H_5F)]^+$ (**10**) | $C_6H_5F$ | 0.098 | 39200 |
| $[(XA_2)U(CH_2Ph)(\eta^x\text{-}C_6H_5F)]^+$ (**11**) | $C_6H_5F$ | 0 | 0 |
| $[(XA_2)U(CH_2SiMe_3)(o\text{-}C_6H_4F_2)]^+$ (**12**) | $o\text{-}C_6H_4F_2$ | 0 | 0 |
| $[(XA_2)Th(CH_2SiMe_3)(\eta^x\text{-}C_6H_5F)]^+$ (**10-Th**) | $C_6H_5F$ | 0.144 | 57600 |

[a] Conditions: 0.005 mmol of catalyst (< 10 mg), 5 mL of solvent, 1 atm of ethylene, 70 °C, 30 min. [b] Activities are measured in $g\cdot mol^{-1}\cdot h^{-1}\cdot atm^{-1}$. For cationic species, $[B(C_6F_5)_4]^-$ is the counteranion.

### 3.4 – Cationic $XA_2$ Uranium(IV) Monoalkyl Polyfluoroarene Complexes

Given the success in utilizing fluorobenzene as a highly labile ligand/solvent for unlocking the catalytic activity of the $[(XA_2)U(CH_2SiMe_3)(\eta^x\text{-arene})]^+$ cation, we explored the use of a variety of polyfluoroarenes on the basis that their electron-deficient π-systems would prove even less competitive toward binding the active site. Following the established protocol, one equiv of $[Ph_3C][B(C_6F_5)_4]$ was admitted to a 1,2-difluorobenzene solution of dialkyl **3** (Scheme 3.6), and immediately the red solution

became a familiar deep brown colour, although numerous attempts to isolate a crystalline product were unsuccessful.

**Scheme 3.6** – Proposed synthesis of monoalkyl uranium(IV) cation **12**, depicting the most likely coordination mode of *o*-$C_6H_4F_2$.

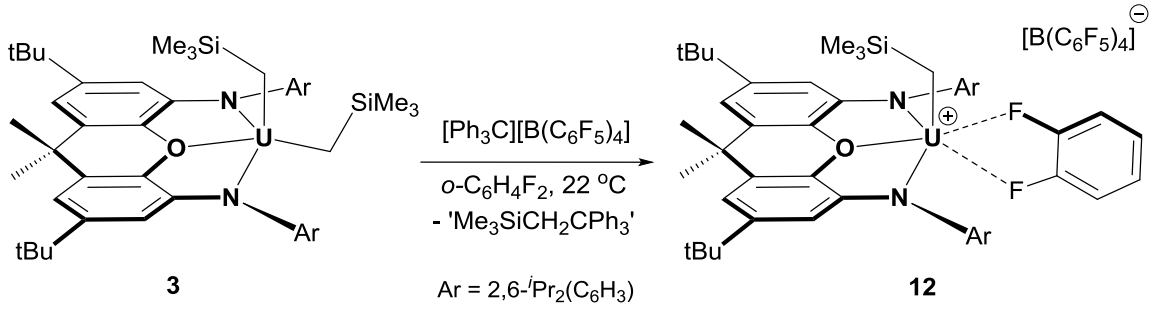


While *o*-$C_6H_4F_2$ is capable of coordinating through either a chelating $\kappa^2$-*F* fashion[260], or facially through the arene ring[259] (Figure 3.11), it is likely that the former is engaged in cation **12** given the steric restrictions imposed on the coordination site by the flanking 2,6-diisopropylphenyl rings.

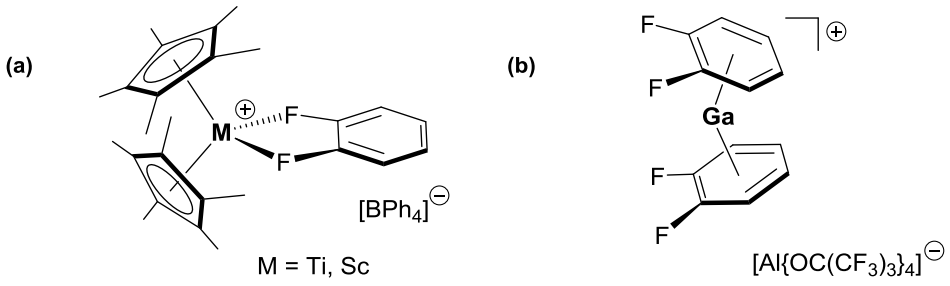


**Figure 3.11** – Coordination modes of *o*-$C_6H_4F_2$ in (a) $[Cp^*_2M(\kappa^2\text{-}F\text{-}C_6H_4F_2)][BPh_4]$ (M = Ti, Sc), and (b) $[(\eta^6\text{-}C_6H_4F_2)_2Ga][Al\{OC(CF_3)_3\}_4]$.

Further evidence in support of a chelating $\kappa^2$-*F* *o*-$C_6H_4F_2$ ligand in **12** is reflected in the catalytic activity of the complex; while **12** is indeed an active ethylene polymerization catalyst (activity = $1.12 \times 10^4$ g of PE·mol$^{-1}$·h$^{-1}$·atm$^{-1}$ at 20 °C; Table 3.4), it exhibits a modest decrease in activity relative to that of fluorobenzene-bound **10**. This suggests that in these $[(XA_2)U(CH_2SiMe_3)(\eta^x\text{-arene})]^+$ systems, the chelating $\kappa^2$-*F* coordination-mode of *o*-$C_6H_4F_2$ is more coordinatively supportive (and thus more competitive for ethylene binding) than π-coordinated $C_6H_5F$. Interestingly, no polyethylene was obtained when the polymerization was carried out at high temperature (70 °C), indicating that cation **12** suffers from reduced thermal stability relative to fluorobenzene-coordinated cation **10**.

To disengage the putative $\kappa^2$-*F* coordination mode that appears to hinder catalytic performance, we explored the use of 1,3-difluorobenzene. In theory, the *meta*-disposition of the relatively bulky fluorine substituents should not only prevent π-coordination, but also limit the ligand to a $\kappa^1$-*F* binding mode, improving the accessibility of the active site. However, while the alkyl abstraction appeared to proceed as usual based on solution colour changes, no polyethylene formed after stirring a solution of **3**/$[Ph_3C][B(C_6F_5)_4]$ in *m*-$C_6H_4F_2$ under ethylene (1 atm. 20 °C) for 30 min, perhaps due to room-temperature instability of the resulting cation in the absence of an arene solvent capable of π- or $\kappa^2$-*F*-coordination.

As 1,3-difluorobenzene failed to provide access to a catalytically active species, we explored the use of hexafluorobenzene as a labile ligand/solvent. While $C_6F_6$ may chelate in a $\kappa^2$-*F* fashion, we reasoned that perfluorination might significantly limit the binding power and furnish improved catalytic performance over **12**. Rather surprisingly,

neutral dialkyl precursor **3** suffers from limited solubility in $C_6F_6$, but nevertheless, the trityl-promoted alkyl abstraction reaction was carried out, and an oily brownish material precipitated which was not amenable to further purification and failed to polymerize ethylene. Similarly, treatment of **3** with $[Ph_3C][B(C_6F_5)_4]$ in α,α,α-trifluorotoluene resulted in a black-green oily intractable mixture, and the reaction was not pursued further.

### 3.5 – Revisiting $XA_2$ Thorium(IV) Ethylene Polymerization Catalysis

The development of methodology that has unlocked dormant catalytic activity in our cationic monoalkyl uranium complexes motivated us to reassess the catalytic profile of the thorium-based precursor $[(XA_2)Th(CH_2SiMe_3)_2]$ (**3-Th**) that was previously reported by the Emslie group[40]. Accordingly, treatment of a colourless fluorobenzene solution of neutral **3-Th** with one equiv of $[Ph_3C][B(C_6F_5)_4]$ resulted in an abrupt colour change to bright yellow, becoming vibrant orange over the course of 3 hours. Despite numerous attempts to isolate a crystalline product, only oily, orange intractable material could be obtained. Therefore, on the basis of the established reactivity profile of **3-Th** with alkyl abstraction agents, and the parallel result observed utilizing uranium dialkyl complex **3**, we have assigned the product as fluorobenzene-bound $[(XA_2)Th(CH_2SiMe_3)(\eta^x\text{-}C_6H_5F)][B(C_6F_5)_4]$ (**10-Th**; Scheme 3.7).

**Scheme 3.7** – Proposed synthesis of monoalkyl thorium(IV) cation **10-Th**.

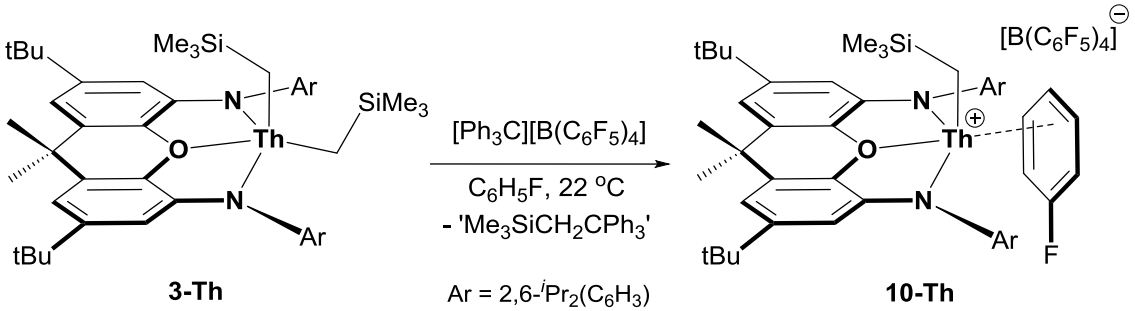


Within minutes of admitting ethylene (1 atm, 20 °C), the approximately 1 millimolar fluorobenzene solution of *in-situ*-generated **10-Th** became noticeably turbid, and upon quenching after 30 min, 0.042 g of off-white solid polyethylene was harvested, corresponding to an activity of $1.68 \times 10^4$ g of polyethylene·mol$^{-1}$·h$^{-1}$·atm$^{-1}$ for cation **10-Th** (Table 3.4). Given that neutral dialkyl precursor **3-Th** reacts with $[Ph_3C][B(C_6F_5)_4]$ in benzene and toluene solutions slowly over the course of 24−48 h to generate cations **6-Th** and **7-Th**, respectively, we repeated the *in-situ* preparation of **10-Th**, but allowed the alkyl abstraction in fluorobenzene solution to stir for 24 h in order to ensure complete cation formation prior to admitting ethylene. Interestingly, the 24 h activation did not result in an increase or decrease in polymer yield or catalytic activity for cation **10-Th**, which suggests that alkyl abstraction from **3-Th** occurs much faster in fluorobenzene solution than in benzene or toluene, likely as a result of the increased polarity of the solvent.

As was also observed in the complementary uranium system (cation **10**), conducting the reaction between **10-Th** and ethylene at elevated temperature (70 °C)

resulted in an approximately 3-fold increase in activity ($5.76 \times 10^4$ g of polyethylene·(mol of Th)$^{-1}$·h$^{-1}$·atm$^{-1}$; Table 3.5), which suggests that **10-Th** is a thermally robust catalyst. To our knowledge, **10-Th** is the most active post-metallocene actinide ethylene polymerization catalyst to date, with [(2-pyridylamidinate)$_2$UCl(μ-Cl)$_2$Li(tmeda)] (2-pyridylamidinate = {(Me$_3$SiN)$_2$C(2-py)}) activated with [Ph$_3$C][B(C$_6$F$_5$)$_4$] and TIBA being nearly 6-times less active, with an activity of $1.02 \times 10^4$ g of polyethylene·(mol of U)$^{-1}$·h$^{-1}$·atm$^{-1}$.[213]

Samples of polyethylene produced using catalysts **10**, **10-Th**, and **12** were sent for analysis by gel permeation chromatography (GPC) in attempt to probe their respective molecular weight averages and dispersities. Unfortunately, polyethylene produced using fluorobenzene-bound uranium cation **10** or the analogous thorium congener **10-Th** was found to be thoroughly insoluble in trichlorobenzene at 140 °C, and as such could not be subjected to GPC analysis; the limited solubility of these polymers at elevated temperature suggests they are of high molecular weight. However, polyethylene formed using the catalyst generated in 1,2-difluorobenzene, cation **12**, could be solubilised, and GPC analysis revealed a polymer of moderate molecular weight, with a $M_w$ of $2.9 \times 10^4$ and $M_n$ of $1.1 \times 10^4$ g·mol$^{-1}$; the relatively low polydispersity index (PDI) of 2.61 suggests that the polymerization is carried out *via* a single-site mechanism.[213] The polyethylene produced using cation **12** is highly comparable to that obtained by Leznoff and co-workers utilizing the neutral dialkyl [($^{t\text{Bu}}$NON)U(CH$_2$SiMe$_3$)$_2$] ($^{t\text{Bu}}$NON = {($^t$BuNSiMe$_2$)$_2$O}$^{2-}$) as a catalyst ($M_w$ of PE = $2.4 \times 10^4$; $M_n$ = $8.9 \times 10^3$ g·mol$^{-1}$; PDI = 2.7).[174]

Rationalizing the modest increase in ethylene polymerization activity observed for thorium cation **10-Th** relative to the analogous uranium cation **10** is not trivial. Eisen and co-workers reported significantly improved catalytic performance in their uranium system [(2-pyridylamidinate)$_2$UCl(μ-Cl)$_2$Li(tmeda)]/[Ph$_3$C][B(C$_6$F$_5$)$_4$]/TIBA relative to the thorium analogue, observing an increase in activity of >$10^4$ g of polyethylene·(mol of An)$^{-1}$·h$^{-1}$·atm$^{-1}$.[213] The authors argued that unlike the 5f$^0$6d$^0$ thorium(IV) ion, the 5f$^2$ uranium(IV) ion may be able to participate in back-donation to the π*-orbital of ethylene to some degree, resulting in improved coordination of the olefin and more facile activation of the double bond. Additionally, the authors noted that based on bond dissociation energies, the U−C bond (300 kJ·mol$^{-1}$) is weaker than the Th−C bond (339 kJ·mol$^{-1}$)[264], permitting more facile insertion of the coordinated ethylene ligand into the U−C bond.[213] Further, Liddle and co-workers computationally demonstrated[171] that cyclometalation in actinide benzyl complexes [(tren$^{TIPS}$)An(CH$_2$Ph)] (tren$^{TIPS}$ = κ$^4$-{N(CH$_2$CH$_2$NSi$^i$Pr$_3$)$_3$}$^{3-}$; An = U, Th) is significantly favoured for the uranium compound as a result of 5f-orbital participation in the stabilization of the σ-bond metathesis transition state. By extension, the uranium 5f-orbital manifold may participate in the stabilization of the 4-membered transition state (Figure 3.12) that has been shown to be important in organoactinide-mediated transformations of olefins[109], perhaps leading to improved ethylene polymerization activities for uranium catalysts relative to the analogous thorium-based systems.

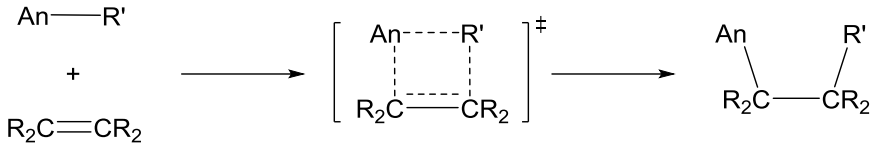


**Figure 3.12** – Four-centre transition state in neutral organoactinide-mediated transformations.

Conversely, Liddle and co-workers have noted that the 5f-orbital manifold is generally inaccessible to the $5f^0 6d^0$ thorium(IV) ion, resulting in complexes where electrostatic interactions are dominant, and as a consequence, thorium–ligand bonds are generally more reactive than the corresponding uranium–ligand bonds.[171]

In the present case, the thorium congener **10-Th** exhibits improved ethylene polymerization activity relative to the analogous uranium-based system **10**, but in the absence of illuminating computational insights,[§] the observed reactivity trend cannot be explicitly rationalized. Qualitatively, a number of factors may be responsible; for example, it may be speculated that increased covalency- and a tighter coordination environment surrounding the smaller uranium(IV) ion in **10** (which may promote favourable dispersion interactions between the arene ring and the ligand architecture) results in a stronger interaction between the fluorobenzene ligand and the uranium cation relative to thorium, leading to an increased barrier to dissociation. However, this behaviour is not reflected in the spectroscopically-observed solution dynamics of the actinide cations. Toluene-coordination in **7-Th** is maintained in $C_6D_5Br$ solution,

[§] Studying arene-coordinated monoalkyl $XA_2$ uranium(IV) complexes computationally has proven exceptionally challenging and non-trivial.

evidenced by the presence of resonances arising from both free- and bound toluene in the $^{1}H$ and $^{13}C$ NMR spectra,[179] and no resonances attributable to the bromobenzene-bound species $[(XA_2)Th(CH_2SiMe_3)(\eta^x\text{-}C_6H_5Br)][B(C_6F_5)_4]$ (**8-Th**) are observed. Conversely, the proteo-arene ligands of uranium cations **6** and **7** are readily displaced by bromobenzene to form **8** in solution, which, taken together, points to stronger An–arene bonding in the thorium system. Perhaps, simply, the larger more sterically-accessible thorium cation in **10-Th** facilitates the superior ethylene polymerization catalysis; theoretical investigations concerning the bonding in arene-coordinated $XA_2$ actinide complexes are currently underway.

By thoroughly understanding the discrete molecular structure of $XA_2$ uranium(IV) cations **6** and **7**, and by leveraging the significantly limited coordinative support of fluoroarene ligands, the previously dormant cationic $[(XA_2)An(CH_2SiMe_3)(\eta^x\text{-arene})]^+$ species can be unleashed as active ethylene polymerization catalysts. This study explicitly highlights that the identity of the solvent in which homogenous ethylene polymerization catalysis takes place is a critical variable, and it raises the question of whether other f-element systems that are reportedly catalytically inactive in toluene solution (at low pressures of ethylene; e.g. 1–2 atm.) may in fact be suffering from coordinative-asphyxiation. For example, even with π-donation of the aryloxide ligand taken into account, Clark's 10-electron $[Cp^{*}Th(OAr)(CH_2SiMe_3)]^+$ (Ar = 2,6-$^{t}Bu_2C_6H_3$) cation would appear to be more electron-deficient than 14-electron $[Cp^{*}_2ThMe]^+$, yet the monocyclopentadienyl species is 100 times less active than the metallocene.[110] Given the sterically open environment in the half-sandwich complex relative to the metallocene,

perhaps toluene-coordination occurs in solution yielding 16-electron $[Cp^{*}Th(OAr)(CH_2SiMe_3)(\eta^6\text{-}C_6H_5Me)]^+$, where the toluene ligand competes with ethylene for the active site, reducing polymerization activity as a consequence.

**Table 3.6** – Crystallographic data collection and refinement parameters for complexes **6**, **7**, and **10**.

| Structure | **6**·2(benzene) | **7**·toluene | **10**·fluorobenzene |
|---|---|---|---|
| Formula | $C_{93}H_{91}BF_{20}N_2OSiU$ | $C_{82}H_{81}BF_{20}N_2OSiU$ | $C_{85.94}H_{82.11}BF_{21.82}N_2OSiU$ |
| Formula wt | 1909.60 | 1767.41 | 1850.45 |
| *T* (K) | 150(2) | 173(2) | 100(2) |
| Cryst. Syst. | Triclinic | Orthorhombic | Orthorhombic |
| Space Group | *P*–1 | *Pca*2(1) | *Pca*2(1) |
| *a* (Å) | 13.916(3) | 26.661(4) | 26.5251(18) |
| *b* (Å) | 17.437(4) | 15.845(3) | 15.7375(11) |
| *c* (Å) | 19.155(4) | 19.116(3) | 18.8824(13) |
| α [deg] | 95.996(3) | 90 | 90 |
| β [deg] | 111.194(3) | 90 | 90 |
| γ [deg] | 95.687(3) | 90 | 90 |
| Volume [$Å^3$] | 4262.7(15) | 8076(2) | 7882.2(9) |
| *Z* | 2 | 4 | 4 |
| Density (calcd; $Mg/m^3$) | 1.488 | 1.454 | 1.559 |
| μ ($mm^{-1}$) | 2.010 | 2.116 | 2.175 |
| *F*(000) | 1924 | 3544 | 3709 |
| Crystal Size ($mm^3$) | 0.458×0.356×0.024 | 0.252×0.219×0.020 | 0.316×0.138×0.098 |
| θ Range for Collection [deg] | 1.525–26.521 | 1.495–24.999 | 1.505–30.839 |
| No. of reflns. Collected | 65558 | 81186 | 120454 |
| No. of Indep. Reflns. | 17563 | 9775 | 24644 |
| Completeness to θ Max (%) | 100.0 | 99.9 | 99.9 |
| Absorption Correction | Numerical | Numerical | Numerical |

| | | | |
|---|---|---|---|
| Max and Min Transmission | 0.9964, 0.5765 | 0.7454, 0.6059 | 0.8492, 0.6622 |
| Data / Parameters | 17563 / 1075 | 9775 / 973 | 24644 / 1021 |
| GOF on $F^2$ | 1.013 | 1.015 | 1.000 |
| Final $R_1$ [$I > 2\sigma(I)$] | R1 = 0.0295<br>wR2 = 0.0664 | R1 = 0.0522<br>wR2 = 0.1029 | R1 = 0.0305<br>wR2 = 0.0643 |
| *R* indices (all data) | R1 = 0.0411<br>wR2 = 0.0702 | R1 = 0.1096<br>wR2 = 0.1274 | R1 = 0.0489<br>wR2 = 0.0694 |

# Chapter 4

# Reactivity of $XA_2$ Organouranium(IV) Complexes with Small Molecules

## 4.1 – Reactions of $[(XA_2)U(CH_2SiMe_3)_2]$ with Anionic Lewis Bases

We have previously demonstrated that the uranium(IV) dialkyl complex $[(XA_2)U(CH_2SiMe_3)_2]$ (**3**) is susceptible to mild alkyl abstraction *via* reaction with strong Lewis acids such as $[Ph_3C]^+$, forming cationic monoalkyl species of the form $[(XA_2)U(CH_2SiMe_3)(\eta^x\text{-arene})]^+$ which behave as thermally robust ethylene polymerization catalysts under carefully curated conditions (*vide supra*, Chapter 3). Herein, we continue to develop the reactivity portfolio of our organometallic $XA_2$ uranium species, exploring reactions between dialkyl **3** and Lewis bases.

### 4.1.1 – $XA_2$ Actinide(IV) Alkyl Exchange Reactivity

Reactions of dialkyl **3** with alkyllithium species were explored in order to probe the accessibility of anionic tris(alkyl) 'ate' complexes supported by the bulky and rigid $XA_2$ ancillary ligand. To this end, 1.1 equiv of $LiCH_2SiMe_3$ were introduced to the dialkyl complex $[(XA_2)U(CH_2SiMe_3)_2]$ (**3**), but the desired tris((trimethylsilyl)methyl) 'ate' species $[(XA_2)U(CH_2SiMe_3)_3]^-$ failed to form in $C_6D_6$, hexane, or toluene; $^1$H NMR spectroscopy showed only unreacted starting materials.[177] However, rather surprisingly, addition of 2.1 equiv of $LiCH_2{}^tBu$ to $[(XA_2)U(CH_2SiMe_3)_2]$ (**3**) in $C_6D_6$ resulted in quantitative conversion to the bis(neopentyl) derivative $[(XA_2)U(CH_2{}^tBu)_2]$ (**4**) over the

course of approximately 1 h, with concomitant release of 2 equiv of $LiCH_2SiMe_3$ (Scheme 4.1), rather than formation of a mixed tris(alkyl) uranium anion. Treatment of complex **4** with up to 80 equiv of $LiCH_2SiMe_3$ in $C_6D_6$ did not re-form detectable amounts of **3** by $^1H$ NMR spectroscopy; thus, the equilibrium in this reaction must lie far to the side of complex **4**. This unusual reaction bears a resemblance to salt metathesis (both alkyl exchange and salt metathesis are classes of transmetalation reactions), but with elimination of $LiCH_2SiMe_3$ instead of a lithium halide.

**Scheme 4.1 –** Conversion of complex **3** to **4** *via* alkyl exchange.

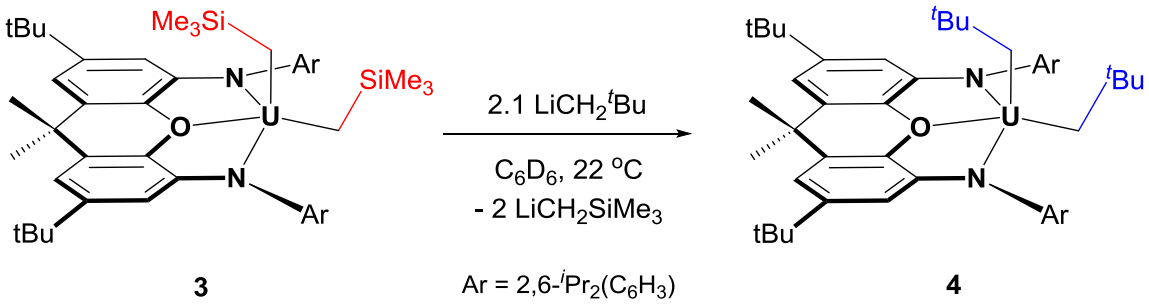


**3** Ar = 2,6-$^i$Pr$_2$(C$_6$H$_3$) **4**

This alkyl metathesis reactivity is not unique to uranium, since the reaction between $[(XA_2)Th(CH_2SiMe_3)_2]$ (**3-Th**) and 15 equiv of $LiCH_2{}^tBu$ cleanly provided $[(XA_2)Th(CH_2{}^tBu)_2]$ (**4-Th**). However, addition of 2.2 equiv of $LiCH_2{}^tBu$ to **3-Th** yielded an approximate 1:1:3:1 mixture of **4-Th**, $[(XA_2)Th(CH_2SiMe_3)(CH_2{}^tBu)]$ (**13-Th**), $LiCH_2SiMe_3$, and $LiCH_2{}^tBu$ (Scheme 4.2). This product distribution was established within 5 min and did not change with extended reaction times (days), consistent with a significantly smaller equilibrium constant for the reaction of **3-Th** with $LiCH_2{}^tBu$, relative to the reaction of uranium complex **3** with $LiCH_2{}^tBu$. Complex **13-Th** is the mixed alkyl species that must form *en route* from **3-Th** to **4-Th**, and both **4-Th** and **13-**

**Th** were characterized *in situ* by $^{1}H$, $^{13}C$, and 2D NMR spectroscopy (at low temperature for **4-Th**).

**Scheme 4.2 –** Reactions of **3-Th** with 2.2 and 15 equiv of $LiCH_2{}^tBu$, respectively.

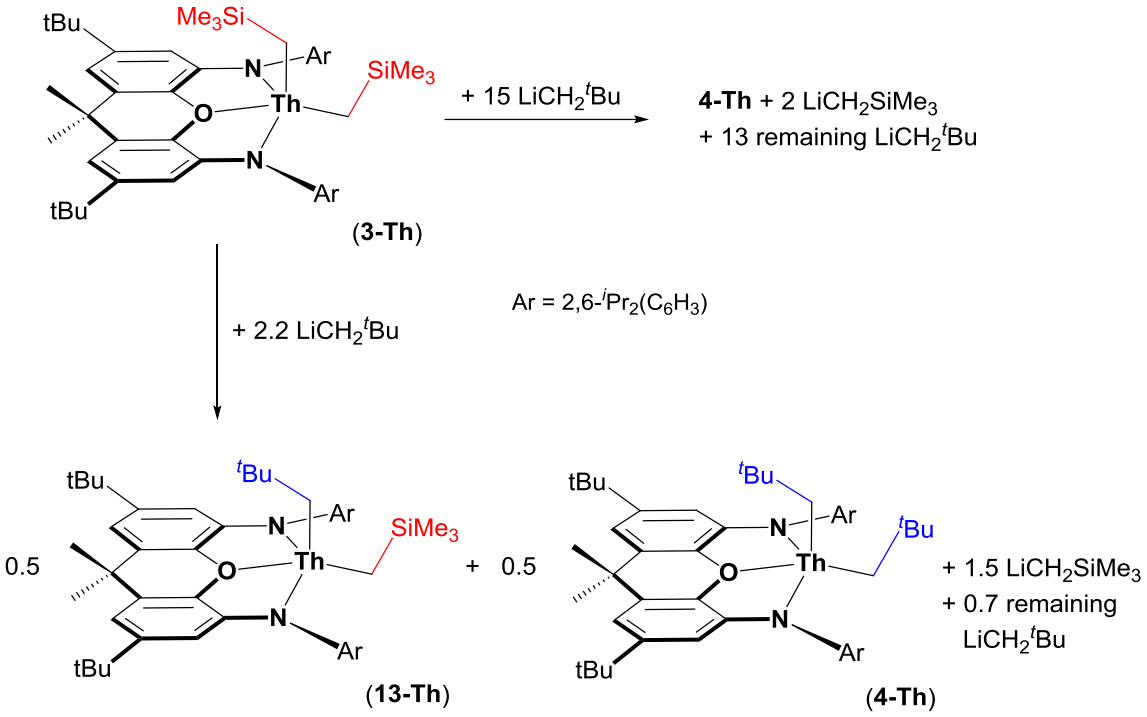


Previously reported alkyl exchange reactions at electropositive d- or f-element centres include (a) synthesis of [{*o*-$C_6H_4$(NDipp)(PPh($C_6H_4$)(=NMes))}LuMe(THF)$_2$] by treatment of [{*o*-$C_6H_4$(NDipp)(PPh($C_6H_4$)(=NMes))}Lu($CH_2SiMe_3$)(THF)] with 10 equiv of $AlMe_3$ in THF,[265] (b) reaction of [{$Me_2$Si(2-Me-$C_9H_5$)$_2$}YMe(THF)] with $AlEt_3$ followed by addition of THF to yield an approximately 1:1 mixture of the starting methyl complex and [{$Me_2$Si(2-Me-$C_9H_5$)$_2$}YEt(THF)],[266] and (c) exchange between a growing polymer chain on a d- or f-element polymerization catalyst and the alkyl group of an

added trialkylaluminium,[267,268,269,270] trialkylboron,[271] dialkylzinc,[269,270,272] or dialkylmagnesium[273] reagent. This last mode of reactivity is typically detrimental to olefin polymerization activity[274] but has found productive use in chain shuttling alkene polymerization[272] and metal-catalyzed "Aufbaureaktion" chemistry.[267,270] Alkyl exchange reactions involving alkyllithium reactions are more scarce, but have been reported for dialkylmercury compounds in combination with alkyllithium reagents; these reactions proceed to completion when the alkyllithium product is insoluble in the solvent employed.[275]

The alkyl exchange reactions herein are also related to salt metathesis-like reactions involving cyclopentadienyl anion elimination from polar metallocenes. These include the reaction of $[\{Cp^{*}_{2}U\}_2(\mu\text{-}\eta^6\text{:}\eta^6\text{-}C_6H_6)]$ with MX (M = K, X = $N(SiMe_3)_2$, $OC_6H_2(CMe_3)_2$-2,6-Me-4; M = Li, X = $CH(SiMe_3)_2$, $^{i}PrNCMeN^{i}Pr$) to form $[\{Cp^{*}XU\}_2(\mu\text{-}\eta^6\text{:}\eta^6\text{-}C_6H_6)]$,[72] reaction of $[MnCp_2]$ with $LiC_2Ph$ in THF to provide 0.5 $[\{CpMn(\mu\text{-}C_2Ph)(THF)\}_2]$,[276] reaction of $[MnCp_2]$ with 1 or 3 equiv of Li(hpp) to afford 0.5 $[\{CpMn(hpp)\}_2]$ or $[\{LiMn(hpp)_3\}_2]$,[277] reaction of $[VCp_2]$ with 2 equiv of Li(hpp) to give 0.25 $[\{V_2(hpp)_4\}Li(\mu\text{-}Cp)Li(\mu\text{-}Cp)Li\{V_2(hpp)_4\}][CpLi(\mu\text{-}Cp)LiCp]$,[278] and reaction of $[CrCp_2]$ with 2 equiv of Li(MeNCHNMe) to yield 0.5 $[Cr_2(MeNCHNMe)_4]$.[279]

### 4.1.2 – $XA_2$ Uranium(IV) Tris((trimethylsilyl)methyl) Complex

The reaction to convert **3** to **4** presumably occurs *via* tris(alkyl) 'ate' intermediates, as shown in Scheme 4.3. These intermediates were not detected in the reaction of **3** with $LiCH_2{}^tBu$ in aromatic solvents, and reaction of complex **3** with up to 20 equiv of $LiCH_2SiMe_3$ in $C_6D_6$ did not provide any evidence for the formation of $[(XA_2)U(CH_2SiMe_3)_3]^-$ by $^1H$ NMR spectroscopy.

**Scheme 4.3 –** Proposed reaction pathway for the conversion of **3** to **4**.

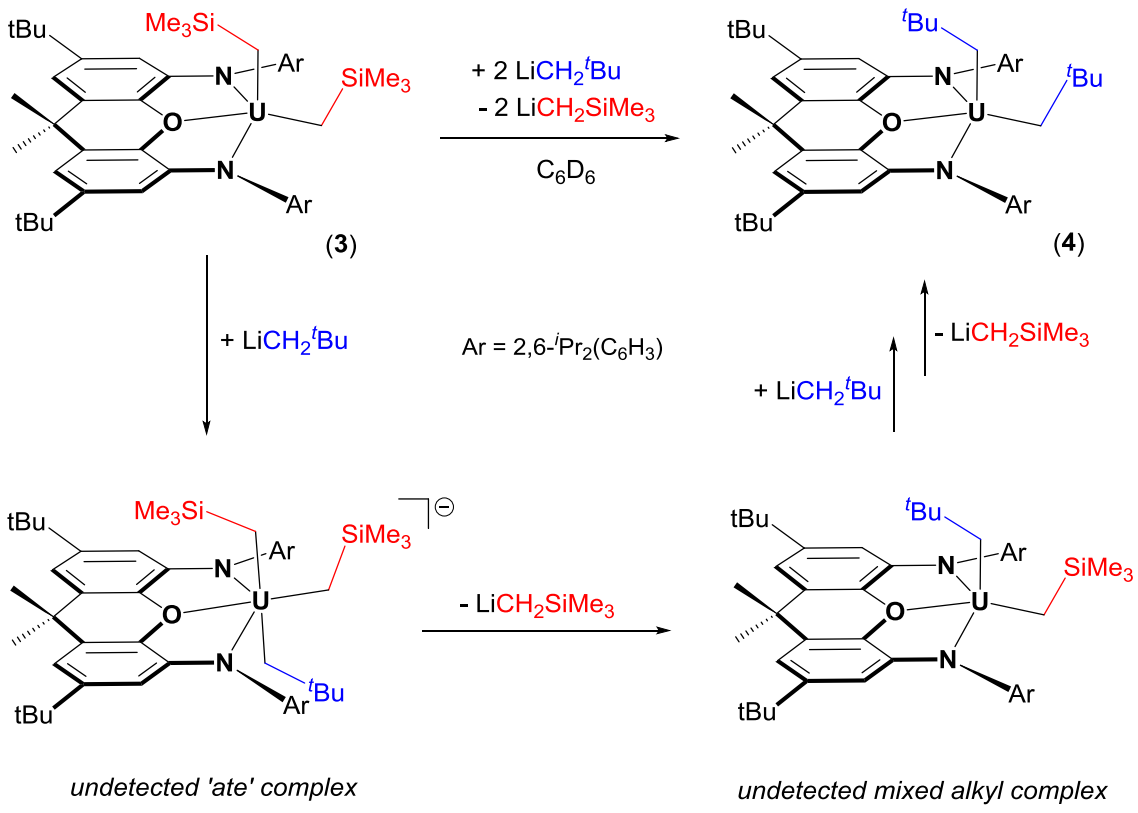


*undetected 'ate' complex*

*undetected mixed alkyl complex*

However, tris(alkyl) 'ate' complexes did prove accessible in ethereal solvents; indeed, upon addition of 1.3 equiv of $LiCH_2SiMe_3$ to a cherry-red THF-$d_8$ solution of **3** at room temperature, the solution immediately became a golden-yellow colour and the $^1$H NMR spectrum acquired after 5 min revealed a clean collection of 20 new, paramagnetically-shifted resonances that were assigned to the tris((trimethylsilyl)methyl) complex $[Li(THF\text{-}d_8)_x][(XA_2)U(CH_2SiMe_3)_3]$ (**14-THF**; Scheme 4.4).

**Scheme 4.4** – *In-situ* formation of $[Li(THF\text{-}d_8)_x][(XA_2)U(CH_2SiMe_3)_3]$ (**14-THF**).

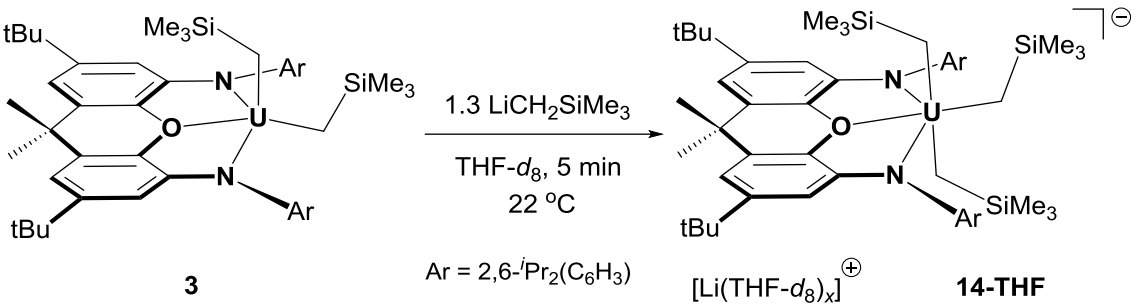


Although the resonances of **14-THF** are relatively sharp at room temperature, the $^1$H NMR spectrum acquired at −50 °C (Figure 4.1) allowed for more accurate integration and definitive assignment of the three sets of U$CH_2$ $\alpha$-protons, which arise at 451.0, 378.0, and −236.9 ppm as extremely broadened singlets.

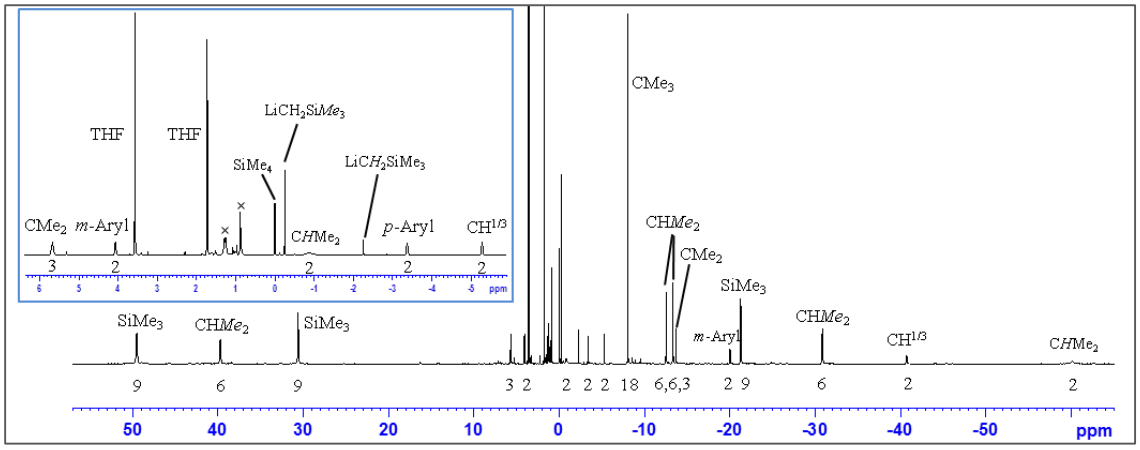


**Figure 4.1** – Selected regions of the $^{1}$H NMR spectrum of [Li(THF-$d_8$)$_x$][(XA$_2$)U(CH$_2$SiMe$_3$)$_3$] (**14-THF**) in THF-$d_8$ at −50 °C (500 MHz). × denotes *n*-pentane. Numbers below the baseline indicate the integration of each peak. Signals for U−C$H_2$ protons, which are located at very high (>100 ppm) and very low (<−100 ppm) frequencies are not shown. The inset shows a blown-up portion of the spectrum.

While bright-yellow **14-THF** is readily generated in THF solution and can be characterized by $^{1}$H NMR spectroscopy without issue, the species begins to decompose in under an hour, typified by a deepening of the solution to a dark amber colour. The decomposition was also observed spectroscopically; $^{1}$H NMR spectroscopy revealed the evolution of SiMe$_4$, the loss of signals corresponding to **14-THF**, and the emergence of a collection of unidentified paramagnetically-shifted resonances, beginning within an hour and completed over the course of approximately one week.

Given the instability of **14-THF** in solution, our initial attempts to develop preparative-scale methodology met with complications. Alkylation reactions were also conducted in neat 1,2-dimethoxyethane (dme) solution in hopes of improving

crystallinity, and while this approach afforded single crystals of the complex as the $[Li(dme)_3]^+$ salt, $[Li(dme)_3][(XA_2)U(CH_2SiMe_3)_3]\cdot 2(dme)$ (**14-dme**·2(dme)), the bulk material afforded by this method was also impure as indicated by $^1H$ NMR spectroscopy. Analytically pure **14-dme** was ultimately prepared by precipitating the salt immediately upon formation; a mixture of the hydrocarbon-soluble dialkyl precursor **3** and 1.1 equiv of $LiCH_2SiMe_3$ in *n*-pentane was cooled to −30 °C, and 3.05 equiv of dme was added. This resulted in immediate precipitation of yellow **14-dme**, which was isolated as a solid powder in 95% yield (Scheme 4.5).

**Scheme 4.5** – Preparation of $[Li(dme)_3][(XA_2)U(CH_2SiMe_3)_3]$ (**14-dme**).

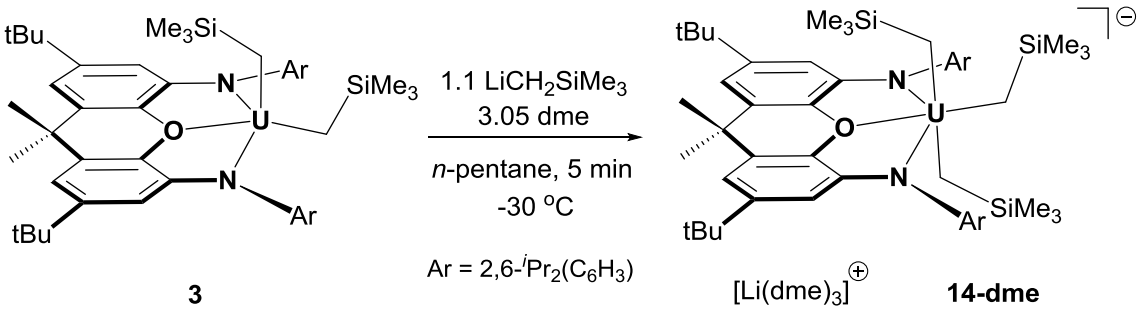


In the solid-state, (Figure 4.2; Table 4.1), **14-dme**·2(dme) features two independent but structurally analogous ion-pairs in the unit cell, each comprised of a $C_s$-symmetric $XA_2$-uranium(IV) anion and distal $[Li(dme)_3]^+$ cation, consistent with the observed collection of $^1H$ NMR resonances. In anion **14**, uranium is six-coordinate, featuring two $CH_2SiMe_3$ ligands bound approximately *trans*- to one another occupying apical positions, and a third $CH_2SiMe_3$ ligand located approximately in the plane of the ancillary ligand backbone. The five anionic donors (N(1), N(2), C(48), C(52), and C(56))

adopt a distorted trigonal-bipyramidal arrangement around the metal centre, with N(1)−U−N(2), N(1)−U−C(48), N(2)−U−C(48), and C(52)−U−C(56) angles of 123.5(3)−124.2(3), 127.4(4)−134.2(3)°, 102.2(3)−108.4(3)°, and 159.1(3)−172.8(4)°, respectively. The neutral diarylether donor is coordinated between the two amido groups, located 0.75 and 0.83 Å out of the NUN plane, approximately capping a face of the aforementioned trigonal bipyramid. As with trichloro 'ate' complex **1**, The N/$C_{eq}$/N-plane of the trigonal bipyramid in anion **14** is significantly tilted relative to the plane of the $XA_2$ ligand, indicated by the considerably expanded angles between the N/O/N- and N/C(48)/N-planes of 27.9 and 33.9°. This tilting of the alkyl ligand-set toward the plane of the $XA_2$ backbone is likely intended to reduce unfavourable steric interactions between the apical $CH_2SiMe_3$ ligands and the isopropyl substituents of the $XA_2$ ancillary.

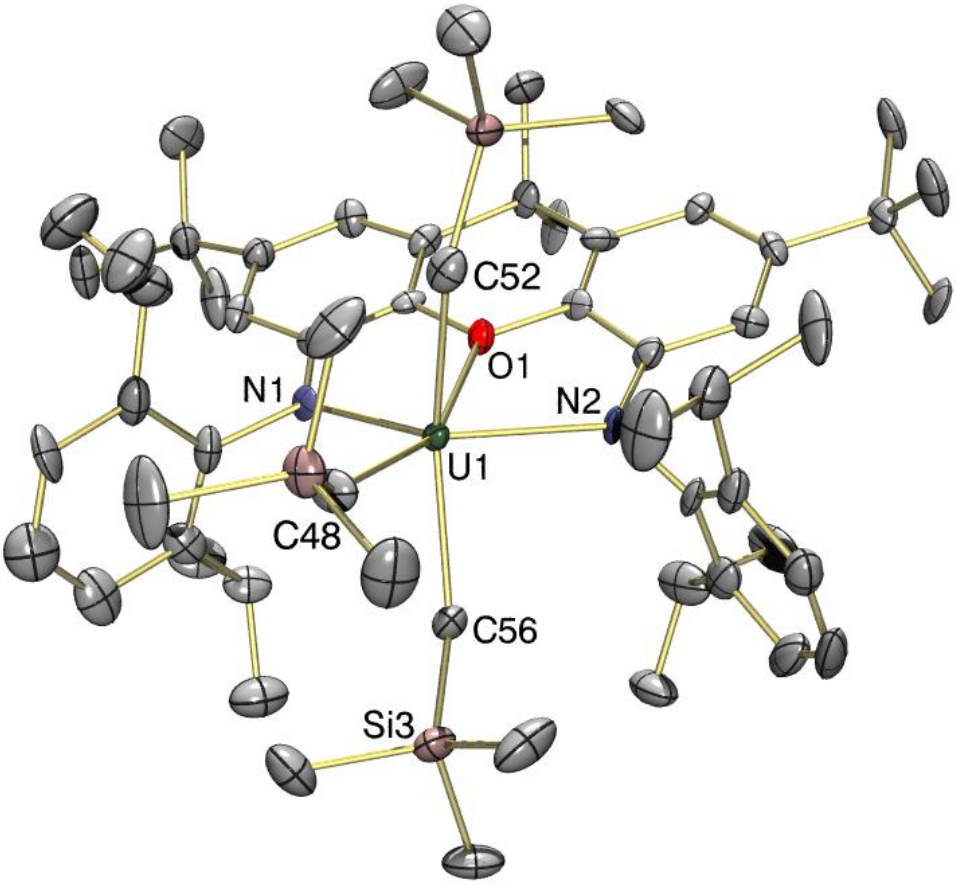


**Figure 4.2** – X-ray crystal structure of $[Li(dme)_3][(XA_2)U(CH_2SiMe_3)_3]\cdot 2(dme)$ (**14-dme**·2(dme)), with thermal ellipsoids at 50% probability. Only one of the two independent anions in the unit cell is shown. Hydrogen atoms, the $[Li(dme)_3]^+$ countercation, and dme lattice solvent are omitted for clarity.

**Table 4.1** – Selected bond lengths (Å) and angles (deg) for $XA_2$ complexes **14-dme**, **15**, and **3** (for comparison).

| Compound | **14-dme** | **15** | **3** |
|---|---|---|---|
| U−O | 2.515(6), 2.551(6) | 2.517(5) | 2.484(5), 2.504(4) |
| U−N | 2.389(9), 2.397(9), 2.374(9), 2.398(8) | 2.363(6), 2.373(6) | 2.261(5), 2.262(5), 2.272(5), 2.280(5) |
| $U-CH_2R^a$ *in plane* | 2.46(1), 2.47(1) | 2.506(9) | 2.393(7), 2.418(7) |

| | | | |
|---|---|---|---|
| U−$CH_2$R[a] *apical* | 2.42(1), 2.50(1), 2.45(1), 2.45(1) | 2.377(9), 2.493(8) | 2.368(7), 2.380(7) |
| Ligand Bend Angle [b] | 4.8, 7.0° | 6.5° | 17.5, 18.8° |
| O···(N/U/N-plane) | 0.75, 0.83 | 0.75 | 0.91, 0.95 |
| U···(N/O/N-plane) | 0.56, 0.62 | 0.54 | 0.64, 0.65 |
| Angle between the N/O/N- and N/$C_{eq}$/N-planes | 27.9, 33.9° | 29.7° | 7.7, 8.4° |
| U−$CH_2$−Si *in plane* | 147.9(6), 149.4(6)° | n/a | 130.5(4), 130.8(3)° |
| U−$CH_2$−Si *apical* | 134.5(6), 140.1(6), 136.2(7), 139.6(6)° | n/a | 128.2(3), 130.4(3)° |
| N(1)···N(2) | 4.20, 4.23 | 4.20 | 4.00, 4.02 |

[a] For **14-dme** and **3**, R = $SiMe_3$, for **15**, R = H. [b] Ligand Bend Angle = the angle between the two aromatic rings of the xanthene ligand backbone.

The U−N, U−O, and U−$CH_2$ bond distances in tris((trimethylsilyl)methyl) anion **14** are elongated by at least 0.04 Å relative to those of the neutral bis((trimethylsilyl)methyl) precursor **3** (the U−N distances in particular), likely a result of the increased- coordination number, electronic saturation, and steric crowding at the uranium centre relative to dialkyl **3**, and the fact that anion **14** bears a net negative charge. Indeed, uranium−ligand bond elongation has previously been observed in 'ate' derivatives relative to the bond distances observed in their neutral precursors. Liddle and co-workers observed U=C, U−$N_{pincer}$, and U−$N_{amido}$ bond elongations of at least 0.05 Å in the mixed imido/amido bis(iminophosphorane)methanediide 'ate' derivative [($BIPM^{TMS}$)U=$NCPh_3$($NHCPh_3$)(K)] ($BIPM^{TMS}$ = $\kappa^3$-{$C(PPh_2NSiMe_3)_2$}$^{2-}$) relative to those of the neutral bis(amido) precursor [($BIPM^{TMS}$)U($NHCPh_3$)$_2$].[280] Additionally, expanded U−$CH_2$ bond distances were observed in Hayton's homoleptic hexabenzyl 'ate'

species $\{[K(THF)]_3[K(THF)_2][U(CH_2Ph)_6]_2\}_x$ (U−$CH_2$ = 2.50(2)−2.63(2) Å)[37] relative to the U−$CH_2$ distances observed for Bart's neutral homoleptic tetrabenzyl complex $[U(CH_2Ph)_4]$ (U−$CH_2$ = 2.446(7)−2.477(7) Å).[44]

While expanded by approximately 0.07 Å relative to those of dialkyl **3**, the U−$CH_2$ distances (2.42(1)−2.50(1) Å) in anion **14** are quite comparable to those observed for Hayton's tris((trimethylsilyl)methyl) 'ate' complex $[Li(dme)_3][U(O^tBu)_2(CH_2SiMe_3)_3]$ (U−C = 2.49(1) Å).[53] Crystallographically-characterized monomeric actinide(IV) tris(alkyl) complexes are surprisingly rare, limited to the aforementioned alkoxy 'ate' species reported by Hayton, and Emslie's [(BDPP*)Th(μ-Me)$_2$Li(dme)] (BDPP* = [2,6-($NC_5H_3$)($CH_2$NAr)($CH_2$N{$C_6H_3{}^i$Pr(C$Me_2$)-2,6}]$^{3-}$); Ar = 2,6-$^i$Pr$_2C_6H_3$), which formed by cyclometalation of the trimethyl 'ate' species [(BDPP)Th$Me_3${Li(dme)}] (BDPP = 2,6-bis(2,6-diisopropylanilidomethyl)pyridine)[178] (Figure 4.3).

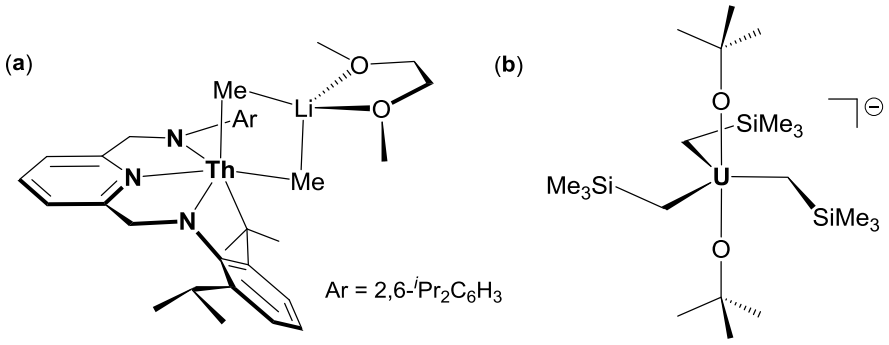


**Figure 4.3** – Other structurally characterized monomeric actinide(IV) tris(alkyl) complexes (**a**) [(BDPP*)Th(μ-Me)$_2$Li(dme)], and (**b**) $[U(O^tBu)_2(CH_2SiMe_3)_3]^-$.

The significant steric crowding in tris(alkyl) 'ate' anion **14** is made apparent not only through elongated uranium−ligand bonds, but also through the considerably

expanded U−C−Si bond angles relative to the ideal 109.5° angle. While quite obtuse, the apical U−C−Si angles in **14**, ranging from 134.5(6)−140.1(6)°, are much closer to those observed in neutral dialkyl **3** than the drastically expanded U−C−Si angles observed for the equatorial alkyl group in anionic **14**, which range from 147.9(6)−149.4(6)°. Although this may be viewed as the result of strengthened C−H−U α-agostic interactions, the steric pressure inflicted upon the equatorial $CH_2SiMe_3$ ligand by the flanking 2,6-diisopropylphenyl groups is likely the cause of such dramatic expansion. Cloke and co-workers observed a U−C−Si angle expanded to a similarly remarkable extent (U−C−Si = 147.5(2)°) in their mixed sandwich complex [($^{TIPS2}$COT)(Cp*****)U($CH_2SiMe_3$)] ($^{TIPS2}$COT = {1,4-($Si^iPr_3$)$_2C_8H_6$}$^{2-}$), which is likely a response to the steric pressure afforded by the bulky $Si^iPr_3$ substituents of the COT ancillary ligand.[155] Additionally, the constrained coordination environment is likely responsible for the distortion of the trigonal bipyramid that is formed by the anionic donors in anion **14**, whereby the steric pressure exerted by the flanking 2,6-diisopropylphenyl groups causes the equatorial $CH_2SiMe_3$ ligand to bend toward N(2), resulting in significant N−U−$C_{eq}$ angle−asymmetry (*i.e.* the N(2)−U−C(48) angle (102.2(3)−108.4(3)°) is considerably more acute than the complimentary N(1)−U−C(48) angle (127.4(4)−134.2(3)°)).

### 4.1.3 – $XA_2$ Uranium(IV) Trimethyl Complex

The reactivity of dialkyl complex **3** is not limited to alkyl exchange with neopentyllithium; addition of 3.3 equiv of MeLi to **3** in THF-$d_8$ cleanly afforded saturated hydrocarbon-insoluble $[Li(THF\text{-}d_8)_x][(XA_2)UMe_3]$ (**15**; Scheme 4.6) *in-situ*. The trimethyl uranium anion $[(XA_2)UMe_3]^-$ (**15**) could also be prepared as the $[Li(dme)_3]^+$ salt from the reaction of $[(XA_2)UCl_2(\mu\text{-}Cl)\{K(dme)_3\}]$ (**1**) with 3 equiv of MeLi in dme (Scheme 4.6). In contrast, attempts to access the putative dimethyl derivative $[(XA_2)UMe_2]$ by reaction of dialkyl complex **3** or trichloro complex **1** with 2 equiv of MeLi in dme, THF, or benzene yielded mixtures of unidentified products, and treatment of trichloro complex **1** with excess $AlMe_3$ in toluene also failed to provide a neutral dimethyl derivative. Much like the tris((trimethylsilyl)methyl) complex **14**, anionic **15** is much less thermally stable than neutral dialkyls **3**, **4**, or **5**, decomposing over several days at room temperature in THF to produce a mixture of unidentified paramagnetic products accompanied by $CH_4$.

**Scheme 4.6** – Synthesis of $[Li(solv)_x][(XA_2)UMe_3]$ {**15**; solv = THF or dme ($x$ = 3)}.

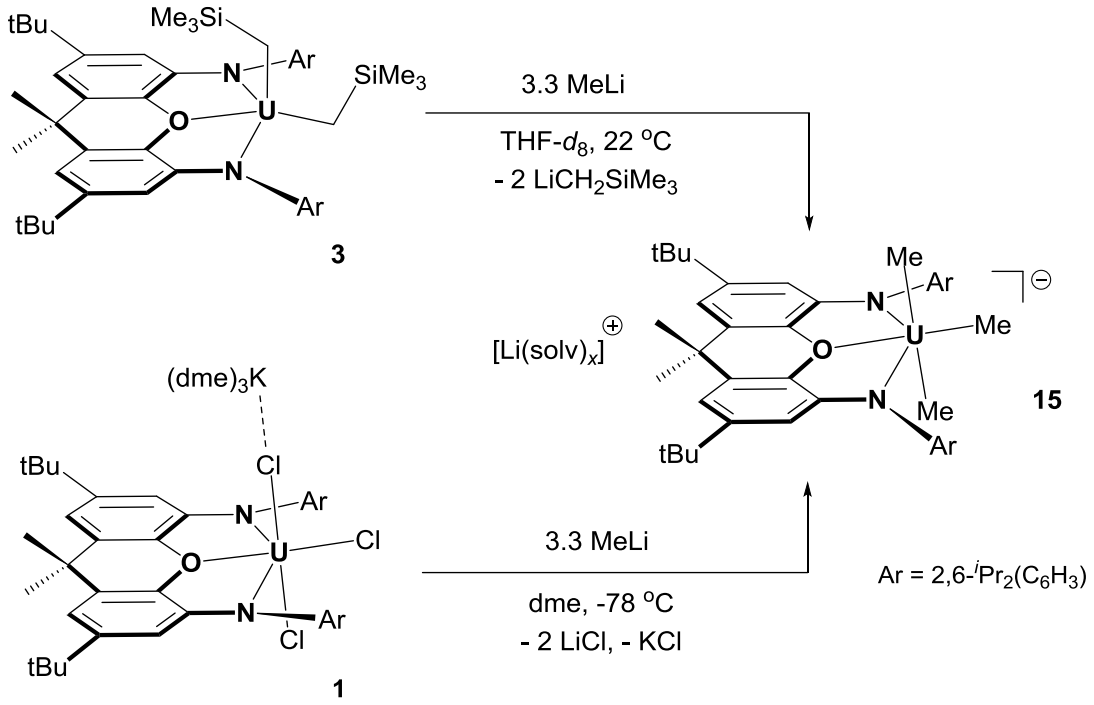


The room-temperature $^1$H NMR spectrum of **15** in THF-$d_8$ features only 9 paramagnetically-shifted resonances, consistent with the expected top–bottom symmetric environment ($C_{2v}$ symmetry). Unfortunately, $^1$H resonances arising from the UC$H_3$ α-protons could not be located (between +400 and −400 ppm); these signals may simply be broadened into the baseline, and indeed, resonances of methyl groups directly bound to uranium are occasionally conspicuously absent.[281]

Golden-yellow X-ray quality crystals of **15**·dme were obtained from dme/hexanes at −30 °C; as with closely-related anion **14**, the ligand backbone in six-coordinate **15** (Figure 4.4; Table 4.1) is quite planar (the angle between the two aryl rings of the xanthene backbone is 6.5° vs. 4.8 and 7.0° in tris(alkyl) 'ate' anion **14**), and uranium is

located 0.54 Å from the NON-donor plane. The five anionic donors (N(1), N(2), and C(48)−C(50)) form a trigonal bipyramid with methyl groups occupying axial positions, reflected by the N(1)−U−N(2), N(1)−U−C(49), N(2)−U−C(49), and C(48)−U−C(50) angles of 124.8(2), 120.3(3), 114.8(3), and 169.9(3)°, respectively. The neutral diarylether donor is coordinated between the two amido groups, located 0.75 Å out of the NUN plane, approximately capping a face of the aforementioned trigonal bipyramid. Much like in anion **14**, the N/$C_{eq}$/N plane of the trigonal bipyramid in **15** is significantly tilted relative to the plane of the $XA_2$ ligand, indicated by the relatively expanded 29.7° angle between the N/O/N- and N/C(49)/N planes, which is again, likely a steric consideration.

The U−N distances of **15** are approximately 0.1 Å longer than those in neutral dialkyl complexes **3** and **4**, and only the U−C(48) distance of 2.377(9) Å falls within the range observed for the U−C bonds in **3** and **4**; the U−C(49) and U−C(50) bonds in **15** are substantially longer at 2.493(8) and 2.506(9) Å. However, the elongated uranium−ligand bond lengths in **15** are comparable to those of anion **14**, and as with **14**, this can be explained on the basis of the increased coordination number at uranium and the overall anionic charge on the complex. Indeed, the U−$C_{Me}$ bond lengths in other crystallographically-characterized uranium(IV) methyl 'ate' complexes are generally elongated as well, ranging from 2.465(7) Å in Andersen's alkoxy 'ate' complex [LiU(Me){OCH($^t$Bu)$_2$}$_4$],[160] to 2.48(1)−2.600(9) Å in Hayton's homoleptic hexamethyl 'ate' species [Li(tmeda)]$_2$[$UMe_6$].[37] The geometry of complex **15** is analogous to that in six-coordinate [($XA_2$)$UCl_2$(μ-Cl){K(dme)$_3$}] (**1**), which also exhibits a considerably

planar xanthene backbone and a trigonal-bipyramidal arrangement of the anionic donors. However, the U−O and U−N distances in **15** are substantially longer than those in [($XA_2$)$UCl_2$(μ-Cl){K(dme)$_3$}] (**1**), most likely due to decreased Lewis acidity, increased steric hindrance, and complete separation of the anionic portion of the complex from the alkali-metal countercation in **15**.

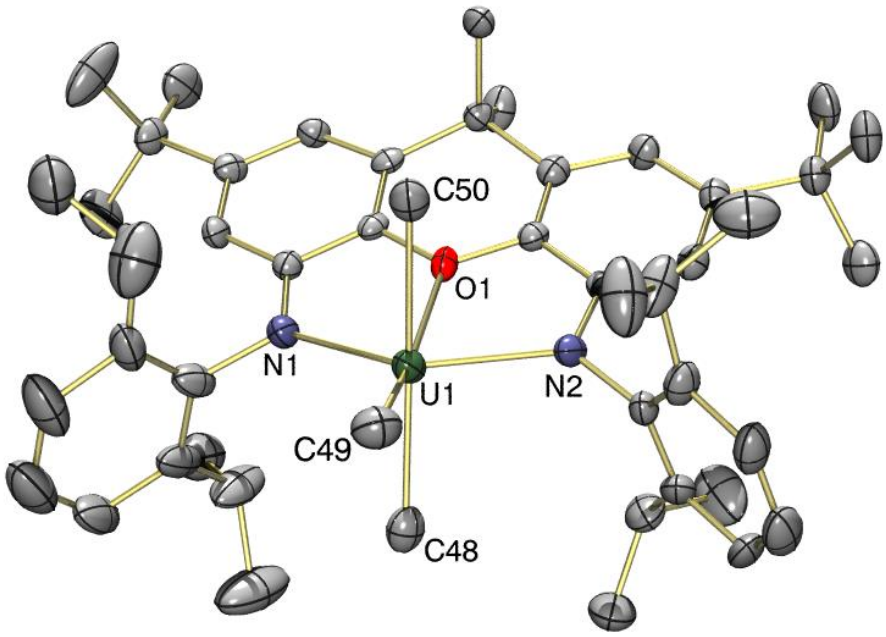


**Figure 4.4** – X-ray crystal structure of [Li(dme)$_3$][($XA_2$)$UMe_3$]·dme (**15**·dme), with thermal ellipsoids at 30% probability (collected at 173 K). Hydrogen atoms, the [Li(dme)$_3$]$^+$ countercation, and dme lattice solvent are omitted for clarity.

While numerous (~40) uranium(IV) methyl complexes have been structurally characterized, the majority are supported by carbocyclic ancillary ligands (substituted cyclopentadienides and cyclooctatetraenides). Crystallographically-characterized post-metallocene uranium(IV) methyl complexes are limited to the tris(amido) species

[UMe{N(SiMe$_3$)$_2$}$_3$],[282] and Cummins' [UMe{N($^t$Bu)(Ar)}$_3$] (Ar = 3,5-Me$_2$C$_6$H$_3$),[159] Edelmann's tris(benzamidinate) [{(Me$_3$SiN)$_2$CPh}$_3$UMe],[164] Andersen's alkoxy[160] and diphosphine[48] species [LiU(Me){OCH($^t$Bu)$_2$}$_4$] and [(dmpe)U(CH$_2$Ph)$_3$(Me)] (dmpe = 1,2-bis(dimethylphosphino)ethane), Shores' diphosphine [(dmpe)$_2$UMe$_4$],[283] and Hayton's homoleptic hexamethyl 'ate' complex [Li(tmeda)]$_2$[UMe$_6$].[37]

The extent to which the reactions of **3** with 2.1 equiv of LiCH$_2$$^t$Bu (in benzene) or 3.3 equiv of MeLi (in THF) lie toward the side of the products (**4** or **15** and LiCH$_2$SiMe$_3$) is remarkable, and likely[§] reflects the increased basicity of neopentyl and methyl anions in comparison with the (trimethylsilyl)methyl anion,[230] leading to stronger uranium−alkyl bonds. The requirement for addition of more than 2 equiv of LiCH$_2$$^t$Bu to convert **3-Th** to **4-Th** is also intriguing in that it highlights distinct differences in the reactivity of thorium and uranium, possibly arising from increased covalency in the uranium congener.

### 4.1.4 – Reactions of [(XA$_2$)U(CH$_2$SiMe$_3$)$_2$] with KCH$_2$Ph

In addition to the reactions of dialkyl [(XA$_2$)U(CH$_2$SiMe$_3$)$_2$] (**3**) with alkyllithium reagents LiCH$_2$SiMe$_3$, LiCH$_2$$^t$Bu, and MeLi, the reaction with benzylpotassium was also investigated. Upon addition of 1 equiv of KCH$_2$Ph to **3** in C$_6$D$_6$ or toluene-$d_8$ solution, $^1$H NMR spectroscopy revealed the evolution of a significant amount of SiMe$_4$ accompanied

[§] The thermodynamic driving force for conversion of **3** to **4** and **15** could alternatively be related to different levels of aggregation for the LiCH$_2$$^t$Bu and MeLi reactants versus the LiCH$_2$SiMe$_3$ product in solution. However, this explanation seems unlikely given that the reaction to form **4** was performed in an aromatic solvent while the reaction to form **15** was performed in THF, and the extent of alkyllithium aggregation in THF can be expected to be significantly less than that in benzene or toluene.

by a new collection of unidentified paramagnetically-shifted resonances, and the loss of signals corresponding to **3**. Although a number of pathways may be accessible, the presence of $SiMe_4$ as a by-product is similar to that previously observed during the decomposition process of tris((trimethylsilyl)methyl) anion **14**, which suggests that a mixed tris(hydrocarbyl) 'ate' species possibly of the form "$[(XA_2)U(CH_2SiMe_3)_2(CH_2Ph)]^-$" was quickly forming and decomposing in solution. Many avenues were explored in attempt to isolate the major product of this reaction, including the use of arene- (benzene, toluene) and ethereal solvents ($OEt_2$, dme, THF), saturated hydrocarbons (hexane, pentane, hexamethyldisiloxane), and mixtures thereof at various temperatures in the preparatory and purification stages of the reaction, as well as the addition of a neutral Lewis base, 4-(dimethylamino)pyridine (DMAP), to potentially stabilize a reactive product. Additionally, encapsulating agents such as 18-crown-6 and [2.2.2]-cryptand were applied in attempt to sequester the potassium cation and improve crystallinity, and countercation metathesis with $[Ph_3P{=}N{=}PPh_3][Cl]$ was attempted to replace the potassium cation outright. However, despite numerous attempts to isolate a crystalline product, only intractable material was obtained.

### 4.1.5 – $XA_2$ Uranium(IV) Tris(alkyl) 'ate' Cyclometalation

As mentioned previously, yellow ethereal solutions of tris(alkyl) 'ate' complexes **14** and **15** begin to decompose in under an hour, typified by a deepening of the solutions to a dark amber colour and $^1H$ NMR spectra that feature new collections of paramagnetically-shifted resonances accompanied by $SiMe_4$ and $CH_4$, respectively, with

loss of the original resonances belonging to **14** and **15**. In order to further explore the reactivity palette of organometallic $XA_2$ uranium species, this decomposition pathway was the subject of further investigation.

Previously, Emslie and co-workers found that the trimethyl 'ate' thorium complex [(BDPP)$ThMe_3${Li(dme)}] underwent cyclometalation at the methine carbon of an isopropyl group of the BDPP ligand to yield [(BDPP*)Th(μ-$Me)_2$Li(dme)] (BDPP* = [2,6-($NC_5H_3$)($CH_2$NAr)($CH_2$N{$C_6H_3$$^i$Pr($CMe_2$)-2,6}]$^{3-}$; Ar = 2,6-$^i$$Pr_2C_6H_3$; Figure 4.3, *vide supra*) over the course of several days in solution, with concomitant evolution of $CH_4$.[178] Given the structural and electronic similarities between [(BDPP)$ThMe_3${Li(dme)}] and [Li(dme)$_3$][($XA_2$)U($CH_2SiMe_3$)$_3$] (**14-dme**), similar decomposition pathways may be likely. Indeed, close inspection of the decomposition products of tris((trimethylsilyl)methyl) anion **14** by $^1$H NMR spectroscopy revealed that a single $C_1$-symmetric product [Li(THF-$d_8$)$_x$][($XA_2$*)U($CH_2SiMe_3$)$_2$] (**16-THF**; $XA_2$* = [4-(NAr)-5-(N{$C_6H_3$$^i$Pr($CMe_2$)-2,6})-2,7-$^t$$Bu_2$-9,9-$Me_2$(xanthene)]$^{3-}$; Ar = 2,6-$^i$$Pr_2C_6H_3$) was formed, accompanied by evolution of precisely one equiv of $SiMe_4$ (Scheme 4.7).

**Scheme 4.7 –** Cyclometalation of **14-THF** to yield **16-THF**.

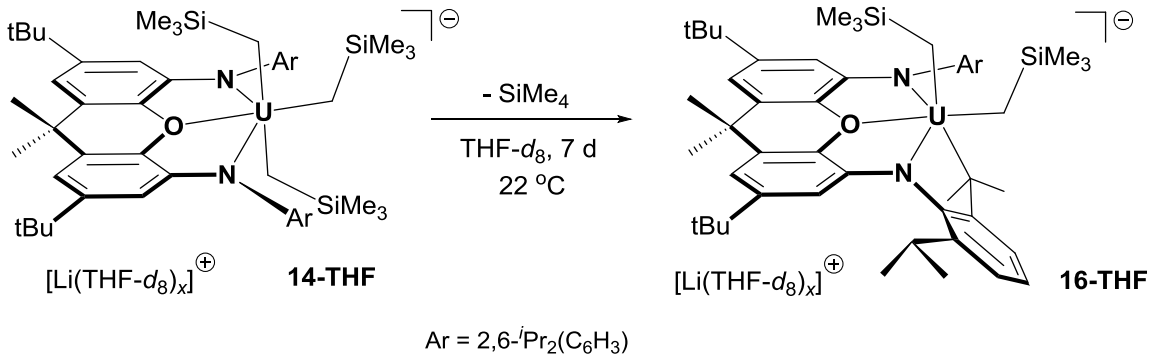


Analogous to the cyclometalated [(BDPP*)Th(μ-Me)$_2$Li(dme)] species, anion **16** is the product of metalation at the methine carbon of an isopropyl group of the $XA_2$ ligand of tris(alkyl) anion **14**. This assignment is corroborated by the presence of 31 paramagnetically-shifted $^1$H NMR resonances (ranging from +79 to −29 ppm), the full complement of signals expected for $C_1$-symmetric anion **16**. Additionally, initial attempts to prepare and crystallize tris(alkyl) 'ate' species **14-dme** afforded not only the desired tris(alkyl) complex, but also pale brown X-ray quality crystals of the cyclometalated derivative [Li(dme)$_3$][($XA_2$*)U($CH_2SiMe_3$)$_2$] (**16-dme**) as the [Li(dme)$_3$]$^+$ salt.

In the solid-state (Figure 4.5; Table 4.2), **16-dme** features a cyclometalated $C_1$-symmetric $XA_2$*-uranium(IV) anion and distal [Li(dme)$_3$]$^+$ cation, consistent with the $^1$H NMR spectral assignment. Uranium adopts a highly distorted six-coordinate geometry, with one $CH_2SiMe_3$ group occupying an apical position and one located approximately in the plane of the ancillary ligand backbone. The metalated $CMe_2Ar$ group is bound below the NUN-plane *cis* to amido donor N(1), forming a five-membered uranacycle, and as a

consequence of cyclometalation, the aryl ring of the metalated isopropyl group is significantly tilted toward the xanthene backbone (*i.e.* the angle between the plane of the aryl ring and the NUN-plane is 58.3° for the metalated ring and 82.3° for the non-metalated ring in anion **16**; cf. the corresponding angles of 76.3, 79.8° and 83.6, 87.8° in the two crystallographically independent molecules of dialkyl **3**). Perhaps to accommodate the strain associated with isopropyl methine cyclometalation, the xanthene backbone of anion **16** is considerably bent away from planarity, a feature atypical for 6-coordinate $XA_2$-uranium species (*i.e.* the angle between the two aryl rings of the xanthene backbone is 26.9° in anion **16** vs. 4.8 and 7.0° in tris(alkyl) 'ate' anion **14** and 6.5° in trimethyl 'ate' anion **15**). Indeed, the strain of isopropyl methine cyclometalation is likely also responsible for other structural phenomena observed in anion **16**, including the expanded U−O distance (2.59(1) Å) relative to those of tris(alkyl) 'ate' anions **14** and **15**.

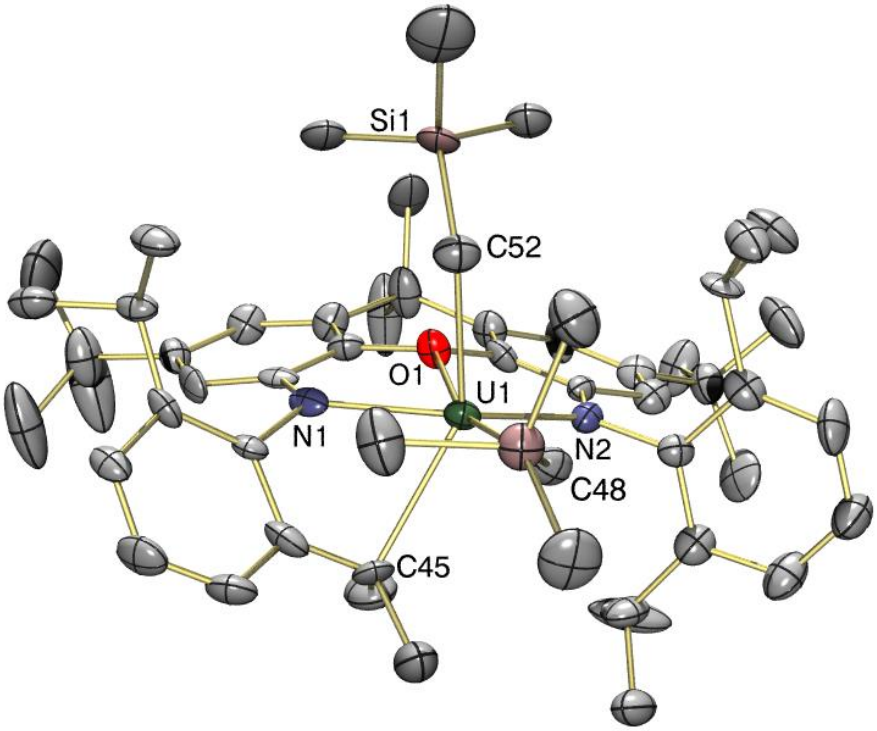


**Figure 4.5** – X-ray crystal structure of $[Li(dme)_3][(XA_2*)U(CH_2SiMe_3)_2]$ (**16-dme**), with thermal ellipsoids at 30% probability. Hydrogen atoms and the $[Li(dme)_3]^+$ countercation are omitted for clarity.

**Table 4.2 –** Selected bond lengths (Å) and angles (deg) for complexes **16-dme** and **14-dme** (for comparison).

| Compound | **16-dme** | **14-dme** |
|---|---|---|
| U−O | 2.59(1) | 2.515(6), 2.551(6) |
| U−N | 2.31(1), 2.35(1) | 2.389(9), 2.397(9), 2.374(9), 2.398(8) |
| U−$CH_2$ *in plane* | 2.47(2) | 2.46(1), 2.47(1) |
| U−$CH_2$ *apical* | 2.46(2) | 2.42(1), 2.50(1), 2.45(1), 2.45(1) |
| U−$CMe_2Ar$ | 2.56(2) | n/a |

| | | |
|---|---|---|
| Ligand Bend Angle[a] | 26.9° | 4.8, 7.0° |
| O···(N/U/N-plane) | 0.82 | 0.75, 0.83 |
| U···(N/O/N-plane) | 0.55 | 0.56, 0.62 |
| U−$CH_2$−Si *in plane* | 130(1)° | 147.9(6), 149.4(6)° |
| U−$CH_2$−Si *apical* | 133(1)° | 134.5(6), 140.1(6), 136.2(7), 139.6(6)° |
| U−$CMe_2$−$C_{ipso}$ | 97(1)° | n/a |
| N(1)···N(2) | 4.12 | 4.20, 4.23 |

[a] Ligand Bend Angle = the angle between the two aromatic rings of the xanthene ligand backbone.

The U−$CMe_2$Ar bond distance of 2.56(2) Å is significantly expanded relative to the remaining U−$C_{alkyl}$ distances of anion **16**, likely, in part, due to the geometric constraints of the $XA_2$* ligand and the strain associated with isopropyl methine cyclometalation. However, the $CMe_2$Ar group may instead be viewed as a substituted benzyl ligand, which tend to bind uranium through elongated U−C bonds relative to those of aliphatic alkyls (*vide supra*, Chapter 3). From this perspective, the U−$CMe_2$Ar distance (2.56(2) Å) is comparable to the U−$CH_2$Ph bond lengths of Hayton's homoleptic hexabenzyl 'ate' species $\{[K(THF)]_3[K(THF)_2][U(CH_2Ph)_6]_2\}_x$ (U−C = 2.50(2)−2.63(2) Å).[37] Likely also a consequence of the geometric constraints of the metalated $XA_2$* ligand, the benzyl-like $CMe_2$Ar ligand features a relatively acute U−$CMe_2$−$C_{ipso}$ angle (97(1)°) and relatively short U−$C_{ipso}$ and U−$C_{ortho}$ contacts (3.10 and 3.05 Å, respectively), which suggests that multi-hapto bonding may be in effect. The U−$CH_2$ and U−N distances in anion **16** are quite comparable to those observed for the tris((trimethylsilyl)methyl) precursor **14**; a reasonable observation given the electronic similarities between the two species.

Cyclometalation of an isopropyl moiety originating from a 2,6-diisopropylphenyl group is fairly common in early transition metal[284] and f-element[285] chemistry, but typically occurs at a *methyl* carbon rather than a *methine* carbon. Rare examples of complexes that engage in isopropyl *methine* metalation include [(BDPP)Lu($AlMe_4$)],[286] [(nacnac)(X)Ti=CH$^t$Bu] (X = Cl, Br, OTf, $BH_4$, $CH_2SiMe_3$; nacnac = {CH(CMeNAr)$_2$}$^-$, Ar = 2,6-$^i$Pr$_2$C$_6$H$_3$),[287] [(BDPP)Th$Me_3${Li(dme)}],[178] [{(Me$_3$Si)$_2$N}$_2$Sn=NAr] (Ar = 2,6-$^i$Pr$_2$C$_6$H$_3$),[288] [(nacnac)$Me_2$Nb=N$^t$Bu],[289] [La$_2$($\mu_2$-NAr)($\mu_3$-NAr){($\mu_2$-Me)$_2$AlMe}(AlMe$_4$)$_2$] (Ar = 2,6-$^i$Pr$_2$C$_6$H$_3$),[290] and [Ar$_2$Ge=C=C($^t$Bu)(Ph)] (Ar = 2,4,6-$^i$Pr$_3$C$_6$H$_2$).[291]

Complex **16-dme** can also be synthesized on a preparative (100 mg) scale by reaction of 1.1 equiv of $LiCH_2SiMe_3$ with dialkyl **3** in neat dme (Scheme 4.8). Immediately upon addition of the alkyllithium, the tris(alkyl) 'ate' anion **14** is formed *in situ* as evidenced by an abrupt colour change from cherry-red to yellow, and the solution was then stirred for approximately 1 week at room temperature to allow for complete cyclometalation of **14**. After work-up, crude **16-dme** was isolated as a brown powder in 73% yield; however, further purification proved challenging, and analytically-pure material could not be obtained as a consequence.

**Scheme 4.8 –** Preparation of cyclometalated 'ate' complex **16-dme** from dialkyl **3**.

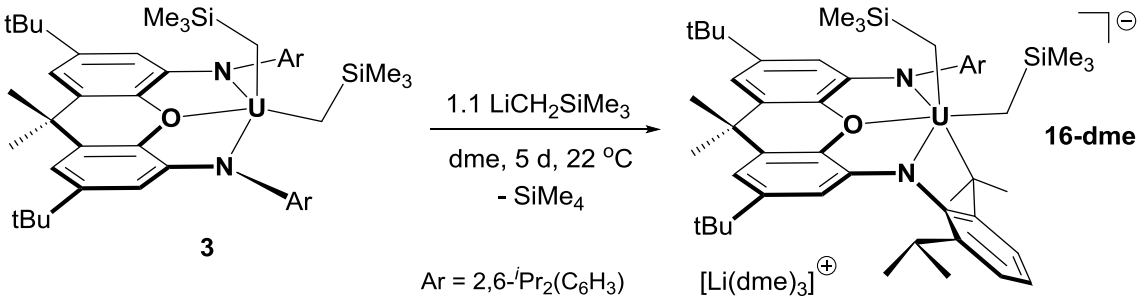


The most plausible mechanism for the C−H activation of an isopropyl group of the tris(alkyl) 'ate' anion **14** *en route* to cyclometalated anion **16** is simple σ-bond metathesis, which may be active *via* a direct pathway (**a** in Figure 4.6), or *via* initial γ C−H activation of a $CH_2Si\mathit{Me}_3$ group, followed by a second σ-bond metathesis (**b** in Figure 4.6). Actinide-mediated γ C−H activation of an alkyl group has been previously observed by several groups; Marks and co-workers reported that thermolysis of the thorium dialkyl $[Cp^*_2Th(CH_2SiMe_3)_2]$ cleanly yielded the thoracyclobutane species $[Cp^*_2Th\{\kappa^2\text{-}(CH_2)_2SiMe_2\}]$, and determined that γ C−H activation was in effect *via* a deuterium-labelling study.[292] Additionally, Leznoff and co-workers observed the formation of a metallacyclic dimer $[(^{t\mathrm{Bu}}NON)U\{CH(SiMe_3)(SiMe_2CH_2)\}]_2$ ($^{t\mathrm{Bu}}NON$ = $\{(^tBuNSiMe_2)_2O\}^{2-}$), which formed as a result of γ C−H activation of individual $\{CH(SiMe_3)_2\}$ ligands.[174]

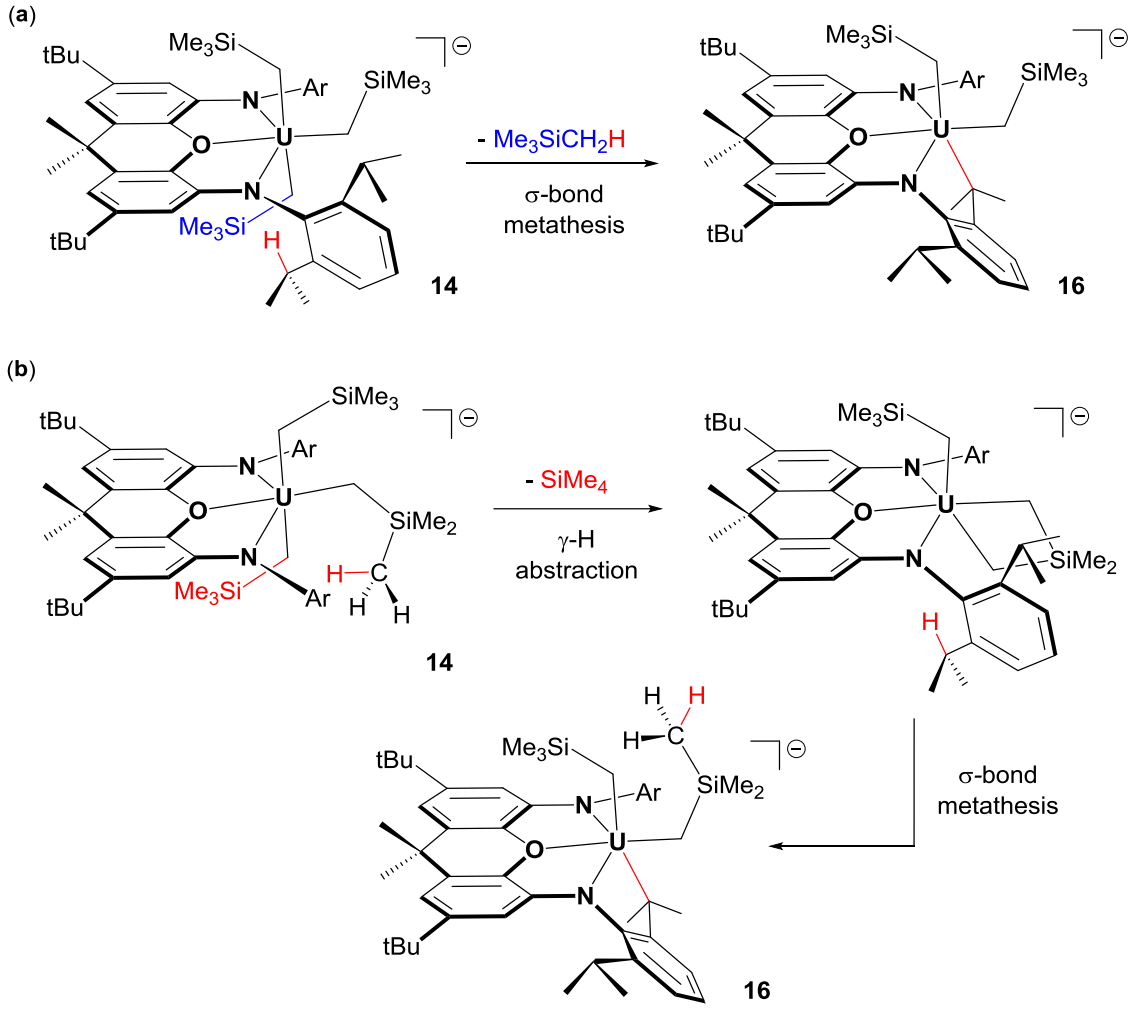


**Figure 4.6 –** Possible σ-bond metathesis mechanisms for the formation of cyclometalated anion **16**: (**a**) direct σ-bond metathesis; (**b**) γ C−H activation of a $CH_2Si\mathit{Me}_3$ group, followed by a second σ-bond metathesis. Ar = 2,6-diisopropylphenyl.

While less likely, an additional pathway invoking the 1,2–addition of an isopropyl methine C−H bond across a *transient uranium alkylidene* linkage arising from initial α-hydrogen abstraction could also provide **16** (Figure 4.7).

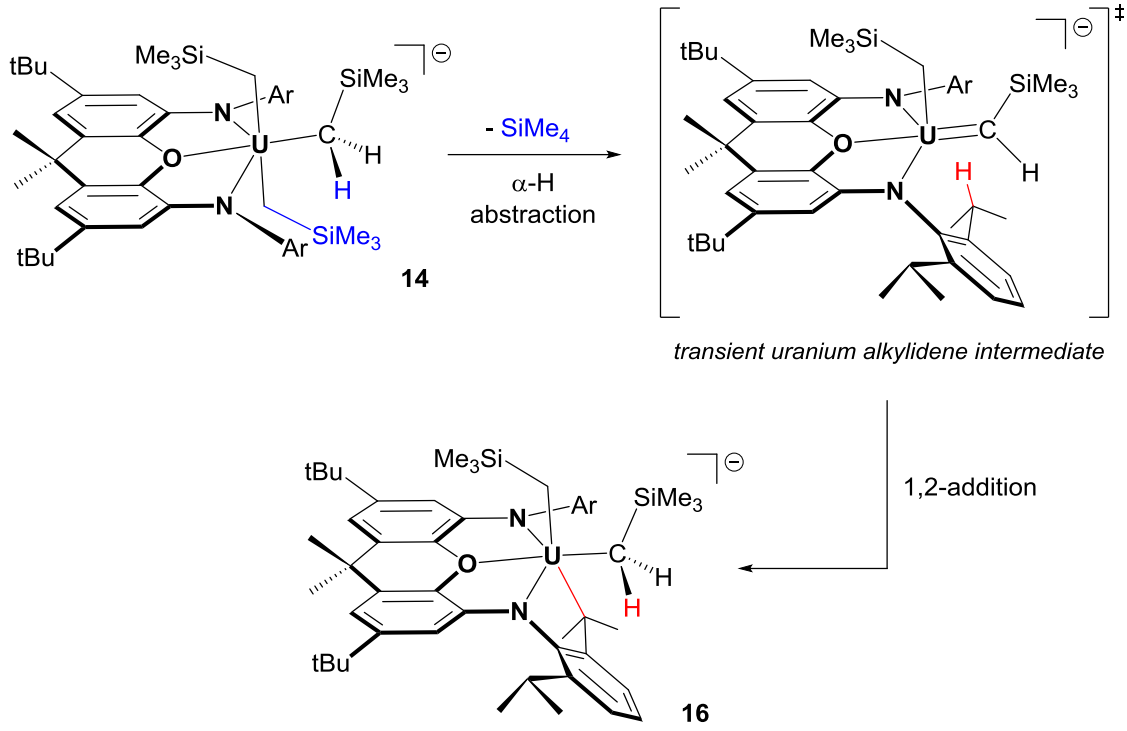


**Figure 4.7** – Possible α-hydrogen abstraction pathway yielding a transient uranium alkylidene intermediate and subsequent 1,2–addition of an isopropyl C−H bond yielding **16**. Ar = 2,6-diisopropylphenyl.

To probe which mechanism is active in this cyclometalative process, the appropriately deuterated tris(alkyl) precursor could be employed, allowing for study of the chemical composition of the silane that is eliminated as a by-product. In the case of **14**, selectively incorporating deuterium at the α-positions to yield the $d_6$-anion $[(XA_2)U(CD_2SiMe_3)_3]^-$ would result in the elimination of the $d_2$-silane $Me_3SiCD_2H$ if either σ-bond metathesis pathway (**a** or **b** in Figure 4.6) is engaged, and the $d_3$-silane $Me_3SiCD_3$ would be eliminated if α-deuterium abstraction *en route* to an alkylidene-type intermediate is active (Figure 4.7). In such a deuterium-labelling scheme, either silane

would be readily identifiable by NMR spectroscopy. Unfortunately, the necessary $d_2$-alkyllithium $LiCD_2SiMe_3$ is not accessible by known chemical methodology, and while the related $d_9$-reagent $LiCH_2Si(CD_3)_3$ can be prepared,[117] the $d_9$-silane $H_3CSi(CD_3)_3$ would be the product of either direct σ-bond metathesis *or* α-hydrogen abstraction, leading to an inconclusive result.

However, Emslie and co-workers were previously able to prepare the appropriately isotopically-labelled species [(BDPP)Th($^{13}CD_3$)$_3${Li(dme)}] in order to probe the mechanism for the formation of the cyclometalated derivative (Figure 4.3, *vide supra*).[178] The authors reported that thermal decomposition of the isotopically-labelled trimethyl 'ate' complex yielded only $^{13}CHD_3$ (rather than $^{13}CD_4$) and [BDPP*)Th(μ-$^{13}CD_3$)$_2$Li(dme)] (rather than the $^{13}CD_3$/$^{13}CHD_2$ species) by $^{13}C$ and $^{13}C\{^1H\}$ NMR spectroscopy.[178] These products are consistent with a σ-bond metathesis pathway, with no evidence to support the α-deuterium abstraction route. Given the structural and electronic similarities between [(BDPP)Th$Me_3${Li(dme)}] and [Li(dme)$_3$][(X$A_2$)U($CH_2SiMe_3$)$_3$] (**14-dme**), it is reasonable to infer that similar cyclometalative mechanisms are in effect in both species. Thus, it is likely that the tris(alkyl) 'ate' anion **14** is converted to metalated **16** by simple σ-bond metathesis, rather than *via* an exotic alkylidene intermediate.

### 4.2 – Reactions of [(XA$_2$)U(CH$_2$SiMe$_3$)$_2$] with Neutral Lewis Bases

Beyond reactions with anionic Lewis bases ($Me_3SiCH_2^-$, $^tBuCH_2^-$, $H_3C^-$, $PhCH_2^-$) neutral dialkyl [(XA$_2$)U(CH$_2$SiMe$_3$)$_2$] (**3**) was also treated with a variety of neutral Lewis bases in attempt to form new base-incorporated dialkyl species or promote further reactivity. This avenue was inspired by the seminal work of Chen and co-workers, who were able to access and structurally-characterize the first rare-earth metal terminal imido complex, formed upon introduction of a neutral Lewis base.[293] The authors utilized a custom amine-appended tridentate β-diketiminato (nacnac) ligand to stabilize an anilido methyl scandium(III) complex [($\kappa^3$-nacnac′)Sc(NHAr)(Me)] ($\kappa^3$-nacnac′ = {(ArN)C(Me)CHC(Me)(NCH$_2$CH$_2$NMe$_2$)}$^-$, Ar = 2,6-$^i$Pr$_2$C$_6$H$_3$); although heating the anilido methyl complex did not lead to any further reactivity, addition of the Lewis base 4-(dimethylamino)pyridine (DMAP) promoted the elimination of CH$_4$ by α-hydrogen abstraction, affording the terminal imido species [($\kappa^3$-nacnac′)Sc=NAr(DMAP)] (Figure 4.8).[293]

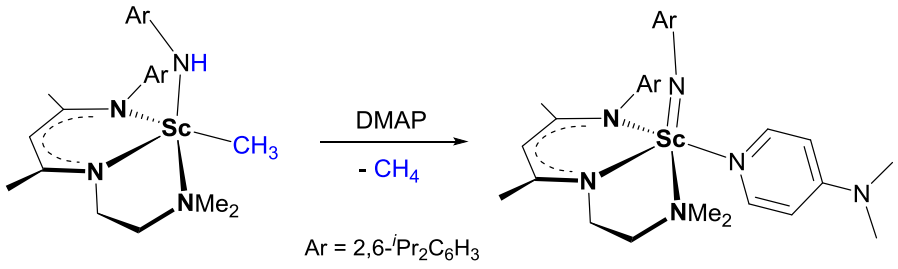


**Figure 4.8 –** Lewis base-promoted α-hydrogen abstraction to yield a terminal imido complex.

With respect to our dialkyl uranium platform **3**, we envisioned that introduction of the appropriate Lewis base may be able to promote a similar α-hydrogen abstraction reaction, but with formation of a yet-unknown neutral uranium alkylidene complex, rather than an imido species (Figure 4.9).

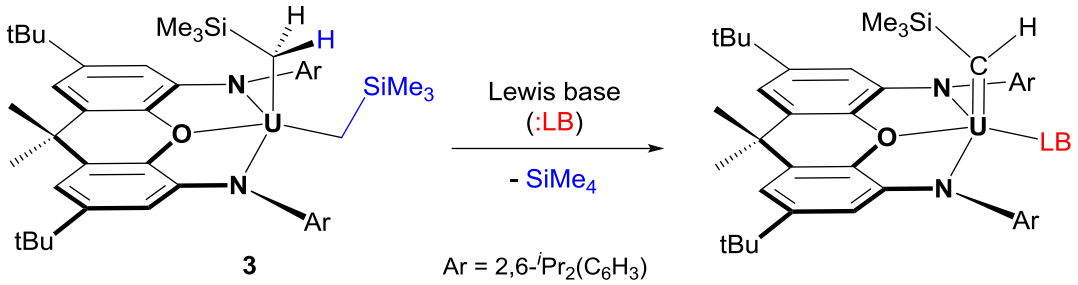


**Figure 4.9 –** Proposed Lewis base-promoted α-hydrogen abstraction of **3**.

While transition-metal carbene/alkylidene species are well established,[294] finding extensive application in organic synthesis[295] and catalysis,[296] analogous species containing f-element–carbon multiple bonds are largely unexplored. The energy mismatch and poor spatial overlap between the f-element- and carbon valence orbitals significantly limits the stabilization of the carbenic centre by π-back-donation in f-element carbene species, and many have cited this as the primary reason for the distinct paucity of progress in this area.[297-299] Indeed, the strong ionic character of f-element complexes results in significant charge polarization in f-element–carbon multiple bonds, and consequently, such species have been classified as *nucleophilic carbenes*.[297]

While few families of complexes exhibiting U=C multiple-bonding character are known,[298] the only isolable uranium carbene species are heteroatom-stabilized, with

phosphorus α- to the carbenic centre in all cases (selected examples are depicted in Figure 4.10); despite considerable interest, no 'true' f-element alkylidene complex has been isolated to-date. α-phosphorus-stabilized uranium carbene species include [$Cp_3U$=CHP(Me)RR′] (R = R′ = Me, Ph; R = Me and R′ = Ph) reported by Gilje and Cramer,[300] and Hayton's [{$(Me_3Si)_2N$}$_3$U=CHP$Ph_3$].[301] Additionally, the groups of Ephritikhine and Liddle have developed families of uranium carbene complexes supported by the bis(thiophosphorano)methandiide ({$C(PPh_2S)_2$}$^{2-}$)[302] and bis(iminophosphorano)methanediide ($BIPM^X$; {$C(PPh_2NR)_2$}$^{2-}$)[303] pincer ligands, respectively. These ligands feature two α-phosphorus substituents that stabilize the central carbenic donor, and assist in facilitating U=C multiple bonding by forcing the carbenic moiety into the coordination sphere, anchoring it through coordination of the remaining donor atoms of the pincer array.

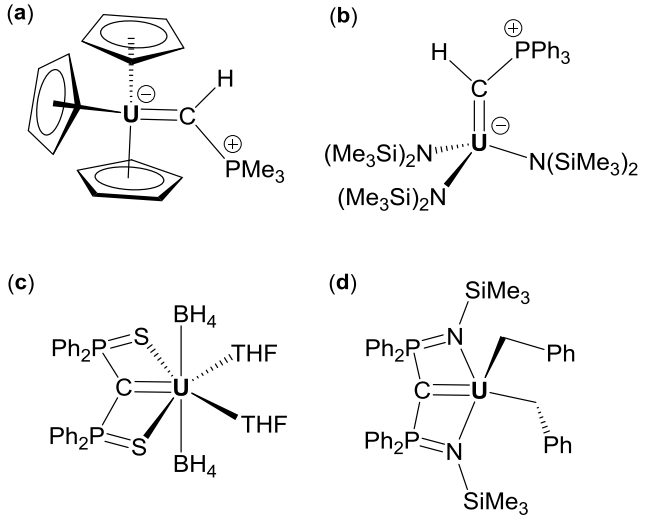


**Figure 4.10 –** Selected examples of α-phosphorus-stabilized uranium carbene complexes: (**a**) [$Cp_3U$=CHP$Me_3$], (**b**) [{$(Me_3Si)_2N$}$_3$U=CHP$Ph_3$], (**c**) [{$\kappa^3$-$C(PPh_2S)_2$}$U(BH_4)_2(THF)_2$], and (**d**) [$(BIPM^{TMS})U(CH_2Ph)_2$].[173]

### 4.2.1 – $XA_2$ Uranium(IV)-Mediated DMAP Activation

Somewhat surprisingly, no reaction occurred between dialkyl **3** and one equiv of $PMe_3$, 2,2′-bipyridine (bipy), or quinuclidine (1-azabicyclo[2.2.2]octane) in $C_6D_6$ at room temperature, with $^1$H NMR spectra revealing only the starting complex **3** and the free Lewis base in solution. Heating the solutions of **3**/Lewis base to 40−45 °C resulted in no change to the respective $^1$H NMR spectra. However, treatment of dialkyl **3** with approximately one equiv of 4-(dimethylamino)pyridine (DMAP) in $C_6D_6$ resulted in an abrupt colour change from orange to reddish-orange, and $^1$H NMR spectroscopy revealed a new, clean collection of extremely broadened paramagnetically-shifted resonances accompanied by $SiMe_4$ and the loss of signals corresponding to **3**. The reaction was repeated on a preparative scale in toluene; the red mixture was stirred for 1 hr and subsequently layered with *n*-pentane and cooled to −30 °C. After several days, orange crystals were harvested; X-ray diffraction analysis did not reveal a uranium(IV) alkylidene species, but rather $[(XA_2)U(CH_2SiMe_3)(\kappa^2\text{-DMAP*})(DMAP)]\cdot 2(\text{toluene})$ (**17**·2(toluene); Figure 4.11 and Table 4.3), a uranium(IV) monoalkyl complex featuring a neutral $\kappa^1$-DMAP ligand and an anionic, cyclometalated $\kappa^2$-*C,N*-DMAP* ligand, where DMAP* is the anion formed upon deprotonating DMAP at the 2-position, $(4\text{-}NMe_2\text{-}NC_5H_3)^-$.

Although one equiv of DMAP was originally introduced to the reaction, no complex bearing only one DMAP derivative was accessible.[§] In attempt to isolate a species featuring one DMAP ligand, the reaction of **3** with one equiv of DMAP was conducted on a preparative scale in *n*-pentane; surprisingly, after stirring for approximately 45 min, a bright yellow solid precipitated from solution. However, the identity of the precipitate was confirmed to be complex **17** by $^{1}$H NMR spectroscopy. Subsequently, the reaction of **3** with 2.1 equiv of DMAP in *n*-pentane afforded **17**·(*n*-pentane) as an analytically-pure bright yellow precipitate, which was isolated by centrifugation in 91% yield (Scheme 4.9).

**Scheme 4.9** – Preparation of [(XA$_2$)U(CH$_2$SiMe$_3$)(κ$^2$-DMAP*)(DMAP)] (**17**).

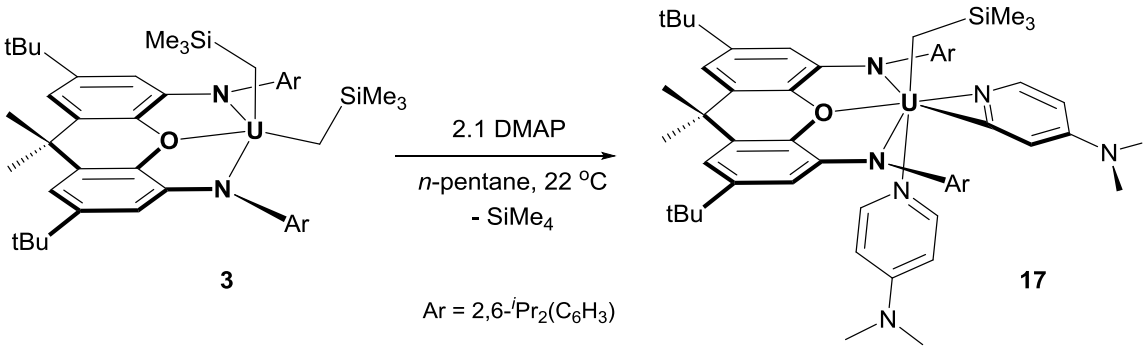


The X-ray crystal structure of **17**·2(toluene) (Figure 4.11; Table 4.3) revealed a seven-coordinate $C_1$-symmetric XA$_2$-uranium(IV) complex featuring an axially-bound

[§] $^{1}$H NMR spectroscopy revealed a slightly different collection of broadened, paramagnetically-shifted resonsances when dialkyl **3** was treated with 1 equiv of DMAP delivered *via* a stock solution. However, complex **17** (containing two equiv of DMAP) was always obtained regardless of reaction stoichiometry, presumably in approx. 50% yield when only 1 equiv of DMAP was used. Therefore, further exploration of the complex formed upon addition of 1 equiv of DMAP to **3** was not pursued.

(trimethylsilyl)methyl ligand, an equatorially-bound cyclometalated $\kappa^2$-*C,N*-DMAP* ligand, and a neutral $\kappa^1$-DMAP ligand coordinated approximately *trans*- to the alkyl substituent. The 4 anionic donors (N(1), N(2), C(48), and C(52)) and pyridyl donor N(3) adopt a distorted trigonal-bipyramidal arrangement around the metal centre, with N(1)−U−N(2), N(1)−U−C(52), N(2)−U−C(52), and C(48)−U−N(3) angles of 125.41(8), 110.8(1), 122.1(1), and 169.0(1)°, respectively. The neutral diarylether donor is located 0.59 Å out of the NUN plane in the direction of the $\kappa^1$-DMAP ligand, coordinated between the two amido groups capping a face of the aforementioned trigonal bipyramid. As typically observed in other $XA_2$ uranium(IV) species with coordination numbers greater than five, the xanthene backbone of the $\kappa^3$-$XA_2$ ligand is quite planar in complex **17**, with a 4.9° angle between the two aryl rings of the xanthene backbone (cf. 1.2° in trichloro **1**, 6.5° in trimethyl **15**, and 4.8, 7.0° in tris(alkyl) **14**).

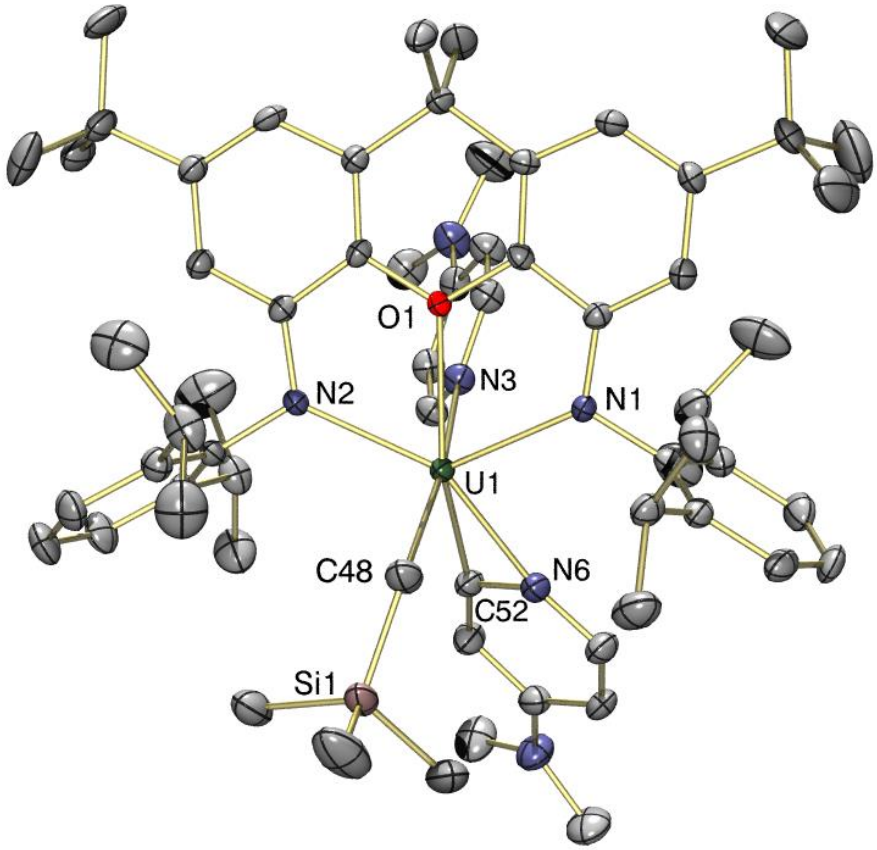


**Figure 4.11** – X-ray structure of [($XA_2$)U($CH_2SiMe_3$)($\kappa^2$-DMAP*)(DMAP)]·2(toluene) (**17**·2(toluene)), with thermal ellipsoids at 50% probability. Hydrogen atoms and two toluene lattice solvent molecules are omitted for clarity.

**Table 4.3** – Selected bond lengths (Å) and angles (deg) for complexes **17** and **18** (vs. **3** for comparison).

| Compound | **17** | **18** | **3** |
|---|---|---|---|
| U−O | 2.542(2) | 2.557(5) | 2.484(5), 2.504(4) |
| U−$N_{pincer}$ | 2.388(2), 2.395(3) | 2.371(6), 2.378(7) | 2.261(5), 2.262(5), 2.272(5), 2.280(5) |
| U−N ($\kappa^1$-pyridyl)[a] | 2.640(3) | 2.579(6) | n/a |

| | | | |
|---|---|---|---|
| U−N ($\kappa^2$-pyridyl*)[b] | 2.367(3) | 2.355(7) | n/a |
| U−$CH_2$ | 2.425(4) | 2.463(8) | 2.368(7), 2.380(7), 2.418(7), 2.393(7) |
| U−C ($\kappa^2$-pyridyl*) | 2.421(3) | 2.429(8) | n/a |
| U−$CH_2$−Si | 132.1(2) | 138.7(4) | 128.2(3), 130.4(3), 130.5(4), 130.8(3) |
| N−U−C ($\kappa^2$-pyridyl*) | 32.6(1)° | 33.1(3)° | n/a |
| Ligand Bend Angle[c] | 4.9° | 4.7° | 17.5, 18.8° |
| Angle between the N/O/N- and N/$C_{eq}$/N-planes | 32.5° | 37.6° | 7.7, 8.4° |
| O···(N/U/N-plane) | 0.59 | 0.67 | 0.91, 0.95 |
| U···(N/O/N-plane) | 0.43 | 0.49 | 0.64, 0.65 |
| N(1)···N(2) | 4.25 | 4.20 | 4.00, 4.02 |

[a] $\kappa^1$-pyridyl = DMAP for **17**, AJ for **18**. [b] $\kappa^2$-pyridyl* = DMAP* for **17**, AJ* for **18**. [c] Ligand Bend Angle = the angle between the two aromatic rings of the xanthene ligand backbone.

The U−O (2.542(2) Å), U−$N_{pincer}$ (2.388(2), 2.395(3) Å), and U−$CH_2$ (2.425(4) Å) distances in complex **17** are generally elongated relative to those of other neutral $XA_2$ uranium(IV) species, likely in part due to increased electronic saturation in seven-coordinate **17**, which is formally a 16-electron complex (cf. formally 12-electron, five-coordinate dialkyls **3** and **4**). Significant steric crowding around the uranium centre in complex **17** also likely contributes to the elongated U−ligand bond distances; while the U−O, U−$N_{pincer}$, and U−$CH_2$ distances of **17** are expanded relative to those of anionic trichloro **1** and trimethyl **15**, which bear relatively small chloro- and methyl ligands, respectively, they are quite comparable to those of the considerably sterically-hindered tris((trimethylsilyl)methyl) 'ate' anion **14**.

Although the lone U−$CH_2$ bond distance in **17** (2.425(4) Å) is expanded relative to those of other neutral $XA_2$ uranium(IV) hydrocarbyl species, it falls within the range observed in other structurally-characterized, neutral uranium(IV) (trimethylsilyl)methyl complexes, which exhibit U−C bond distances ranging from 2.40(2)−2.44(2) Å in Leznoff's [($^{DIPP}$NCOCN)U($CH_2SiMe_3$)$_2$] ($^{DIPP}$NCOCN = κ$^3$-{($ArNCH_2CH_2$)$_2$O}$^{2-}$, Ar = 2,6-$^i$Pr$_2$C$_6$H$_3$),[60] to 2.464(4) Å in Cloke's mixed sandwich complex [($^{TIPS2}$COT)(Cp*****)U($CH_2SiMe_3$)] ($^{TIPS2}$COT = {1,4-(Si$^i$Pr$_3$)$_2$C$_8$H$_6$}$^{2-}$).[155] Furthermore, elongation of U−$C_{alkyl}$ distances has been observed in other monoalkyl uranium(IV) complexes bearing cyclometalated κ$^2$-*C,N*-pyridyl ligands (*vide infra*). For instance, the U−$C_{Me}$ distances in Kiplinger's [Cp*****$_2$UMe{κ$^2$-*C,N*-pyridyl}] complexes range from 2.445(9)–2.467(4) Å,[304,305] significantly expanded relative to those of the dimethyl precursor [Cp*****$_2$UMe$_2$] (U−$C_{Me}$ = 2.414(7), 2.424(7) Å).[125]

The nitrogen donor of the neutral κ$^1$-DMAP ligand in complex **17** is coordinated to uranium through a relatively long bond (U−N(3) = 2.640(3) Å), but this distance is comparable to U−N bond lengths in other structurally-characterized uranium(IV) κ$^1$-DMAP complexes, which are limited to Andersen's [(Cp′)$_2$U=O(DMAP)] (Cp′ = {η$^5$-1,2,4-$^t$Bu$_3$($C_5H_2$)}$^-$; U−N = 2.535(4) Å),[116] Liddle's [(BIPM$^{TMS}$)U=NCPh$_3$(DMAP)$_2$] (BIPM$^{TMS}$ = κ$^3$-{C($PPh_2NSiMe_3$)$_2$}$^{2-}$; U−$N_{DMAP}$ = 2.580(5), 2.586(5) Å),[306] and Zi's [Cp*****$_2$U{η$^2$-$C_2$($SiMe_3$)$_2$}(DMAP)] (U−N = 2.632(6) Å).[307] Unsurprisingly, the cyclometalated, anionic κ$^2$-*C,N*-DMAP* ligand in complex **17** is bound to uranium more intimately than neutral DMAP, with tighter U−N and U−C contacts of 2.367(3) and

2.421(3) Å, respectively. The DMAP* ligand is coordinated *edge-on*, forming a three-membered metallacycle with an acute N(6)−U−C(52) angle of 32.6(1)°.

Uranium-mediated C−H activation of pyridyl derivatives yielding complexes which feature cyclometalated, anionic $\kappa^2$-*C,N*-pyridyl ligands has been previously observed by several groups. Dormond and co-workers originally observed that the four-membered metallacycle [{$(Me_3Si)_2N$}$_2$U{$\kappa^2$-*C,N*-$CH_2SiMe_2NSiMe_3$}] cleanly activates an α-C−H bond of pyridine (and of pyridyl derivatives), yielding orthometalated products of the form [{$(Me_3Si)_2N$}$_3$U{$\kappa^2$-*C,N*-(4-R′-6-R-$NC_5H_2$)}] (R = H, R′ = H, Me; R = Me, R′ = H), which were spectroscopically characterized.[308] Scott and co-workers reported that the cyclometalated triamidoamine uranium(IV) complex [($tren^{TBS*}$)U] ($tren^{TBS*}$ = $\kappa^5$-{$N(CH_2CH_2NR)_2(CH_2CH_2NSi(Me)(^tBu)(CH_2)\}^{4-}$; R = $SiMe_2{}^tBu$) also activates pyridine, forming [($tren^{TBS}$)U($\kappa^2$-*C,N*-$NC_5H_4$)] ($tren^{TBS}$ = $\kappa^4$-{$N(CH_2CH_2NSiMe_2{}^tBu)_3\}^{3-}$; **a** in Figure 4.12).[309] [($tren^{TBS}$)U($\kappa^2$-*C,N*-$NC_5H_4$)] was structurally-authenticated, revealing an anionic $\kappa^2$-*C,N*-pyridyl ligand symmetrically bound *edge-on* to uranium, forming a three-membered metallacycle with identical[§] U−N and U−C distances of 2.469(9) Å, and an acute N−U−C angle of 29.2(2)°.[309] Later, Kiplinger and co-workers demonstrated that [Cp**$_2$UMe$_2$] could also activate C−H bonds of pyridyl derivatives, yielding similar edge-on $\kappa^2$-*C,N*-pyridyl products of the form [Cp**$_2$UMe{$\kappa^2$-*C,N*-(4-R′-6-R-$NC_5H_2$)}] (R = H, R′ = H, $^t$Bu; R = Me, R′ = H; **b** in Figure 4.12), with U−N and U−C distances of

[§] The authors noted that [($tren^{TBS}$)U($\kappa^2$-*C,N*-$NC_5H_4$)] suffered from exchange disorder associated with the $\kappa^2$-$NC_5H_4$ ligand in the solid state; see Boaretto, R.; Roussel, P.; Alcock, N. W.; Kingsley, A. J.; Munslow, I. J.; Sanders, C. J.; Scott, P. *J. Organomet. Chem.* **1999**, *591*, 174.

2.394(3)−2.424(6) Å and 2.386(3)−2.406(7) Å, respectively, and N−U−C angles ranging from 31.8(3)–32.9(1)°.[304,305] Additionally, Diaconescu and co-workers reported that similar pyridyl C−H activation chemistry could be achieved utilizing the 1,1′-diamidoferrocene species [(FcNN)U($CH_2Ph$)$_2$] (FcNN = {Fc($NSiMe_2{}^tBu$)$_2$}$^{2-}$), which reacts with pyridyl derivatives to furnish complexes of the form [(FcNN)U($CH_2Ph$){κ$^2$-*C*,*N*-(6-R-$NC_5H_3$)}] (R = H, Me; **c** in Figure 4.12); the U−N and U−C distances range from 2.370(4)−2.393(3) Å and 2.397(3)−2.406(5) Å, respectively, and the N−U−C angles are 32.5(1)°.[310]

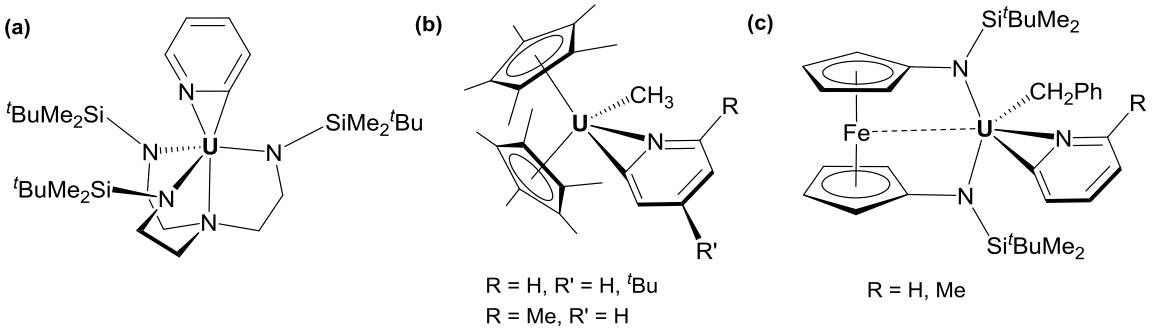


**Figure 4.12 –** Structurally-characterized uranium complexes featuring cyclometalated κ$^2$-*C*,*N*-pyridyl ligands.

The N(6)−U−C(52) angle and U−N(6) and U−C(52) bond lengths in **17** are in close agreement with those observed in comparable *edge-on* κ$^2$-*C*,*N*-pyridyl complexes of uranium, and while **17** is the first example of a uranium complex featuring a cyclometalated κ$^2$-*C*,*N*-DMAP* ligand, analogous C−H activation at the α-position of DMAP has been observed for thorium. Zi and co-workers reported that the metallacyclopropene species [(Cp′)$_2$Th(η$^2$-$C_2Ph_2$)] (Cp′ = {η$^5$-1,2,4-$^tBu_3(C_5H_2)$}$^-$)

activates DMAP to yield the $\kappa^2$-DMAP* alkenyl thorium complex [$(Cp')_2Th(\kappa^1$-C(Ph)CHPh)($\kappa^2$-*C*,*N*-DMAP*)], though this species was not structurally-characterized.[311]

The room-temperature $^1$H NMR spectrum of complex **17** in $C_6D_6$ or toluene-$d_8$ is clean but thoroughly uninformative, featuring 8 extremely broadened resonances located between +10 and −10 ppm. The significant broadening of the resonances is a clear indication that **17** is highly fluxional in solution; although the nature of the fluxional process is unclear, rotation of the asymmetrically-bound $\kappa^2$-DMAP* ligand about the U−C(52) bond is a reasonable possibility, perhaps combined with neutral DMAP coordination and de-coordination to yield isomers with different arrangements of the DMAP, DMAP*, and $CH_2SiMe_3$ ligands within the coordination pocket of the $XA_2$ ligand. At low-temperature (approximately −80 °C), the $^1$H NMR resonances of complex **17** only sharpen to limited extent, indicating that while de-coalescence is taking place, the complex remains fluxional in solution at low temperature (Figure 4.13). As a consequence, the low-temperature $^1$H NMR spectrum of **17** is uninformative. However, at high temperature (80 °C), the signals coalesce to yield an averaged $^1$H NMR spectrum featuring 23 paramagnetically shifted resonances located between +31 and −72 ppm, indicative of an approximately $C_s$-symmetric isomer of complex **17** (Figure 4.13). Although **17** can tolerate brief heating at 80 °C, decomposition begins at 50 °C as indicated by accelerated $SiMe_4$ evolution, and continues at high temperature to yield a mixture of unidentified paramagnetic products.

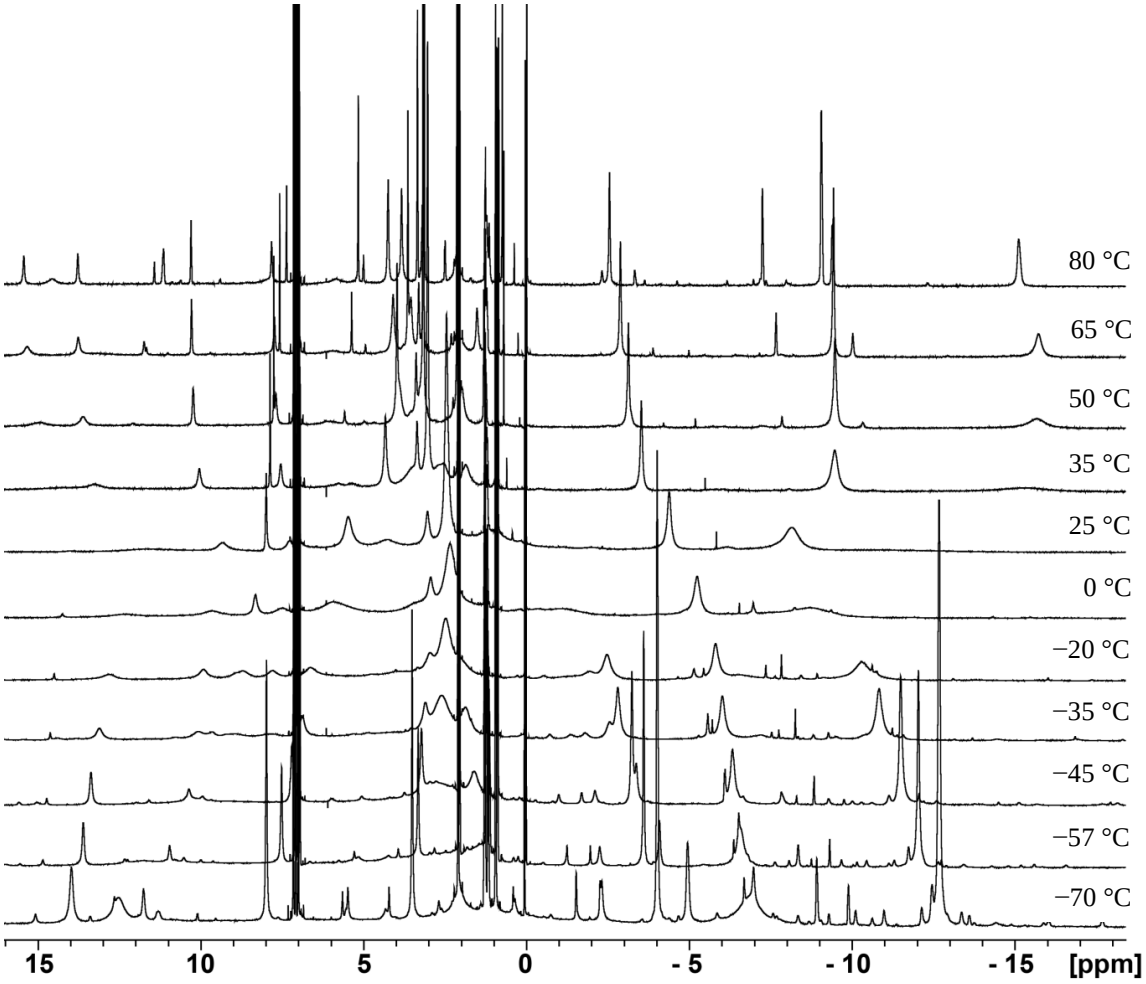


**Figure 4.13 –** Selected regions of the $^{1}$H NMR spectra of [(XA$_2$)U(CH$_2$SiMe$_3$)($\kappa^2$-DMAP*)(DMAP)] (**17**) in toluene-$d_8$ at temperatures ranging from +80 to −70 °C (500 MHz). Resonances located at high (>15 ppm) and low (<−15 ppm) frequencies are not shown. Signals corresponding to toluene-$d_8$, SiMe$_4$, CMe$_3$, and *n*-pentane are truncated in the +80 °C spectrum.

Although no intermediates could be detected by $^{1}$H NMR spectroscopy, the formation of complex **17** most likely proceeds by initial DMAP coordination to dialkyl **3** forming [(XA$_2$)U(CH$_2$SiMe$_3$)$_2$($\kappa^1$-DMAP)], followed by cyclometalative α-C−H activation of the bound DMAP ligand to yield [(XA$_2$)U(CH$_2$SiMe$_3$)($\kappa^2$-DMAP*)] and

$SiMe_4$. Subsequently, coordination of a second DMAP ligand to the $[(XA_2)U(CH_2SiMe_3)(\kappa^2\text{-DMAP*})]$ intermediate occurs, yielding complex **17**. Mechanistically, although several pathways for the formation of **17** can be envisioned, the cyclometalative C−H activation of DMAP likely occurs *via* a simple σ-bond metathesis pathway, as is common for coordinatively-unsaturated, electropositive f-element complexes.[312]

In order to definitively ascertain the mechanism of the cyclometalative DMAP C−H activation *en route* to the formation of complex **17**, a deuterium-labelling scheme was employed utilizing 2,6-DMAP-$d_2$, an isotopomer with deuterium selectively incorporated at the α-positions prepared in-house by known chemical methodology.[313] As depicted in Figure 4.14, several avenues[§] for the formation of complex **17** can be considered which yield products with varying deuteration patterns; (**a**) straight-forward σ-bond metathesis, (**b**) base-induced γ C−H activation followed by a second σ-bond metathesis, or (**c**) base-induced α-hydrogen abstraction yielding a transient uranium alkylidene species, followed by 1,2-addition of an *ortho* C−H bond of coordinated DMAP across the U=C linkage.

[§] Pathways leading to **17** which involve the initial activation of an isopropyl methine C−H bond (whether *via* base-induced σ-bond metathesis or *via* 1,2-addition across a U=CHR bond) followed by transfer of a DMAP proton to the metalated isopropyl group to form the cyclometalated DMAP* ligand are ruled out, as in either case, the coordinated neutral DMAP ligand would end up *trans*- to the cyclometalated isopropyl group, with a (trimethylsilyl)methyl ligand in the *cis*-position effectively blocking DMAP from transfering a proton to the cyclometalated isopropyl group. Formation of an intermediate with a cyclometalated isopropyl group in the equatorial position is unlikely given the considerable strain it would invoke.

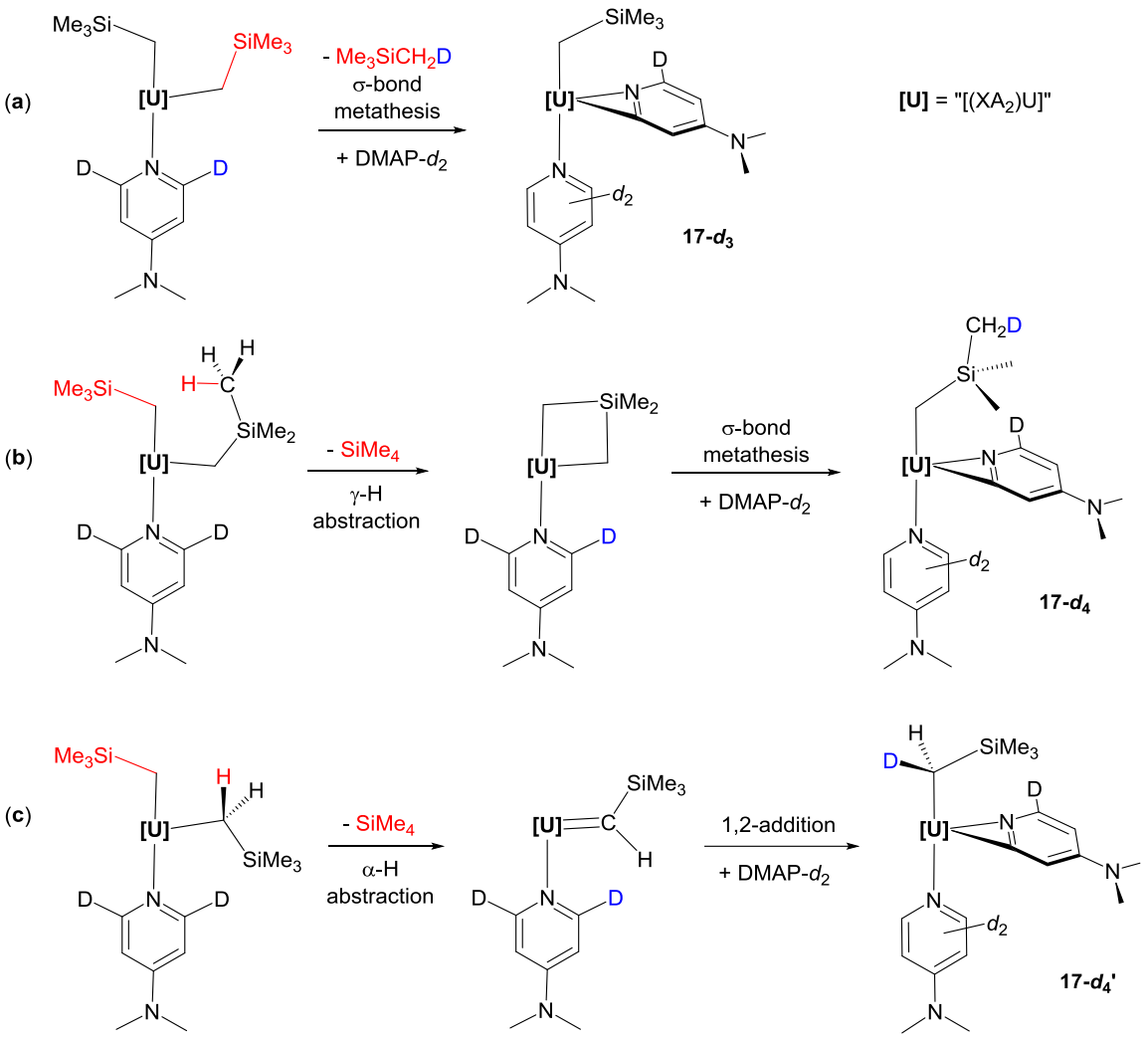


**Figure 4.14 –** Plausible mechanisms for the formation of complex **17**.

To probe the mechanism, the reaction between dialkyl **3** and DMAP-$d_2$ was monitored *in-situ* by $^1$H NMR spectroscopy; the silane by-product was readily identified as the $d_1$-silane $Me_3SiCH_2D$, consistent with a σ-bond metathesis mechanism (pathway **a** in Figure 4.14). Although the fluxional behaviour of complex **17** did not permit identification of the deuterated isotopomer of the uranium product (labelled **17-*d*$_3$**, **17-*d*$_4$**,

or **17-*d*$_4$′** in Figure 4.14), the deuterated uranium product was isolated in pure form[§] and purposefully decomposed in solution by careful addition of $H_2O$ in order to analyze the organic decomposition products by $^2$H NMR spectroscopy. In a sealable NMR tube, a solution of the deuterated uranium product in $C_6H_6$ was treated with excess $H_2O$ and the tube was quickly sealed; $^2$H NMR spectroscopy revealed only $^2$H resonances attributable to DMAP-$d_2$ and DMAP-$d_1$, as well as $C_6H_5D$ present at low natural-abundance in the $C_6H_6$ solvent. No $d_1$-silane $Me_3SiCH_2D$ was observed, indicating that neither **17-*d*$_4$** nor **17-*d*$_4$′** (the products of pathways **b** and **c** in Figure 4.14, respectively) were formed, and no deuterium was incorporated into the $XA_2$ ligand, ruling out the involvement of an intermediate featuring a cyclometalated $XA_2$* ligand.[¶] This outcome confirms that no other competitive mechanism was active in the formation of complex **17**. Kiplinger and co-workers similarly demonstrated that a σ-bond metathesis pathway was also responsible for the formation of the analogous complex [Cp*$_2$UMe(κ$^2$-*C*,*N*-$NC_5H_4$)].[304] To probe the mechanism, the authors monitored the reaction of [Cp*$_2$$UMe_2$] with pyridine-$d_5$ in solution; $^1$H NMR spectroscopy revealed the exclusive formation of the $d_4$-complex [Cp*$_2$UMe(κ$^2$-*C*,*N*-$NC_5D_4$)] and $CH_3D$ as the lone methane isotopomer, products consistent with a σ-bond metathesis mechanism.[304]

[§] The $d_3$-isotopomer **17-*d*$_3$** was prepared by treating dialkyl **3** with 2 equiv of DMAP-$d_2$ on a preparative scale in *n*-pentane; **17-*d*$_3$** precipitated as a bright yellow solid.

[¶] If an intermediate of appropriate ligand orientation featuring a cyclometalated isopropyl group such as [($XA_2$*)U($CH_2SiMe_3$)(κ$^1$-DMAP-$d_2$)] could form, cyclometalative C−H activation of the DMAP-$d_2$ ligand would result in deuterium-incorporation into the $XA_2$ ligand (as $CDMe_2ArN$).

### 4.2.2 – $XA_2$ Uranium(IV)-Mediated 9-azajulolidine Activation

To expand the scope of the reactivity of organometallic $XA_2$ uranium species with pyridyl-based ligands, dialkyl **3** was treated with 9-azajulolidine (AJ), a commercially-available, bulky DMAP derivative featuring a fused tricyclic structure. To this end, 2.1 equiv of 9-azajulolidine were added to a solution of **3** in $C_6D_6$, resulting in a subtle deepening of the red colour; much like for the reaction of **3** with DMAP, $^1$H NMR spectroscopy revealed a clean but extremely broadened collection of resonances accompanied by $SiMe_4$, and loss of signals corresponding to **3**. The reaction was repeated on a preparative scale in *n*-pentane (Scheme 4.10); after stirring for approx 4 h, the faintly turbid solution was cooled to −30 °C. After several days, a yellow-brown crystalline solid was deposited, identified as $[(XA_2)U(CH_2SiMe_3)(\kappa^2\text{-AJ*})(AJ)]$ (**18**) by X-ray diffraction crystallography, obtained in nearly quantitative yield.

**Scheme 4.10** – Preparation of $[(XA_2)U(CH_2SiMe_3)(\kappa^2\text{-AJ*})(AJ)]$ (**18**).

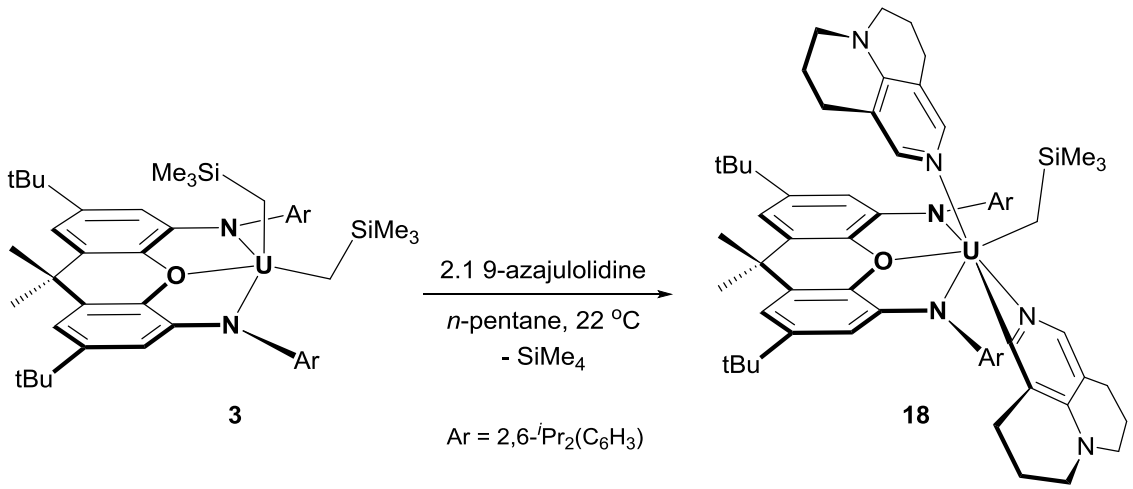

In the solid-state (Figure 4.15; Table 4.3), **18**·2(*n*-pentane) bears a number of structural features consistent with those observed for the related DMAP complex, **17**; both seven-coordinate, $C_1$-symmetric $XA_2$-uranium(IV) complexes feature a lone alkyl group, a cyclometalated $\kappa^2$-*C,N*-pyridyl* derivative bound *edge-on*, and a neutral $\kappa^1$-coordinated pyridyl ligand. However, in **18**, these ligands are organized differently within the coordination environment of the $XA_2$ ancillary; the $\kappa^2$-*C,N*-AJ* ligand occupies an axial position approximately *trans* to the neutral $\kappa^1$-AJ donor, and the (trimethylsilyl)methyl group is bound *cis* to both AJ moieties, presumably to limit unfavourable steric interactions between the $XA_2$ ligand and the bulky AJ groups. The 4 anionic donors (N(1), N(2), C(48), and C(52)) and pyridyl donor N(5) adopt a distorted trigonal-bipyramidal arrangement around the metal centre, with N(1)−U−N(2), N(1)−U−C(48), N(2)−U−C(48), and C(52)−U−N(5) angles of 124.2(2), 113.0(2), 120.3(2), and 161.0(3)°, respectively. The neutral diarylether donor is bound relatively far (0.67 Å) above the NUN plane in the direction of the neutral $\kappa^1$-AJ ligand, coordinated between the two amido groups, capping a face of the aforementioned trigonal bipyramid. The N/$C_{eq}$/N-plane of the trigonal bipyramid in **18** is heavily tilted relative to the plane of the $XA_2$ ligand, more so than in any other $XA_2$ uranium complex, as indicated by the considerably expanded angle between the N/O/N- and N/C(48)/N-planes of 37.6°. This is likely a consequence of the significant steric pressure asserted by the fused ring systems of the AJ groups bound to uranium.

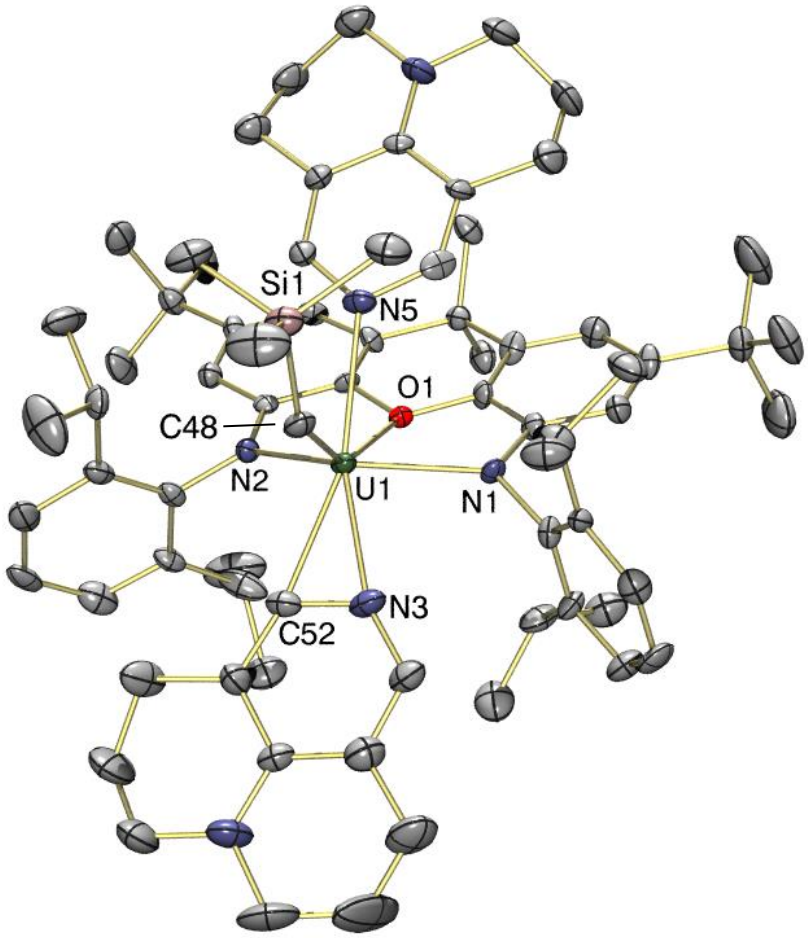


**Figure 4.15** – X-ray crystal structure of [(XA$_2$)U(CH$_2$SiMe$_3$)($\kappa^2$-AJ*)(AJ)]·2(*n*-pentane) (**18**·2(*n*-pentane)), with thermal ellipsoids at 50% probability. Hydrogen atoms and lattice solvent are omitted for clarity.

The U−O (2.557(5) Å), U−N$_{pincer}$ (2.371(6), 2.378(7) Å), and U−C(52) (2.429(8) Å) bond distances, and N(3)−U−C(52) angle (33.1(3)°) in complex **18** are quite comparable to those observed for the related DMAP analogue **17**, but despite the bulky, fused ring-systems of the AJ substituents, the neutral (U−N$_{AJ}$ = 2.579(6) Å) and cyclometalated (U−N$_{AJ*}$ = 2.355(7) Å) pyridyl groups are bound to uranium through

tighter U−N contacts in **18** (cf. $U-N_{DMAP}$ and $U-N_{DMAP*}$ distances of 2.640(3) and 2.367(3) Å in **17**, respectively), possibly a result of the increased donor ability of 9-azajulolidine relative to DMAP.[314] Perhaps as a consequence of the increased electronic saturation afforded to uranium by the superior AJ donors (relative to DMAP), the $U-CH_2$ distance of 2.463(8) Å in **18** is expanded relative to that in **17** ($U-CH_2$ = 2.425(4) Å), but this may also be the result of steric congestion in the coordination sphere of the metal. Indeed, such steric crowding is also likely responsible for the considerably expanded U−C−Si angle of 138.7(4)°, though expansion for the purpose of strengthening a potential C−H−U α-agostic interaction cannot be ruled out.

Much like for complex **17**, the room-temperature $^1$H NMR spectrum of **18** in $C_6D_6$ or toluene-$d_8$ is clean but thoroughly uninformative, featuring seven extremely broadened resonances located between +8 and −21 ppm, indicating that **18** is highly fluxional in solution. As for **17**, the origin of the fluxional process is unknown, but processes involving rotation about the U−C(52) bond of the cyclometalated $\kappa^2$-AJ* ligand, as well as de-coordination and subsequent re-coordination of the neutral $\kappa^1$-AJ ligand to form a species with a different spatial distribution of ligands relative to the coordination environment of the $XA_2$ ancillary are reasonable possibilities. At low-temperature (approximately −80 °C), a complex $^1$H NMR spectrum is observed which features > 60 relatively sharp, paramagnetically-shifted resonances, significantly more than would be expected for any one isomer of complex **18** alone. This suggests that a mixture of isomers is present in solution at low-temperature, possibly arising from a combination of the aforementioned processes. Unfortunately, at elevated temperature (approximately 60 °C),

the $^{1}$H NMR resonances of complex **18** are only marginally coalesced; the spectrum features 14 broad resonances located between +11 and −29 ppm, from which little can be gleaned regarding the structure of complex **18** in solution. Complex **18** is less thermally-stable than closely-related **17**, as significant thermal decomposition begins at 40 °C in solution as indicated by accelerated $SiMe_4$ evolution.

From a mechanistic perspective, the cyclometalative C−H activation of AJ *en route* to the formation of complex **18** likely occurs *via* a simple σ-bond metathesis pathway highly analogous to that observed for the formation of closely-related **17**. A deuterium labelling study was not carried out, but an alternate mechanism is not expected given the structural- and electronic similarities between DMAP and AJ, and between uranium products **17** and **18**. Although 9-azajulolidine has been utilized as a ligand/co-catalyst in copper-catalyzed post-Ullmann C(aryl)−E (E = N, O, S) bond-forming reactions,[315] AJ-containing copper species were not described by the authors. Consequently, **18** is the first metal complex of AJ to be identified and crystallographically characterized.

Rather intriguingly, despite providing dialkyl **3** with 2 equiv of either DMAP or AJ, only one pyridyl ligand is activated *en route* to the formation of complexes **17** and **18**, respectively, which now join five other uranium(IV) $\kappa^2$-*C,N*-pyridyl complexes that feature an intact alkyl group. Diaconescu *et al*. observed similar behaviour, as 2 equiv of pyridine (or 2-picoline (2-Me-$NC_5H_4$)) was introduced to the dibenzyl precursor [(FcNN)U($CH_2Ph)_2$], yet only the mono-activated product [(FcNN)U($CH_2Ph$)($\kappa^2$-*C,N*-pyridyl)] was formed.[310] Kiplinger *et al.* observed that the $\kappa^2$-py* species [Cp**$_2$UMe($\kappa^2$-

*C,N*-$NC_5H_4$)] engages in pyridyl ligand-exchange in the presence of 5 equiv of 2-picoline, yielding the cyclometalated $\kappa^2$-*C,N*-(α-picolyl) complex [Cp*****$_2$UMe{$\kappa^2$-*C,N*-(6-Me($NC_5H_3$)}] along with liberated pyridine, with no evidence for the formation of a bis($\kappa^2$-*C,N*-pyridyl) species.[304] The selective C−H activation of a *single* pyridyl ligand despite the presence of intact U−C linkages and excess pyridyl substrate is remarkable and puzzling, especially given that further pyridyl coordination can indeed be accommodated (*i.e* Kiplinger's pyridyl exchange mechanism likely involves a species of the form [Cp*****$_2$UMe($\kappa^2$-*C,N*-$NC_5H_4$)($\kappa^1$-2-picoline)], and complexes **17** and **18** both feature a coordinated $\kappa^1$-pyridyl ligand in addition to the cyclometalated $\kappa^2$-pyridyl* moiety).

**Table 4.4** – Crystallographic data collection and refinement parameters for complexes **14-dme**, **15**, and **16-dme**.

| Structure | **14-dme**·2(dme) | **15**·dme | **16-dme** |
|---|---|---|---|
| Formula | $C_{71}H_{125}Li\ N_2O\ Si_3U$ | $C_{66}H_{111}Li\ N_2O_9U$ | $C_{67}H_{113}Li\ NO_7Si_2U$ |
| Formula wt | 1447.96 | 1321.54 | 1359.74 |
| *T* (K) | 100(2) | 173(2) | 100(2) |
| Cryst. Syst. | Orthorhombic | Triclinic | Orthorhombic |
| Space Group | *Pca*2(1) | *P*–1 | *P*2(1)2(1)2(1) |
| *a* (Å) | 25.0530(18) | 14.259(4) | 12.785(2) |
| *b* (Å) | 25.4722(18) | 14.344(4) | 22.414(3) |
| *c* (Å) | 25.8586(18) | 17.959(5) | 25.160(4) |
| α [deg] | 90 | 76.978(5) | 90 |
| β [deg] | 90 | 81.499(5) | 90 |
| γ [deg] | 90 | 83.966(6) | 90 |
| Volume [Å$^3$] | 16502(2) | 3529.4(17) | 7209.9(19) |

| | | | |
|---|---|---|---|
| *Z* | 8 | 2 | 4 |
| Density (calcd; $Mg/m^3$) | 1.166 | 1.244 | 1.253 |
| μ ($mm^{-1}$) | 2.055 | 2.350 | 2.332 |
| *F*(000) | 6064 | 1376 | 2832 |
| Crystal Size ($mm^3$) | 0.450×0.190×0.050 | 0.20×0.20×0.02 | 0.370×0.120×0.020 |
| θ Range for Collection [deg] | 0.799–28.322 | 1.98–26.50 | 1.619–25.414 |
| No. of reflns. Collected | 96542 | 41002 | 54610 |
| No. of Indep. Reflns. | 38301 | 14468 | 12825 |
| Completeness to θ Max (%) | 100.0 | 99.1 | 97.1 |
| Absorption Correction | Numerical | Multi-scan | Numerical |
| Max and Min Transmission | 0.9915, 0.6330 | 1.00, 0.805 | 1.000, 0.5548 |
| Data / Parameters | 38301 / 1541 | 14468 / 712 | 12825 / 732 |
| GOF on $F^2$ | 1.018 | 0.985 | 0.983 |
| Final $R_1$ [$I > 2\sigma(I)$] | R1 = 0.0538 wR2 = 0.1121 | R1 = 0.0653 wR2 = 0.1220 | R1 = 0.0700 wR2 = 0.1513 |
| *R* indices (all data) | R1 = 0.1089 wR2 = 0.1323 | R1 = 0.1435 wR2 = 0.1498 | R1 = 0.1207 wR2 = 0.1755 |

**Table 4.5** – Crystallographic data collection and refinement parameters for complexes **17** and **18**.

| Structure | **17**·2(toluene) | **18**·2(*n*-pentane) |
|---|---|---|
| Formula | $C_{76.59}H_{105.24}N_6OSiU$ | $C_{83}H_{125}N_6OSiU$ |
| Formula wt | 1392.04 | 1489.00 |
| *T* (K) | 100(2) | 100(2) |
| Cryst. Syst. | Triclinic | Orthorhombic |
| Space Group | *P*–1 | *Pca*2(1) |
| *a* (Å) | 10.9088(14) | 27.049(2) |
| *b* (Å) | 14.7669(19) | 13.2390(10) |

| | | |
|---|---|---|
| *c* (Å) | 23.527(3) | 21.6950(16) |
| α [deg] | 84.947(2) | 90 |
| β [deg] | 80.749(2) | 90 |
| γ [deg] | 76.410(3) | 90 |
| Volume [Å$^3$] | 3630.9(8) | 7769.1(10) |
| *Z* | 2 | 4 |
| Density (calcd; Mg/m$^3$) | 1.273 | 1.273 |
| μ (mm$^{-1}$) | 2.297 | 2.152 |
| *F*(000) | 1442 | 3116 |
| Crystal Size (mm$^3$) | 0.305×0.256×0.058 | 0.280×0.132× 0.048 |
| θ Range for Collection [deg] | 2.133–27.677 | 1.538–28.300 |
| No. of reflns. Collected | 46320 | 58825 |
| No. of Indep. Reflns. | 16763 | 19268 |
| Completeness to θ Max (%) | 99.6 | 100.0 |
| Absorption Correction | Numerical | Numerical |
| Max and Min Transmission | 0.9137, 0.7123 | 0.9833, 0.6844 |
| Data / Parameters | 16763 / 784 | 19268 / 804 |
| GOF on $F^2$ | 1.045 | 0.991 |
| Final $R_1$ [$I > 2\sigma(I)$] | R1 = 0.0346 wR2 = 0.0765 | R1 = 0.0451 wR2 = 0.0923 |
| *R* indices (all data) | R1 = 0.0439 wR2 = 0.0789 | R1 = 0.0781 wR2 = 0.1018 |

# Chapter 5

# Ligand Evolution: XAT Potassium–Alkane Complexes and XAd Thorium(IV) Hydrocarbyl Complexes

Adapted with permission from: Andreychuk, N. R., and Emslie, D. J. H. *Angew. Chem. Int. Ed.* **2013**, *52*, 1696–1699. Copyright 2013 John Wiley & Sons.

## 5.1 – XAT: An Exceptionally Bulky $XA_2$ Analogue

### 5.1.1 – Ligand Synthesis and XAT Dipotassium–Alkane Complexes

Previous ventures in $XA_2$ (and related BDPP) thorium[40,179,180] and uranium[177,187] chemistry aimed at developing thermally-robust and highly active cationic monoalkyl actinide catalysts for use in the insertion-polymerization of olefins met with numerous hurdles. In particular, the coordination of facially-bound arene solvent molecules (**a** and **b** in Figure 5.1), the benzyl moiety of a benzylborate counterion (**c** in Figure 5.1), or remaining neutral dialkyl precursor complex (**d** in Figure 5.1) was established as a persistent structural motif which, through competition with ethylene for the active site, asphyxiated any potential catalytic activity.

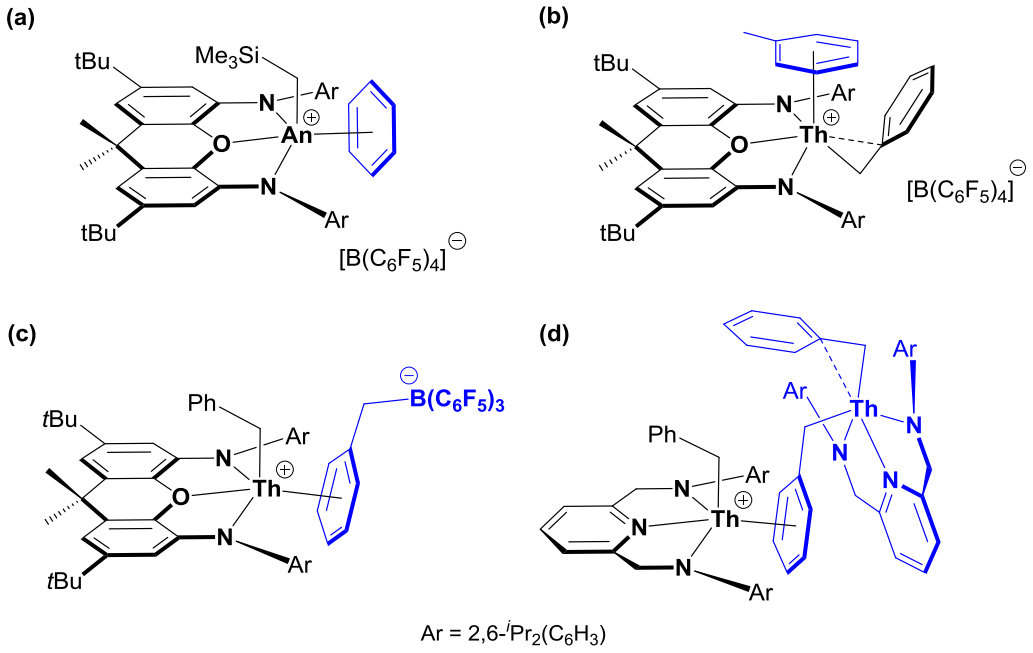


**Figure 5.1** – Coordinated arenes in cationic $XA_2$ and BDPP actinide complexes: **a)** benzene in $[(XA_2)An(CH_2SiMe_3)(\eta^6\text{-}C_6H_6)]^+$ (An = U (**6**), Th (**6-Th**)), **b)** toluene in $[(XA_2)Th(CH_2Ph)(\eta^6\text{-}C_6H_5Me)][B(C_6F_5)_4]$ (**9-Th**), **c)** the benzylborate counteranion $[PhCH_2B(C_6F_5)_3]^-$ in $[(XA_2)Th(CH_2Ph)][PhCH_2B(C_6F_5)_3]$, and **d)** neutral $[(BDPP)Th(CH_2Ph)_2]$ in $[(BDPP)Th(\eta^2\text{-}CH_2Ph)(\mu\text{-}\eta^1\text{:}\eta^6\text{-}CH_2Ph)Th(\eta^1\text{-}CH_2Ph)(BDPP)][B(C_6F_5)_4]$ (BDPP = 2,6-bis(2,6-diisopropylanilidomethyl)pyridine).

Through electronic tuning of the coordinated arene by utilizing electron-deficient fluoroarenes we have been able to unlock latent ethylene polymerization behaviour in $XA_2$ actinide cations of the form $[(XA_2)An(CH_2SiMe_3)(\text{fluoroarene})]^+$ (An = U (cations **10** and **12**); An = Th (cation **10-Th**)). However, despite reasonable catalytic activities achieved using these systems, the use of fluoroarene solvents for olefin polymerization is not likely to be a viable solution in industry, and as such, ancillary ligand evolution was

explored as a circumventive strategy in an attempt to completely disengage such cation−arene interactions.

Inspired by the work of Power and co-workers who have pioneered the use of *m*-terphenyl derivatives as sterically-demanding ancillary ligands for the stabilization of highly reactive, low-coordinate species across the periodic table,[316] we designed an extremely bulky [$XA_2$] analogue, 4,5-bis(2,6-dimesitylanilido)-2,7-di-*tert*-butyl-9,9-dimethylxanthene, [XAT],[317] which bears sterically-imposing 2,6-dimesitylphenyl (Dmp) groups flanking the metal coordination pocket. We envisioned that these Dmp flanking groups could potentially disfavour cation−arene interactions, and possibly promote more facile olefin polymerization catalysis as a result. Additionally, bulky mesityl groups are expected to thoroughly protect the axial coordination sites of actinide derivatives, leading to low coordination numbers and possibly greater control over reactivity patterns. The *o*-methyl substituents of the terminal mesityl groups insist on an orthogonal disposition of the mesityl rings with respect to the central *N*-aryl ring, providing sufficient room for metal-binding in the NON pocket and ideally preventing cyclometalation, a common degradation pathway travelled by electropositive metal alkyl species.[318]

Palladium-catalyzed coupling of 4,5-dibromo-2,7-di-*tert*-butyl-9,9-dimethylxanthene with 2 equiv of 2,6-dimesitylaniline, which was prepared in-house by known chemical methodology,[319] afforded 4,5-bis(2,6-dimesitylanilino)-2,7-di-*tert*-butyl-9,9-dimethylxanthene, $H_2$[XAT] (**19**) (Scheme 5.1), an extremely sterically-hindered analogue of the known 4,5-bis(2,6-diisopropylanilino)-2,7-di-*tert*-butyl-9,9-dimethylxanthene ($H_2[XA_2]$)[40] and 4,5-bis(2,4,6-trimethylanilino)-2,7-di-*tert*-butyl-9,9-

dimethylxanthene[214] proligands. The resulting crude semi-solid was recrystallized from an EtOH/toluene mixture to yield proligand **19** as a colourless microcrystalline solid in 66% yield, and the procedure can be scaled to produce multi-gram quantities. It is noteworthy that despite the considerable steric profile of the 2,6-dimesitylaniline starting material, a mixed bromo/amino xanthene intermediate (4-bromo-5-(2,6-dimesitylanilino)-2,7-di-*tert*-butyl-9,9-dimethylxanthene) was not observed *en route* to the synthesis of proligand **19**. Reaction of $H_2$[XAT] (**19**) with excess KH in toluene-$d_8$ cleanly yielded the dipotassium complex "[$K_2$(XAT)]" (**20**); the reaction was repeated on a preparatory scale, and upon filtration and layering with hexanes at −30 °C, vibrant yellow X-ray quality crystals of [$K_2$(XAT)(*n*-hexane)]·toluene (**20a**·toluene; Scheme 5.2; Figure 5.2; Table 5.1) were obtained.

**Scheme 5.1 –** Synthesis of proligand $H_2$[XAT] (**19**).

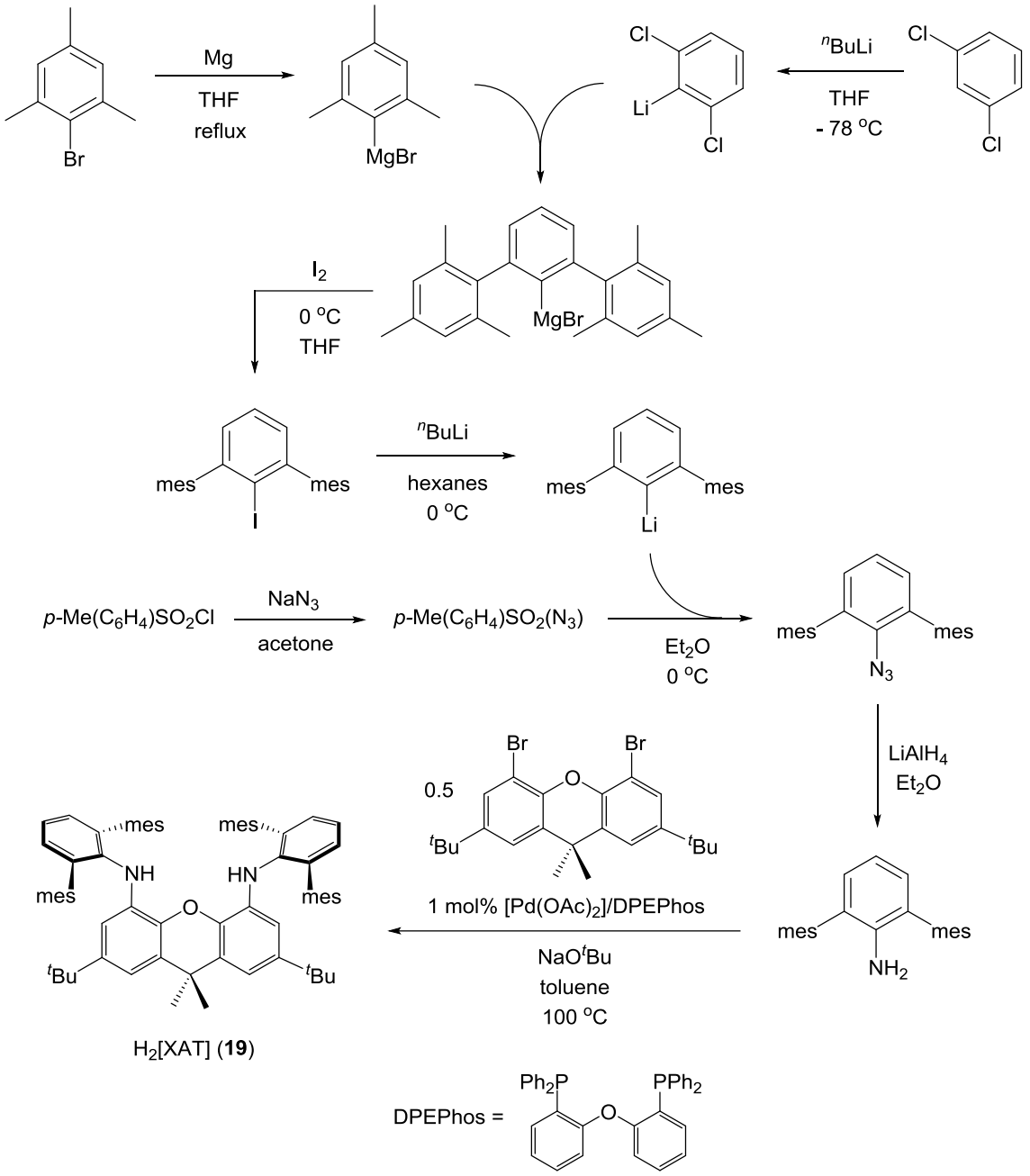

**Scheme 5.2 –** Synthesis of [$K_2$(XAT)(hydrocarbon)$_x$] (**20a–f**).

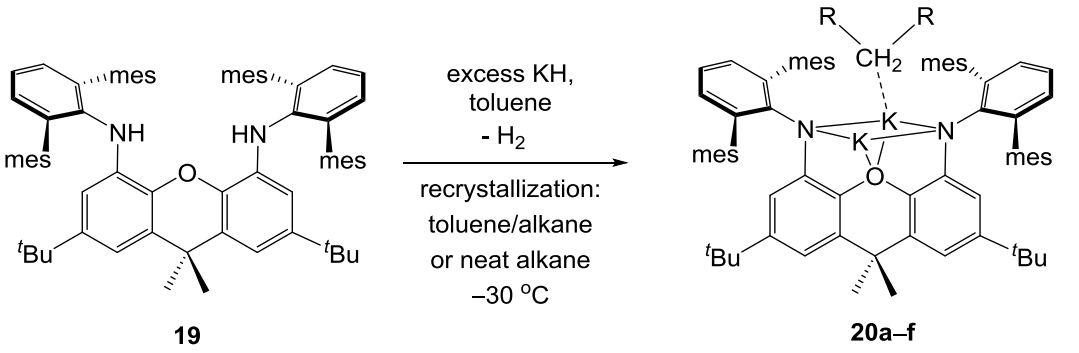


[$K_2$(XAT)(*n*-hexane)]·toluene (**20a**)
[$K_2$(XAT)(toluene)]·0.5(toluene) (**20e**)
[$K_2$(XAT){$(Me_3Si)_2O$}$_2$] (**20f**)

[$K_2$(XAT)(alkane)]·alkane
alkane = *n*-pentane (**20b**)
alkane = 3-methylpentane (**20c**)
alkane = cyclopentane (**20d**)

In the solid state (Figure 5.2; Table 5.1), the two potassium atoms of [$K_2$(XAT)(*n*-hexane)]·toluene (**20a**·toluene) are bound to bridging amido- and ether donors, forming a distorted square-pyramidal $K_2N_2O$ core with oxygen in the apical site, as indicated by N(1)−K−N(2) and K(1)−N−K(2) angles of 93.43(5)−98.06(5)° and 82.82(4)−84.74(5)°, respectively. Additionally, each potassium atom is further supported by π-electron density provided by the flanking mesityl substituents of the 2,6-dimesitylphenyl groups, which exert sufficient steric pressure to maintain a planar xanthene backbone (the angle between the two aryl rings of the xanthene backbone is only 4.72° in complex **20a**).

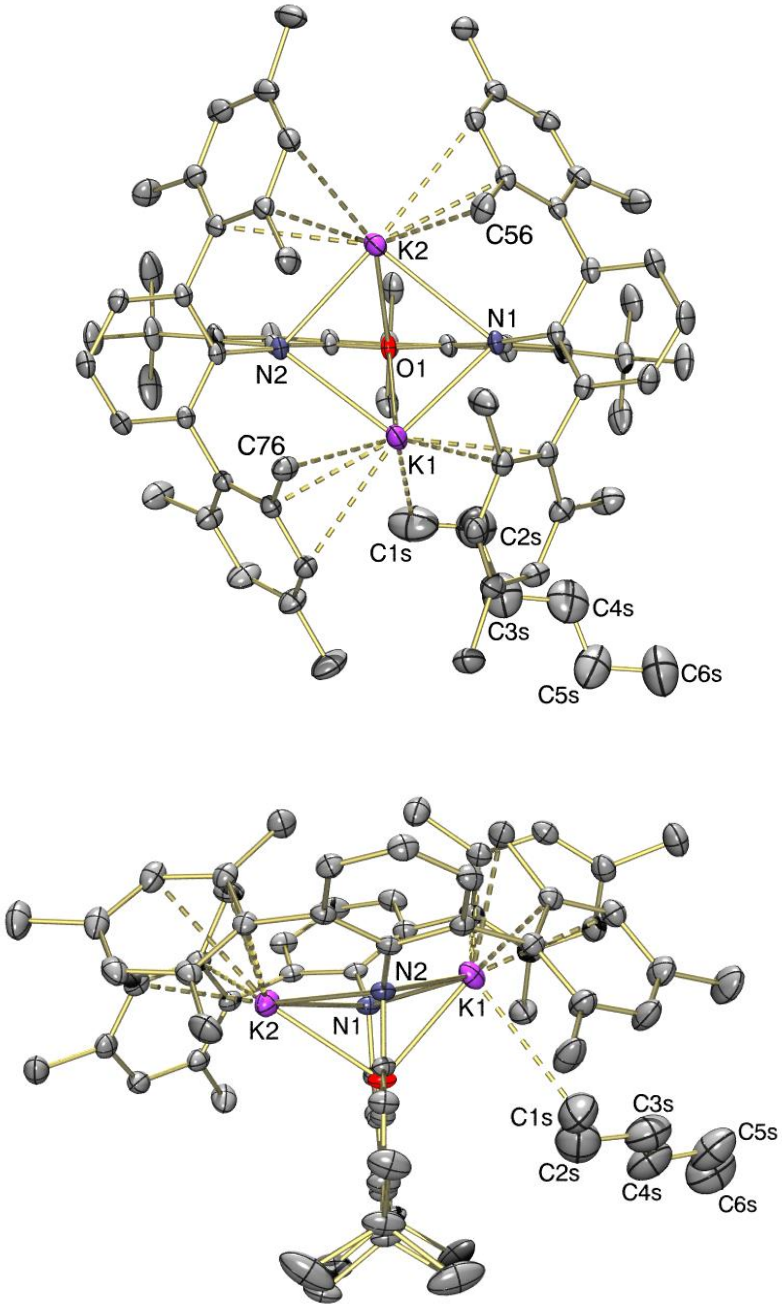


**Figure 5.2** – Two views of the X-ray crystal structure of [$K_2$(XAT)(*n*-hexane)]·toluene (**20a**·toluene), with thermal ellipsoids at 50% probability. Hydrogen atoms and toluene lattice solvent are omitted for clarity.

**Table 5.1 –** Selected Bond Lengths (Å) and Angles (deg) For XAT Complexes **20a–c**.

| Compound | **20a** | **20b** | **20c** |
|---|---|---|---|
| K−O | 2.570(2), 2.598(2) | 2.557(2), 2.583(2) | 2.534(3), 2.602(3) |
| K−N | 2.758(2)–3.105(2) | 2.772(2)–3.025(2) | 2.785(3)–2.987(3) |
| K−$C_{hydrocarbon}$ | 3.284(4) | 3.358(5) | 3.215(5) |
| K−$C_{mesityl}$ | 3.002(2)–3.404(2) | 2.986(2)–3.409(3) | 2.989(4)–3.456(4) |
| K(1)···K(2) | 3.89 | 3.90 | 3.88 |
| K−C−C | 115.9(3)° | 152.6(4)° | 170.1(3)° |

**Table 5.2 –** Selected Bond Lengths (Å) and Angles (deg) For XAT Complexes **20d–f**.

| Compound | **20d** | **20e** | **20f** |
|---|---|---|---|
| K−O | 2.585(3), 2.612(4) | 2.586(2), 2.619(2) | 2.571(2), 2.588(2) |
| K−N | 2.898(4)– 2.955(4) | 2.900(2)– 2.982(2) | 2.869(3)– 3.006(2) |
| K−$C_{hydrocarbon}$ | 3.42(3), 3.48(1) | 3.285(7), 3.305(9) | 3.282(5), 3.332(5 |
| K−$C_{mesityl}$ | 3.074(6)– 3.393(5) | 3.019(3)– 3.399(3) | 3.068(3)– 3.472(3) |
| K(1)···K(2) | 4.01 | 3.98 | 3.92 |
| K−C−E[a] | 82(1)°, 92(1)° | 100.7(6)°, 107.9(5)° | 171, 176° |

[a] For **20d** and **20e**, E = C; for **20f**, E = Si.

Complex **20a** features K−N bond lengths (2.758(2)−3.105(2) Å) which are comparable to those observed in Villinger's bridging (terphenyl)amido dipotassium species [$K_2${μ-NH(Dmp)}$_2$] (Dmp = 2,6-dimesitylphenyl; K−N = 2.716(2)−2.829(2) Å);[320] the modest K−N bond expansion observed in **20a** is likely attributable to the steric constraints of the XAT ligand, and the additional coordination of the ether donor to each potassium centre. Indeed, the neutral diarylether donor in **20a** is bound to each potassium atom through K−O bond distances (2.570(2)−2.598(2) Å) that are significantly shorter

than those observed in the comparable species $[K_2(THF)_4(Xanthdim)]$ (Xanthdim = {4,5-(nacnac)$_2$-2,7-$^t$Bu$_2$-9,9-Me$_2$(xanthene)}$^{2-}$, nacnac = {C(CHNAr)$_2$}$^-$, Ar = 2,3-Me$_2$C$_6$H$_3$; K−O$_{diarylether}$ = 2.900(2)−2.936(2) Å) reported by Limberg and co-workers,[321] Turculet's bis(phosphido) complex [K$_2$($^{tBu}$POP)] ($^{tBu}$POP = {4,5-($^t$BuP)$_2$-9,9-Me$_2$(xanthene)}$^{2-}$; K−O = 2.869(2)−3.401(2) Å),[322] and Kamalov's [K([1.5]dibenzo-18-crown-6)][CrClO$_3$] (K−O$_{diarylether}$ = 2.753(3) Å),[323] likely a consequence of the structural constraints imposed by the XAT ligand.

An unexpected feature of complex **20a** is the close approach of a molecule of *n*-hexane to K(1), with a K(1)-C(1S) distance of 3.284(4) Å. Metal–alkane complexes are of considerable importance because of their involvement in alkane C−H activation reactions[324] and hydrocarbon adsorption in alkali-metal-containing zeolites.[325] However, observable metal–alkane complexes are scarce as a consequence of the poor donor/acceptor character of alkanes and the low polarity of C−H bonds.[326] Examples detected by NMR spectroscopy include [(C$_5$R$_5$)Re(CO)$_2$(alkane)],[327,328] [(C$_5$R$_5$)M(CO)(PF$_3$)(alkane)] (M = Re or Mn),[328] [(Cp)Mn(CO)$_2$(alkane)],[329] [TpRe(CO)$_2$(alkane)],[330] [(PONOP)Rh(CH$_4$)]$^+$ (PONOP = 2,6-($^t$Bu$_2$PO)$_2$C$_5$H$_3$N),[331] [(C$_6$Et$_6$)W(CO)$_2$(*n*-pentane)],[332] and [(C$_6$Et$_6$)Re(CO)$_2$(alkane)]$^+$,[333] but none of these complexes have proven sufficiently robust to allow isolation or crystallization. At the other end of the spectrum are the crystallographically characterized metal–alkane complexes[334] which have not been observed in solution. The only members of this group (Figure 5.3) are the iron(II) 'double A-frame' porphyrin–heptane complex [Fe(DAP)(*n*-heptane)] (DAP = 'double A-frame' porphyrin) reported by Reed and co-workers,[335] the

uranium(III)–alkane complexes [{(ArO)$_3$tacn}U(alkane)] ({(ArO)$_3$tacn}$^{3-}$ = 1,4,7-tris(3,5-di-*tert*-butyl-2-hydroxybenzyl)-1,4,7-triazacyclononane; alkane = cyclohexane, cyclopentane, methylcyclohexane, methylcyclopentane, neohexane) reported by Meyer and co-workers,[336] and the cationic rhodium(I)−alkane complexes [(R$_2$PCH$_2$CH$_2$PR$_2$)Rh(alkane)][BAr′$_4$] (R = $^i$Bu, Cy, cyclopentyl, alkane = norbornane (C$_7$H$_{12}$); R = Cy, alkane = *n*-pentane; Ar′ = 3,5-(CF$_3$)$_2$C$_6$H$_3$) reported by Weller and co-workers,[337] and in all cases the metal–alkane interaction is considered to possess some degree of covalency, perhaps with additional stabilization from interactions between the alkane and the ligand framework. Compound **20a** is the first main-group-metal−alkane complex to have been observed crystallographically.

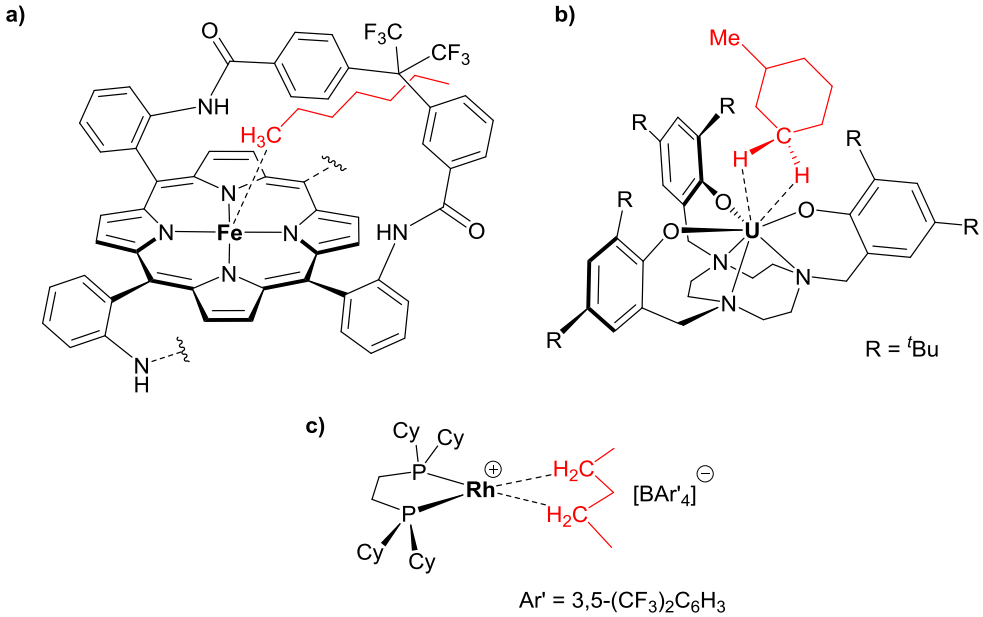


**Figure 5.3** – Selected examples of structurally-characterized metal−alkane complexes: **a)** [Fe(DAP)(*n*-heptane)], **b)** [{(ArO)$_3$tacn}U(methylcyclohexane)], and **c)** [(Cy$_2$PCH$_2$CH$_2$PCy$_2$)Rh(*n*-pentane)][BAr′$_4$]. For clarity, the second organic linker arm of the DAP ligand in [Fe(DAP)(*n*-heptane)] (**a**) is not depicted.

The Fe−$C_{alkane}$ distances in Reed's iron porphyrin heptane complex are 2.5 and 2.8 Å (the heptane molecule and the Fe atoms are disordered; calculated Fe−C distances for methane, ethane, propane, and butane complexes are 2.68–2.70 Å),[335] the U−$C_{alkane}$ distances in Meyer's uranium–alkane complexes range from 3.731(8) to 3.864(7) Å (the calculated U−C distance for the methylcyclohexane complex is 3.974 Å),[336] and the Rh−C distances in Weller's rhodium−alkane complexes range from 2.388(5) to 2.522(5) Å.[337] To enable a rough comparison between the M−C (M = metal) distances in the more ionic uranium complex and complex **20a**, ionic radii for $U^{3+}$ and $K^{+}$ (1.03 and 1.38 Å for a coordination number of six)[11] may be subtracted from the crystallographic M−C distances, yielding values of 2.70–2.83 and 1.90 Å, respectively. The K−C distance in complex **20a** is therefore notably short, and even falls at the lower end of the range of K−C distances observed for face-on potassium–benzene and potassium–toluene interactions, which are typically 3.2 to 3.5 Å.[338,339] The potassium–alkane interaction in **20a** can be surmised to involve a weak electrostatic potassium–alkane interaction stabilized by additional interactions between the alkane and the hydrophobic ligand pocket (*vide infra*).

An analogous intermolecular potassium–alkane interaction is not observed at K(2), perhaps as a result of crystal packing forces as the *para*-methyl carbon C(48) of a mesityl group in an adjacent [$K_2$(XAT)(*n*-hexane)] molecule is positioned 3.538(3) Å from K(2). However, both potassium atoms in **20a** are forced into close proximity with flanking mesityl groups and the xanthene backbone, leading to a large number of K−$C_{arene}$ and K−$C_{methyl}$ distances that are below 3.50 Å (Figure 5.2). In particular, the

intramolecular K−$C_{methyl}$ distances K(2)−C(56) and K(1)−C(76) are 3.180(3) and 3.230(3) Å, respectively, comparable to the intramolecular K–$CHR_3$ interactions observed in the sterically encumbered $[\{KSi(SiMe_3)_3\}_2]$,[339] $[KC(SiMe_3)_3]_n$,[340] and $[K_2(OEt_2)\{O\{SiMe_2C(SiMe_3)_2\}_2\}]_n$,[341] which feature K−C distances that range from 3.138(3) to 3.433(3) Å. The intramolecular K−$C_{mesityl}$ distances in **20a** range from 3.002(2)−3.404(2) Å, and these contacts are highly analogous to those observed in Villinger's comparable complex $[K_2\{\mu\text{-}NH(Dmp)\}_2]$ (Dmp = 2,6-dimesitylphenyl), which features K−$C_{mesityl}$ distances of 3.079(2)−3.393(3) Å.[320]

To further probe the disposition of the $[K_2(XAT)]$ moiety to interact with the hydrocarbon solvent, alternative crystallization conditions were explored. The reaction of $H_2$[XAT] (**19**) with excess KH in toluene was scaled up (400 mg scale), and after centrifugation, sonication in hexane, and filtering at low temperature, a bright yellow solid was obtained; the product was shown to have the composition $K_2(XAT)(hexane)_{0.6}(toluene)_{0.9}$ by $^1$H NMR spectroscopy. Layering a toluene solution of $K_2(XAT)(hexane)_{0.6}(toluene)_{0.9}$ with *n*-pentane followed by cooling to –30 °C furnished X-ray quality crystals of $[K_2(XAT)(n\text{-pentane})]\cdot(n\text{-pentane})$ (**20b·**(*n*-pentane)). Additionally, cooling concentrated 3-methylpentane, cyclopentane, toluene, or $O(SiMe_3)_2$ solutions of $K_2(XAT)(hexane)_{0.6}(toluene)_{0.9}$ to –30 °C yielded X-ray quality crystals of $[K_2(XAT)(3\text{-methylpentane})]\cdot 3\text{-methylpentane}$ (**20c·**3-methylpentane), $[K_2(XAT)(cyclopentane)]\cdot cyclopentane$ (**20d·**cyclopentane), $[K_2(XAT)(toluene)]\cdot 0.5(toluene)$ (**20e·**0.5(toluene)), and $[K_2(XAT)\{(Me_3Si)_2O\}_2]$ (**20f**), respectively (Scheme 5.2; Tables 5.1 and 5.2; Figures 5.4−5.8). The central cores of

structures **20b–f** are analogous to that in **20a** (each potassium atom is NON-coordinated and engages in intramolecular potassium–carbon interactions with surrounding mesityl groups), and in every case either one (**20b–e**) or two (**20f**) intermolecular K–$H_3CR$ or K–$H_2CR_2$ interactions are observed. These interactions involve the 1-position of *n*-pentane and 3-methylpentane, one of the $CH_2$ groups in cyclopentane, and a methyl group of toluene and of hexamethyldisiloxane, leading to K−C distances of 3.358(5) Å in **20b**, 3.215(5) Å in **20c**, 3.42(3) and 3.48(1) Å in **20d**,[§] 3.285(7) and 3.305(9) Å in **20e**, and 3.282(5) and 3.332(5) Å in **20f** (bound cyclopentane in **20d** and toluene in **20e** are disordered over two positions). In **20e**, toluene bridges between adjacent [$K_2$(XAT)] molecules through K–$C_{arene}$ interactions with distances of 3.240(7), 3.425(9), and 3.433(8) Å. The K−C−C angles in primary alkyl complexes **20a**, **20b**, and **20c** are 115.9(3)°, 152.6(4)°, and 170.1(3)°, respectively, while the K−$CH_2$−$CH_2$ angles in cyclopentane complex **20d** are 82(1)° and 92(1)°. The K−$C_{methyl}$–C angles in toluene complex **20e** are 100.7(6)° and 107.9(5)°, and the K−C−Si angles in hexamethyldisiloxane complex **20f** are 171° and 176°.

[§] The K–C distances in **20d** should be viewed with some caution since bound cyclopentane is disordered over two positions and restraints had to be applied to ensure reasonable C–C bond distances (DFIX was used to set all five C–C distances to 1.41 Å with an ESD of 0.01 Å).

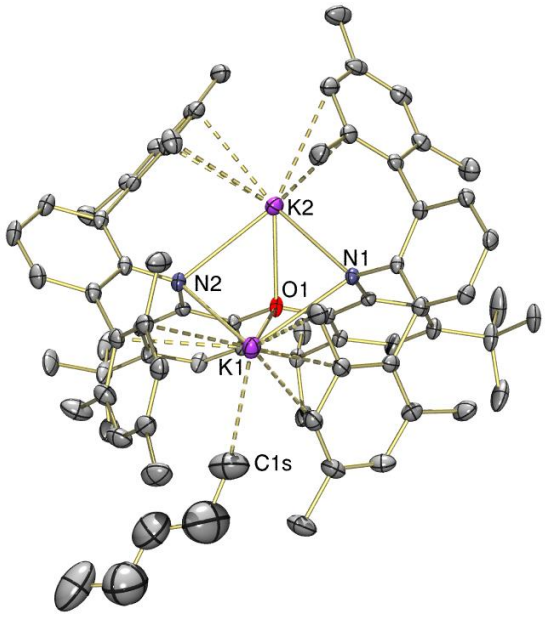


**Figure 5.4** – X-ray crystal of [$K_2$(XAT)(*n*-pentane)]·(*n*-pentane) (**20b**·(*n*-pentane), with thermal ellipsoids at 50% probability. Hydrogen atoms and lattice solvent are omitted for clarity.

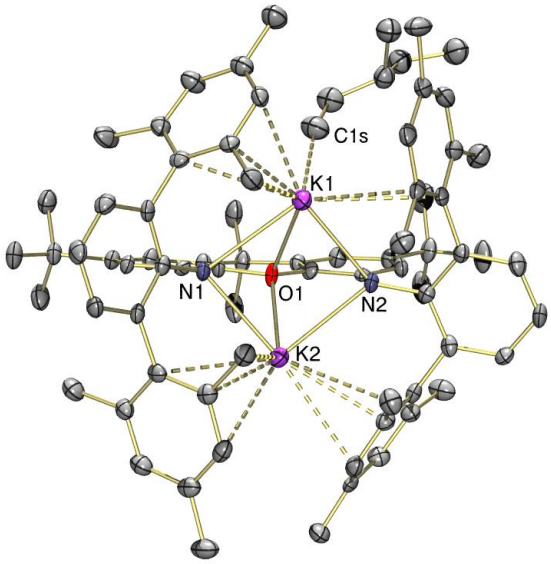


**Figure 5.5** – X-ray crystal structure of [$K_2$(XAT)(3-methylpentane)]·3-methylpentane (**20c**·3-methylpentane), with thermal ellipsoids at 50% probability. Hydrogen atoms and 3-methylpentane lattice solvent are omitted for clarity.

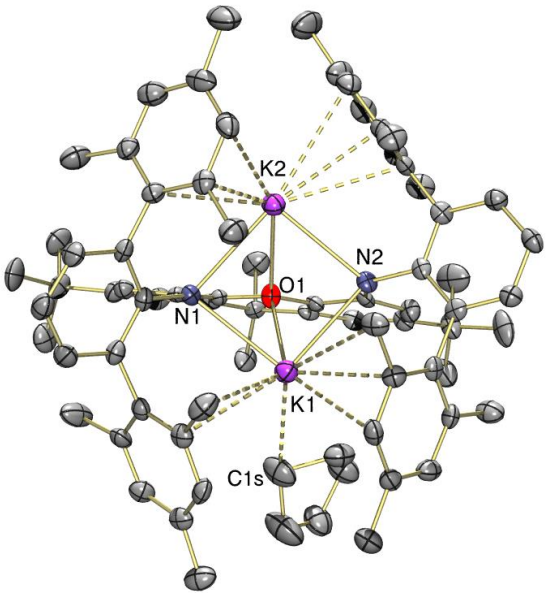


**Figure 5.6** – X-ray crystal structure of [$K_2$(XAT)(cyclopentane)]·cyclopentane (**20d**·cyclopentane), with thermal ellipsoids at 50% probability. Hydrogen atoms and cyclopentane lattice solvent are omitted for clarity. Only one of the two orientations of cyclopentane is shown.

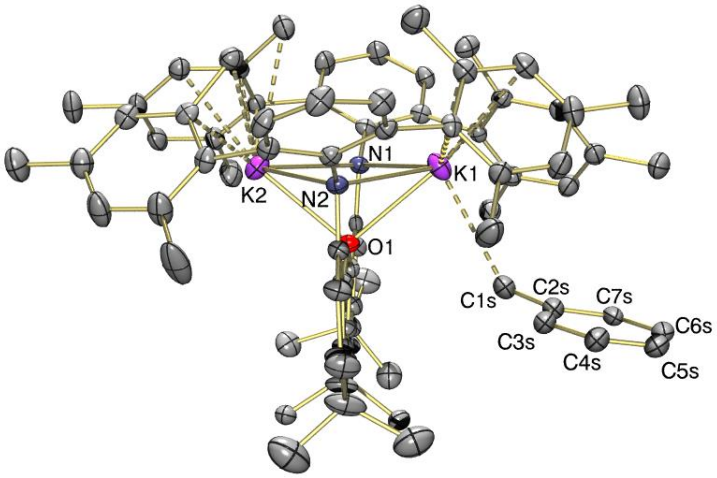


**Figure 5.7** – X-ray crystal structure of [$K_2$(XAT)(toluene)]·0.5(toluene) (**20e**·0.5(toluene)), with thermal ellipsoids at 50% probability. Hydrogen atoms and lattice solvent are omitted for clarity. Only one of the two orientations of toluene is shown. The interactions between C(5S) and C(6S) and K(2) of the neighbouring [$K_2$(XAT)] unit are not shown.

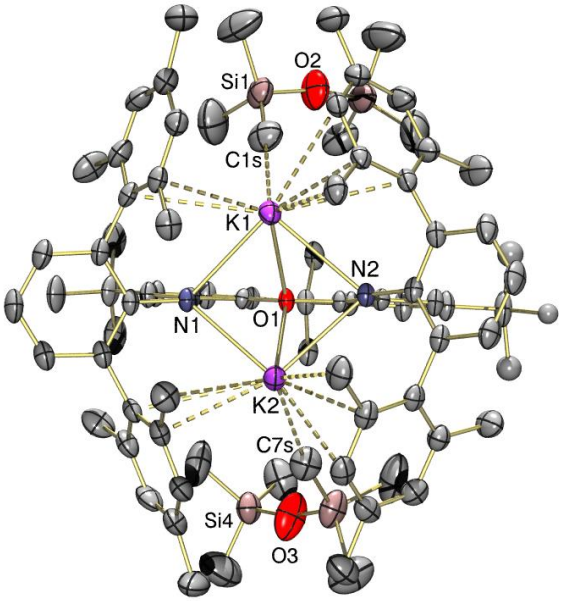


**Figure 5.8** – X-ray crystal structure of $[K_2(XAT)\{(Me_3Si)_2O\}_2]$ (**20f**), with thermal ellipsoids at 30% probability (collected at 223 K). Hydrogen atoms are omitted for clarity. One *tert*-butyl group is disordered and so was refined isotropically, and only one of the two orientations of the disordered *tert*-butyl group is shown.

**Table 5.3** – Crystallographic data collection and refinement parameters for complexes **20a–c**.

| Structure | **20a**·toluene | **20b**·(*n*-pentane) | **20c**·3-methylpentane |
|---|---|---|---|
| Formula | $C_{84}H_{100}K_2N_2O$ | $C_{81}H_{102}K_2N_2O$ | $C_{83}H_{106}K_2N_2O$ |
| Formula wt | 1231.86 | 1197.85 | 1225.90 |
| *T* (K) | 100(2) | 296(2) | 100(2) |
| Cryst. Syst. | Monoclinic | Monoclinic | Monoclinic |
| Space Group | *P*2(1)/*c* | *P*2(1)/*c* | *P*2(1)/*c* |
| *a* (Å) | 22.2287(13) | 22.2840(12) | 22.480(8) |
| *b* (Å) | 14.7664(9) | 14.7045(7) | 14.679(5) |
| *c* (Å) | 23.6055(13) | 23.5209(12) | 23.929(9) |
| α [deg] | 90 | 90 | 90 |

| | | | |
|---|---|---|---|
| β [deg] | 113.6980(10) | 113.6080(10) | 115.411(6) |
| γ [deg] | 90 | 90 | 90 |
| Volume [Å$^3$] | 7094.9(7) | 7062.2(6) | 7132(4) |
| *Z* | 4 | 4 | 4 |
| Density (calcd; Mg/m$^3$) | 1.153 | 1.127 | 1.142 |
| μ (mm$^{-1}$) | 0.180 | 0.179 | 0.179 |
| *F*(000) | 2656 | 2592 | 2656 |
| Crystal Size (mm$^3$) | 0.76×0.49×0.38 | 0.40×0.35×0.30 | 0.31×0.30×0.06 |
| θ Range for Collection [deg] | 1.67–27.98 | 1.75–26.43 | 1.68–23.35 |
| No. of reflns. Collected | 90818 | 81611 | 60401 |
| No. of Indep. Reflns. | 17048 | 14519 | 10288 |
| Completeness to θ Max (%) | 99.6 | 99.8 | 99.3 |
| Absorption Correction | Numerical | Numerical | Numerical |
| Max and Min Transmission | 0.9346, 0.8751 | 0.9482, 0.9317 | 0.9893, 0.9466 |
| Data / Parameters | 17048 / 829 | 14519 / 932 | 10288 / 805 |
| GOF on $F^2$ | 1.038 | 1.028 | 1.001 |
| Final $R_1$ [$I > 2\sigma(I)$] | R1 = 0.0605<br>wR2 = 0.1668 | R1 = 0.0589<br>wR2 = 0.1474 | R1 = 0.0574<br>wR2 = 0.1170 |
| *R* indices (all data) | R1 = 0.0842<br>wR2 = 0.1865 | R1 = 0.0871<br>wR2 = 0.1692 | R1 = 0.1310<br>wR2 = 0.1475 |

**Table 5.4** – Crystallographic data collection and refinement parameters for complexes **20d–f**.

| Structure | **20d**·cyclopentane | **20e**·0.5(toluene) | **20f** |
|---|---|---|---|
| Formula | $C_{81}H_{98}K_2N_2O$ | $C_{81.5}H_{89.5}K_2N_2O$ | $C_{83}H_{114}K_2N_2O_3Si_4$ |
| Formula wt | 1193.82 | 1191.25 | 1378.32 |
| *T* (K) | 100(2) | 100(2) | 223(2) |

| Cryst. Syst. | Monoclinic | Monoclinic | Monoclinic |
|---|---|---|---|
| Space Group | *P*2(1)/*c* | *P*2(1)/*n* | *P*2(1)/*c* |
| *a* (Å) | 12.824(6) | 12.924(2) | 20.689(2) |
| *b* (Å) | 20.329(9) | 21.037(3) | 16.4916(17) |
| *c* (Å) | 27.078(12) | 24.765(4) | 24.651(2) |
| α [deg] | 90 | 90 | 90 |
| β [deg] | 103.099(8) | 95.374(3) | 97.120(2) |
| γ [deg] | 90 | 90 | 90 |
| Volume [$Å^3$] | 6875(5) | 6703.4(18) | 8345.8(14) |
| *Z* | 4 | 4 | 4 |
| Density (calcd; $Mg/m^3$) | 1.153 | 1.180 | 1.097 |
| μ ($mm^{-1}$) | 0.184 | 0.189 | 0.216 |
| *F*(000) | 2576 | 2554 | 2976 |
| Crystal Size ($mm^3$) | 0.24×0.15× 0.05 | 0.41×0.37× 0.09 | 0.47×0.32× 0.18 |
| θ Range for Collection [deg] | 1.84–23.31 | 1.72–26.26 | 1.85–25.54 |
| No. of reflns. Collected | 60237 | 76369 | 88763 |
| No. of Indep. Reflns. | 9919 | 13518 | 15449 |
| Completeness to θ Max (%) | 99.6 | 99.7 | 99.1 |
| Absorption Correction | Numerical | Numerical | Numerical |
| Max and Min Transmission | 0.9909, 0.9571 | 0.9832, 0.9266 | 0.9622, 0.9054 |
| GOF on $F^2$ | 1.000 | 1.061 | 1.102 |
| Data / Parameters | 9919 / 795 | 13518 / 867 | 15449 / 889 |
| Final $R_1$ [$I > 2\sigma(I)$] | $R_1$ = 0.0690 $wR_2$ = 0.1315 | $R_1$ = 0.0589 $wR_2$ = 0.1450 | $R_1$ = 0.0638 $wR_2$ = 0.1544 |
| *R* indices (all data) | $R_1$ = 0.1780 $wR_2$ = 0.1758 | $R_1$ = 0.1060 $wR_2$ = 0.1707 | $R_1$ = 0.1288 $wR_2$ = 0.1859 |

Compounds **20a–f** illustrate the extent to which intermolecular K–$H_3CR$ and K–$H_2CR_2$ interactions are a common feature of the solid-state structures of [$K_2$(XAT)]. However, attempts to observe alkane or $O(SiMe_3)_2$ binding by $^1H$ or $^{13}C$ NMR spectroscopy in 3-methylpentane/toluene-$d_8$ (−80 °C), 3-methylpentane (−110 °C), cyclopentane (−80 °C), or $O(SiMe_3)_2$ (−60 °C; $^1H$ NMR spectroscopy only) were unsuccessful, possibly as a result of rapid exchange between free and bound solvent.

DFT calculations were carried out by the Emslie group to probe the nature of the potassium−alkane interaction in 3-methylpentane complex **20c**, which is the complex featuring the shortest K−$C_{alkane}$ distance. This computational investigation revealed that a combination of electrostatic bonding (including a significant cation-induced dipole[342] contribution) and dispersion interactions (between the alkane and the hydrophobic pocket formed by the surrounding ligand framework) are responsible for supporting the potassium−alkane interactions, rather than σ-donation from alkane C−H bonds to potassium.[317] The effectiveness of the rigid hydrophobic binding pocket in [$K_2$(XAT)] to promote and stabilize even very weak potassium–alkane interactions (as shown crystallographically in the solid state and computationally in the gas phase)[317] also suggests that in combination with catalytically relevant metals, ligands featuring a rigid hydrophobic binding pocket (including XAT) may have untapped potential in alkane C−H activation chemistry.

### 5.1.2 – Reactions of "[$K_2$(XAT)]" with Actinide(IV) Halide Precursors

Despite numerous attempts at installing the XAT ligand onto thorium and uranium, no new actinide-containing complex could be isolated. Attempted transmetalation of the dipotassium precursor [$K_2$(XAT)] (**20**) with actinide(IV) chloro starting materials [$ThCl_4(dme)_2$] and $UCl_4$ failed to provide access to the originally targeted putative XAT actinide chloro complexes, [(XAT)$AnCl_2$] (An = Th, U). Regardless of stoichiometry (upwards of 6 equiv of actinide precursor), temperature (−30 to 80 °C), time (<1 h to 72 h), or solvent (benzene, dme, THF), reaction mixtures routinely yielded intractable material, typically containing proligand $H_2$[XAT] (**19**) as a major decomposition product, as indicated by $^1$H NMR spectroscopy. The apparent incompatibility of the XAT dianion with actinide(IV) precursors is likely an unintended consequence of the considerably bulky steric profile of the XAT ancillary ligand, which may be unable to accommodate the two chloride co-ligands that would be present in the target actinide chloro complexes. As a result, further development of XAT as an ancillary ligand in organoactinide chemistry was not pursued.

## 5.2 – XAd: A Third-Generation NON-Donor Ancillary Ligand

While the terphenyl-appended second-generation XAT ligand proved unsuitable as an ancillary for tetravalent actinide metals, the evolution of $XA_2$ with the goal of accessing cationic organoactinide species free from arene-coordination remained a priority. In that vein, a third generation ligand was designed featuring 1-adamantyl groups pendant to the amido donors, 4,5-bis(1-adamantylamido)-2,7-di-*tert*-butyl-9,9-

dimethylxanthene, XAd. In replacing the aryl groups of $XA_2$ with roughly spherical 1-adamantyl substituents, we envisioned a supporting ligand which offers a coordination environment featuring relatively open axial sites and enhanced steric protection in the plane of the xanthene ligand backbone, making the equatorial site significantly less accessible. As a consequence, the redistributed steric bulk in XAd is expected to limit the approach of an arene to the vacant site *cis* to an axially-bound alkyl substituent in cationic XAd organoactinide fragments of the form "$[(XAd)An(CH_2SiMe_3)]^+$" (Figure 5.9). By disfavouring competitive *cis* cation–arene binding, more facile actinide–olefin coordination is expected for cationic XAd organoactinide catalysts relative to the first-generation $XA_2$-based systems, potentially leading to improved catalytic polymerization activities.

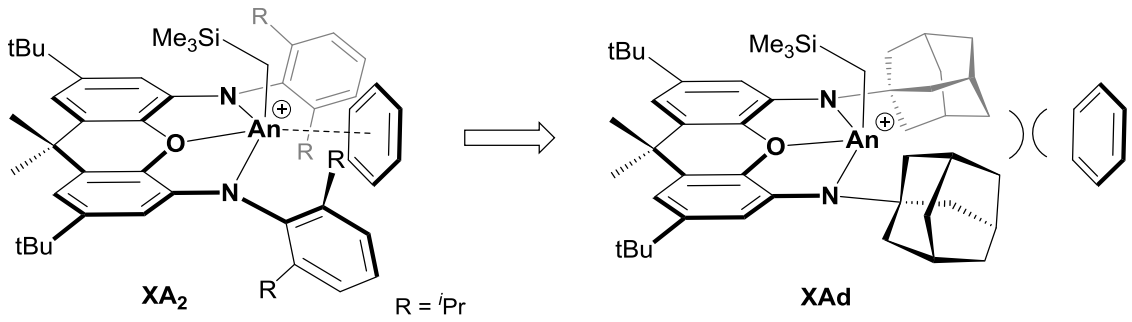


**Figure 5.9** – Potential disengagement of cation–arene binding as a consequence of steric bulk re-positioning in the third-generation pincer ligand XAd.

### 5.2.1 – XAd Ligand Synthesis and Dipotassium Complex

The third-generation NON-donor proligand, $H_2$[XAd] (**21**), was synthesized by palladium-catalyzed coupling[40,214] of 4,5-dibromo-2,7-di-*tert*-butyl-9,9-dimethylxanthene

with 2 equiv of commercially-available 1-adamantylamine (Scheme 5.3), and was obtained as a white solid upon recrystallization from ethanol/toluene in 81% yield.

**Scheme 5.3** – Synthesis of proligand $H_2$[XAd] (**21**).

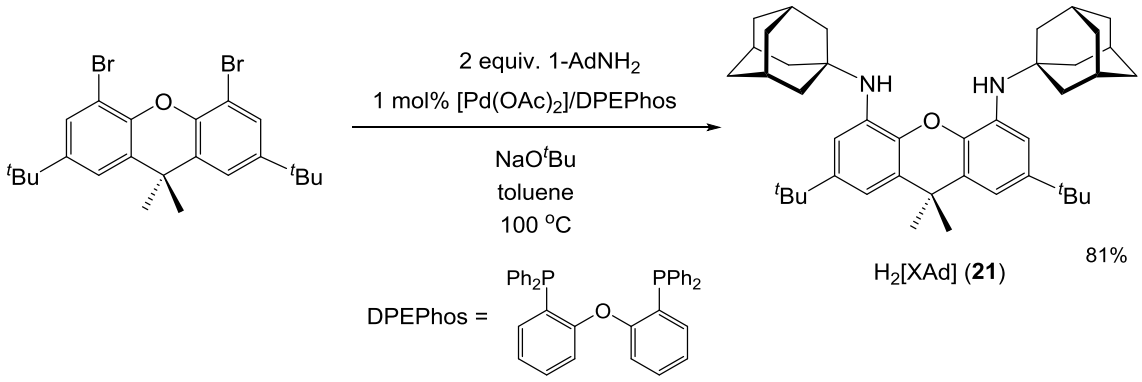


As with $H_2$[$XA_2$], proligand **21** was dried by stirring a toluene solution with excess NaH to remove any residual moisture and ethanol, both of which result in decomposition of amido actinide complexes. However, in contrast to the reactivity profile of $H_2$[$XA_2$], deprotonation of $H_2$[XAd] with KH does not proceed rapidly to form an appreciably soluble dipotassium salt in ethereal solvents (e.g. THF, dme). For example, while ether-soluble [$K_2$($XA_2$)(dme)$_2$] is formed within 5 h at room temperature,[40] only poorly-soluble "[$K_2$(XAd)(THF)$_x$]" (**22**) resulted from heating proligand **21** with excess KH in THF at 65 °C for 72 h. Alternatively, conducting the reaction in dme yielded highly insoluble [$K_2$(XAd)(dme)] (**22-dme**) after stirring for 7 days at room temperature, and solubility issues precluded the isolation of **22-dme** as an analytically-pure precursor. [$K_2$(XAd)(dme)] (**22-dme**) can also be more efficiently prepared by stirring proligand **21** with 2.5 equiv of $KCH_2Ph$ for 12 h in dme at −78 °C. Attempts to recrystallize the

dipotassium species "[$K_2$(XAd)]" (**22**) from THF/hexanes yielded colourless crystals of [{K(THF)$_3$}$_2$(XAd)] (**22-THF**), but **22-THF** underwent rapid desolvation upon removal of THF solvent, with ensuing decomposition to yield proligand **21** as confirmed by $^1$H NMR spectroscopy, precluding its use as an isolable precursor. Consequently, for the development of XAd actinide chemistry, [$K_2$(XAd)(dme)] (**22-dme**) was most conveniently generated using benzylpotassium as described above, and utilized *in situ*.

### 5.2.2 – XAd Thorium(IV) Chloro Derivative

Attempts to prepare the putative salt-free XAd thorium dichloride complex "[(XAd)$ThCl_2$]" met with complications, as the limited solubility of the dipotassium precursor **22-dme** necessitated use of ethereal solvents, from which removal of alkali-metal−halide salts can be problematic. However, a KCl salt-occluded thorium chloro species [(XAd)$ThCl_4K_2$]·*x*(dme) (**23**·*x*(dme)) could be obtained by transmetalation of *in-situ* generated [$K_2$(XAd)(dme)] (**22-dme**) with [$ThCl_4$(dme)$_2$] in dme solution,[§] which was isolated as an off-white solid in 64 % yield (for $x = 2$) after centrifugation, trituration in hexanes, and subsequent filtration (Scheme 5.4). In this complex, dme is not believed to be coordinated to thorium, as the amount of dme present varied from batch to batch (from approximately 0.5 to 2 equiv). Complex **23**·dme was characterized by $^1$H and $^{13}$C{$^1$H} NMR spectroscopy, as well as elemental analysis.

[§] Alternatively, the presumed THF-containing species [(XAd)$ThCl_4K_2$]·*x*(THF) (**23**·*x*(THF)) could be generated- and utilized *in-situ* by conducting the transmetalation reaction of *in-situ* generated [$K_2$(XAd)(THF)$_x$] (**22-THF**) with [$ThCl_4$(dme)$_2$] in THF solution.

**Scheme 5.4** – Synthesis of chloro complex [(XAd)ThCl$_4$K$_2$]·*x*(dme) (**23·***x*(dme); *x* = 0.5–2), depicted as a trichloro 'ate' species.

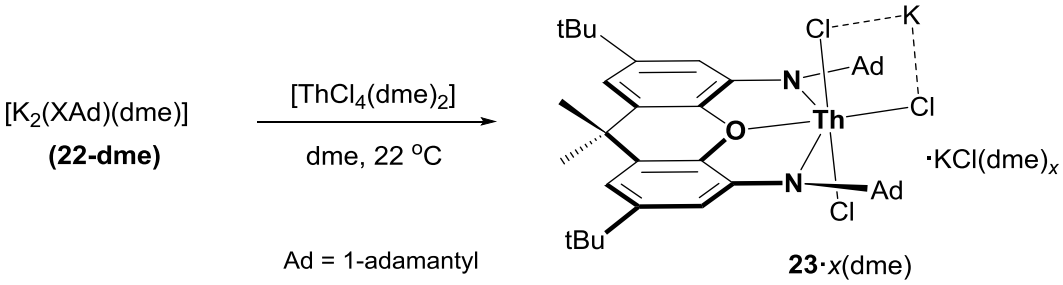


Despite numerous attempts at obtaining crystals of suitable quality for X-ray diffraction, only microcrystalline **23·***x*(dme) could be obtained, precluding explicit structural authentication of the chloro species. Although it is not apparent by inspection of the clean $^1$H or $^{13}$C{$^1$H} NMR spectra, the inclusion of two equiv of KCl in **23·***x*(dme) was established through multiple elemental analyses, which revealed %CHN values uniformly (e.g. 6.89−6.98 % for C) lower than those expected for the salt-free species "[(XAd)ThCl$_2$(dme)]". Indeed, elemental analyses obtained for both [(XAd)ThCl$_4$K$_2$]·dme (**23·**dme) and [(XAd)ThCl$_4$K$_2$]·2(dme) (**23·**2(dme)) revealed %CHN values that strongly indicate retention of 2 equiv of KCl salt in complex **23**. Furthermore, the presence of KCl in complex **23** is additionally corroborated by various physical observations, including poor solubility in aromatic solvents and poor crystallinity. Leznoff and co-workers observed similar LiCl salt-retention in their bis(amido)ether thorium complex [($^{t\text{Bu}}$NON)ThCl$_5$Li$_3$]·dme ($^{t\text{Bu}}$NON = {($^t$BuNSiMe$_2$)$_2$O}$^{2-}$), which was prepared *via* a comparable transmetalation reaction of dilithium precursor [Li$_2$($^{t\text{Bu}}$NON)] with [ThCl$_4$(dme)$_2$] in ethereal solutions.[175] The authors similarly utilized elemental analysis as a frontier characterization tool in order to

establish the inclusion of LiCl in their thorium chloro species, as X-ray quality crystals of [($^{t\text{Bu}}$NON)ThCl$_5$Li$_3$]·dme could not be obtained.[175]

### 5.2.3 – XAd Thorium(IV) Dialkyl Complex

Reaction of *in-situ* generated [(XAd)ThCl$_4$K$_2$]·*x*(THF) (**23**·*x*(THF)) with 2.1 equiv of LiCH$_2$SiMe$_3$ at 0 °C in THF solution afforded neutral, base-stabilized dialkyl complex [(XAd)Th(CH$_2$SiMe$_3$)$_2$(THF)] (**24**; Scheme 5.5), which was obtained as a white solid in 43% yield after trituration in hexane and subsequent centrifugation. Bis((trimethylsilyl)methyl) complex **24** is highly soluble in ethereal- and aromatic solvents, and fairly soluble in saturated hydrocarbons.

**Scheme 5.5** – Synthesis of dialkyl complex [(XAd)Th(CH$_2$SiMe$_3$)$_2$(THF)] (**24**).

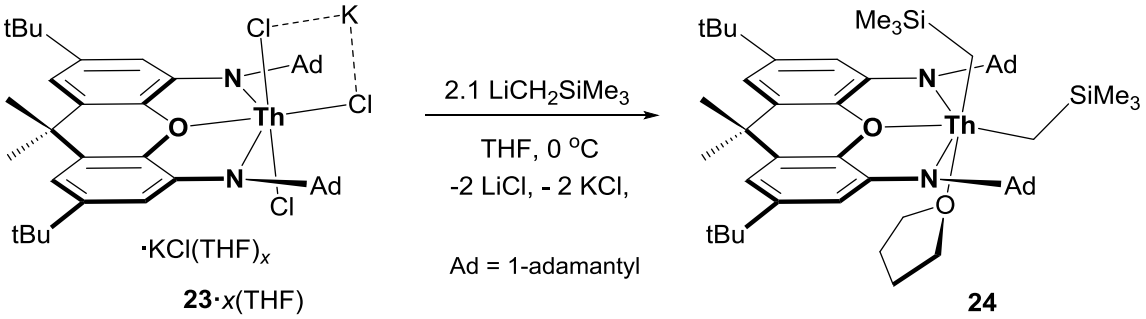


The room-temperature $^1$H NMR spectrum of dialkyl **24** in C$_6$D$_6$ features twelve resonances located between 7.10 and 0.09 ppm including a single set of sharp ThC*H*$_2$ and ThCH$_2$Si*Me*$_3$ signals, indicating that coalescence has been achieved between the rapidly exchanging axial and in-plane alkyl substituents. To facilitate this exchange, the bound THF ligand must be dissociating and re-coordinating rapidly, which is supported by the

broadening observed for the two OC$H_2$C$H_2$ resonances of coordinated THF. Alternatively, the $^1$H NMR spectrum of **24** could be explained by predominance of a top−bottom symmetric ($C_{2v}$ symmetry) isomer of dialkyl **24** which features *trans*-disposed (trimethylsilyl)methyl groups bound in axial positions and a THF ligand occupying the site roughly in the plane of the xanthene backbone, *cis* to each alkyl substituent.

The X-ray crystal structure of dialkyl **24** (Figure 5.10; Table 5.4) revealed a six-coordinate XAd-thorium(IV) complex of approximate $C_s$-symmetry, with one (trimethylsilyl)methyl group located roughly in the plane of the XAd ligand, one occupying an axial site, and a THF ligand coordinated approximately *trans* to the axial alkyl substituent.

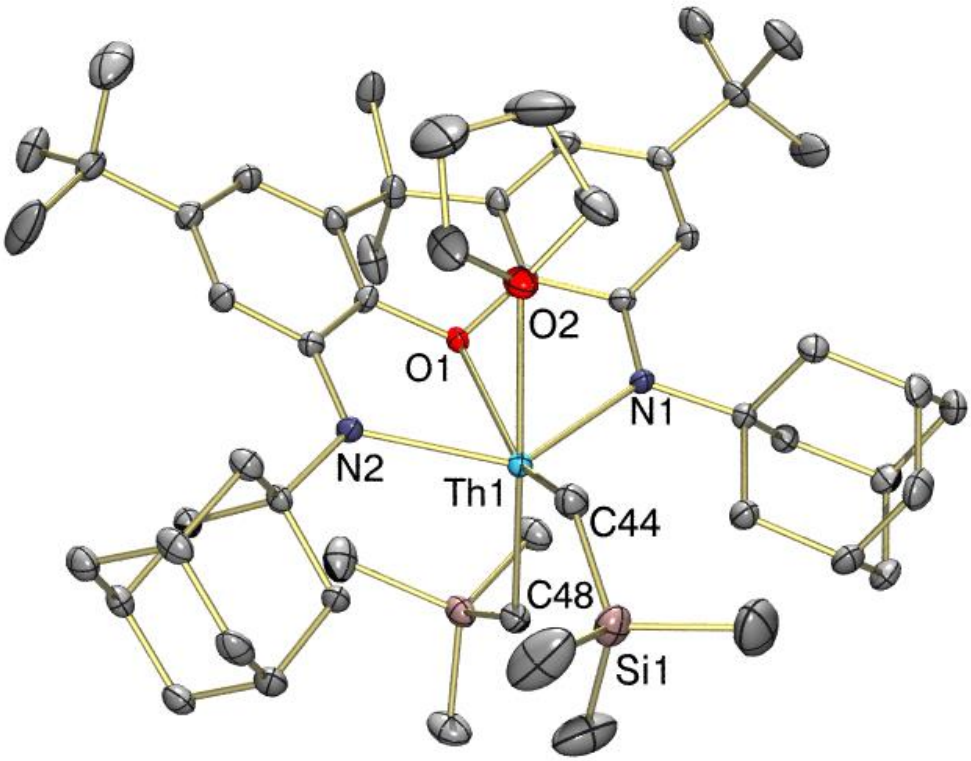


**Figure 5.10** – X-ray crystal structure of [(XAd)Th($CH_2SiMe_3$)$_2$(THF)] (**24**), with thermal ellipsoids at 50% probability. Hydrogen atoms are omitted for clarity. The 1-adamantyl methylene carbon atoms closest to thorium are C(25) (of the Ad substituent on N(1)), and C(35) (of the Ad substituent on N(2)).

**Table 5.5** – Selected bond lengths (Å) and angles (deg) for complexes **24** and **25** (and **3-Th** for comparison).

| Compound | **24** | **25** | **3-Th** |
|---|---|---|---|
| Th−$O_{xanthene}$ | 2.564(2) | 2.492(5) | 2.535(4) |
| Th−N | 2.360(2), 2.368(2) | 2.375(6), 2.379(6) | 2.291(4), 2.312(4) |
| Th−$O_{THF}$ | 2.692(2) | n/a | n/a |
| Th−$C_{apical}$ | 2.549(3) | n/a | 2.467(6) |
| Th−$C_{in\text{-}plane}$ | 2.528(3) | n/a | 2.484(6) |
| Th···$CH_2R_2$ *1-adamantyl* | 3.150(3), 3.221(3) | 3.215(7), 3.253(7) | n/a |

| | | | |
|---|---|---|---|
| Th−$CH_2$ *gem-allyl* | n/a | 2.750(7), 2.760(7) | n/a |
| Th−CH *meso-allyl* | n/a | 2.797(7), 2.805(7) | n/a |
| Th−$CHSiMe_3$ *allyl* | n/a | 2.784(7), 2.801(7) | n/a |
| Th−$CH_2$−Si | 119.8(1), 129.6(2) | n/a | 126.8(3), 127.6(3) |
| Ligand Bend Angle[a] | 32.7° | 12.0° [c] | 9.0° |
| Allyl fold angle[b] | n/a | 115.3, 116.8° | n/a |
| Th···(N/O/N-plane) | 0.33 | 0.03 | 0.48 |
| O···(N/Th/N-plane) | 0.53 | 0.04 | 0.66 |
| N(1)···N(2) | 4.28 | 4.31 | 4.06 |

[a]Ligand Bend Angle = the angle between the two aromatic rings of the xanthene ligand backbone. [b]Allyl fold angle = the angle between the $C_3$ allyl plane and the plane passing through the thorium atom and the two terminal allyl carbon atoms. [c] The xanthene backbone in **25** is twisted rather than bent.

The 4 anionic donors (N(1), N(2), C(44), and C(48)) and THF donor O(2) adopt a distorted trigonal-bipyramidal arrangement around the thorium centre, with N(1)−Th−N(2), N(1)−Th−C(44), N(2)−Th−C(44), and C(48)−Th−O(2) angles of 129.87(7), 112.06(9), 102.68(8), and 172.00(7)°, respectively, and the neutral diarylether donor is coordinated between the two amido groups, approximately capping an edge of the aforementioned trigonal bipyramid. However, the donor atoms that are bound in the equatorial plane of the distorted trigonal bipyramid in complex **24** (N(1), N(2), and C(44)) are bent toward the axially-bound THF ligand, resulting in moderate pyramidalization at thorium, with the sum of the N−Th−N and N−Th−$C_{eq}$ angles equal to 344.6° in **24** (cf. the sum of the comparable angles of trimethyl 'ate' anion $[(XA_2)UMe_3]^-$ (**15**); ∑(N−U−N, N−U−$C_{eq}$) = 359.9°). As a consequence, the thorium atom in complex **24** lies 0.54 Å above the N/$C_{eq}$/N plane (for comparison, the uranium atom in anion **15** lies 0.00 Å from the N/$C_{eq}$/N plane). The observed pyramidalization at thorium is likely a

consequence of the steric pressure inflicted on the equatorial site by the bulky 1-adamantyl substituents flanking the coordination pocket, and may additionally be facilitated by the relatively long Th−$O_{THF}$ distance of 2.692(2) Å in complex **24**.

As with all six-coordinate $XA_2$ organouranium complexes, the N/$C_{eq}$/N plane in thorium dialkyl **24** is tilted relative to the plane of the XAd ligand, as indicated by the 13.5° angle between the N/O/N- and N/C(44)/N-planes. This likely occurs in order to reduce unfavourable steric interactions between the in-plane $CH_2SiMe_3$ ligand and the 1-adamantyl substituents of the XAd ancillary. However, in contrast to six-coordinate $XA_2$ complexes, the xanthene backbone in **24** is significantly bent away from planarity, with a 32.7° angle between the two aryl rings of the xanthene backbone (cf. 1.2° in trichloro complex **1**, 6.5° in trimethyl anion **15**, and 4.8 and 7.0° in tris((trimethylsilyl)methyl) anion **14**). It is possible that in the absence of sterically restrictive isopropyl groups located above and below the NON-donor array, facile xanthene-bending can be more easily accommodated.

The Th−N, Th−$O_{xanthene}$, and Th−$CH_2$ distances in complex **24** are expanded by 0.03−0.07 Å relative to those of the corresponding $XA_2$ bis((trimethylsilyl)methyl complex [$(XA_2)Th(CH_2SiMe_3)_2$] (**3-Th**) reported by Emslie and co-workers,[40] likely a consequence of the increased coordination number and steric crowding at the thorium centre of formally 12-electron **24** relative to that of 10-electron **3-Th**, as well as the superior donor ability of the alkylamide donors of XAd. Although structurally-authenticated complexes featuring adamantylamide−thorium linkages have not been previously reported, the Th−N distances in dialkyl **24** (2.360(2), 2.368(2) Å) are

comparable to those of *tert*-butylamide−thorium species [($^{t\text{Bu}}$NON)Th(O$^{i}$Pr)$_3$Li(OEt$_2$)] ($^{t\text{Bu}}$NON = {($^{t}$BuNSiMe$_2$)$_2$O}$^{2-}$; Th−N = 2.38(1) Å),[343] and [{Me$_2$Si(η$^5$-C$_5$Me$_4$)($^{t}$BuN)}Th{N(SiMe$_3$)$_2$}(μ-Cl)]$_2$ (Th−N$_{tBu}$ = 2.335(5) Å)[344] reported by Leznoff and Marks, respectively. The Th−O$_{THF}$ distance of 2.692(2) Å is relatively long, but is comparable to that observed for Liddle's six-coordinate triamidoamine thorium complex [(tren$^{TBS}$)ThCl(THF)] (tren$^{TBS}$ = κ$^4$-{N(CH$_2$CH$_2$NSiMe$_2$$^{t}$Bu)$_3$}$^{3-}$; Th−O = 2.648(9) Å).[170]

The Th−CH$_2$ distances (2.528(3), 2.549(3) Å) in complex **24** are similar to- or modestly elongated relative to those of the six additional structurally-characterized neutral thorium (trimethylsilyl)methyl complexes, namely Marks' bis(metallocene) [Cp**$_2$Th(CH$_2$SiMe$_3$)$_2$] (Th−CH$_2$ = 2.46(1), 2.51(1) Å),[345] and *ansa*-metallocene [{Me$_2$Si(η$^5$-C$_5$Me$_4$)$_2$}Th(CH$_2$SiMe$_3$)$_2$] (Th−CH$_2$ = 2.48(2), 2.54(1) Å), Leznoff's diamido(ether) complex [($^{DIPP}$NCOCN)Th(CH$_2$SiMe$_3$)$_2$] ($^{DIPP}$NCOCN = κ$^3$-{(ArNCH$_2$CH$_2$)$_2$O}$^{2-}$, Ar = 2,6-$^{i}$Pr$_2$C$_6$H$_3$; Th−CH$_2$ = 2.490(7), 2.513(8) Å),[175] Clark's aryloxide species [Cp**Th(OAr)(CH$_2$SiMe$_3$)$_2$] (Ar = 2,6-$^{t}$Bu$_2$C$_6$H$_3$; Th−CH$_2$ = 2.460(9), 2.488(2),[110] and [Th(OAr)$_2$(CH$_2$SiMe$_3$)$_2$] (Ar = 2,6-$^{t}$Bu$_2$C$_6$H$_3$; Th−CH$_2$ = 2.44(2), 2.49(2),[162] and Mazzanti's 'salan' complex [(salan$^{t\text{Bu2}}$)Th(CH$_2$SiMe$_3$)$_2$] (salan$^{t\text{Bu2}}$ = κ$^4$-{*N,N′*-bis(2-methylene-4,6-di-*tert*-butylphenoxy)-*N,N′*-dimethyl-1,2-diaminoethane}; Th−CH$_2$ = 2.529(3) Å).[185]

The Th−C−Si angles of 119.8(1) and 129.6(2)° in dialkyl **24** are expanded relative to the ideal 109.5° angle, and while this may be a consequence of steric hindrance within the coordination sphere, it also suggests that the alkyl groups are engaged in α-agostic C−H−Th interactions.[60,162] Indeed, the presence of such α-agostic interactions has been

corroborated spectroscopically, whereby a $^{1}J_{C,H}$ of 100.4 Hz is observed for the $CH_2SiMe_3$ groups in the $^{1}H$-coupled $^{13}C$ NMR spectrum of **24** in $C_6D_6$ at room temperature. This coupling constant is significantly lower than typically expected for an $sp^3$-hybridized carbon atom, and compares well with values observed for related complexes.[346] Additionally, a methylene carbon atom from each 1-adamantyl group approaches thorium relatively closely (Th−C(25) = 3.150(3) Å, Th−C(35) = 3.221(3) Å), suggestive of Th−H−$C_{Ad}$ γ-agostic interactions in the solid state. However, such γ-agostic interactions are not maintained in solution, as a $^{1}J_{C,H}$ of 123.7 Hz is observed for the NC$CH_2$ groups of the freely-rotating 1-adamantyl substituents in the $^{1}H$-coupled $^{13}C$ NMR spectrum of **24**, which is highly comparable to that observed for a typical $sp^3$-hybridized carbon atom.[117]

Unlike Emslie's thorium dialkyl complex [$(XA_2)Th(CH_2SiMe_3)_2$] (**3-Th**), which can be dissolved in THF and readily recovered as a base-free species by evaporation of the solvent *in vacuo*, the THF ligand of dialkyl **24** cannot be removed under reduced pressure. The presence of coordinated THF in complex **24** is not desirable and poses potential issues for subsequent cation formation; although cationic organometallic species featuring THF can be prepared for electrophilic metals, such as Piers and co-workers' anilido-imine yttrium cation [($^{Dipp}$NN)Y($CH_2SiMe_2Ph$)(THF)][$PhMe_2SiCH_2B(C_6F_5)_3$] ($^{Dipp}$NN = κ$^2$-[ArN{$C_6H_4$-*o*-C(H)(NAr)}]$^-$, Ar = 2,6-$^{i}Pr_2C_6H_3$),[347] unwanted side-reactions involving coordinated Lewis bases can occur when coupled with activators such as $B(C_6F_5)_3$. For example, the [(THF)$B(C_6F_5)_3$] adduct can form, inhibiting cation formation.[348] Additionally, Lewis acidic metal cations (as well as activating reagents) can

promote THF ring-opening, leading to unexpected products such as $[Zr_3(O^tBu)_6(\mu_2\text{-}O^tBu)_3(\mu_3\text{-}O^tBu)\{\mu_3\text{-}O(CH_2)_3CH_3\}][B(C_6F_5)_4]$, which was reported to form in the reaction of $[Zr(O^tBu)_4]$ with $B(C_6F_5)_3$ in the presence of THF by Lorber and co-workers.[349] Lewis base coordination also suppresses catalytic activity and can influence other aspects of polymerization,[350] which additionally reinforces the benefit of base-free systems in this field. Consequently, rather than pursuing cationic derivatives of base-stabilized dialkyl **24**, we sought to disengage ethereal base-coordination by opting for bulkier hydrocarbyl ligands.

### 5.2.4 – XAd Thorium(IV) Bis(allyl) Complex

Although alkyls of sufficient steric influence could likely be utilized to disengage Lewis base coordination, leading to base-free XAd thorium dialkyl systems, we instead became interested in the use of bulky allyl ligands. Allyl complexes of thorium are rare; early efforts by Wilke and co-workers yielded the prototypical homoleptic tetra(allyl) species $[(C_3H_5)_4Th]$, which the authors described as a yellow crystalline solid that decomposes at 0 °C.[351] Marks and co-workers later developed heteroleptic systems, such as the tris(cyclopentadienyl) thorium allyl complex $[Cp_3Th(C_3H_5)]$, though neither complex was structurally-characterized.[352] Structurally-authenticated examples of thorium allyl complexes are limited to Hanusa's homoleptic tetra(allyl) species $[\{1\text{-}(SiMe_3)C_3H_4\}_4Th]$ and $[\{1,3\text{-}(SiMe_3)_2C_3H_3\}_4Th]$,[59] Evans' bis(metallocene) complex $[Cp^*_2Th(\eta^3\text{-}C_3H_5)(\eta^1\text{-}C_3H_5)]$,[353] and Walter and Zi's 'tuck-in' complex $[(Cp')\{\eta^5,\eta^1\text{-}(1,2\text{-}{}^tBu_2\text{-}C_5H_2\text{-}4\text{-}(CMe_2CH_2)\}Th\{1\text{-}(Ph)C_3H_4\}]$ ($Cp' = \{\eta^5\text{-}1,2,4\text{-}{}^tBu_3(C_5H_2)\}^-$).[311] We

envisioned that bulky allyl co-ligands in combination with the rigid XAd pincer ligand would yield base-free and thermally robust organothorium diallyls and cationic monoallyl derivatives thereof. In that vein, reaction of [(XAd)ThCl$_4$K$_2$]·2(dme) (**23**·2(dme)) with a 2.2 equiv of K[1-(SiMe$_3$)C$_3$H$_4$] (K[allyl$^{TMS}$]; prepared in the Emslie group *via* a slight modification of the original literature procedure[354]) at −78 °C in toluene solution afforded neutral, base-free bis(allyl) complex [(XAd)Th(η$^3$-allyl$^{TMS}$)$_2$] (**25**; Scheme 5.6). Bis(allyl) **25** was obtained as a vibrant yellow solid in approximately quantitative yield, and is highly soluble in ethereal, aromatic, and hydrocarbon solvents.

**Scheme 5.6** – Synthesis of bis(allyl) complex [(XAd)Th(η$^3$-allyl$^{TMS}$)$_2$] (**25**).

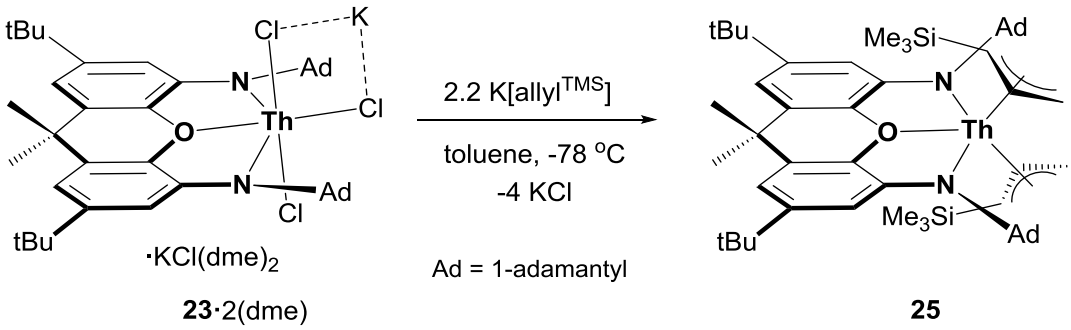


The X-ray crystal structure of **25**·2(toluene) (Figure 5.11; Table 5.4) revealed an XAd thorium(IV) bis(allyl) complex of approximate $C_2$ symmetry, with each allyl$^{TMS}$ ligand adopting an η$^3$-bonding mode, coordinated above and below the plane of the XAd ligand, respectively. If we view each allyl ligand of complex **25** as the occupant of two coordination sites, thorium is seven-coordinate; the amido donors (N(1) and N(2)) and terminal carbon atoms of the allyl ligands (C(44) and C(50)) adopt a distorted tetrahedral arrangement around the metal centre, and the neutral diarylether donor is bound between

the two amido groups, capping an edge of the aforementioned tetrahedron. While xanthene-backbone *bending* is typically observed in $XA_2$ and XAd actinide complexes, the xanthene backbone is uniquely *twisted* in complex **25**. This backbone twisting can be illustrated using the angles between the N/O/N-plane and the planes formed by each individual aromatic ring of the ligand backbone; the plane of the arene ring bound to N(2) is tilted 10.3° relative to the NON-plane, placing the arene above the NON-plane, whereas the plane of the arene ring bound to N(1) is tilted 11.6° relative to the NON-plane in the opposite direction, positioning this arene below the NON-plane. As a result of tri-hapto coordination of each allyl ligand in complex **25**, the bulky silyl groups are brought in tightly toward both faces of the ligand backbone, resulting in unfavourable steric interactions, and the observed xanthene twisting likely occurs to mitigate the steric pressure exerted by these substituents.

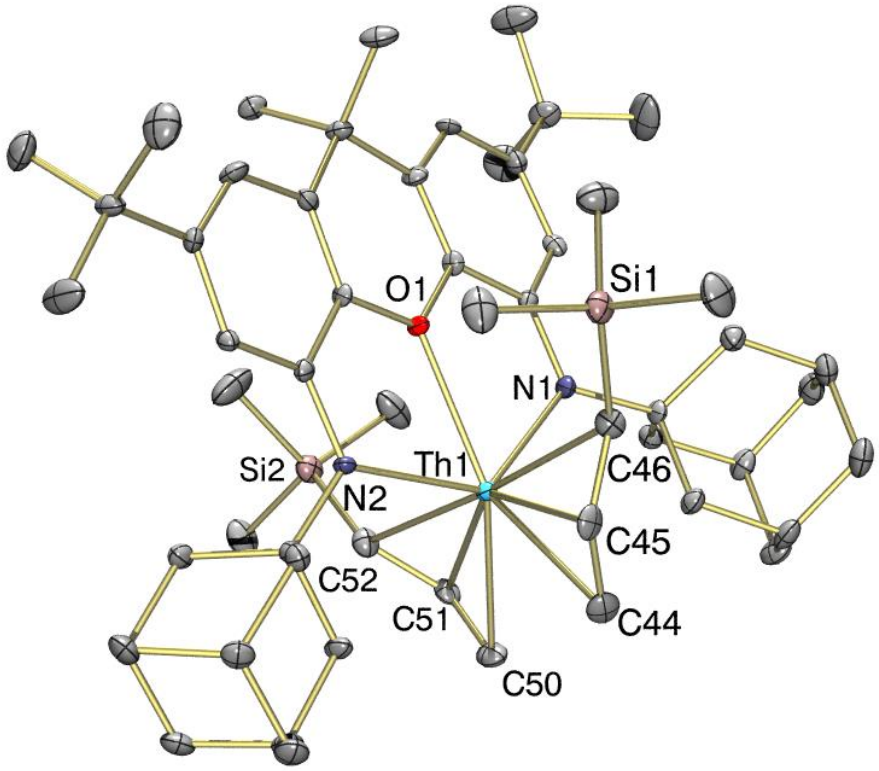


**Figure 5.11** – X-ray crystal structure of [(XAd)Th($\eta^3$-allyl$^{TMS}$)$_2$]·2(toluene) (**25**·2(toluene)), with thermal ellipsoids at 50% probability. Hydrogen atoms and toluene lattice solvent are omitted for clarity. The 1-adamantyl methylene carbon atoms closest to thorium are C(37) (of the Ad substituent on N(1)), and C(25) (of the Ad substituent on N(2)).

Although modest thorium–ligand bond elongation might be expected in the formally 14-electron bis(allyl) complex **25**, the Th−N (2.375(6), 2.379(6) Å) and Th−O (2.492(5) Å) distances are equal within error (Th−N) or very slightly shorter (Th−O) relative to those observed for the 12-electron dialkyl complex **24**, perhaps a consequence of thorium residing only 0.03 Å from the NON-plane (cf. thorium lies 0.33 Å above the NON-plane in dialkyl complex **24**). The Th−C$_{allyl}$ distances range from 2.750(7) to

2.805(7) Å and are unremarkable, in line with Th−$C_{allyl}$ contacts observed in other thorium–$\eta^3$-allyl complexes, which range from 2.617(5)−2.984(6) Å).[59,311] The $SiMe_3$ substituent of each allyl ligand in **25** is in a *syn* configuration (Figure 5.12), as was observed for all $SiMe_3$ groups in Hanusa's tetra(allyl) complexes, and as with the homoleptic species, the central *meso*-carbon of each allyl ligand in **25** is tipped away from the metal, as illustrated by fold angles of 115.3 and 116.8°, respectively (cf. the allyl fold angles in [{1-($SiMe_3$)$C_3H_4$}$_4$Th] range from 119.8−121.4°; fold angle = the angle between the $C_3$ allyl plane and the plane passing through the thorium atom and the two terminal allyl carbon atoms; Figure 5.12). Additionally, as with dialkyl **24**, a methylene carbon atom from each 1-adamantyl group of complex **25** approaches thorium relatively closely (Th−C(25) = 3.253(7) Å, Th−C(37) = 3.215(7) Å), suggestive of Th−H−$C_{Ad}$ γ-agostic interactions in the solid state.

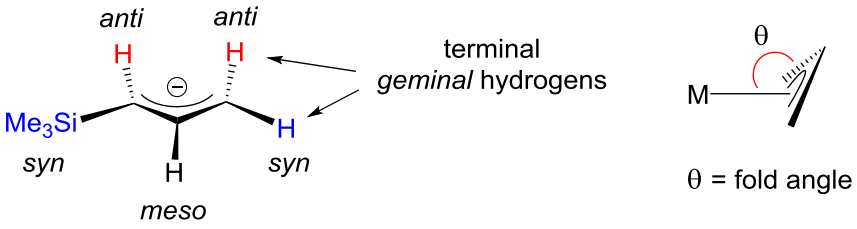


**Figure 5.12** – Naming protocol for the chemical environments of the {1-($SiMe_3$)$C_3H_4$}$^-$ ligand, and depiction of the fold angle of an $\eta^3$-allyl complex.

The room-temperature $^1$H NMR spectrum of **25** in toluene-$d_8$ (Figure 5.13) features resonances indicative of a side−side and top−bottom symmetric isomer of bis(allyl) complex [(XAd)Th($\eta^3$-allyl$^{TMS}$)$_2$], with resonances corresponding to the terminal (*gem*) protons, central *meso* proton, and *anti* proton of each allyl ligand (as well

as the signal corresponding to the equivalent 1-adamantyl NC($CH_2$)$_3$ methylene protons) broadened nearly completely into the baseline. The broadening observed for these resonances is attributed to dynamic allyl ligand behaviour, whereby averaging of the geminal *syn* and *anti* protons (of the allyl $CH_2$ group) occurs as a consequence of rapid allyl 'flipping', most likely *via* a π–σ–π intramolecular conversion (Figure 5.14), which has been proposed to occur for the allyl ligands in other thorium–allyl complexes.[59,352]

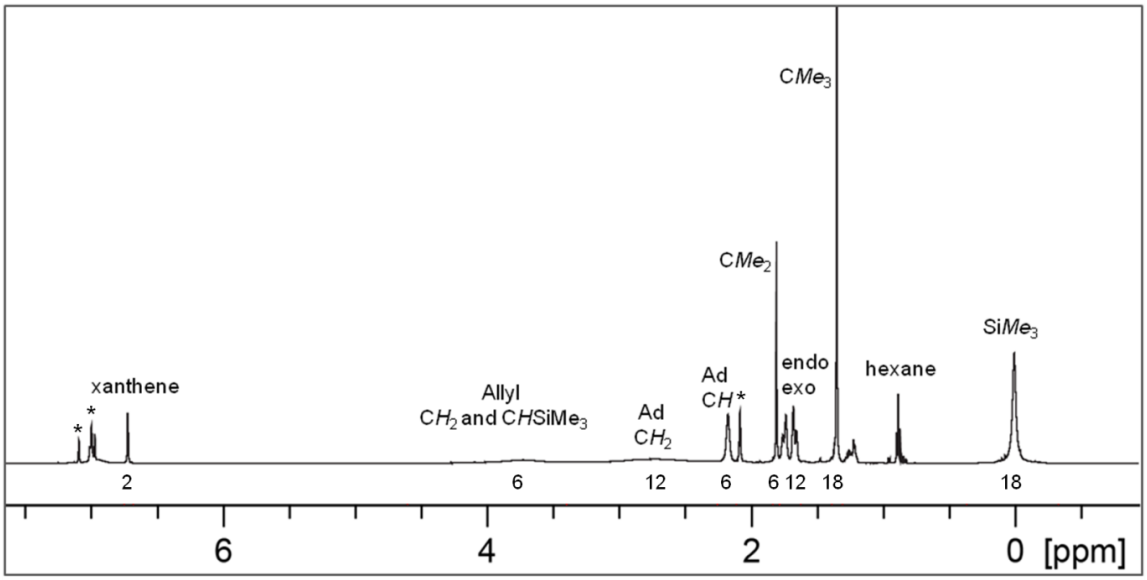


**Figure 5.13** – $^1$H NMR spectrum of bis(allyl) complex **25** in toluene-$d_8$ at room temperature (500 MHz). Numbers below the baseline indicate the approximate integration of each peak. ***** denotes toluene-$d_8$. The *meso*-C*H* resonance is broadened into the baseline and obscured by toluene-$d_8$ signals; the second xanthene peak is obscured by toluene-$d_8$ signals as well.

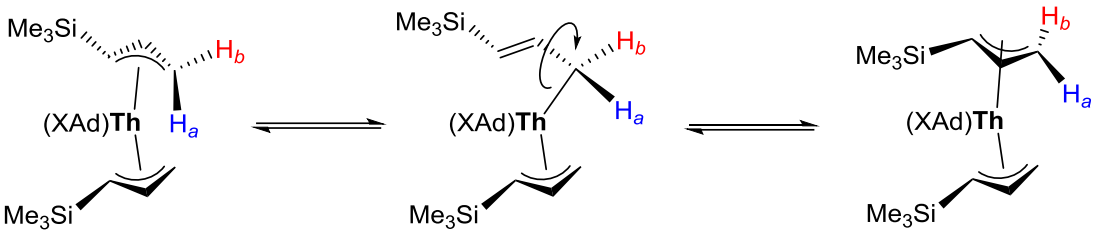


**Figure 5.14** – Exchange of the *geminal* $H_a$ and $H_b$ protons *via* a π–σ–π intramolecular conversion.

Indeed, upon warming complex **25** in toluene-$d_8$ to high temperature (87 °C), coalescence occurred, and $^1$H NMR resonances corresponding to a single, averaged π-coordinated allyl ligand environment were observed (Figure 5.15) that arise from two allyl ligands per XAd ligand based on integrations (*i.e.* the terminal *gem* protons of both allyl ligands appear as a doublet integrating to 4H ($^3J_{H,H}$ = 11.8 Hz), the central *meso* proton environment appears as a multiplet (2H), the *anti* proton environment appears as a doublet (2H; $^3J_{H,H}$ = 15.7 Hz), and the Si*Me*$_3$ protons appear as a singlet (18H). The allyl ligands are characterized as $\eta^3$ π-coordinated based on the observed $^3J_{H,H}$ coupling constants, which fall within the range observed for vicinal *cis* and *trans* alkenyl protons (7–18 Hz) (cf. smaller $^3J_{H,H}$ values (e.g. 6 Hz) are typical for R*CH*$_2$−C*H*=CH$_2$).[355]

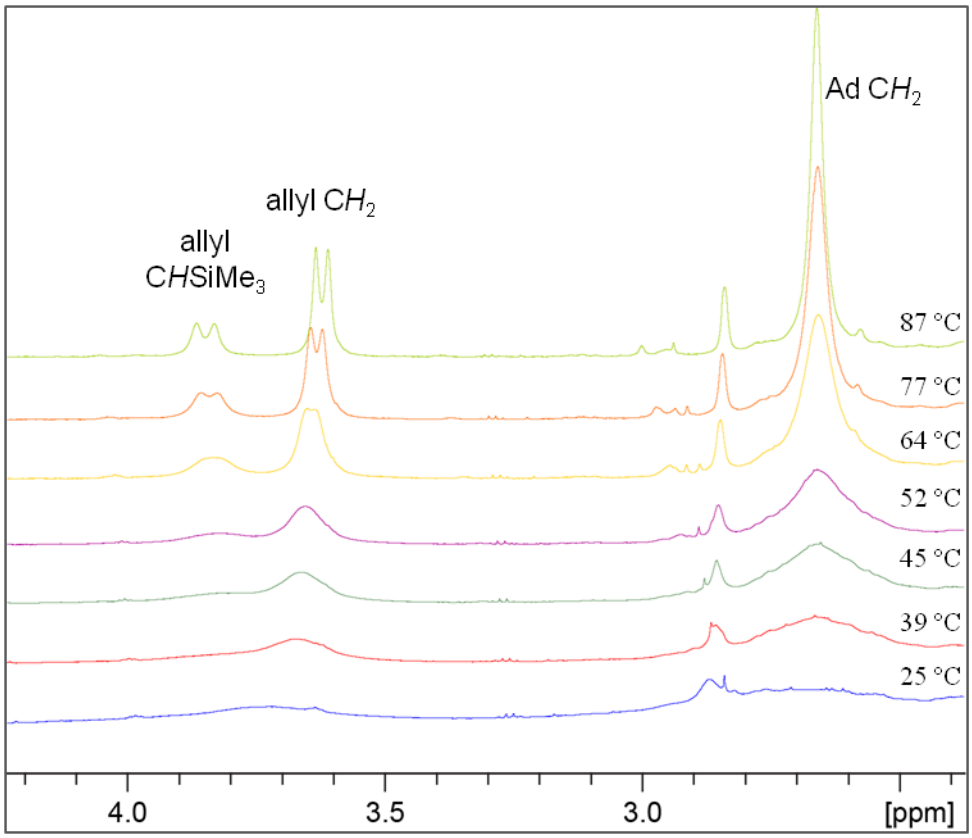


**Figure 5.15** – Selected region of the $^{1}$H NMR spectra of bis(allyl) complex **25** in toluene-$d_8$ at temperatures ranging from +25 to +87 °C (500 MHz).

At low temperature (−63 °C), a more complex spectrum is observed (Figure 5.16); most notable are three singlets attributable to three unique Si*Me*$_3$ environments, and nine doublets (two of which are obscured by 1-adamantyl C*H*$_2$ signals, *vide infra*) attributable to chemically inequivalent terminal *gem* protons and *anti* C*H*SiMe$_3$ protons. Taken together, this collection of resonances is indicative of an approximately 1:1:1 mixture of *three* chemically distinct {1-(SiMe$_3$)C$_3$H$_4$} ligand environments, which indicates the presence of a mixture of isomers in solution. Each allyl ligand environment is characterized as π-bound, as indicated by $^{3}J_{cis\text{-H,H}}$ values ranging from 8.4–8.9 Hz, and $^{3}J$-

$^{trans}$-H,H values ranging from 16.1–18.4 Hz, which are typical of vicinal alkenyl protons.[355] The 2D [$^1$H-$^1$H] COSY NMR spectrum of complex **25** acquired at −63 °C (Figure 5.17) definitively corroborates the presence of three unique π-bound {1-(SiMe$_3$)C$_3$H$_4$} ligand environments, and additionally indicates that the SiMe$_3$ substituents are in *syn* configurations based on the presence of two *anti* protons and one *syn* proton for each of the unique allyl environments (as evidenced by the distribution of $^3J_{trans}$ and $^3J_{cis}$ values).

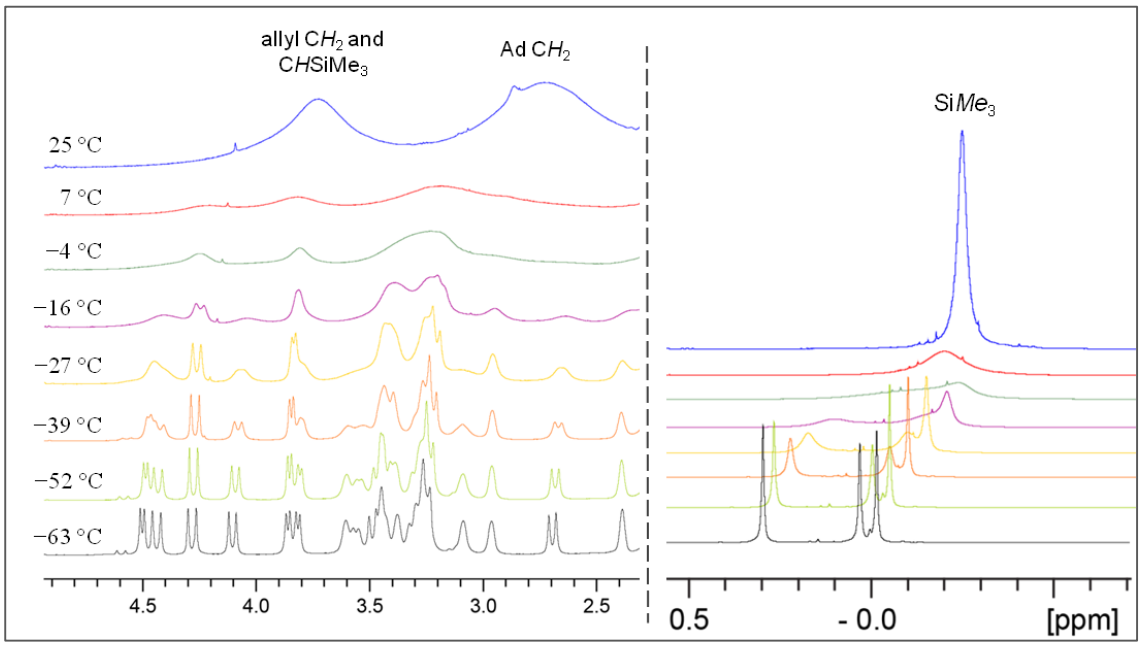


**Figure 5.16** – Selected regions of the $^1$H NMR spectra of bis(allyl) complex **25** in toluene-$d_8$ at temperatures ranging from +25 to −63 °C (500 MHz).

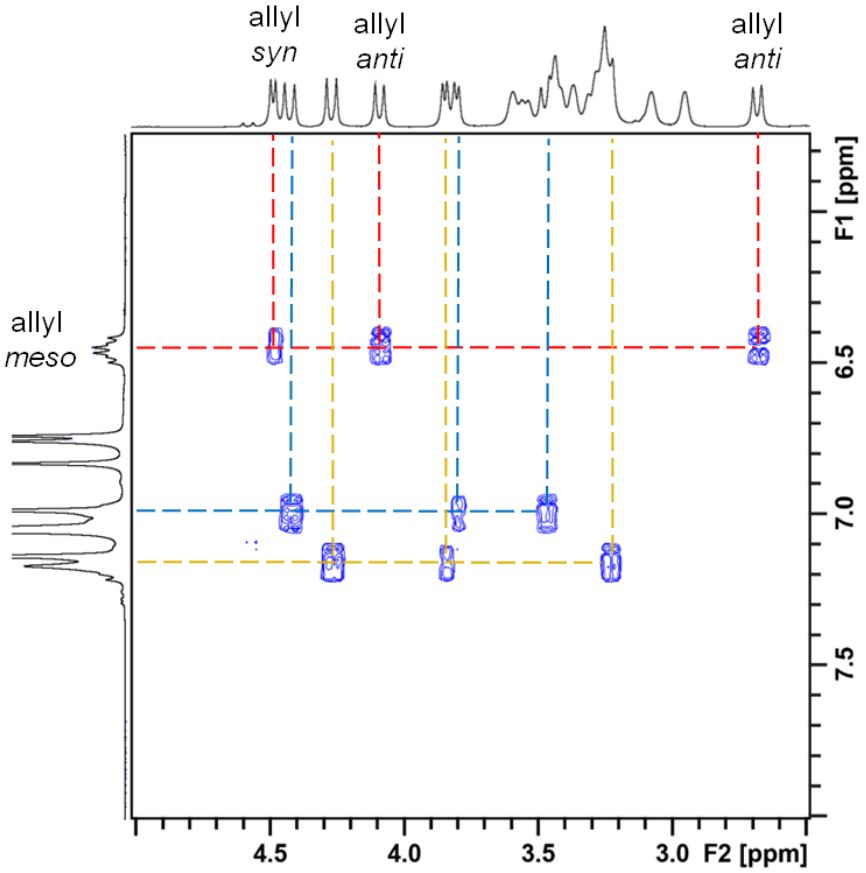


**Figure 5.17** – Selected region of the 2D [$^{1}$H–$^{1}$H] COSY NMR spectrum of bis(allyl) complex **25** in toluene-$d_8$ at −63 °C (500 MHz), highlighting the presence of three unique π-allyl environments.

The bis(allyl) complex is proposed to exist as two isomers in solution at low-temperature, depicted as **25** and **25′** (Figure 18), in an approximate 1:2 ratio, respectively. $C_2$-symmetric **25** features top–bottom and side–side symmetry, giving rise to one chemical environment each for the Si*Me*$_3$, C*Me*$_3$, and C*Me*$_2$ groups, respectively. By contrast, $C_1$-symmetric **25′** features top–bottom and side–side asymmetry, giving rise to *two* unique environments each for the respective aforementioned Si*Me*$_3$, C*Me*$_3$, and C*Me*$_2$

groups. This distribution of environments aligns with those observed in the low-temperature $^{1}H$ and $^{13}C\{^{1}H\}$ NMR spectra of the bis(allyl) species, validating this assignment.

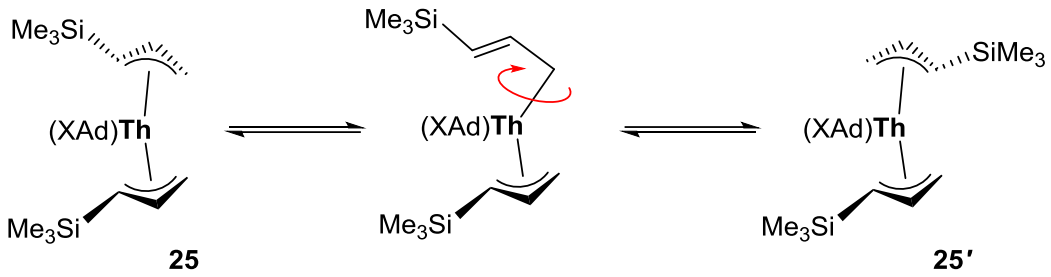


**Figure 5.18** – Isomerization of complex **25** to form **25′** *via* π–σ–π intramolecular conversion of a {1-($SiMe_3$)$C_3H_4$} group.

The original homoleptic tetra(allyl) complex [($C_3H_5$)$_4$Th] reported by Wilke and co-workers[51] suffered from limited thermal stability, decomposing at temperatures above 0 °C. By replacing allyl groups with resilient cyclopentadienyl supporting ligands, the resulting heteroleptic thorium allyl complex [$Cp_3Th(C_3H_5)$] developed by Marks and co-workers[352] exhibited drastically improved thermal stability, decomposing at 210 °C. The rigid XAd ancillary similarly serves to improve thermal robustness in thorium allyl systems, as heteroleptic bis(allyl) complex **25** can withstand heating at 85 °C for a period of 15 h with minimal decomposition, and is only <5% decomposed after heating at 155 °C for 10 min. By contrast, Hanusa's homoleptic tetra(allyl) complex [{1-($SiMe_3$)$C_3H_4$}$_4$Th] decomposed at 90 °C.[53]

Having prepared a thermally-robust, base-free bis(hydrocarbyl) XAd thorium complex, we sought to generate a cationic monoallyl derivative, and probe its ability to

polymerize ethylene. Emslie and co-workers previously demonstrated the utility of the trityl cation as an alkide abstracting agent capable of abstracting a multi-hapto coordinated benzyl ligand from [(XA$_2$)Th(CH$_2$Ph)$_2$] (**5-Th**) to afford the cationic monobenzyl species [(XA$_2$)Th(CH$_2$Ph)($\eta^6$-C$_6$H$_5$Me)][B(C$_6$F$_5$)$_4$] (**9-Th**), and from [(BDPP)Th(CH$_2$Ph)$_2$] to afford the cationic dimer [(BDPP)Th($\eta^2$-CH$_2$Ph)($\mu$-$\eta^1$:$\eta^6$-CH$_2$Ph)Th($\eta^1$-CH$_2$Ph)(BDPP)][B(C$_6$F$_5$)$_4$].[179] Given the electronic similarities between a multi-hapto coordinated benzyl ligand and a π-bound allyl group, we reasoned that the trityl cation should be an effective allyl abstractor. Following the established protocol, 1 equiv of [Ph$_3$C][B(C$_6$F$_5$)$_4$] was admitted to a light yellow fluorobenzene solution of bis(allyl) **25**, in attempt to generate the monoallyl fragment [(XAd)Th($\eta^x$-allyl$^{TMS}$)]$^+$; the 1-adamantyl substituents of the XAd ligand are expected to disfavour *cis* arene-coordination, though *trans* arene-coordination may be engaged. Upon addition of the [Ph$_3$C][B(C$_6$F$_5$)$_4$] activator, the solution became pale yellow; the 1 millimolar solution was subsequently exposed to ethylene (1 atm, 20 °C), but unfortunately, after 1 h under dynamic ethylene and subsequent quenching with acidified methanol, no polyethylene was produced.

The observed catalytic inactivity of **25**/[Ph$_3$C][B(C$_6$F$_5$)$_4$] in fluorobenzene solution may be due to a number of factors. As was hypothesized for the proposed monobenzyl species [(XA$_2$)U(CH$_2$Ph)($\eta^x$-C$_6$H$_5$F)][B(C$_6$F$_5$)$_4$] (**11**), it is possible that the stability imparted to the cationic [(XAd)Th($\eta^x$-allyl$^{TMS}$)]$^+$ fragment by π-coordination of the lone allyl ligand precludes its subsequent involvement in ethylene insertion-polymerization. Additionally, it is possible that allyl abstraction was not complete to a sufficient extent

after the 1 hour induction period, or that the trityl cation is incapable of abstracting an allyl moiety, but may instead engage in unwanted reactivity leading to decomposition of the neutral bis(allyl) precursor. Proposed avenues for future work in XAd thorium chemistry are described in detail in Chapter 6.

**Table 5.6** – Crystallographic data collection and refinement parameters for complexes **24** and **25**

| Structure | **24** | **25**·2(toluene) |
|---|---|---|
| Formula | $C_{55}H_{88}N_2O_2Si_2Th$ | $C_{69}H_{100}N_2OSi_2Th$ |
| Formula wt | 1097.49 | 1261.72 |
| *T* (K) | 120(2) | 100(2) |
| Cryst. Syst. | Monoclinic | Triclinic |
| Space Group | *P*2(1)/*n* | *P*–1 |
| *a* (Å) | 11.8753(13) | 11.7100(12) |
| *b* (Å) | 19.058(2) | 11.8425(12) |
| *c* (Å) | 24.429(3) | 23.928(3) |
| α [deg] | 90 | 82.182(2) |
| β [deg] | 100.431(2) | 76.962(2) |
| γ [deg] | 90 | 78.177(2) |
| Volume [$Å^3$] | 5437.4(11) | 3150.0(6) |
| *Z* | 4 | 2 |
| Density (calcd; $Mg/m^3$) | 1.341 | 1.330 |
| μ ($mm^{-1}$) | 2.826 | 2.447 |
| *F*(000) | 2264 | 1308 |
| Crystal Size ($mm^3$) | 0.390×0.110×0.060 | 0.273×0.209×0.064 |
| θ Range for Collection [deg] | 2.004–33.374 | 0.877–26.372 |
| No. of reflns. Collected | 92036 | 85255 |

| | | |
|---|---|---|
| No. of Indep. Reflns. | 20473 | 12862 |
| Completeness to θ Max (%) | 99.9 | 99.8 |
| Absorption Correction | Numerical | Numerical |
| Max and Min Transmission | 0.8782, 0.5232 | 0.8822, 0.6466 |
| Data / Parameters | 20473 / 559 | 12862 / 658 |
| GOF on $F^2$ | 0.997 | 1.286 |
| Final $R_1$ [$I > 2\sigma(I)$] | R1 = 0.0403<br>wR2 = 0.0665 | R1 = 0.0539<br>wR2 = 0.1445 |
| *R* indices (all data) | R1 = 0.0757<br>wR2 = 0.0762 | R1 = 0.0567<br>wR2 = 0.1457 |

# Chapter 6

# Conclusions and Future Directions

## 6.1 – Conclusions

The development of non-carbocyclic actinide systems has become a significant research thrust over the course of the past decade, with new, carefully crafted ligand platforms affording access to species which feature intriguing chemical linkages, and which often promote unusual reactivity. Research in the Emslie group has previously led to frontier advancements in this burgeoning area, namely the development of non-carbocyclic organothorium species supported by the diamido pincer ligands $XA_2$ and BDPP. Herein, the exploration of actinide systems supported by rigid xanthene-based diamido pincer ligands was advanced through development of the complementary $XA_2$ uranium chemistry, and through the continued evolution of the ligand design. This work has demonstrated that $XA_2$ and related pincer ligands are (a) versatile in their ability to accommodate electronic changes at the metal centre without significant deviation from their intended architectural mandate, (b) that they are highly suitable for support of low-coordinate and highly electrophilic organouranium fragments, and (c) that they are readily amenable to steric and electronic tuning, all hallmarks of attractive ancillary ligand platforms. Additionally, we have unlocked latent catalytic ethylene polymerization behaviour in cationic $XA_2$ actinide systems, and explored C−H bond activation chemistry

promoted by uranium. Specific developments in this thesis which support these conclusions are described below.

Having previously demonstrated valuable utility as a chemically robust ancillary for the support of thorium(IV) systems, the dianionic pincer ligand (4,5-bis(2,6-diisopropylanilido)-2,7-di-*tert*-butyl-9,9-dimethylxanthene), $XA_2$, was deployed for the development of uranium chemistry. In that vein, facile transmetalation of the dipotassium complex $[K_2(dme)_x(XA_2)]$ with $UCl_4$ furnished access to a salt-occluded $XA_2$ uranium(IV) chloro species, $[(XA_2)UCl_2(\mu\text{-}Cl)\{K(dme)_3\}]$, and subsequent one-electron reduction of this complex afforded a stable, crystalline uranium(III) derivative, $[(XA_2)UCl(dme)]$. Access to this tandem of chloro species demonstrates the ability of $XA_2$ to accommodate significant electronic changes at the metal centre, supporting complexes featuring the smaller uranium(IV) ion (ionic radius = 0.89 Å) and larger uranium(III) ion (1.03 Å), relative to thorium(IV) (0.94 Å).[11]

To support metals with differing electronic profiles, the $XA_2$ ligand is able to bend at the diarylether linkage of the xanthene backbone, allowing for modulation of the An−O and An−N bond lengths. For example, the xanthene backbone of the six-coordinate uranium(IV) chloro species is fairly planar, with a 1.2° angle between the planes formed by each aromatic ring of the backbone (where each plane is defined by the six carbon atoms of each aromatic ring). Upon reduction, the xanthene backbone bends significantly (20.9°) as a means of facilitating longer uranium–ligand bonds to the larger U(III) ion. Through its support of uranium in various oxidation states [including low-valent uranium(III)], $XA_2$ has additionally proven resistant to reductive degradation. For

comparison, Lappert and co-workers observed reductive imine cleavage and forceful rearrangements of their β-diketaminato (nacnac) ligand system upon introduction to uranium.[356]

In complexes of uranium(IV), changes in coordination number and/or geometry are also easily managed by $XA_2$, typically through a combination of the aforementioned backbone flexing in conjunction with modulation of the NON-donor array positioning with respect to the metal centre. For example, the five-coordinate dialkyl complex $[(XA_2)U(CH_2SiMe_3)_2]$ features a fairly bent xanthene backbone (average of 18.2°) and in this complex, the NON-donor array of the $XA_2$ ligand is positioned so that the neutral diarylether donor is located an average of 0.93 Å from the N/U/N-plane. Upon coordination of a third (trimethylsilyl)methyl ligand to form the six-coordinate $[(XA_2)U(CH_2SiMe_3)_3]^-$ anion, the xanthene backbone planarizes (average of 5.9°) to accommodate the additional steric bulk of a second axially-bound alkyl group, and as a result, the NON-donor array is re-positioned, with the diarylether donor now located an average of 0.79 Å from the N/U/N-plane. Importantly, although the $XA_2$ ligand features some inherent flexibility, the donor array remains meridionally- rather than facially-coordinated, and the steric protection afforded by the 2,6-diisopropylphenyl groups flanking the metal coordination pocket is maintained for all $XA_2$ complexes prepared thus far.

In addition to proving quite versatile in its ability to make structural accommodations for metal fragments with varied electronic and steric demands, $XA_2$ has demonstrated an ability to stabilize electrophilic, low-coordinate uranium species, and to

resist cyclometalation or other decomposition pathways, except under pressing conditions. For example, several thermally-robust low-coordinate uranium(IV) dialkyl complexes have been prepared, including the formally 12-electron $[(XA_2)U(CH_2SiMe_3)_2]$, $[(XA_2)U(CH_2Ph)_2]$, and the first structurally-characterized neutral uranium neopentyl complex $[(XA_2)U(CH_2{}^tBu)_2]$. While other groups have attempted to prepare uranium neopentyl derivatives, unexpected ancillary ligand-centred reactivity or unwanted cyclometalation was often observed, highlighting the ability of $XA_2$ to support organouranium species that proved inaccessible with other ligand systems. Electrophilic low-coordinate monoalkyl uranium cations bearing $XA_2$ also exhibit exceptional thermal stability, withstanding heating of up to 80 °C with gradual decomposition over 8 hours. While arene-bound cationic $XA_2$ actinide systems have previously resisted utility as ethylene polymerization catalysts, dormant catalytic activity has been unearthed through electronic tuning of the arene ligand. Indeed, activities up to $5.76 \times 10^4$ g of polyethylene·(mol of An)$^{-1}$·h$^{-1}$·atm$^{-1}$ have been achieved using fluoroarene-coordinated cations $[(XA_2)U(CH_2SiMe_3)(\eta^3\text{-}C_6H_5F)]^+$, $[(XA_2)U(CH_2SiMe_3)(o\text{-}C_6H_4F_2)]^+$, and $[(XA_2)Th(CH_2SiMe_3)(\eta^x\text{-}C_6H_5F)]^+$, the former representing the first structurally-characterized f-element complex bearing a π-coordinated fluoroarene ligand, and the latter representing the most active post-metallocene actinide ethylene polymerization catalyst to date. Additionally, $XA_2$ has proven adept at supporting complexes that exhibit nucleophilic behaviour, as the dialkyl complex $[(XA_2)U(CH_2SiMe_3)_2]$ readily promotes C−H activation of pyridines to afford new monoalkyl uranium(IV) species bearing

cyclometalated $\kappa^2$-*C,N*-pyridyl ligands, which deuterium labeling established as the products of σ-bond metathesis.

Finally, as an additional research thrust, we focused on the evolution of the xanthene-based diamido ligand motif. Ligand systems that have experienced rapid uptake in the organometallic chemistry community typically offer simple/cost-effective syntheses, superior properties (*i.e.* donor function/distribution, optimal steric shielding, thermal and chemical stability, advantageous solubility/crystallinity characteristics), and modularity in design. Previous research in the Emslie group, as well as research presented herein is highly complementary of the functional properties the xanthene-based NON-donor platform exhibits as a supporting ligand in organoactinide chemistry, and through exploration of ligand evolution, the modularity of the $XA_2$ ligand design has now been explicitly demonstrated. The palladium-catalyzed coupling of functionalized amines with 4,5-dibromo-2,7-di-*tert*-butyl-9,9-dimethylxanthene is amenable to a variety of amine substrates; the use of extremely bulky 2,6-dimestylaniline afforded the 2$^{nd}$ generation ligand 4,5-bis(2,6-dimesitylanilido)-2,7-di-*tert*-butyl-9,9-dimethylxanthene, XAT, and the use of 1-adamantylamine afforded the 3$^{rd}$ generation ligand 4,5-bis(1-adamantylamido)-2,7-di-*tert*-butyl-9,9-dimethylxanthene, XAd. The development of these 2$^{nd}$ and 3$^{rd}$ generation xanthene-based diamido ligands led to the study of crystallographically-authenticated potassium–alkane complexes, as well as new thorium hydrocarbyl complexes that exhibit impressive thermal stability. Indeed, the modularity of the xanthene-based NON-donor platform serves to add to its attractiveness as a highly

versatile and chemically robust ancillary ligand system that offers rapid tunability of its electronic and steric profile.

## 6.2 – Future Directions

As highlighted above, xanthene-based diamido ancillary ligands have proven quite suitable for the support of a wide variety of organoactinide systems that engage in diverse reactivity manifolds, and offer significant potential in other areas as well. Outlined below are various potential avenues for the future of this research thrust, including some initial results from various initiatives currently in their early stages of development in the Emslie group, as well as possible future investigations.

### 6.2.1 – Low-Valent $XA_2$ Uranium Chemistry and Small Molecule Activation.

While one-electron reduction of the uranium(IV) chloro species [$(XA_2)UCl_2(\mu\text{-}Cl)\{K(dme)_3\}$] yielded [$(XA_2)UCl(dme)$], a stable uranium(III) derivative, the majority of the research delineated herein was focused toward the development of uranium(IV) chemistry. However, the monochloro uranium(III) species has shown initial promise as a potential precursor for further derivatization. Early investigations in the Emslie group have revealed divergent avenues of reactivity stemming from [$(XA_2)UCl(dme)$], namely, access to organouranium(III) species, and to further-reduced arene-bridged dimers that behave as U(II) synthetic equivalents.

While the chemistry of uranium(IV) alkyl complexes has experienced considerable growth, development of the corresponding uranium(III) alkyl species has

remained a synthetic challenge.[111] Bart and co-workers have recently begun the development of post-metallocene uranium(III) alkyl chemistry utilizing a bis(scorpionate) $(Tp')_2$ ($Tp' = \{HB(3,5\text{-}Me_2pz)_3\}^-$) platform as an ancillary support system, gaining access to complexes of the form $[Tp'_2UR]$ (R = $CH_2Ph$, $CH_2SiMe_3$, Me, $^nBu$) by alkylation of the corresponding uranium(III) halide complex $[Tp'_2UI]$.[63,169] Early results in the Emslie group suggest that the uranium(III) monochloride complex $[(XA_2)UCl(dme)]$ can similarly serve as precursor to uranium(III) alkyl species, as alkylation with $LiCH_2SiMe_3$ at low temperature has afforded the uranium(III) (trimethylsilyl)methyl derivative $[(XA_2)U(CH_2SiMe_3)(dme)]$ (Scheme 6.1). We envision a more complete development of this area, by expanding the scope of accessible $XA_2$ uranium(III) hydrocarbyl species, and investigating their reactivities.

**Scheme 6.1** – Formation of an $XA_2$ uranium(III) alkyl derivative in the Emslie group.

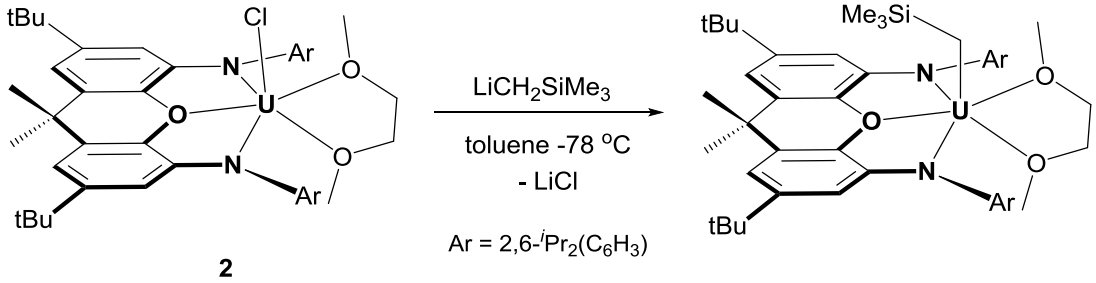


While organouranium(III) species appear accessible *via* transmetalation with alkyllithium reagents at low temperature, attempted room-temperature alkylation of $[(XA_2)UCl(dme)]$ instead resulted in reduction, yielding a complex featuring a reduced bridging arene, $[\{(XA_2)U(\kappa^1\text{-dme})\}_2(\mu\text{-}\eta^6\text{:}\eta^6\text{-toluene})]$. Such 'inverse-sandwich' complexes of uranium bearing reduced bridging arene ligands have been a growing area

of interest for nearly 20 years, investigated primarily by the groups of Cummins,[357] Evans,[71] Diaconescu,[358] Arnold,[359] Mazzanti,[360] and Liddle.[361] Most notably, while such uranium species behave as 'U(II) synthetic equivalents' which promote multi-electron reductions, the bridging arene ligands have been shown to be reduced, acting as 'electron storage sinks'.[362] Early investigations in the Emslie group suggest that the "[$(XA_2)U$]" fragment is similarly capable of supporting the reduced-arene bridged 'inverse-sandwich' motif in various forms; reduction of [$(XA_2)UCl_2(\mu\text{-}Cl)\{K(dme)_3\}$] with 2 equiv of potassium naphthalenide in dme yielded [$\{(XA_2)U(ClK(dme)_2\}_2(\mu\text{-}\eta^6\text{:}\eta^6\text{-naphthalene})$], which can be converted to [$\{(XA_2)U(\kappa^1\text{-dme})\}_2(\mu\text{-}\eta^6\text{:}\eta^6\text{-toluene})$] by addition of toluene. Indeed, both of these reduced uranium dimers have demonstrated capability as reducing agents, reacting with organic azides to form higher-valent uranium imido species (Scheme 6.2).

**Scheme 6.2** – Formation of $XA_2$ uranium imido species *via* multi-electron reductions of organoazide compounds.

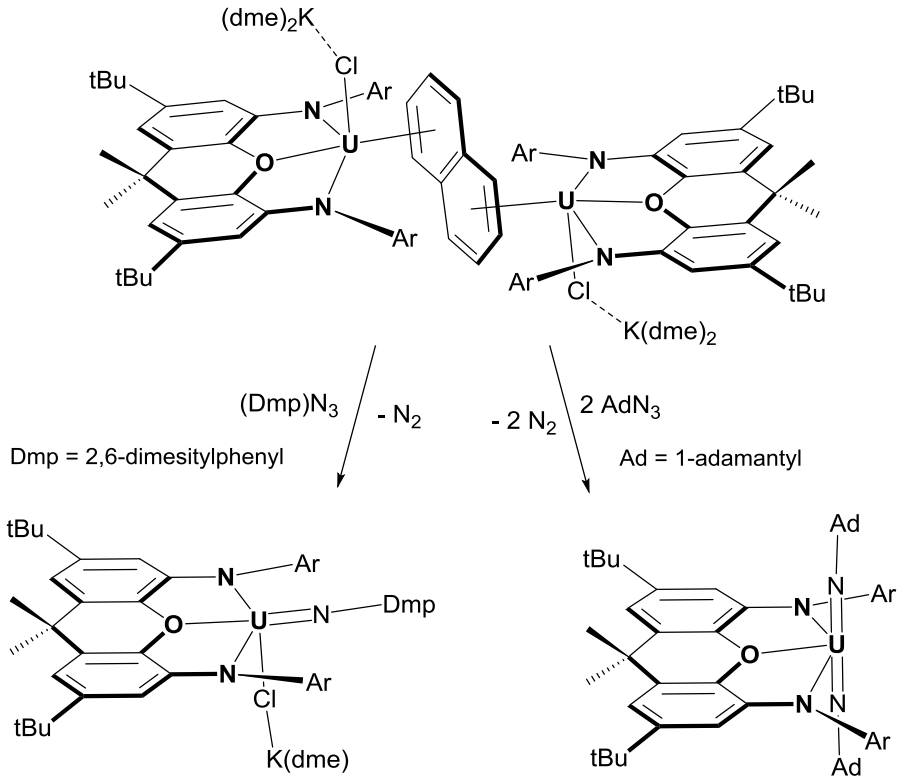


Future work in this area will involve the development of additional 'inverse-sandwich' complexes of uranium (preliminary results suggest an anthracene-bridged species is accessible), and further exploration of their respective reduction chemistries, with a focus on activating small inorganic molecules (*i.e.* $P_4$, $N_2$).

### 6.2.2 – Organometallic $XA_2$ Uranium(IV) Chemistry

A major focus of the research presented in this thesis is the development of neutral, cationic, and anionic $XA_2$ uranium(IV) alkyl species, which have proven accessible, thermally-stable, and reactive. To expand the scope of this research thrust, the

development of hydride derivatives will be pursued in the future, as the vast majority of known actinide hydride species are supported by carbocyclic ancillary ligands. Preliminary results in the Emslie group indicate that $XA_2$ uranium polyhydride complexes are accessible, as evidenced by the formation of a tentatively assigned hydride cluster complex *via* the reaction of uranium(IV) chloro precursor $[(XA_2)UCl_2(\mu\text{-}Cl)\{K(dme)_3\}]$ with an alkali-metal hydride reagent. Future work in this area will involve expanding the scope of accessible hydride derivatives, as well as exploration of their respective chemistries.

The development of cationic $XA_2$ monoalkyl species for use in ethylene polymerization has met with a variety of challenges to date, namely the persistent π-coordination of arene ligands, which serves as a barrier to ethylene binding and subsequent insertion. Attempts to mitigate this form of catalytic deactivation, including electronic tuning of the arene ligand, have resulted in access to latent catalytic behaviour in our cationic actinide species, and further evaluation of their catalytic profile will be administered in the future. Ethylene polymerization catalyzed by fluoroarene complexes of the form $[(XA_2)An(CH_2R)(C_6H_xF_{6-x})]^+$ (An = U, Th; R = $SiMe_3$, $^t$Bu, Ph) could be further explored, including reactions at elevated temperatures (100 °C) and pressures (up to 50 atm). Additionally, although fluoroarene solvents have provided access to catalytically active cations, the use of such solvents is not expected to be industrially-viable, and so continued development of cationic $XA_2$ systems is warranted given the catalytic inactivity of $XA_2$ actinide cations bearing proteo-arenes. One such approach could involve the preparation of arene-free systems; for example, by utilizing $B(C_6F_5)_3$ as

a soluble alkide abstracting agent in conjunction with dialkyl precursor $[(XA_2)U(CH_2SiMe_3)_2]$ in hexane solution, a contact ion-pair featuring the weakly-coordinating anion $[Me_3SiCH_2B(C_6F_5)_3]^-$ may be accessible, given the absence of available arene ligands (Scheme 6.3). Such species are expected to demonstrate improved solubility in saturated hydrocarbons, which circumvents the issues surrounding the presence of arene molecules as a desirable consequence.

**Scheme 6.3** – Proposed synthesis of arene-free cationic $XA_2$ uranium species, with proposed subsequent introduction of ethylene to assess insertion-polymerization capabilities.

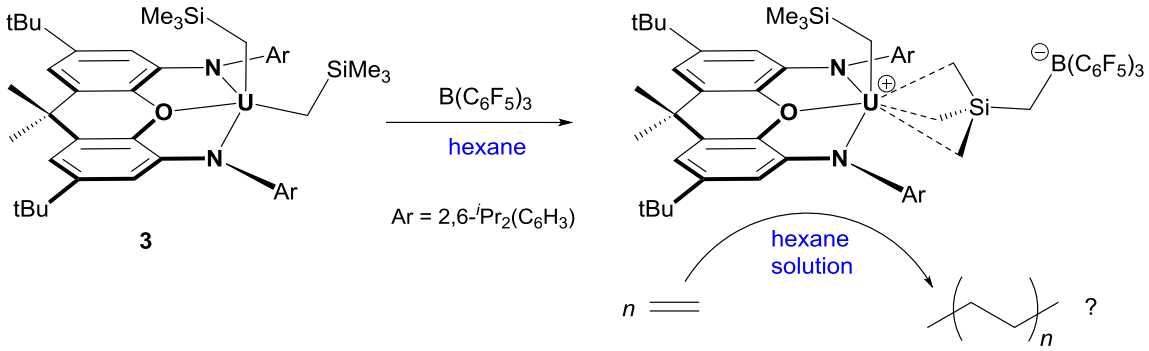


In addition to further development of $XA_2$ actinide cations as olefin polymerization catalysts, the synthetic utility of such cationic monoalkyl species will also be explored. For instance, bromobenzene-bound mono((trimethylsilyl)methyl) uranium cation $[(XA_2)U(CH_2SiMe_3)(C_6H_5Br)]^+$ could serve as a useful precursor for accessing synthetically challenging neutral mixed alkyl species, such as $[(XA_2)UMe(CH_2SiMe_3)]$ (Scheme 6.4), which have been proposed as intermediates in actinide-centered alkyl exchange chemistry (*vide supra*; Chapter 4).

**Scheme 6.4** – Proposed synthesis of a mixed alkyl complex from a cationic monoalkyl precursor.

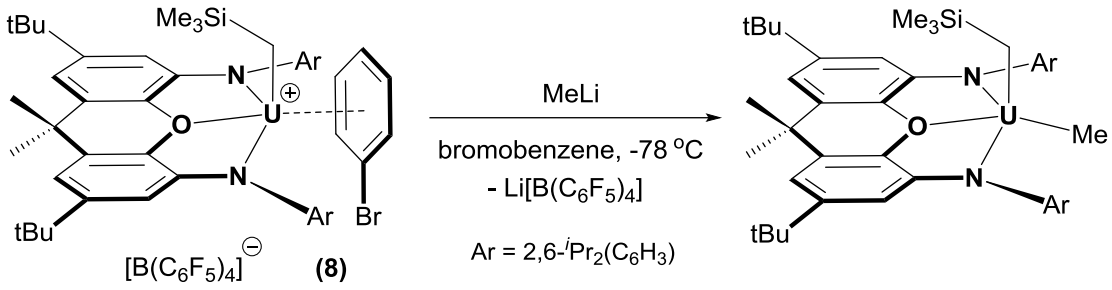


### 6.2.3 – New Avenues in XAT Chemistry

While the bulky 2nd generation ligand 4,5-bis(2,6-dimesitylanilido)-2,7-di-*tert*-butyl-9,9-dimethylxanthene (XAT) has thus far proven untenable as an ancillary for the support of tetravalent actinides, XAT offers entry into a variety of other intriguing avenues. The observation that dipotassium XAT species feature close approach of hydrocarbon solvent molecules to the potassium centre(s) in the solid state (*i.e. n*-hexane in $[K_2(XAT)(n\text{-hexane})]\cdot$toluene) highlights the potential for the hydrophobic binding pocket(s) formed from the XAT ligand framework to encourage incorporation of small, nonpolar molecules into the coordination sphere of a metal, a phenomenon that is highly relevant toward developing complexes capable of activating challenging substrates (e.g. hydrocarbons). Early investigations geared toward broadening the scope of XAT chemistry have led to the development of a trilithium species, $[Li_3(C_4H_9)(XAT)]$ (carried out by Adam Pantaleo, an undergraduate student in the Emslie group under the supervision of N. R. Andreychuk), which features the incorporation of an *n*-butyllithium

unit into the XAT binding pocket in solution as well as the solid-state. This observation serves to further demonstrate the utility of the bulky hydrophobic XAT ligand architecture in facilitating access to complexes which feature the uptake of nonpolar molecules. In the future, the use of sterically bulky alkyllithium reagents (e.g. $^{t}$BuLi) or LiH may be explored in order to furnish access to the desired dilithium species "[$Li_2$(XAT)]", and its ability to form complexes featuring lithium–alkane interactions may be subsequently pursued. Additionally, to investigate the extent to which the XAT ligand system is capable of facilitating industrially-relevant transformations (such as the C−H activation of saturated hydrocarbon molecules), we intend to explore the preparation of complexes featuring catalytically relevant metals (e.g. [$Rh_2$(XAT)], potentially prepared by transmetalation of "[$K_2$(XAT)]" with [{(COD)Rh(μ-Cl)}$_2$] (COD = 1,5-cyclooctadiene)) and explore their respective reactivity profiles.

Inspired by the work of Jones and co-workers who have pioneered low-valent magnesium(I) dimers of the form [LMgMgL] (L = nacnac, guanidinate, reduced α-diimine)[363] for use as soluble utility reducing agents, we envisioned XAT as a suitable ancillary for the support of similar low-valent Group 2 dimers. Given the NON-donor set and tendency of XAT to form polymetallic species, a single XAT ligand will be employed to support an alkali-earth metal dimer of the form [$Ae_2$(XAT)] (Ae = alkali-earth metal). We have initially targeted magnesium systems (Scheme 6.5) in order to establish the suitability of XAT for such an application, but intend to expand the scope to include heavier alkali earth metals if possible, and explore their capacity to behave as potent reducing agents.

**Scheme 6.5** – Proposed synthesis of $[(MgI)_2(XAT)]$ and subsequent reduction.

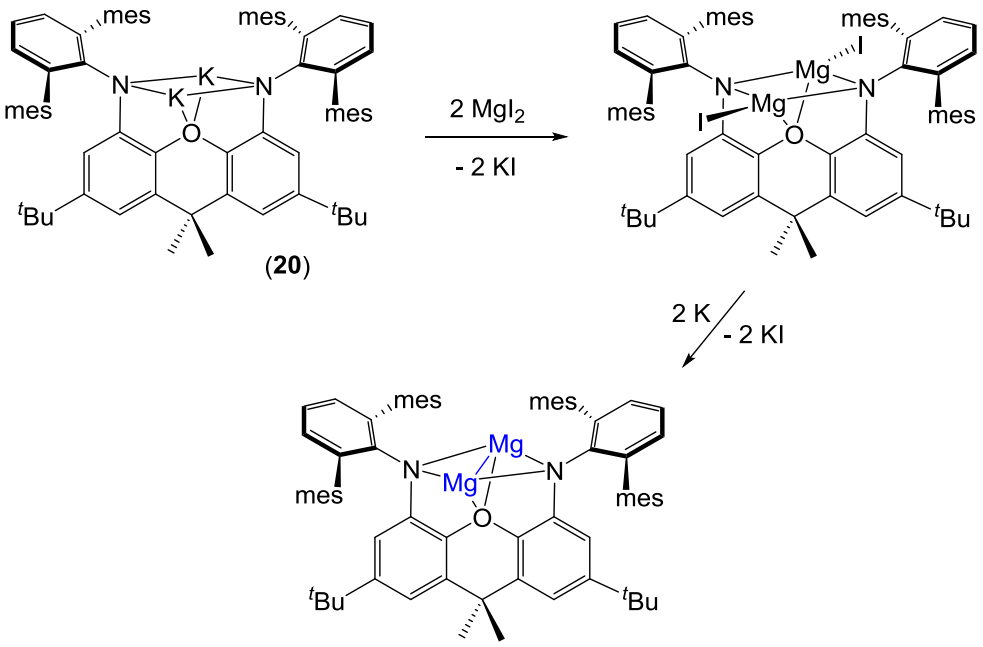


### 6.2.4 – Continued Exploration of XAd Thorium(IV) Chemistry and Hydroamination Catalysis.

Initial inroads into the chemistry of thorium species supported by the 3rd generation NON-donor pincer ligand 4,5-bis(1-adamantylamido)-2,7-di-*tert*-butyl-9,9-dimethylxanthene (XAd) has led to the development of the thermally robust hydrocarbyl derivatives $[(XAd)Th(CH_2SiMe_3)_2(THF)]$ and $[(XAd)Th(\eta^3\text{-allyl}^{TMS})_2]$, and investigations pertaining to their catalytic capabilities have begun in earnest. With regard to the latter bis(allyl) complex, the formation of a cationic mono(allyl) derivative for application in ethylene polymerization remains a principle focus. To that end, preliminary work in this area has involved the attempted *in-situ* generation of a cationic species of the form $[(XAd)Th(\eta^x\text{-allyl}^{TMS})]^+$ *via* abstraction of a single allyl ligand from

[(XAd)Th($\eta^3$-allyl$^{TMS}$)$_2$] using [Ph$_3$C][B(C$_6$F$_5$)$_4$] as an activator. However, after stirring a 1:1 mixture of the neutral bis(allyl) precursor with the alkide abstracting reagent for 1 h and subsequently exposing the solution to dynamic ethylene for an additional hour, addition of acidified methanol did not result in the precipitation of polyethylene. In our ongoing investigation in this area, we intend to monitor the reaction between the neutral bis(allyl) precursor [(XAd)Th($\eta^3$-allyl$^{TMS}$)$_2$] and the alkide abstracting agent [Ph$_3$C][B(C$_6$F$_5$)$_4$] utilizing $^1$H NMR spectroscopy in order to determine whether this reaction proceeds, as it is quite possible that trityl-mediated allyl abstraction is not as facile as the corresponding abstraction of an alkyl group, and may require heating or extended reaction times. If the trityl cation proves untenable for the abstraction of an allyl ligand, protonation of [(XAd)Th($\eta^3$-allyl$^{TMS}$)$_2$] with 1 equiv of [NPh$_2$MeH][B(C$_6$F$_5$)$_4$] will be explored, as Okuda and co-workers have successfully demonstrated the viability of this protocol for the preparation of monocationic bis(allyl) lanthanide complexes of the form [Ln($\eta^3$-C$_3$H$_5$)$_2$(THF)$_3$][B(C$_6$F$_5$)$_4$] (Ln = Y, Ln, Nd) using neutral tris(allyl) precursors.[364] Once cationic mono(allyl) XAd thorium species have been prepared and authenticated, their ability to catalyze ethylene polymerization will be evaluated.

In addition to investigating the ability of our neutral and cationic organoactinide complexes to catalyze the insertion-polymerization of ethylene, we have also become interested in utilizing such species as catalysts for intramolecular hydroamination, which essentially involves the addition of an N−H bond across an unsaturated C−C linkage (such as an alkene or alkyne) contained within the same molecule. Hydroamination is a well-documented process, carried out extensively by transition metals[365] and

lanthanides,[366] and actinide-catalyzed systems are becoming increasingly common.[367] Preliminary studies indicate that $XA_2$ and XAd organoactinide systems are capable of catalyzing the intramolecular hydroamination of 2,2-diphenylpent-4-en-1-amine as indicated by the complete conversion of the aminoalkene to the cyclized product 2-methyl-4,4-diphenylpyrrolidine by $^1$H NMR spectroscopy (Scheme 6.6 and Table 6.1).

**Scheme 6.6** – Actinide-catalyzed intramolecular hydroamination of 2,2-diphenylpent-4-en-1-amine.

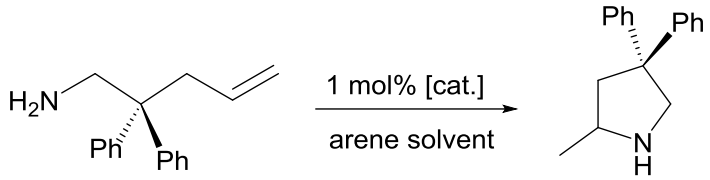


**Table 6.1** – Preliminary results for the intramolecular hydroamination of 2,2-diphenylpent-4-en-1-amine.

| **[cat.]** | **Solvent**[a] | **Temp** (°C) | **Time** (h) |
|---|---|---|---|
| $[(XAd)Th(CH_2SiMe_3)_2(THF)]$ | $C_6D_6$ | 70 °C | 17 |
| $[(XA_2)U(CH_2SiMe_3)_2]$ | $C_6D_5Br$ | 60 °C | 3[b] |
| $[(XA_2)U(CH_2SiMe_3)(\eta^3\text{-}C_6H_5Me)][B(C_6F_5)_4]$ | $C_6D_5Br$ | 60 °C | 3[c] |

[a] [substrate] = 0.167 M. [b] $[(XA_2)U(CH_2SiMe_3)_2]$ can also catalyze the intramolecular hydroamination of the substrate at room temperature (requires 48 h). [c] the toluene-coordinated cation $[(XA_2)U(CH_2SiMe_3)(\eta^3\text{-}C_6H_5Me)][B(C_6F_5)_4]$ does not catalyze the hydroamination of the substrate at room temperature (monitored over a 24 h period).

Although these preliminary results demonstrate the viability of xanthene-based actinide catalysts for the hydroamination of aminoalkenes, the catalysts investigated are less active than the related species $[(^{t\text{Bu}}NON)Th(CH_2SiMe_3)_2]$ ($^{t\text{Bu}}$NON =

{($^{t}$BuNSiMe$_2$)$_2$O}) and [($^{DIPP}$NCOCN)U(CH$_2$SiMe$_3$)$_2$] ($^{DIPP}$NCOCN = $\kappa^3$-{(ArNCH$_2$CH$_2$)$_2$O}$^{2-}$; Ar = 2,6-$^{i}$Pr$_2$C$_6$H$_3$) reported by Leznoff and co-workers,[175] who noted complete (or near-complete) conversions of 2,2-diphenylpent-4-en-1-amine to the cyclized product at room temperature in 1−2 hours.[§] Future work in this area will involve broadening the scope through trial of additional XA$_2$ and XAd organoactinide species, as well as investigating additional aminoalkene substrates, and by investigating the potential for such complexes to catalyze *intermolecular* hydroamination of alkynes with amines.

[§] Leznoff *et al.* conducted trials using 10 mol% catalyst loadings, so explicit comparisons are difficult to make (cf. 1 mol% catalyst loadings were used herein).

# Chapter 7

# Experimental Details

## 7.1 – General Details

### 7.1.1 – Laboratory Equipment and Apparatus

An argon-filled MBraun UNIlab glove box equipped with a –30 °C freezer was employed for the manipulation and storage of air-sensitive ligands and complexes. Preparative reactions were performed on a double manifold high vacuum line equipped with an Edwards RV12 vacuum pump (ultimate pressure 1.5 x $10^{-3}$ torr) using standard techniques,[368] and vacuum was measured periodically using a Varian Model 531 Thermocouple Gauge Tube with a Model 801 Controller. Residual oxygen and moisture was removed from the argon, nitrogen, ethylene, or deuterium ($D_2$) stream by passage through an Oxisorb-W scrubber from Matheson Gas Products. Commonly utilized specialty glassware includes the swivel frit assembly, thick-walled Straus flasks equipped with Teflon stopcocks, J-Young or Wilmad-LabGlass LPV NMR tubes, Wilmad-LabGlass LPV EPR tubes, and Starna 1-Q-10/GS UV-Vis-NIR cells with spectrosil far-UV quartz windows (transparent from 170 nm to 2700 nm), quartz to pyrex graded seals and Teflon stopcocks. Where indicated, a Branson 2510 Ultrasonic bath was used to sonicate/triturate reaction mixtures. A VWR Clinical 200 Large Capacity Centrifuge (with 28° fixed-angle rotors that hold 12 × 15 mL or 6 × 50 mL tubes in combination with VWR high-performance polypropylene conical centrifuge tubes) located within a glove

box was used where indicated. Sonication was employed in several NMR tube reactions in lieu of stirring. If sonication was continued for extended periods of time, the water in the sonicator was changed periodically (approximately every 30 min) to prevent excessive heating of the reaction.

### 7.1.2 – Solvents

Anhydrous $CH_2Cl_2$, 1,2-dimethoxyethane (dme) and diethylether ($OEt_2$), along with 1,3-dichlorobenzene (98%), 3-methylpentane (≥99%), cyclopentane (99%), $O(SiMe_3)_2$ (≥98%), 1,3,5-trimethylbenzene (mesitylene) (98%), α,α,α-trifluorotoluene (≥99%), fluorobenzene (99%), hexafluorobenzene (99%), 1,2-difluorobenzene (98%), 1,3-difluorobenzene (≥99%), and bromobenzene (99%) were purchased from Sigma-Aldrich and dried as described below. Hexanes, *n*-pentane, *n*-heptane, acetic acid, benzene and toluene were purchased from Caledon (dried as described below), ethanol was purchased from Commercial Alcohols (Comalc), and deuterated solvents ($C_6D_6$, toluene-$d_8$, THF-$d_8$, $C_6D_5Br$, $CDCl_3$, $CD_2Cl_2$, $Et_2O$-$d_{10}$) were purchased from ACP Chemicals.

Hexanes, *n*-pentane, *n*-heptane, benzene, THF, $OEt_2$, and dme were initially dried and distilled at atmospheric pressure from sodium/benzophenone, while 3-methylpentane, cyclopentane and mesitylene were dried and distilled under reduced pressure (< 10 mTorr) from sodium/benzophenone. Toluene and $O(SiMe_3)_2$ were dried and distilled at atmospheric pressure from sodium. $CH_2Cl_2$ was dried and distilled at atmospheric pressure- while α,α,α-trifluorotoluene, fluorobenzene, hexafluorobenzene, 1,2-

difluorobenzene, and 1,3-difluorobenzene were dried and distilled under reduced pressure (< 10 mTorr) from 4 Å molecular sieves. Bromobenzene was dried and distilled under reduced pressure (< 10 mTorr) at elevated temperature (60 °C) from 4 Å molecular sieves. 1,3-dichlorobenzene was dried and distilled under reduced pressure (< 10 mTorr) at elevated temperature (30 °C) from $P_2O_5$. Deuterated solvents were dried over sodium/benzophenone ($C_6D_6$, toluene-$d_8$, THF-$d_8$, $Et_2O$-$d_{10}$), $CaH_2$ ($CH_2Cl_2$), or 4 Å molecular sieves ($C_6D_5Br$), and degassed *via* three freeze–pump–thaw cycles prior to use.

Unless otherwise stated, all solvents were stored over an appropriate drying agent (dme, $OEt_2$, THF, THF-$d_8$ toluene, toluene-$d_8$, mesitylene, benzene, $C_6D_6$, 3-methylpentane, cyclopentane = $Na/Ph_2CO$; hexanes, *n*-pentane, *n*-heptane, $O(SiMe_3)_2$ = $Na/Ph_2CO$/tetraglyme; $CH_2Cl_2$ = $CaH_2$; α,α,α-trifluorotoluene, fluorobenzene, hexafluorobenzene, 1,2-difluorobenzene, 1,3-difluorobenzene, bromobenzene, $C_6D_5Br$ = 4 Å molecular sieves) and introduced to reactions or solvent storage flasks *via* vacuum transfer with condensation at –78 °C.

### 7.1.3 – Reagents and Starting Materials

$[Th(NO_3)_4(H_2O)_4]$, $UO_3$, neopentyl chloride, $AlMe_3$ (98% in Sure-Pak cylinder), trityl tetrakis(pentafluorophenyl)borate (97 %; used as received) were purchased from Strem Chemicals. Xanthone, $^t$BuCl, anhydrous $FeCl_3$, $Br_2$, 1-adamantylamine, DMAP, 9-azajulolidine, quinuclidine, bipy, $PMe_3$, $Me_3SiCl$, naphthalene, [$^n$Bu$_4$N]Br, TlOEt, NaO$^t$Bu, DPEPhos, $[FeCp_2]$, $Pd(OAc)_2$, KO$^t$Bu, $I_2$, tosyl chloride, Rh on alumina (5%), Li granules (containing 0.5 % Na), Na, K, NaH, KH (30 wt.% in mineral oil), $NaN_3$,

$LiAlH_4$, MesBr, 3-(trimethylsilyl)propene (H[allyl$^{TMS}$]), tetraglyme, Mg turnings, $LiCH_2SiMe_3$ (1.0M in *n*-pentane), $^{t}$BuLi (1.70 M in *n*-pentane), $^{s}$BuLi (1.40 M in cyclohexane), $^{n}$BuLi (1.60 M in hexane), MeLi (1.60 M in $OEt_2$), [2.2.2]-cryptand, 18-crown-6, and deuterium (99.9 atom%) were purchased from Sigma-Aldrich. $K[B(C_6F_5)_4]$ was purchased from Boulder Scientific, $C_6F_5Br$ was purchased from Oakwood chemicals, 2,6-diisopropylaniline was purchased from Lancaster, and hexachloropropene was purchased from Karl Industries. Argon, $N_2$, and ethylene of 99.999 % purity were purchased from Praxair.

Prior to use, solid $LiCH_2SiMe_3$, $^{t}$BuLi and MeLi were obtained by removal of solvent *in vacuo* (MeLi was additionally washed with *n*-pentane and dried *in vacuo* prior to use). Tetraglyme was distilled from sodium/benzophenone, mesityl bromide and 2,6-diisopropylphenyl were dried and distilled from $CaH_2$, tosyl azide was dried over 4 Å molecular sieves, and solid KH was obtained by filtration and washing with hexanes. In addition, $^{n}$BuLi solutions were titrated using *N*-benzylbenzamide in THF at –45 °C.[369] DMAP, 9-azajuloliene, quinuclidine, and bipy were sublimed under reduced pressure (<10 mTorr) prior to use. 1-adamantylamine was dried *in vacuo* prior to use, but the amine slowly sublimes under reduced pressure (<10 mTorr). Before use, all traces of moisture and ethanol were eliminated from $H_2[XA_2]$ by stirring with NaH (4 equiv) in toluene for 16 hours at room temperature, followed by filtration and evaporation to dryness *in vacuo*. [2.2.2]-cryptand and 18-crown-6 were dried by dissolving each solid in diethylether, and stirring the ethereal solutions over 4 Å molecular sieves for > 1 week, at which point the solids (disintegrated sieves) were removed *via* centrifugation, and $Et_2O$

was removed *in vacuo* to afford the dry reagent. Unless otherwise stated, dried/purified reagents were subsequently stored under argon.

Tosyl azide,[370] 2,6-dimesitylphenylamine,[319] 4,5-dibromo-2,7-di-*tert*-butyl-9,9-dimethylthioxanthene,[371] $H_2[XA_2]$,[40] $UCl_4$,[20] $[(XA_2)ThCl_2(dme)]$,[40] $[(XA_2)Th(CH_2SiMe_3)_2]$ (**3-Th**),[40] $LiCH_2{}^tBu$,[372] $KCH_2Ph$,[373] DMAP-$d_2$,[313] $Tl[B(C_6F_5)_4]$,[374] and $H_2NCH_2C(Ph)_2CH_2CHCH_2$,[375] were prepared using literature procedures. $[^nBu_4N][B(C_6F_5)_4]$ was prepared *via* a slight modification of the original literature procedure[376] (using $K[B(C_6F_5)_4]$ in place of $[Li(OEt_2)_x][B(C_6F_5)_4]$) and dried thoroughly before use. $[ThCl_4(dme)_2]$ was prepared using two different methods: a modified version of the procedure reported by Gambarotta and co-workers,[15] and a modified version of the procedure reported by Kiplinger and co-workers.[16] (stirring $[ThCl_4(H_2O)_4]$ with excess $Me_3SiCl$ in dme for 12 h at 50 °C). Solutions of potassium naphthalenide were prepared immediately before use by stirring potassium (1.00*x* mmol) in dme (~10 mL per 0.15 mmol of K) with naphthalene (1.05*x* mmol) at room temperature until no solid remained (~30 min). $K[1\text{-}(SiMe_3)C_3H_4]$ ($K[allyl^{TMS}]$) was prepared in the Emslie group *via* a slight modification of the original literature procedure[354] (lithiation of 3-(trimethylsilyl)propene ($H[allyl^{TMS}]$) was accomplished using $^s$BuLi, and the desired potassium salt was obtained by subsequent transmetalation with $KO^tBu$ in THF at –78 °C).

### 7.1.4 – NMR Spectroscopy

Nuclear magnetic resonance spectroscopy ($^1H$, $^2H$, $^{13}C\{^1H\}$, $^{13}C$, $^{19}F$, $^{29}Si$, $^{13}C$_uDEFT, $^{13}C$_DEPT-135, DEPTq, $^1H$,$^1H$_COSY, $^1H$,$^{13}C$_HSQC, $^1H$,$^{13}C$_HMBC)

experiments were performed on Bruker AV-200, DRX-500 and AV-600 spectrometers. Spectra were obtained at 298 K unless otherwise specified. $^{1}$H NMR and $^{13}$C NMR spectra are referenced relative to $SiMe_4$ through a resonance of the employed deuterated solvent or proteo impurity of the solvent; $C_6D_6$ (δ 7.16 ppm), toluene-$d_8$ (δ 7.09, 7.01, 6.97, 2.08 ppm), $CD_2Cl_2$ (δ 5.32 ppm), diethylether-$d_{10}$ (δ 3.34, 1.07 ppm) $C_6D_5Br$ (δ 7.30, 7.02, 6.94 ppm), and THF-$d_8$ (δ 3.58, 1.72 ppm) for $^{1}$H NMR, and $C_6D_6$ (δ 128.06 ppm), $CD_2Cl_2$ (53.84 ppm), $C_6D_5Br$ (δ 130.9, 129.3, 126.1, 122.3 ppm), toluene-$d_8$ (δ 137.48, 128.87, 127.96, 125.13, 20.43) and THF-$d_8$ (67.21, 25.31 ppm) for $^{13}$C{$^{1}$H} NMR. $^{19}$F and $^{29}$Si NMR spectra were referenced using an external standard of $CFCl_3$ (0.0 ppm) and $SiMe_4$ (0.0 ppm), respectively. Temperature calibration was performed using a methanol-$d_4$ sample, as outlined in the Bruker VTU user manual.[377] Low temperature NMR spectra in neat non-deuterated cyclopentane, 3-methylpentane and $O(SiMe_3)_2$ were obtained using a quartz 3 mm J-young tube (containing the air-sensitive solution) supported by a ring of Teflon tape inside of a 5 mm NMR tube containing diethylether-$d_{10}$ (~ 0.1 mL).

Herein, for $XA_2$, *Aryl* = 2,6-diisopropylphenyl and for XAT, *Aryl* = 2,6-dimesitylphenyl. The numbering scheme ($CH^{1,8}$, $C^{2,7}$, $CH^{3,6}$, $C^{4,5}$, $C^{10/13}$ and $C^{11,12}$) for the xanthene ligand backbone is shown in Figure 7.1. Some peaks in the $^{1}$H NMR spectra of paramagnetic uranium(IV) complexes could be assigned based on integration. Occasionally, the *para*-aryl, $CH^{1,8}$, $CH^{3,6}$ and *tert*-butyl signals could be readily identified as they are often unaffected by the presence/absence of top-bottom symmetry on the NMR timescale. Furthermore, the *para*-Ar signal often appeared as a triplet at room

temperature, allowing definite assignment. The significantly broadened signals (typically integrating to approximately 2H) that are shifted to particularly low- or high- frequencies in the $^{1}$H NMR spectra of paramagnetic uranium complexes were speculatively assigned as the UC$H_2$ α-protons given their close proximity to the paramagnetic uranium(IV) centre.

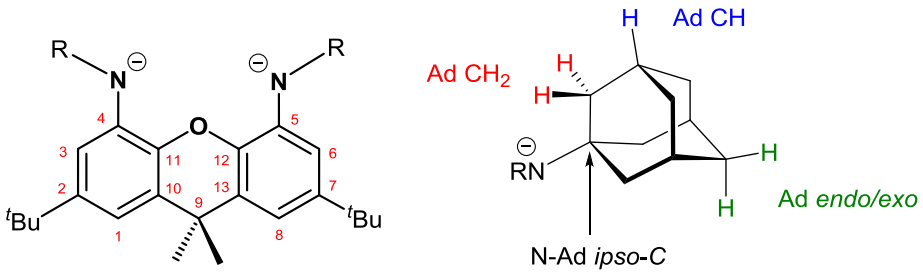


**Figure 7.1** – Numbering scheme for the xanthene backbone of dianionic pincer-type ligands $XA_2$, XAT, and XAd, and naming protocol for the 1-adamantyl substituents of XAd.

### 7.1.5 – X-ray Diffraction and Other Instrumentation and Analysis

X-ray crystallographic analyses were performed on suitable crystals coated in Paratone oil and mounted on a SMART APEX II diffractometer with a 3 kW Sealed tube Mo generator in the McMaster Analytical X-Ray (MAX) Diffraction Facility. Crystal mounting, X-ray data collection (typically at 100 K), and structure solution and refinement were carried out by Dr. Hilary Jenkins and Dr. Jim Britten of the McMaster Analytical X-Ray (MAX) Diffraction Facility.

Combustion elemental analyses were performed on a Thermo EA1112 CHNS/O analyzer by Ms. Meghan Fair or Dr. Steve Kornic of this department, and on a Carlo Erba

EA 1110CHN elemental analyzer at Simon Fraser University by Mr. Farzad Haftbaradaran (with sample preparation conducted by Dr. Wen Zhou of the Leznoff research group at Simon Fraser University).

Electrochemical studies were carried out using a PAR (Princeton Applied Research) model 283 potentiostat (using PAR PowerCV software) in conjunction with a three-electrode cell under an argon atmosphere in an MBraun glove box. The auxiliary electrode was a platinum wire and the pseudo-reference electrode was a silver wire. The working electrode was a glassy carbon disk (3.0 mm diameter, Bioanalytical Systems) for compound **1**. Solutions were $1 \times 10^{-3}$ mol·L$^{-1}$ in the test compound and 0.1 mol·L$^{-1}$ in [$^{n}$Bu$_4$N][B(C$_6$F$_5$)$_4$] as the supporting electrolyte. All CVs were referenced using [FeCp$^{*}_2$] as an internal calibrant, all potentials are quoted versus [FeCp$_2$]$^{0/+1}$, and peak potentials for irreversible redox reactions are quoted at a scan rate of 200 mV·s$^{-1}$. Under the conditions used, $E_{1/2}$ for [FeCp$^{*}_2$]$^{0/+1}$ is −0.48 V versus [FeCp$_2$]$^{0/+1}$.[378]

Gel permeation chromatograms (GPC) were recorded on an Agilent PL220 high temperature instrument equipped with differential refractive index (DRI) and viscometry (VS) detectors at the University of Warwick, Coventry, UK by Dr. Daniel W. Lester and Dr. Ian Hancox. The system was equipped with 2 × PLgel Mixed D columns (300 × 7.5 mm) and a PLgel 5 µm guard column. Samples were dissolved in trichlorobenzene and left to solubilize for 12 h on an Agilent PL SP260VS at 140 °C, and all data was calibrated against polystyrene. The mobile phase was trichlorobenzene stabilized with 250 ppm BHT and run at a flow rate of 1 mL·min$^{-1}$ at 160 °C.

## 7.2 – Synthetic Procedures and Characterization Pertaining to Chapter 2

### [(XA$_2$)UCl$_2$(μ-Cl){K(dme)$_3$}] (1)

KH (0.118 g, 2.94 mmol) and H$_2$[XA$_2$] (0.900 g, 1.34 mmol) in dme (60 mL) were stirred at room temperature overnight. To this mixture, solid UCl$_4$ (0.508 g, 1.34 mmol) was added, resulting in a colour change from green, initially, to orange-brown. After stirring for an additional 12 h, the solution was evaporated to dryness *in vacuo* and the solid residue was redissolved in dme (20 mL). The suspension was centrifuged to remove insoluble KCl and layered with hexanes at –30 °C. After several days, an orange solid was collected and dried *in vacuo* to provide 1.276 g of **1** (0.96 mmol, 72% yield). X-ray quality red-orange crystals of **1**·dme were grown from dme/hexane at −30 °C. **$^1$H NMR (THF-$d_8$, 600.1 MHz, 298 K):** $\delta$ 16.08 (broad s, 4H, C*H*Me$_2$), 9.68, –2.16 (s, 2 × 12H, CH*Me*$_2$), 3.42 (s, 18H, OC*H*$_3$, *free dme*), 3.26 (s, 12H OC*H*$_2$, *free dme*), 1.50 (s, 2H, Aryl-*para* CH), –0.14 (s, 4H, Aryl-*meta* CH), –4.27 (s, 18H, CMe$_3$), –5.68, –19.99 (s, 2 × 2H, CH$^{1,8}$ and CH$^{3,6}$), –6.08 (s, 6H, CMe$_2$). **Anal. Calcd. for C$_{59}$H$_{92}$N$_2$O$_7$Cl$_3$KU:** C, 53.49; H, 7.00; N, 2.11 %. Found: C, 53.71; H, 6.83; N, 2.49 %.

### [(XA$_2$)UCl(dme)]·toluene (2·toluene)

A solution of [(XA$_2$)UCl$_2$(μ-Cl){K(dme)$_3$}] (**1**) (0.200 g, 0.151 mmol) in dme (10 mL) was added at –30 °C to a dme solution of potassium naphthalenide (0.154 mmol). The solution turned from green to dark brown within 15 min, and stirring was continued for another 12 h, during which time the color changed to dark green. After evaporation to

dryness *in vacuo*, the solid residue was redissolved in toluene and the mixture was centrifuged to remove a small amount of insoluble material before layering with hexanes and cooling to –30 °C. After two days, dark green X-ray-quality crystals of **2**·4.5(toluene) were obtained, and drying *in vacuo* provided **2**·toluene as a green-black powder (0.094 g, 0.091 mmol, 60% yield). **$^1$H NMR (THF-$d_8$, 600.1 MHz, 298 K):** $\delta$ 9.96, 9.60 (s, 2 x 2H, $CH^{1,8}$ and $CH^{3,6}$), 8.49 (app t, 2H, $^3J_{H,H}$ = 7 Hz, Aryl-*para* CH), 8.18, 6.15 (d, 2 × 2H, $^3J_{H,H}$ = 7 Hz, Aryl-*meta* CH), 5.04, 2.06 (s, 2 × 3H, C$Me_2$), 3.33 (s, 4H, OC$H_2$), 3.04 (s, 6H, OC$H_3$), 2.89 (s, 18H, $CMe_3$), 1.68, –2.17 (broad s, 2 × 2H, C$H$$Me_2$), 0.26, –0.92, –2.04, –8.69 (s, 4 × 6H, CH$Me_2$). **Anal. Calcd. for $C_{58}H_{80}N_2O_3ClU$:** C, 61.83; H, 7.16; N, 2.49 %. Found: C, 61.65; H, 7.22; N, 2.61 %.

**[($XA_2$)U($CH_2SiMe_3$)$_2$]·(*n*-pentane) (3·*n*-pentane)**

A mixture of [($XA_2$)$UCl_2$(μ-Cl){K(dme)$_3$}] (**1**) (1.05 g, 0.80 mmol) and $LiCH_2SiMe_3$ (0.158 g, 1.67 mmol) in hexanes (65 mL) was stirred at –78 °C and then warmed slowly to room temperature; stirring was continued for a total of 12 h. The red solution was evaporated to dryness *in vacuo*, and the solid residue was extracted with hexanes (10 mL). The suspension was centrifuged to remove insoluble KCl and LiCl, and the red mother liquors were again evaporated to dryness, yielding a bright red solid. The solid was dissolved in a minimum amount of *n*-pentane (7 mL) and cooled to –30 °C. After a few days, bright red crystals were collected in two batches and dried *in vacuo* to provide 0.721 g of **3**·(*n*-pentane) (0.62 mmol, 78% yield). Alternatively, crystallization from minimal hexanes at –30 °C afforded X-ray quality crystals of **3**·2(*n*-hexane); drying *in*

*vacuo* provided **3** in comparable yield (64%). **$^1$H NMR (benzene-$d_6$, 200 MHz, 298 K):** $\delta$ 12.30, 7.32 (broad s, 2 × 2H, CH$^{1,8}$ and CH$^{3,6}$), 7.25 (t, $^3J_{H,H}$ = 8 Hz, 2H, Aryl-*para* CH), 2.82 (s, 18H, CMe$_3$). **$^1$H NMR (toluene-$d_8$, 500.1 MHz, 298 K):** $\delta$ 11.41, 8.27 (broad s, 2 × 2H, CH$^{1,8}$ and CH$^{3,6}$), 7.56 (t, $^3J_{H,H}$ = 9.3 Hz, 2H, Aryl-*para* CH), 2.87 (s, 18H, CMe$_3$). UC$H_2$ protons were not observed at room temperature. **$^1$H NMR (toluene-$d_8$, 500.1 MHz, 213 K):** $\delta$ 178.2, –222.3 (extremely broad s, 2 × 2H, UC$H_2$), 25.00, 13.51 (broad s, 2 × 3H, C$Me_2$), 17.93, 4.71 (broad s, 2 × 2H, CH$^{1,8}$ and CH$^{3,6}$), 17.69, –2.08 (broad s, 2 × 9H, Si$Me_3$), 6.45 (broad s, 2H, Aryl-*para* CH), 5.54, 1.33 (broad s, 2 × 2H, Aryl-*meta* CH), 3.40 (s, 18H, CMe$_3$), –3.14, –14.47, –16.61, –26.85 (broad s, 4 × 6H, CH$Me_2$), –29.86, –96.02 (v broad s, 2 × 2H, C$H$Me$_2$). **Anal. Calcd for $C_{55}H_{84}N_2OSi_2U$:** C, 60.97; H, 7.81; N, 2.59%. Found: C, 61.05; H, 8.06; N, 2.38%.

**[(XA$_2$)U(CH$_2$$^t$Bu)$_2$]·(*n*-pentane) (4·*n*-pentane)**

*Method 1*. A mixture of [(XA$_2$)UCl$_2$(μ-Cl){K(dme)$_3$}] (**1**) (0.250 g, 0.19 mmol) and LiCH$_2$$^t$Bu (0.031 g, 0.39 mmol) in hexanes (25 mL) was stirred at –78 °C and then warmed slowly to room temperature; stirring was continued for a total of 12 h. The deep red solution was evaporated to dryness *in vacuo*, and the solid residue was extracted with a minimum amount of *n*-pentane. The suspension was centrifuged to remove insoluble KCl and LiCl, and the deep red mother liquors were cooled to –30 °C. After a few days, deep red crystals were collected in two batches and dried *in vacuo* to provide 0.146 g of **4**·(*n*-pentane) (0.13 mmol, 69% yield). Alternatively, crystallization from a minimum

amount of hexanes at –30 °C provided X-ray quality crystals of **4**·(*n*-hexane) in comparable yield.

*Method 2.* Complex **4** was generated *in situ* by reaction of **3**·(*n*-pentane) (0.015 g, 0.013 mmol) with 2.1 equiv of $LiCH_2{}^tBu$ (0.0021 g, 0.027 mmol) in benzene-$d_6$. After approximately 1 h of sonication, $^1$H NMR indicated complete conversion of **3** to **4** (the reaction was usually complete after 20 min) with concomitant release of $LiCH_2SiMe_3$. *Method 2* was not pursued as a means to isolate pure **4**, since both **4** and $LiCH_2SiMe_3$ are highly soluble in hydrocarbon solvents. **$^1$H NMR (benzene-$d_6$, 500.1 MHz, 298 K):** $\delta$ 141.1, –142.1 (extremely broad s, 2 × 2H, UC$H_2$), 20.02, –2.43 (v broad s, 2 × 9H, $CH_2CMe_3$), 17.51, 10.17 (v broad s, 2 × 3H, C$Me_2$), 14.71, 4.05 (s, 2 × 2H, $CH^{1,8}$ and $CH^{3,6}$), 5.57 (t, $^3J_{H,H}$ = 8 Hz, 2H, Aryl-*para* CH), 4.42, 2.02 (v broad s, 2 × 2H, Aryl-*meta* CH), 2.61 (s, 18H, $CMe_3$), –3.89, –16.84, (v broad s, 2 × 6H, CH$Me_2$), –9.21 (v broad s, 12H, CH$Me_2$ {×2}), –27.15, –49.21 (v broad s, 2 × 2H, C$H$Me$_2$). **$^1$H NMR (toluene-$d_8$, 500.1 MHz, 298 K):** $\delta$ 134.5, –138.8 (extremely broad s, 2 × 2H, UC$H_2$), 18.78, –2.77 (v broad s, 2 × 9H, $CH_2CMe_3$), 16.66, 9.80, (v broad s, 2 × 3H, C$Me_2$), 14.26, 4.63 (s, 2 × 2H, $CH^{1,8}$ and $CH^{3,6}$), 5.71 (t, $^3J_{H,H}$ = 8.6 Hz, 2H, Aryl-*para* CH), 4.88, 2.29 (v broad s, 2 × 2H, Aryl-*meta* CH), 2.66 (s, 18H, $CMe_3$), –3.43, –8.48, –8.92, –16.73 (v broad s, 4 × 6H, CH$Me_2$), –24.98, –48.17 (v broad s, 2 × 2H, C$H$Me$_2$). **$^1$H NMR (toluene-$d_8$, 500.1 MHz, 223 K):** $\delta$ 223.3, –221.5 (extremely broad s, 2 × 2H, UC$H_2$), 33.64, –2.39 (broad s, 2 × 9H, $CH_2CMe_3$), 28.61, 15.47 (broad s, 2 × 3H, C$Me_2$), 20.13, 0.81 (broad s, 2 × 2H, $CH^{1,8}$ and $CH^{3,6}$), 4.45 (broad t, 2H, Aryl-*para* CH), 3.02 (s, 18H, $CMe_3$), 1.81, –1.12 (broad s, 2 × 2H, Aryl-*meta* CH), –7.35, –16.10, –16.48, –25.70 (broad s, 4 × 6H,

CH*Me*$_2$), –46.92, –84.92 (v. broad s, 2 × 2H, C*H*Me$_2$). **Anal. Calcd for $C_{62}H_{96}N_2OU$:** C, 66.28; H, 8.61; N, 2.49%. Found: C, 66.76; H, 8.01; N, 2.39%.

**[(XA$_2$)U(CH$_2$Ph)$_2$] (5)**

A mixture of [(XA$_2$)UCl$_2$(μ-Cl){K(dme)$_3$}] (**1**) (0.200 g, 0.15 mmol) and 2 equiv of KCH$_2$Ph (0.039 g, 0.30 mmol) in diethylether (30 mL) was stirred initially at –94 °C, then at –78 °C, before warming slowly to room temperature; stirring was continued for a total of 12 h. The deep-brown solution was evaporated to dryness *in vacuo*, and the solid residue was extracted with a minimum amount of hexanes (~11 mL). The suspension was centrifuged to remove insoluble KCl, and the deep-brown mother liquors were evaporated to dryness *in vacuo*, yielding iridescent blackish solid residue. The solids were dissolved in minimal *n*-pentane (~8 mL) and cooled to –30 °C. After several days, black crystalline **5** was collected in two batches and dried *in vacuo* to provide 0.123 g of **5** (0.112 mmol, 74% yield). X-ray quality crystals of **5**·THF were obtained from THF/hexane at –30 °C. **$^1$H NMR (toluene-*d*$_8$, 500.1 MHz, 298 K):** $\delta$ 100.92, 61.75 (v. broad s, 2 × 2H, UC*H*$_2$), 51.04, 18.59, 12.90, −4.30, −8.34, −13.85 (v. broad s, 6 × 2H, Aryl-*meta* CH {× 2}, benzyl-*ortho* CH {× 2}, benzyl-*meta* CH {× 2}), 41.07, −62.32 (v. broad s, 2 × 2H, C*H*Me$_2$), 34.47, 1.25, −5.95, −7.19 (v. broad s, 4 × 6H, CH*Me*$_2$), 9.36, −12.38 (v. broad s, 2 × 1H, benzyl-*para* CH), 4.59 (t, $^3J_{H,H}$ = 6 Hz, 2H, Aryl-*para* CH), 0.85, −5.17 (v. broad s, 2 × 3H, C*Me*$_2$), −2.20, −13.46 (s, 2 × 2H, CH$^{1,8}$ and CH$^{3,6}$), −3.08 (s, 18H, CMe$_3$). **$^1$H NMR (toluene-*d*$_8$, 500.1 MHz, 262 K):** $\delta$ 124.45, 82.22 (v. broad s, 2 × 2H, UC*H*$_2$), 55.18, 21.28, 13.94, −6.98, −11.61, −18.58 (broad s, 6 × 2H, Aryl-*meta* CH {× 2},

benzyl-*ortho* CH {× 2}, benzyl-*meta* CH {× 2}), 49.38, −72.24 (broad s, 2 × 2H, C*H*Me$_2$), 41.30, 0.40, −7.66, −9.17 (broad s, 4 × 6H, CH*Me*$_2$), 11.19, −15.72 (broad s, 2 × 1H, benzyl-*para* CH), 4.06 (broad s, 2H, Aryl-*para* CH), 2.89, −5.90 (broad s, 2 × 3H, C*Me*$_2$), −3.04, −17.67 (broad s, 2 × 2H, CH$^{1,8}$ and CH$^{3,6}$), −3.94 (s, 18H, CMe$_3$). **Anal. Calcd for C$_{61}$H$_{76}$N$_2$OU:** C, 67.14; H, 7.02; N, 2.57%. Found: C, 67.22; H, 7.23; N, 2.67%.

## 7.3 – Synthetic Procedures and Characterization Pertaining to Chapter 3

### [(XA$_2$)U(CH$_2$SiMe$_3$)(η$^6$-C$_6$H$_6$)][B(C$_6$F$_5$)$_4$]·2(benzene) (6·2(benzene))

Solid trityl tetrakis(pentafluorophenyl)borate [Ph$_3$C][B(C$_6$F$_5$)$_4$] (0.079g, 0.087 mmol) was quickly added to a stirring solution of [(XA$_2$)U(CH$_2$SiMe$_3$)$_2$]·(*n*-pentane) (**3**·*n*-pentane) (0.100 g, 0.087 mmol) in benzene (10 mL) at room temperature. The bright red solution immediately darkened to a deep yellow-brown colour, and stirring was continued at room temperature for ~ 1 hour. The deep brown solution was then layered with hexanes and cooled to –30 °C. After several days, X-ray quality deep brown crystals of **6**·2(benzene) were collected, washed with benzene and *n*-pentane, and dried *in vacuo* to provide 0.119 g of **6**·2(benzene) (0.062 mmol, 72% yield). **$^1$H NMR (bromobenzene-*d*$_5$ + 100 equiv of benzene-*d*$_6$, 500.1 MHz, 298 K):** $\delta$ 79.47, 9.88 (broad s, 2 × 2H), 32.75, 32.52, 22.25, 19.69, –12.55 (s, 5 × 2H), 22.17, 17.28, 7.60, –7.39 (s, 4 × 6H, CH*Me*$_2$), 4.31 (s, 18H, CMe$_3$), –11.44, –16.64 (s, 2 × 3H, C*Me*$_2$), –12.13 (s, 9H, SiMe$_3$), –39.45 (v. broad s, 2H, UC*H*$_2$). **Anal. Calcd for C$_{93}$H$_{91}$N$_2$OSiUBF$_{20}$:** C, 58.49; H, 4.80; N, 1.47%. Found: C,

58.62; H, 4.73; N, 1.22%. Conducting the alkyl abstraction in benzene-$d_6$ followed by identical work-up yielded the deuterobenzene isotopologue **6-*d*$_6$** in comparable yield. **$^2$H NMR (bromobenzene + 5 equiv of benzene-*d*$_6$, 600.1 MHz, 298 K):** $\delta$ −29.8 (v broad s, $\eta^6$-$C_6D_6$). The corresponding $\eta^6$-$C_6H_6$ resonance was observed at −29.43 ppm in the $^1$H NMR spectrum of **6** in neat bromobenzene-$d_5$.

**[(XA$_2$)U(CH$_2$SiMe$_3$)($\eta^3$-C$_6$H$_5$Me)][B(C$_6$F$_5$)$_4$]·2(toluene) (7·2(toluene))**

Solid trityl tetrakis(pentafluorophenyl)borate [Ph$_3$C][B(C$_6$F$_5$)$_4$] (0.099 g, 0.108 mmol) was quickly added to a stirring solution of [(XA$_2$)U(CH$_2$SiMe$_3$)$_2$]·(*n*-pentane) (**3**·*n*-pentane) (0.125 g, 0.108 mmol) in toluene (10 mL) at room temperature. The red solution immediately darkened to a deep yellow-brown colour, and stirring was continued at room temperature for ~ 30 min. The deep brown solution was then layered with hexanes and cooled to –30 °C. After several days, deep brown crystalline **7**·2(toluene) was collected, washed with toluene and *n*-pentane, and dried *in vacuo* to provide 0.172 g of **7**·2(toluene) (0.088 mmol, 81% yield). X-ray quality crystals of **7**·toluene were grown from toluene/hexanes at –30 °C, and were additionally utilized for elemental analysis. **$^1$H NMR (bromobenzene-*d*$_5$ + 100 equiv of toluene-*d*$_8$, 500.1 MHz, 298 K):** $\delta$ 78.97, 10.59 (broad s, 2 × 2H), 32.84, 32.75, 22.33, 19.89, –12.57 (s, 5 × 2H), 22.26, 17.62, 7.60, –7.63 (s, 4 × 6H, CH*Me*$_2$), 4.32 (s, 18H, CMe$_3$), –11.42, –17.14 (s, 2 × 3H, C*Me*$_2$), –12.11 (s, 9H, SiMe$_3$), –37.16 (v. broad s, 2H, UC*H*$_2$). **Anal. Calcd for C$_{89}$H$_{89}$N$_2$OSiUBF$_{20}$ [3·(C$_6$H$_5$Me)]:** C, 57.48; H, 4.82; N, 1.51%. Found: C, 57.00; H, 4.81; N, 1.66%. Conducting the alkyl abstraction in toluene-$d_8$ followed by identical work-up yielded the

deuterotoluene isotopologue **7-*d*$_8$** in comparable yield. **$^2$H NMR (bromobenzene + 5 equiv of toluene-*d*$_8$, 600.1 MHz, 298 K):** $\delta$ −17.36 (m, 2D, *o*/*m*-C*D*), −19.23 (broad s, 3D, C$D_3$), −22.74 (m, 2D, *o*/*m*-C*D*), −67.14 (m, 1D, *p*-C*D*). The corresponding *o*/*m*-C*H*, C$H_3$, *o*/*m*-C*H*, and *p*-C*H* resonances were observed at −17.05, −19.20, −22.63, −67.53 ppm in the $^1$H NMR spectrum of **7** in neat bromobenzene-$d_5$.

**[(XA$_2$)U(CH$_2$SiMe$_3$)(η$^x$-C$_6$D$_5$Br)][B(C$_6$F$_5$)$_4$] (8) (*in situ*)**

A sample (approx. 0.010 g) of cation **6**, **7**, or **10** was taken up in ~0.6 mL bromobenzene-$d_5$ to afford a deep brown solution. Five minutes after mixing, $^1$H NMR revealed signals predominantly corresponding to **8**. **(bromobenzene-*d*$_5$, 500.1 MHz, 298 K):** $\delta$ 79.79, 9.72 (broad s, 2 × 2H), 32.95, 32.69, 22.35, 19.77, –12.61 (s, 5 × 2H), 22.28, 17.28, 7.63, –7.61 (s, 4 × 6H, CH*Me*$_2$), 4.33 (s, 18H, CMe$_3$), –11.46, –16.67 (s, 2 × 3H, C*Me*$_2$), –12.25 (s, 9H, SiMe$_3$), –40.76 (v broad s, 2H, UC*H*$_2$).

**[(XA$_2$)U(CH$_2$SiMe$_3$)(η$^3$-C$_6$H$_5$F)][B(C$_6$F$_5$)$_4$] (10)**

Solid trityl tetrakis(pentafluorophenyl)borate [Ph$_3$C][B(C$_6$F$_5$)$_4$] (0.079g, 0.087 mmol) was quickly added to a stirring solution of [(XA$_2$)U(CH$_2$SiMe$_3$)$_2$]·(*n*-pentane) (**3**·*n*-pentane) (0.100 g, 0.087 mmol) in fluorobenzene (10 mL) at room temperature. The bright red solution immediately darkened to a deep brown colour, and stirring was continued at room temperature for 30 mins. The brown solution was evaporated to dryness, yielding a deep brown residue which was re-dissolved in a minimum amount of fluorobenzene (~ 1 mL), layered with *n*-pentane, and cooled to –30 °C. After several days, deep brown

microcrystalline **10** was collected, washed with *n*-pentane (3 × 5 mL), and dried *in vacuo* to provide 0.140 g of **10** (0.079 mmol, 91% yield). X-ray quality crystals of **10**·fluorobenzene were grown from fluorobenzene/*n*-pentane at –30 °C. **$^{1}$H NMR (bromobenzene-$d_5$, 600.1 MHz, 298K):** Cation **10** is readily converted to bromobenzene-bound cation **8** in $C_6D_5Br$, therefore, the $^{1}$H NMR spectrum is identical to that of **10**, but with one equivalent of free fluorobenzene. **$^{19}$F{$^{1}$H} NMR (bromobenzene-$d_5$, 200.1 MHz, 298K):** $\delta$ –112.83 (s, 1F, free $C_6H_5F$ ), –133.41 (s, 8F, *o*-$C_6F_5$), –163.43 (s, 4F, *p*-$C_6F_5$), –167.41 (s, 8F, *m*-$C_6F_5$). **Anal. Calcd for $C_{81}H_{78}N_2OSiUBF_{21}$:** C, 54.92; H, 4.44; N, 1.58%. Found: C, 54.96; H, 4.61; N, 1.55%.

**General Procedure for Ethylene Polymerization**

The appropriate actinide(IV) dialkyl precursor (0.005 mmol, < 10 mg) was dissolved in 4−5 mL of deoxygenated, anhydrous solvent in a 25 mL round bottomed flask in the glovebox. For reactions where cationic species were generated *in-situ* utilizing $[Ph_3C][B(C_6F_5)_4]$ as an activating agent, the trityl salt (0.005g, 0.005 mmol) was added as a solid to the stirring precursor solution, accompanied by an abrupt colour change. For reactions where An = U, the solution was allowed to stir for ~ 30 minutes; for An = Th, the solution stirred for 3 h or 24 h. Once activated, the solution was degassed, and dynamic ethylene (1 atm) was admitted; for reactions conducted at high-temperature, the mixture was heated to 70 °C prior to introducing ethylene. After 30 min under ethylene, the reaction was quenched by venting the ethylene that remained in the headspace and adding ~ 5−10 mL of acidified methanol (10 % conc. hydrochloric acid in methanol). The

precipitated polymer solids were collected on a fritted glass funnel, washed with methanol, and dried first in a 60 °C oven, and subsequently *in vacuo*.

## 7.4 – Synthetic Procedures and Characterization Pertaining to Chapter 4

### [(XA$_2$)Th(CH$_2$$^t$Bu)$_2$] (4-Th) (*in-situ)*

A mixture of [(XA$_2$)Th(CH$_2$SiMe$_3$)$_2$]·0.5{O(SiMe$_3$)$_2$} (**3-Th**·0.5{O(SiMe$_3$)$_2$}) (0.020 g, 0.017 mmol) and 15 equivalents of LiCH$_2$$^t$Bu (0.022 g, 0.26 mmol) were taken up in toluene-$d_8$ to afford a colourless solution. Immediately after, $^1$H NMR revealed new signals corresponding to **4-Th** and free LiCH$_2$SiMe$_3$, with concomitant loss of **3-Th**. **$^1$H NMR (toluene-$d_8$, 600.1 MHz, 298 K):** $\delta$ 7.25 (broad s, 6H, Aryl-*meta* & Aryl-*para*), 6.76, 6.03 (d, $^4J_{H,H}$ 2 Hz, 2 × 2H**,** CH$^{1,8}$ & CH$^{3,6}$), 3.63 (v. broad s, 4H, C*H*Me$_2$), 1.66 (s, 6H, CMe$_2$), 1.41, 1.15 (broad s, 2 × 12H, CH*Me*$_2$), 1.32 (broad s, 4H, ThC*H*$_2$), 1.18 (s, 18H, CMe$_3$), 0.90 (broad s, 18H, ThCH$_2$C*Me*$_3$). **$^1$H NMR (toluene-$d_8$, 500.1 MHz, 213 K):** $\delta$ 7.28 (m, $^3J_{H,H}$ 7 Hz, 4H, Aryl-*meta* & Aryl-*para*), 7.16 (d, $^3J_{H,H}$ 7 Hz, 2H, Aryl-*meta*), 6.79, 6.14 (s, 2 × 2H**,** CH$^{1,8}$ & CH$^{3,6}$), 4.19, 3.20 (broad sept, $^3J_{H,H}$ 6.3 Hz, 2 × 2H**,** C*H*Me$_2$), 1.74, 1.54 (broad s, 2 × 3H, CMe$_2$), 1.60, 1.36, 1.22, 1.10 (broad d, $^3J_{H,H}$ 6.2 Hz, 4 × 6H, CH*Me*$_2$), 1.29, 0.71 (broad s, 2 × 9H, ThCH$_2$C*Me*$_3$), 1.17 (broad s, 18H, CMe$_3$) 0.97, –0.30 (broad s, 2 × 2H, ThC*H*$_2$CMe$_3$). **$^{13}$C{$^1$H} NMR (toluene-$d_8$, 150 MHz, 298 K):** $\delta$ 148.14 (*C*$^{2,7}$), 147.86 (Aryl-*C*$_{ortho}$), 146.24 (*C*$^{4,5}$), 141.93 (*C*$^{11,12}$), 136.32 (Aryl-*C*$_{ipso}$), 130.02 (*C*$^{10,13}$), 128.04 (Aryl-*C*$_{para}$), 125.38 (Aryl-*C*$_{meta}$), 110.56, 109.89 (*C*H$^{1,8}$ & *C*H$^{3,6}$), 37.94 (ThCH$_2$*C*Me$_3$), 35.66 (ThCH$_2$C*Me*$_3$), 35.24 (*C*Me$_2$), 35.03 (*C*Me$_3$), 31.67

(C*Me*$_3$), 29.0 (*C*HMe$_2$), 26.25, 25.17 (CH*Me*$_2$). **$^{13}$C{$^1$H} NMR (toluene-*d*$_8$, 150 MHz, 213 K):** $\delta$ 147.96, 147.32 (2 × Aryl-*C*$_{ortho}$), 147.78 (*C*$^{2,7}$), 146.06 (*C*$^{4,5}$), 142.24 (*C*$^{11,12}$), 135.81, 120.59 (2 × Th*C*H$_2$CMe$_3$), 135.02 (Aryl-*C*$_{ipso}$), 129.91 (*C*$^{10,13}$), 128.18, 125.40 (Aryl-*C*$_{para}$ & Aryl-*C*$_{meta}$), 110.33, 109.37 (*C*H$^{1,8}$ & *C*H$^{3,6}$), 39.11, 36.37 (2 × ThCH$_2$*C*Me$_3$), 36.05, 23.96 (2 × C*Me*$_2$), 35.97, 35.35 (2 × ThCH$_2$C*Me*$_3$), 35.13 (*C*Me$_2$), 34.90 (*C*Me$_3$), 31.43 (C*Me*$_3$), 29.44, 28.08 (2 × *C*HMe$_2$), 27.03, 25.77, 25.36, 24.33 (4 × CH*Me*$_2$).

**[(XA$_2$)Th(CH$_2$SiMe$_3$)(CH$_2$$^t$Bu)] (13-Th) (*in-situ)***

A mixture of [(XA$_2$)Th(CH$_2$SiMe$_3$)$_2$]·0.5{O(SiMe$_3$)$_2$} (**3-Th**·0.5{O(SiMe$_3$)$_2$}) (0.020 g, 0.017 mmol) and 2.2 equivalents of LiCH$_2$$^t$Bu (0.003 g, 0.04 mmol) were taken up in toluene-*d*$_8$ to afford a colourless solution. Immediately after, $^1$H NMR revealed new signals corresponding to an approximate 1:1:3:1 mixture of **13-Th**, [(XA$_2$)Th(CH$_2$$^t$Bu)$_2$] (**4-Th**), free LiCH$_2$SiMe$_3$, and LiCH$_2$$^t$Bu, with concomitant loss of **3-Th**. **$^1$H NMR of 13-Th (toluene-*d*$_8$, 600.1 MHz, 298 K):** $\delta$ 7.29, 7.21 (dd, $^3J_{H,H}$ 7.7 Hz; $^4J_{H,H}$ 1.7 Hz, 2 × 2H**,** Aryl-*meta*), 7.26 (t, $^3J_{H,H}$ 7.7 Hz, 2H**,** Aryl-*para*), 6.77, 6.04 (d, $^4J_{H,H}$ 2 Hz, 2 × 2H, CH$^{1,8}$ & CH$^{3,6}$), 3.83, 3.32 (broad sept, $^3J_{H,H}$ 7 Hz, 2 × 2H**,** C*H*Me$_2$), 1.70, 1.64 (s, 2 × 3H, CMe$_2$), 1.50, 1.32, 1.25, 1.08 (d, $^3J_{H,H}$ 7 Hz, 4 × 6H, CH*Me*$_2$), 1.19 (s, 18H, CMe$_3$), 0.74 (s, 9H, ThCH$_2$C*Me*$_3$), 0.21 (broad s, 2H, ThC*H*$_2$CMe$_3$), 0.05 (s, 9H, ThCH$_2$Si*Me*$_3$), -0.11 (broad s, 2H, ThC*H*$_2$SiMe$_3$). **$^{13}$C{$^1$H} NMR of 13-Th (toluene-*d*$_8$, 150 MHz, 298 K):** $\delta$ 148.36, 147.86 (2 × Aryl-*C*$_{ortho}$), 148.23 (*C*$^{2,7}$), 145.92 (*C*$^{4,5}$), 142.0 (*C*$^{11,12}$), 135.66 (Aryl-*C*$_{ipso}$), 129.79 (*C*$^{10,13}$), 128.26 (Aryl-*C*$_{para}$), 125.55, 125.48 (2 × Aryl-*C*$_{meta}$), 110.49,

110.19 (*C*H$^{1,8}$ & *C*H$^{3,6}$), 37.44 (ThCH$_2$*C*Me$_3$), 35.54 (ThCH$_2$C*Me*$_3$), 35.26 (*C*Me$_2$), 35.12 (*C*Me$_3$), 33.87, 28.33 (2 × C*Me*$_2$), 31.63 (C*Me*$_3$), 29.43, 28.47 (2 × *C*HMe$_2$), 26.92, 25.91, 25.46, 24.77 (4 × CH*Me*$_2$), 3.48 (ThCH$_2$Si*Me*$_3$).

**[Li(THF)$_x$][(XA$_2$)U(CH$_2$SiMe$_3$)$_3$] (14-THF) (*in-situ*)**

A mixture of [(XA$_2$)U(CH$_2$SiMe$_3$)$_2$]·(*n*-pentane) (**3**·*n*-pentane) (0.010 g, 0.009 mmol) and 1.3 equiv of LiCH$_2$SiMe$_3$ (0.0011 g, 0.011 mmol) were dissolved in THF-$d_8$ in a sealable NMR tube to afford a yellow solution. Five minutes after mixing, $^1$H NMR revealed new signals corresponding to **14-THF**, with concomitant loss of **3**. **$^1$H NMR (THF-$d_8$, 500.1 MHz, 298 K):** $\delta$ 314.6, 268.8, –161.0 (extremely broad s, 3 × 2H, UC*H*$_2$), 35.08, 23.20, –14.20 (v broad s, 3 × 9H, CH$_2$Si*Me*$_3$), 28.34, –9.54, –11.39, –24.50 (v. broad s, 4 × 6H, CH*Me*$_2$), 5.85, –12.40 (v broad s, 2 × 2H, Aryl-*meta* CH), 4.70, –9.50 (v broad s, 2 × 3H, C*Me*$_2$), 0.19 (t, $^3J_{H,H}$ = 7 Hz, 2H, Aryl-*para* CH), –1.49, –28.03 (s, 2 × 2H, CH$^{1,8}$ and CH$^{3,6}$), –1.65, –56.37 (v broad s, 2 × 2H, C*H*Me$_2$), –5.34 (s, 18H, CMe$_3$). **$^1$H NMR (THF-$d_8$, 500.1 MHz, 223 K):** $\delta$ 451.0, 378.0, –236.9 (extremely broad s, 3 × 2H, UC*H*$_2$), 49.48, 30.58, –21.27 (broad s, 3 × 9H, CH$_2$Si*Me*$_3$), 39.69, –12.53, –13.32, –30.85 (broad s, 4 × 6H, CH*Me*$_2$), 5.68, –13.68 (broad s, 2 × 3H, C*Me*$_2$), 4.07, –20.03 (broad s, 2 × 2H, Aryl-*meta* CH), –0.86, –60.16 (v broad s, 2 × 2H, C*H*Me$_2$), –3.37 (broad s, 2H, Aryl-*para* CH), –5.28, –40.72 (broad s, 2 × 2H, CH$^{1,8}$ and CH$^{3,6}$), –8.04 (s, 18H, CMe$_3$).

**[Li(dme)$_3$][(XA$_2$)U(CH$_2$SiMe$_3$)$_3$] (14-dme)**

*Preparatory scale.* A mixture of [(XA$_2$)U(CH$_2$SiMe$_3$)$_2$]·(*n*-pentane) (**3**·*n*-pentane) (0.100 g, 0.087 mmol) and 1.1 equivalents of LiCH$_2$SiMe$_3$ (0.009 g, 0.095 mmol) were dissolved in minimal *n*-pentane (~ 2 mL) to afford a red solution. The solution was cooled to –30 °C, and 3.05 equivalents of 1,2-dimethoxyethane (dme) were quickly added *via* microsyringe to the rapidly stirring mixture. Immediately upon addition of dme, a yellow precipitate evolved and the supernatant became a pale orange colour. The mixture continued to stir for ~ 5 minutes and the mother liquors were then discarded, affording a yellow-brown solid. The powder was washed with *n*-pentane (~ 3 mL) and dried, yielding 0.119 g of yellow-brown **14-dme** (0.082 mmol, 95 % yield). X-ray quality crystals of **14-dme**·2(dme) were obtained by conducting the reaction in neat dme; the yellow solution was layered with *n*-pentane and cooled to –30 °C. After several days, a mixture of yellow **14-dme**·2(dme) crystals were obtained alongside brown crystals of cyclometalated **16-dme**. The $^1$H NMR spectrum of isolated complex **14-dme** is identical to that of the *in situ* generated **14-THF**, but with 3 equiv of free dme in solution. **$^1$H NMR (THF-*d*$_8$, 600.1 MHz, 298 K):** $\delta$ 314.6, 268.8, –161.0 (extremely broad s, 3 × 2H, UC*H*$_2$) 35.08, 23.20, –14.20 (v. broad s, 3 × 9H, CH$_2$Si*Me*$_3$), 28.34, –9.54, –11.39, –24.50 (v. broad s, 4 × 6H, CH*Me*$_2$), 5.85, –12.40 (v. broad s, 2 × 2H, Aryl-*meta* CH), 4.70, –9.50 (v. broad s, 2 × 3H, C*Me*$_2$), 3.42 (s, 12H, OC*H*$_2$, *free dme*), 3.26 (s, 18H, OC*H*$_3$, *free dme*), 0.19 (t, $^3J_{H,H}$ = 7 Hz, 2H, Aryl-*para* CH), –1.49, –28.03 (s, 2 × 2H, CH$^{1,8}$ and CH$^{3,6}$), –1.65, –56.37 (v. broad s, 2 × 2H, C*H*Me$_2$), –5.34 (s, 18H, CMe$_3$). **Anal. Calcd for** C$_{71}$H$_{125}$N$_2$O$_7$Si$_3$LiU**:** C, 58.89; H, 8.70; N, 1.93 %. Found: C, 58.99; H, 8.87; N, 2.35%.

**[Li(dme)$_3$][(XA$_2$)UMe$_3$] (15)**

*Method 1*. A mixture of [(XA$_2$)UCl$_2$(μ-Cl){K(dme)$_3$}] (**1**) (0.150 g, 0.11 mmol) and MeLi (0.008 g, 0.37 mmol) in dme (20 mL) were stirred at –78 °C and then warmed slowly to room temperature; stirring was continued for a total of 12 h. The yellow solution was evaporated to dryness *in vacuo*, and the solid residue was extracted with toluene (20 mL). The suspension was filtered to remove insoluble KCl and LiCl, and the yellow filtrate was evaporated to dryness *in vacuo*. The solid residue was taken up in minimal dme and layered with hexanes. After a few days at –30 °C, X-ray quality crystals of **15**·dme were obtained and dried *in vacuo* to provide 0.046 g of **15**·dme (0.035 mmol, 31% yield). The low yield likely results from losses during extraction as a consequence of poor solubility in toluene.

*Method 2*. Complex **15** can be prepared cleanly *in situ* (as the [Li(THF)$_x$]$^+$ salt) by reaction of dialkyl **3**·(*n*-pentane) (0.010 g, 0.009 mmol) and MeLi (0.0007 g, 0.03 mmol) in THF-$d_8$. Upon mixing, the solution became a bright yellow colour, and after 30 min of sonication, $^1$H NMR revealed new signals corresponding to anionic [(XA$_2$)UMe$_3$]$^-$ with concomitant loss of neutral **3** and release of LiCH$_2$SiMe$_3$. **$^1$H NMR (THF-$d_8$, 500.1 MHz, 298 K):** $\delta$ 6.29, –7.04 (broad s, 2 × 12H, CH*Me*$_2$), –1.53 (t, $^3J_{H,H}$ = 6 Hz, 2H, Aryl-*para* CH), –2.26 (s, 6H, CMe$_2$), –2.44, –28.86 (s, 2 × 2H, CH$^{1,8}$ and CH$^{3,6}$), –4.59 (v broad s, 4H, C*H*Me$_2$), –5.69 (s, 18H, CMe$_3$), –5.84 (d, $^3J_{H,H}$ = 5 Hz, 4H, Aryl-*meta* CH). Signals corresponding to the UC*H*$_3$ protons were not located between +400 and –400 ppm. **Anal. Calcd for C$_{62}$H$_{101}$N$_2$O$_7$LiU** prepared using method 1: C, 60.47; H, 8.27; N, 2.27%. Found: C, 60.79; H, 7.73; N, 2.08%.

**[Li(THF)$_x$][(XA$_2$*)U(CH$_2$SiMe$_3$)$_2$] (16-THF) (*in-situ*)**

Solid [Li(dme)$_3$][(XA$_2$)U(CH$_2$SiMe$_3$)$_3$] (**14-dme**) (0.011 g, 0.008 mmol) was dissolved in THF-$d_8$ in a sealable NMR tube to afford a yellow solution. Over the course of approximately one week, the solution gradually became a deep amber colour; monitoring by $^1$H NMR revealed the growth of new signals corresponding to the cyclometalated species **16-THF**, with concomitant loss of **14-dme** and evolution of 1 equiv of SiMe$_4$. **$^1$H NMR (THF-$d_8$, 600.1 MHz, 298 K):** $\delta$ 78.73, 64.96 (broad s, 2 × 3H, UC*Me*$_2$Ar), 17.65, 5.06, 4.38, 1.32, −4.60, −5.69, −14.98, −19.35 (broad s, 8 × 3H, C*Me*$_2$, CH*Me*$_2$ {× 3}), 48.11, 45.95, 18.26, 9.42, 8.46, 5.58, 4.17, 2.92, 1.39, −1.56, −2.98, −3.80, −6.66, −9.33, −14.54, −22.93, −28.05 (broad s, 17 × 1H, CH$^1$, CH$^3$, CH$^6$, CH$^8$, C*H*Me$_2$ {× 3}, Aryl-*meta* CH {× 4}, Aryl-*para* CH {× 2}, UC*H*$_2$ {× 2}), 13.14, 4.04, −6.53, −9.04 (broad s, 4 × 9H, C*Me*$_3$ {× 2}, Si*Me*$_3$ {× 2}), 3.42 (s, 12H, OC*H*$_2$, *free dme*), 3.26 (s, 18H, OC*H*$_3$, *free dme*).

**[Li(dme)$_3$][(XA$_2$*)U(CH$_2$SiMe$_3$)$_2$] (16-dme)**

*Preparatory Scale.* Solid LiCH$_2$SiMe$_3$ (0.009 g, 0.095 mmol, 1.1 equiv) was added to a rapidly stirring solution of [(XA$_2$)U(CH$_2$SiMe$_3$)$_2$]·(*n*-pentane) (**3**·*n*-pentane) (0.100 g, 0.087 mmol) in dme (4 mL) at room temperature. Immediately upon addition, the cherry red solution became yellowy-amber, indicative of [(XA$_2$)U(CH$_2$SiMe$_3$)$_3$]$^-$ formation *in situ*. Stirring continued at room temperature for approximately one week to complete the cyclometalation process, at which point the deep red-brown solution was evaporated to dryness *in vacuo* yielding a deep brown residue. The residue was dissolved in a minimum

amount of dme (1 mL) and layered with *n*-pentane. Cooling the mixture at –30 °C for several days resulted in the precipitation of a deep brown oily residue. The residue was washed with *n*-pentane (5 mL), dried *in vacuo*, and finally triturated in *n*-pentane (20 mL) using a sonicating bath. Volatiles were removed *in vacuo* to afford 0.086 g of **16-dme** (0.063 mmol, 73 % yield) as a deep brown powder. X-ray quality crystals of **16-dme** were obtained alongside **14-dme**·2(dme) after attempted crystallization of **14-dme** from dme/*n*-pentane at –30 °C. The $^{1}$H NMR spectrum of isolated **16-dme** is identical to that of **16-THF** produced *in situ*, but with 3 equiv of free dme present. Despite numerous attempts, isolated **16-dme** always contained small amounts of unidentified paramagnetic impurities, and as a consequence, satisfactory elemental analyses could not be obtained for this complex.

**[(XA$_2$)U(CH$_2$SiMe$_3$)($\kappa^2$-DMAP*)(DMAP)]·(*n*-pentane) (17·*n*-pentane)**

Solid DMAP (0.022g, 0.182 mmol) was quickly added to a stirring solution of [(XA$_2$)U(CH$_2$SiMe$_3$)$_2$]·(*n*-pentane) (**3**·*n*-pentane) (0.100 g, 0.087 mmol) in *n*-pentane (3 mL) at room temperature. The red solution stirred for approx. 45 minutes before copious yellow solids precipitated, and the mixture continued to stir for an additional 15 minutes. Additional *n*-pentane (5 mL) was added, and the mixture was centrifuged. The mother liquors were removed and the bright yellow solids were dried *in vacuo* to yield 0.103 g of **17**·*n*-pentane (0.078 mmol, 91% yield). X-ray quality orange crystals of **17**·2(toluene) were grown from toluene/*n*-pentane at –30 °C. Reaction of **3** with 2,6-DMAP-$d_2$ followed by identical work-up yielded the $d_3$-isotopologue **17-*d*$_3$** in comparable yield. **$^{1}$H NMR**

**(toluene-$d_8$, 500.1 MHz, 298 K):** $\delta$ 9.81, 7.40 (extremely broad s, 2 × 2H), 8.05 (broad s, 2H), 4.88, −4.08 (v broad s, 2 × 6H), 3.29 (v broad s, 8H {2H + 6H}), 2.83 (v broad s, 24H {18H ($CMe_3$) + 6H}), −9.33 (extremely broad s, 9H, $SiMe_3$). **$^1$H NMR (toluene-$d_8$, 500.1 MHz, 355 K):** $\delta$ 30.45, 16.52, −19.19 (broad s, 3 × 1H, DMAP* 3-CH, DMAP* 5-CH, DMAP* 6-CH), 15.43, 14.55, 13.77, 11.14, 7.82, 7.36, 3.19, 1.14 (broad s, 8 × 2H, $CH^{1,8}$, $CH^{3,6}$, Aryl-*meta* CH {× 2}, C*H*$Me_2$ {× 2}, 2,6-DMAP CH, 3,5-DMAP CH), 10.29 (t, $^3J_{H,H}$ = 8.2 Hz, 2H, Aryl-*para* CH), 5.16, 4.24, 3.82, 3.34, −2.56, −15.12 (broad s, 6 × 6H, CH*Me*$_2$ {× 4}, DMAP N*Me*$_2$, DMAP* N*Me*$_2$), 3.13 (s, 18H, $CMe_3$), −7.25, −9.40 (broad s, 2 × 3H, C*Me*$_2$), −9.06 (broad s, 9H, $SiMe_3$), −71.49 (v broad s, 1 × 2H, UC*H*$_2$). **Anal. Calcd for $C_{70}H_{104}N_6OSiU$:** C, 64.09; H, 7.99; N, 6.41%. Found: C, 64.03; H, 8.13; N, 6.54%.

**[(XA$_2$)U(CH$_2$SiMe$_3$)($\kappa^2$-AJ*)(AJ)] (18)**

**S**olid 9-azajulolidine (0.032g, 0.182 mmol) was quickly added to a stirring solution of [(XA$_2$)U(CH$_2$SiMe$_3$)$_2$]·(*n*-pentane) (**3**·*n*-pentane) (0.100 g, 0.087 mmol) in *n*-pentane (4 mL) at room temperature. The red-orange solution stirred for 4 hours, at which point the faintly turbid mixture was cooled to –30 °C. After several days, 0.128 g of yellow-brown crystalline **18**·2(*n*-pentane) was harvested (0.086 mmol, 99% yield); drying *in vacuo* provided **18** in comparable yield. X-ray quality yellow-brown crystals of **18**·2(*n*-pentane) were grown from *n*-pentane at –30 °C. **$^1$H NMR (toluene-$d_8$, 600.1 MHz, 303 K):** $\delta$ 7.65, 2.04, −6.19, −7.77, −11.06, −20.74 (extremely broad s × 6), −3.14 (v broad s). **$^1$H NMR (toluene-$d_8$, 600.1 MHz, 333 K):** $\delta$ 10.08, 9.13, 7.52, 5.76, 2.27, −1.24, −6.41, −11.45,

−19.27, −28.44 (extremely broad s × 10), 9.04 (s), 4.37, 3.36, −4.90 (v broad s × 3). **Anal. Calcd for $C_{73}H_{100}N_6OSiU$:** C, 65.25; H, 7.50; N, 6.25%. Found: C, 65.29; H, 7.92; N, 6.40%.

### 7.5 – Synthetic Procedures and Characterization Pertaining to Chapter 5

#### $H_2$[XAT] (19)

4,5-dibromo-2,7-di-*tert*-butyl-9,9-dimethylxanthene (3.42 g, 7.12 mmol), 2,6-dimesitylaniline (4.69 g, 14.23 mmol), NaO$^t$Bu (1.92 g, 19.92 mmol), $Pd(OAc)_2$ (0.018 g, 0.08 mmol) and DPEPhos (0.064 g, 0.119 mmol) were heated at 95 °C in toluene (~100 mL) for 3 days. The brown-orange reaction mixture was then quenched with water, extracted with toluene (3 × 30 mL), and dried over $MgSO_{4(s)}$ before removing volatiles *in vacuo*. The resulting pale yellow-orange oil was recrystallized from boiling ethanol/toluene (~10:1) and dried for 48 h at 90 °C to afford $H_2$[XAT] (**19**) as a white solid in 66% yield (3.97 g, 4.06 mmol). **$^1$H NMR ($CD_2Cl_2$, 600.1 MHz, 298 K):** $\delta$ 7.19 (t, 2H, $^3J_{H,H}$ = 7.6 Hz, N-aryl *para* CH), 7.04 (d, 4H, $^3J_{H,H}$ = 7.6 Hz, N-aryl *meta* CH), 6.64 (broad s, 4H, Mes Ar-*H*), 6.63 (d, 2H, $^4J_{H,H}$ = 2.3 Hz, CH$^{1,8}$), 6.46 (d, 2H, $^4J_{H,H}$ = 2.3 Hz, CH$^{3,6}$) 6.44 (broad s, 4H, Mes Ar-*H*'), 4.67 (broad s, 2H, N*H*), 2.05 (s, 12H, Mes C$H_3$), 1.96 (s, 12H, Mes C$H_3$), 1.88 (s, 12H, Mes C$H_3$), 1.21 (s, 6H, C$Me_2$), 1.15 (s, 18H, C$Me_3$). **$^{13}$C{$^1$H} NMR ($CD_2Cl_2$, 150 MHz, 298 K):** $\delta$ 143.27 (N-aryl *ipso*-*C* + xanthene C$^{2,7}$), 139.79 (xanthene *C*$^{11,12}$), 137.1 (Mes *C*$CH_3$), 137.0 (N-aryl *o*-*C*), 136.6 (Mes *C*$CH_3$), 136.41 (Mes *ipso*-*C*), 135.95 (Mes *C*$CH_3$), 134.08 (xanthene *C*$^{4,5}$), 130.71 (N-aryl

*m*-*C*H), 128.29, 128.19 (2 x Mes Ar-*C*H + xanthene $C^{10,13}$), 123.56 (N-aryl *p*-*C*H), 116.88 ($CH^{1,8}$), 116.78 ($CH^{3,6}$), 34.51 (*C*Me$_3$), 34.02 (*C*Me$_2$), 33.17 (C*Me*$_2$), 31.48 (C*Me*$_3$), 21.61, 20.87, 20.83 (3 x Mes *C*H$_3$). **Anal. Calcd. For $C_{71}H_{80}N_2O$:** C, 87.25; H, 8.25; N, 2.87 %. Found: C, 87.20; H, 8.77; N, 2.93 %.

**[K$_2$(XAT)] (20) (*in-situ*)**

A mixture of H$_2$[XAT] (**19**) (0.020 g, 0.02 mmol), KH (0.003 g, 0.08 mmol), and toluene-$d_8$ (~0.6 mL) was sealed in a J-Young tube and heated at 80 °C for 5 days; complete conversion to bright yellow [K$_2$(XAT)] (**20**) was verified by $^1$H and $^{13}$C NMR. **$^1$H NMR (toluene-$d_8$, 600.1 MHz, 298 K):** $\delta$ 7.00−7.06 (m(8), 6H, $^3J_{H,H}$ = 7.39 Hz, N-aryl *m*- and *p*-, AB$_2$ coupled spin-system), 6.63 (br. s, 4H, Mes Ar-*H*), 6.59 (br. s, 4H, Mes Ar-*H*), 6.18 (d, 2H, $^4J_{H,H}$ = 2.3 Hz, C$H^{1,8}$), 6.05 (d, 2H, $^4J_{H,H}$ = 2.3 Hz, C$H^{3,6}$), 2.38 (s, 12H, Mes *o*-C*H*$_3$), 2.08 (s, 12H, Mes *p*-C*H*$_3$), 2.06 (s, 12H, Mes *o*′-C*H*$_3$), 1.48 (s, 6H, C*Me*$_2$), 1.32 (s, 18H, C*Me*$_3$). **$^{13}$C{$^1$H} NMR (toluene-$d_8$, 150 MHz, 298 K):** $\delta$ 158.84 (N-aryl *ipso*-*C*), 148.86 (xanthene $C^{4,5}$), 144.22 (xanthene $C^{2,7}$), 142.57 (Mes *ipso*-*C*), 139.71 (N-aryl *ortho*-*C*), 139.31 (Mes *o*-*C*CH$_3$), 135.26 (Mes *p*-*C*CH$_3$), 134.88 (Mes *o*-*C*CH$_3$), 133.73 (xanthene $C^{11,12}$), 130.57 (N-aryl *m*-*C*H), 130.05 (Mes Ar-*C*H), 128.63 (xanthene $C^{10,13}$), 126.44 (Mes Ar-*C*H), 120.80 (N-aryl *p*-*C*H), 109.98 ($CH^{3,6}$), 101.94 ($CH^{1,8}$), 34.83 (*C*Me$_3$), 34.56 (*C*Me$_2$), 32.94 (C*Me*$_2$), 32.08 (C*Me*$_3$), 22.48 (Mes *o*-*C*H$_3$), 21.36 (Mes *p*-*C*H$_3$), 21.19 (Mes *o*-*C*H$_3$).

**[$K_2$(XAT){$(Me_3Si)_2O$}$_2$] (20f)**

*Preparative scale*: A mixture of $H_2$[XAT] (**19**) (0.200 g, 0.21 mmol) and KH (0.033 g, 0.82 mmol) in toluene (20 mL) was heated at 80 °C for 6 days. After cooling to room temperature, volatiles were removed *in vacuo* and the residue was extracted with minimal toluene (8 mL) followed by centrifugation to remove insoluble material (excess KH). The resulting deep brown-yellow solution was evaporated to dryness *in vacuo* and $O(SiMe_3)_2$ (65 mL) was added. The mixture was sonicated and a small quantity of insoluble brown residue was removed by filtration to yield a bright yellow solution. Volatiles were then removed *in vacuo*, and a small volume of $O(SiMe_3)_2$ (~15 mL) was added to the crude product. The slurry was sonicated, cooled in a –78 °C bath and filtered cold, yielding a vibrant yellow powder which was washed with cold $O(SiMe_3)_2$ (3 × 8 mL). After drying *in vacuo*, [$K_2$(XAT){$(Me_3Si)_2O$}$_2$] (**20f**) was isolated in 41% yield (0.117 g, 0.08 mmol). The low yield is due to appreciable solubility of crude **20** in $O(SiMe_3)_2$. The $^1$H NMR spectrum (toluene-$d_8$) of this isolated material matches that for [$K_2$(XAT)] (**20**) generated *in situ* in toluene-$d_8$, except with an additional peak at 0.10 ppm (s, 36 H, 2 × O(Si*Me*$_3$)$_2$). **$^1$H NMR ($C_6D_6$, 200.1 MHz, 298 K):** $\delta$ 7.09 (br. s, 6H, N-aryl *m*- and *p*-*H*), 6.63 (br. s, 4H, Mes Ar-*H*), 6.58 (br. s, 4H, Mes Ar-*H*), 6.25 (br. s, 2H, C*H*$^{1,8}$), 6.13 (br. s, 2H, C*H*$^{3,6}$), 2.44 (s, 12H, Mes *o*-C*H*$_3$), 2.08 (s, 12H, Mes *p*-C*H*$_3$), 2.06 (s, 12H, Mes *o*′-C*H*$_3$), 1.55 (s, 6H, C*Me*$_2$), 1.39 (s, 18H, C*Me*$_3$), 0.12 (s, 36 H, 2 × O(Si*Me*$_3$)$_2$). **Anal. Calcd. For $C_{83}H_{114}N_2O_3Si_4K_2$:** C, 72.33; H, 8.34; N, 2.03 %. Found: C, 71.46; H, 7.66; N, 1.77 %.

**X-ray Quality Crystals of [$K_2$(XAT)(hydrocarbon)$_x$] (20a–f)**

A mixture of $H_2$[XAT] (**19**) (0.400 g, 0.41 mmol) and KH (0.066 g, 1.64 mmol) was heated at 80 °C in toluene (~45 mL) for 6 days before evaporation to dryness *in vacuo*. The brown-yellow residue was extracted with minimal toluene, centrifuged to remove insoluble material, and evaporated to dryness *in vacuo*. The brown-yellow solid was then sonicated in hexanes (~15ml) and filtered at –78 °C to provide a bright yellow solid after washing with cold hexanes. This product was shown to have the composition $K_2$(XAT)(hexane)$_{0.6}$(toluene)$_{0.9}$ by $^1$H NMR spectroscopy (0.230 g; 0.19 mmol; 46% yield; the low yield is due to high solubility of the product in hexanes), but a satisfactory elemental analysis was not obtained. Layering a toluene solution of $K_2$(XAT)(hexane)$_{0.6}$(toluene)$_{0.9}$ with hexanes or *n*-pentane followed by cooling to –30 °C furnished X-ray quality crystals of [$K_2$(XAT)(*n*-hexane)]·toluene (**20a·**toluene) and [$K_2$(XAT)(*n*-pentane)]·(*n*-pentane) (**20b·**(*n*-pentane)), respectively. Cooling concentrated 3-methylpentane, cyclopentane, toluene, or O($SiMe_3$)$_2$ solutions of $K_2$(XAT)(hexane)$_{0.6}$(toluene)$_{0.9}$ to –30 °C yielded X-ray quality crystals of [$K_2$(XAT)(3-methylpentane)]·3-methylpentane (**20c·**3-methylpentane), [$K_2$(XAT)(cyclopentane)]·cyclopentane (**20d·**cyclopentane), [$K_2$(XAT)(toluene)]·0.5(toluene) (**20e·**0.5(toluene)), and [$K_2$(XAT){($Me_3Si$)$_2$O}$_2$] (**20f**), respectively.

**$H_2$[XAd] (21)**

4,5-dibromo-2,7-di-*tert*-butyl-9,9-dimethylxanthene (7.28 g, 15.16 mmol), 1-adamantylamine (4.59 g, 30.31 mmol), NaO$^t$Bu (4.08 g, 42.42 mmol), $Pd(OAc)_2$ (0.040 g, 0.18 mmol) and DPEPhos (0.142 g, 0.26 mmol) in toluene (~200 mL) were heated to 95 °C for 14 days. The cream-coloured reaction mixture was then quenched with water, extracted with toluene (3 × 20 mL), and dried over $MgSO_{4(s)}$ before removing volatiles *in vacuo*, yielding an oily cream-coloured solid. The solids were taken up in a refluxing ethanol/toluene mixture (~10:1), and upon cooling, $H_2$[XAd] (**21**) precipitated as a white solid (7.63 g, 12.29 mmol) in 81% yield. **$^1$H NMR ($C_6D_6$, 600.1 MHz, 298 K):** $\delta$ 7.27 (d, 2H, $^4J_{H,H}$ = 2.2 Hz, C*H*$^{3,6}$), 7.06 (d, 2H, $^4J_{H,H}$ = 2.2 Hz, C*H*$^{1,8}$), 4.20 (s, 2H, N*H*), 2.11 (d, 12H, $^3J_{H,H}$ = 2.6 Hz, Ad C*H*$_2$), 2.01 (br. s, 6H, Ad C*H*), 1.70 (s, 6H, C*Me*$_2$), 1.59 (appt. q, 12H, $^2J_{H,H}$ = 11.7 Hz, Ad C*H*$_2$ *endo/exo*), 1.40 (s, 18H, C*Me*$_3$). **$^{13}$C{$^1$H} NMR ($C_6D_6$, 150 MHz, 298 K):** $\delta$ 145.03 (*C*CMe$_3$), 139.64 (xanthene *C*$^{11,12}$), 134.32 (xanthene *C*$^{4,5}$), 130.0 (xanthene *C*$^{10,13}$), 114.91 (*C*H$^{3,6}$), 112.45 (*C*H$^{1,8}$), 52.59 (N-Ad *ipso-C*), 44.25 (Ad *C*H$_2$), 36.92 (Ad *endo/exo*), 35.47 (*C*Me$_2$), 34.71 (*C*Me$_3$), 32.08 (C*Me*$_2$), 31.91 (C*Me*$_3$), 30.29 (Ad *C*H). **Anal. Calcd. For $C_{43}H_{60}N_2O$:** C, 83.17; H, 9.74; N, 4.51 %. Found: C, 83.25; H, 9.77; N, 4.41 %.

**[$K_2$(XAd)] (22) (*in situ*)**

A mixture of $H_2$[XAd] (0.020 g, 0.032 mmol), 4 equiv of KH (0.005 g, 0.129 mmol), and THF-$d_8$ (~0.6 mL) was sealed in a J-Young tube and heated to 65 °C. Immediately, $H_{2(g)}$ evolution began, and the mixture continued heating for 3 days. Complete conversion of

proteo ligand **21** to $K_2$[XAd] (**22**; likely as a (THF-$d_8$)$_x$ adduct) was verified by $^1$H and $^{13}$C NMR. **$^1$H NMR (THF-$d_8$, 600.1 MHz, 298 K):** δ 6.24 (d, 2H, $^4J_{H,H}$ = 2.0 Hz, C$H^{3,6}$), 5.67 (d, 2H, $^4J_{H,H}$ = 2.0 Hz, C$H^{1,8}$), 2.08 (br. s, 6H, Ad C$H$), 2.01 (br. s, 12H, Ad C$H_2$), 1.73 (appt. t, 12H, $^2J_{H,H}$ = 14.6 Hz, Ad C$H_2$ *endo/exo*), 1.46 (s, 6H, C$Me_2$), 1.23 (s, 18H, C$Me_3$). **$^{13}$C{$^1$H} NMR (THF-$d_8$, 150 MHz, 298 K):** δ 149.02 (xanthene $C^{4,5}$), 143.78 ($C$CMe$_3$), 137.97 (xanthene $C^{11,12}$), 127.26 (xanthene $C^{10,13}$), 106.84 ($C$H$^{3,6}$), 95.76 ($C$H$^{1,8}$), 52.66 (N-Ad *ipso-C*), 45.07 (Ad $C$H$_2$), 38.73 (Ad *endo/exo*), 35.21 ($C$Me$_2$), 34.85 ($C$Me$_3$), 32.54 (C$Me_2$), 32.43 (C$Me_3$), 31.73 (Ad $C$H).

**[$K_2$(XAd)(dme)] (22-dme) (*in-situ; preparatory scale*)**

*Method 1*: A mixture of $H_2$[XAd] (0.500 g, 0.81 mmol), 2.5 equiv of KCH$_2$Ph (0.262 g, 2.0 mmol) and dme (60 mL) was stirred at −78 °C and then slowly warmed to room temperature; stirring was continued for a total of 12 h. The grey slurry was evaporated to dryness *in vacuo*, yielding an off-white solid. $^1$H NMR spectroscopy (THF-$d_8$) confirmed the identity of crude product to be [$K_2$(XAd)(dme)] (**22-dme**), which was subsequently used without further purification.

*Method 2*: Alternatively, a mixture of $H_2$[XAd] (0.500 g, 0.81 mmol), KH (0.071 g, 1.77 mmol), and dme (~35 mL) was stirred for ~ 1 week at room temperature, over which time a light pink precipitate formed. Volatiles were removed *in vacuo*, yielding a pale pink solid; $^1$H NMR spectroscopy (THF-$d_8$) indicated complete conversion from proligand **21** to crude [$K_2$(XAd)(dme)] (**22-dme**), which was subsequently used without further purification. X-ray quality crystals of [$K_2$(XAd)(THF)$_6$] (**22-THF**) were obtained from

THF/hexane at −30 °C; however, **22-THF** readily de-solvates and decomposes to yield proligand **21**, precluding its use as an isolable precursor. The $^{1}$H NMR spectrum (THF-$d_8$) of isolated crude **22-dme** is identical to that of **22** produced *in situ*, but with the addition of one equiv of free dme.

**[(XAd)ThCl$_4$K$_2$]·*x*(dme) (23·*x*(dme))**

*Method 1*: A mixture of $H_2$[XAd] (0.500 g, 0.81 mmol), 2.5 equiv of $KCH_2Ph$ (0.262 g, 2.0 mmol) and dme (60 mL) was stirred at −78 °C and then slowly warmed to room temperature; stirring was continued for a total of 12 h. The grey slurry was evaporated to dryness *in vacuo*, yielding solid off-white [$K_2$(XAd)(dme)] (**22-dme**). To this, [$ThCl_4(dme)_2$] (0.446 g, 0.81 mmol) was added, and dme (50 mL) was condensed in at −78 °C. The mixture warmed to room temperature and was stirred for a total of 24 h. The white slurry was evaporated to dryness *in vacuo*, yielding a solid residue which was extracted with dme (25 mL) and centrifuged to remove any insoluble material. The mother liquors were evaporated to dryness, hexane was added (60 mL), and the white slurry was sonicated. The solids were collected by filtration and washed with 3 × 15 mL hexane to yield 0.647 g of [(XAd)ThCl$_4$K$_2$]·2(dme) (**23**·2(dme)) (0.517 mmol, 64 % yield) as a white solid powder. The amount of dme accompanying complex **23** varied by batch (ranging from 0.5 to ~2 equiv).

*Method 2*: Alternatively, a mixture of $H_2$[XAd] (0.500 g, 0.81 mmol), KH (0.071 g, 1.77 mmol) and dme (35 mL) was stirred for approximately 1 week at room temperature, over which time a pink precipitate formed. Volatiles were removed *in vacuo*, yielding crude

[$K_2$(XAd)(dme)] (**22-dme**), to which [$ThCl_4(dme)_2$] (0.446 g, 0.81 mmol) and THF (30 mL) were added. The resulting slurry was stirred for 48 h at room temperature, over which time the solution became pale yellow and copious white solids precipitated; volatiles were subsequently removed *in vacuo*. The solids were extracted with minimal dme, centrifuged to remove any insoluble material, and the mother liquors were removed *in vacuo* to yield a yellowish off-white solid. The solid was sonicated in hexane, filtered, and washed with 3 × 15 mL hexane to afford 0.200 g of [(XAd)$ThCl_4K_2$]·(dme) (**23·**dme) as an off-white solid (0.172 mmol, 21% yield). The low yield is likely due to incomplete extraction with dme and subsequent loss of product during centrifugation. **$^1$H NMR** (on **23·**dme prepared using method 2) **(THF-*d*$_8$, 600.1 MHz, 298 K):** δ 6.69 (d, 2H, $^4J_{H,H}$ = 1.7 Hz, C*H*$^{3,6}$), 6.58 (d, 2H, $^4J_{H,H}$ = 1.7 Hz, C*H*$^{1,8}$), 3.43 (s, 4H, free dme C*H*$_2$), 3.27 (s, 6H, free dme C*H*$_3$), 2.59 (br. s, 12H, Ad C*H*$_2$), 2.24 (br. s, 6H, Ad C*H*), 1.82 (appt. q, 12H, $^2J_{H,H}$ = 12.1 Hz, Ad C*H*$_2$ *endo/exo*), 1.70 (s, 6H, C*Me*$_2$), 1.30 (s, 18H, C*Me*$_3$). **$^{13}$C{$^1$H} NMR (THF-*d*$_8$, 150 MHz, 298 K):** δ 146.47 (*C*CMe$_3$), 143.06 (xanthene *C*$^{4,5}$), 140.34 (xanthene *C*$^{11,12}$), 127.23 (xanthene *C*$^{10,13}$), 112.36 (*C*H$^{3,6}$), 109.73 (*C*H$^{1,8}$), 72.55 (free dme *C*H$_2$), 58.69 (free dme *C*H$_3$), 56.61 (N-Ad *ipso*-*C*), 41.28 (Ad *C*H$_2$), 37.40 (Ad *endo/exo*), 35.09 (*C*Me$_3$), 34.56 (*C*Me$_2$), 33.93 (C*Me*$_2$), 31.73 (C*Me*$_3$), 30.77 (Ad *C*H). **Anal. Calcd. For $C_{47}H_{68}N_2O_3ThCl_4K_2$** (for complex **23·**dme prepared using method 2): C, 48.62; H, 5.90; N, 2.41 %. Found: C, 48.80; H, 6.09; N, 2.12 %.

**[(XAd)Th($CH_2SiMe_3$)$_2$(THF)] (24)**

A mixture of $H_2$[XAd] (0.200 g, 0.32 mmol), KH (0.028 g, 0.71 mmol) and dme (25 mL) was stirred for ~10 days at room temperature, over which time a pale pink precipitate formed. Volatiles were removed *in vacuo* yielding crude pale pink [$K_2$(XAd)(dme)] (**22-dme**), to which [$ThCl_4$(dme)$_2$] (0.179 g, 0.32 mmol) and THF (25 mL) were added. The resulting slurry was stirred for 48 h at room temperature, becoming cloudy and yellowish upon formation of '[(XAd)$ThCl_4K_2$]·*x*(THF)' (**23·***x*(THF)). A separate flask was charged with solid $LiCH_2SiMe_3$ (0.062 g, 0.66 mmol) and THF (10 mL), and both solutions were cooled to 0 °C. The alkyllithium solution was added dropwise *via* cannula to *in situ*-generated '[(XAd)$ThCl_4K_2$]·*x*(THF)' (**23·***x*(THF)); once added, the mixture slowly warmed to room temperature and was stirred for an additional 12 h. The volatiles were removed *in vacuo*, yielding a grey solid, which was dissolved in toluene (10 mL) and centrifuged to remove insoluble KCl and LiCl salts. The golden-coloured mother liquors were removed *in vacuo* to afford an off-white solid, which was subsequently sonicated in hexane, collected by centrifugation, and dried *in vacuo* to yield 0.150 g of dialkyl **24** (0.137 mmol) as a white solid in 43% yield. The low yield may be due to appreciable solubility of **24** in hexane. X-Ray quality crystals of **24** were obtained from a saturated hexane solution at −30 °C. **$^1$H NMR ($C_6D_6$, 600.1 MHz, 298 K):** $\delta$ 7.10 (br. s, 2H, C*H*$^{3,6}$), 6.75 (br. s, 2H, C*H*$^{1,8}$), 3.46 (br. s, 4H, coordinated THF C*H*$_2^{2,5}$), 2.92 (v. br. s, 12H, Ad C*H*$_2$), 2.36 (br. s, 6H, Ad C*H*), 1.95, 1.76 (appt. d, 2 × 6H, $J_{H,H}$ = 11.9 Hz, Ad C*H*$_2$ *endo/exo*), 1.71 (s, 6H, C*Me*$_2$), 1.39 (s, 18H, C*Me*$_3$), 0.90 (br s, 4H, coordinated THF C*H*$_2^{3,4}$), 0.33 (s, 18H, $CH_2$Si*Me*$_3$), 0.09 (s, 4H, C*H*$_2$$SiMe_3$). **$^{13}$C{$^1$H} NMR ($C_6D_6$, 150**

**MHz, 298 K):** $\delta$ 146.40 (*C*CMe$_3$), 143.28 (xanthene *C*$^{4,5}$), 141.97 (xanthene *C*$^{11,12}$), 128.90 (xanthene *C*$^{10,13}$), 112.22 (*C*H$^{3,6}$), 108.36 (*C*H$^{1,8}$), 85.68 (Th*C*H$_2$TMS), 70.36 (coordinated THF 2,5-*C*H$_2$), 57.22 (N-Ad *ipso*-*C*), 41.02 (Ad *C*H$_2$), 37.27 (Ad *endo/exo*), 34.96 (*C*Me$_3$), 34.37 (*C*Me$_2$), 32.72 (C*Me*$_2$), 31.91 (C*Me*$_3$), 30.22 (Ad *C*H), 25.08 (coordinated THF 3,4-*C*H$_2$), 4.65 (ThCH$_2$Si(*C*H$_3$)$_3$). **Anal. Calcd. For C$_{55}$H$_{88}$N$_2$O$_2$Si$_2$Th:** C, 60.19; H, 8.08; N, 2.55 %. Found: C, 60.48; H, 7.89; N, 2.53 %.

**[(XAd)Th(η$^3$-allyl$^{TMS}$)$_2$] (25)**

A mixture of [(XAd)ThCl$_4$K$_2$]·2(dme) (**23**·2(dme)) (0.130 g, 0.104 mmol) and approximately 3 equiv of K[1-(SiMe$_3$)C$_3$H$_4$] (0.049 g, 0.319 mmol) in toluene (35 mL) was stirred at −78 °C and then warmed slowly to room temperature; stirring was continued for a total of 24 h. Upon initial introduction of the toluene solvent, the solution became a bright yellow colour. After 24 h of stirring, the solvent was removed *in vacuo* to afford a bright yellow solid residue. The residue was extracted with O(SiMe$_3$)$_2$ (10 mL), and insoluble material (KCl) was removed by centrifugation. The yellow mother liquors were evaporated to dryness *in vacuo*, yielding 0.112 g of bis(allyl) complex **25** as a vibrant yellow solid (0.104 mmol, 100% yield). X-ray quality crystals of **25**·2(toluene) were obtained from toluene/hexane at –30 °C. **$^1$H NMR (toluene-*d*$_8$, 600.1 MHz, 350 K):** δ 6.94 (d, $^4J_{H,H}$ = 2.03 Hz, 2H, C*H*$^{3,6}$), 6.92 (m, 2H, *meso*-allyl CH$_2$C*H*), 6.69 (d, $^4J_{H,H}$ = 2.03 Hz, 2H, C*H*$^{1,8}$), 3.81 (br d, $^3J_{H,H}$ = 15.7, 2H, *anti*-allyl-C*H*SiMe$_3$), 3.60 (br d, $^3J_{H,H}$ = 11.8, 4H, *gem*-allyl-C*H*$_2$), 2.63 (br s, 12H, Ad-C*H*$_2$), 2.17 (br s, 6H, Ad-C*H*), 1.76 (s, 6H, C*Me*$_2$), 1.70 (m, 12H, Ad-*exo,endo*), 1.33 (s, 18H, C*Me*$_3$), −0.05 (s, 18H, Th-allyl-

CHSi*Me*$_3$). **$^{13}$C{$^1$H} NMR (toluene-*d*$_8$, 600.1 MHz, 350 K):** δ 159.16 (*meso*-allyl-$CH_2$*C*H), 146.53 (*C*$^{2,7}$), 143.14 (*C*$^{4,5}$), 141.49 (*C*$^{11,12}$), 128.60 (*C*$^{10,13}$), 112.14 (*C*$^{3,6}$), 110.23 (*C*$^{1,8}$), 96.80 (Th-allyl-*C*HSiMe$_3$), 86.17 (*gem*-allyl-*C*$H_2$), 57.89 (N-Ad *ipso*-*C*), 40.27 (Ad-*C*$H_2$), 37.64 (Ad-*endo*,*exo*), 35.10 (*C*Me$_3$), 34.17 (*C*Me$_2$), 34.05 (C*Me*$_2$), 31.91 (C*Me*$_3$), 30.29 (Ad-*C*H), 1.00 (Th-allyl-CHSi*Me*$_3$). **Anal. Calcd. For $C_{55}H_{84}N_2OSi_2Th$:** C, 61.31; H, 7.86; N, 2.60 %. Found: C, 60.67; H, 7.57 ; N, 2.53 %.

## References

(1) Jensen, W. B. *J. Chem. Educ.* **1982**, *59*, 634. Jensen, W. B. *Foundations of Chemistry* **2015**, *17*, 23.

(2) Katz, J. J.; Morss, L. R.; Edelstein, N.; Fuger, J., *The Chemistry of the Actinide and Transactinide Elements (Set Vol.1-6)*, Springer Netherlands: 2010.

(3) Cotton, S., *Lanthanide and Actinide Chemistry*, Wiley: 2007.

(4) Starks, D. F.; Parsons, T. C.; Streitwieser, A.; Edelstein, N. *Inorg. Chem.* **1974**, *13*, 1307.

(5) Baumgärtner, F.; Fischer, E. O.; Kanellakopulos, B.; Laubereau, P. *Angew. Chem.* **1969**, *81*, 182.

(6) Baumgärtner, F.; Fischer, E. O.; Kanellakopulos, B.; Laubereau, P. *Angew. Chem. Int. Ed. Engl.* **1966**, *5*, 134.

(7) Laubereau, P. G.; Burns, J. H. *Inorg. Nucl. Chem. Lett.* **1970**, *6*, 59. Baumga¨rtner, F.; Fischer, E. O.; Billich, H.; Dornberger, E.; Kanellakopulos, B.; Roth, W.; Stieglitz, L. *J. Organomet. Chem.* **1970**, *22*, C17.

(8) Laubereau, P. G.; Burns, J. H. *Inorg. Chem.* **1970**, *9*, 1091.

(9) MacDonald, M. R.; Fieser, M. E.; Bates, J. E.; Ziller, J. W.; Furche, F.; Evans, W. J. *J. Am. Chem. Soc.* **2013**, *135*, 13310.

(10) Marks, T. J.; Kennelly, W. J.; Kolb, J. R.; Shimp, L. A. *Inorg. Chem.* **1972**, *11*, 2540. Marks, T. J.; Kolb, J. R. *Chem. Rev.* **1977**, *77*, 263.

(11) Shannon, R. D. *Acta Cryst.* **1976**, *A32*, 751.

(12) Parry, J. S.; Cloke, F. G. N.; Goles, S. J.; Hursthouse, M. B. *J. Am. Chem. Soc.* **1999**, *121*, 6867.

(13) Geckeis, H., Gmelin Handbook of Inorganic and Organometallic Chemistry, 8th Ed., Thorium Suppl. Vol. C 4, Springer-Verlag, 1993, Section 6.1.2: Thorium Tetrachloride, ThCl4, p 65.

(14) Dean, O. C.; Chandler, J. M. *Nucl. Sci. Eng.* **1957**, *2*, 57.

(15) Athimoolam, A.; Gambarotta, S.; Korobkov, I. *Organometallics* **2005**, *24*, 1996.

(16) Cantat, T.; Scott, B. L.; Kiplinger, J. L. *Chem. Commun.* **2010**, *46*, 919.

(17) Travia, N. E.; Monreal, M. J.; Scott, B. L.; Kiplinger, J. L. *Dalton Trans.* **2012**, *41*, 14514.

(18) Wilkerson, M. P.; Burns, C. J.; Paine, R. T.; Scott, B. L. *Inorg. Chem.* **1999**, *38*, 4156.

(19) Khan, I. A.; Ahuja, H. S.; Bagnall, K. W.; L., S. *Inorg. Synth.* **1982**, *21*, 187.

(20) Kiplinger, J. L.; Morris, D. E.; Scott, B. L.; Burns, C. J. *Organometallics* **2002**, *21*, 5978.

(21) Patel, D.; Wooles, A. J.; Hashem, E.; Omorodion, H.; Baker, R. J.; Liddle, S. T. *New J. Chem.* **2015**, *39*, 7559.

(22) Schnaars, D. D.; Wu, G.; Hayton, T. W. *Dalton Trans.* **2008**, 6121.

(23) Berthet, J.-C.; Thuéry, P.; Ephritikhine, M. *Inorg. Chem.* **2005**, *44*, 1142.

(24) Bagnall, K. W.; Brown, D.; Jones, P. J.; Du Preez, J. G. H. *J. Chem. Soc.* **1965**, 350.

(25) Carmichael, C. D.; Jones, N. A.; Arnold, P. L. *Inorg. Chem.* **2008**, *47*, 8577.

(26) Cloke, F. G. N.; Hitchcock, P. B. *J. Am. Chem. Soc.* **2002**, *124*, 9352.

(27) Evans, W. J.; Kozimor, S. A.; Ziller, J. W.; Fagin, A. A.; Bochkarev, M. N. *Inorg. Chem.* **2005**, *44*, 3993.

(28) Clark, D. L.; Sattelberger, A. P.; Bott, S. G.; Vrtis, R. N. *Inorg. Chem.* **1989**, *28*, 1771. Avens, L. R.; Bott, S. G.; Clark, D. L.; Sattelberger, A. P.; Watkin, J. G.; Zwick, B. D. *Inorg. Chem.* **1994**, *33*, 2248. Clark, D. L.; Sattelberger, A. P. *Inorg. Synth.* **1997**, *31*, 307.

(29) La Pierre, H. S.; Heinemann, F. W.; Meyer, K. *Chem. Commun.* **2014**, *50*, 3962.

(30) Moody, D. C.; Zozulin, A. J.; Salazar, K. V. *Inorg. Chem.* **1982**, *21*, 3856.

(31) H. Gilman; R. G. Jones; E. Bindschadler; D. Blume; G. Karmas; G. A. Martin; Nobis, J. F., Jr.; J. R. Thirtle; H. L. Yale; Yoeman, F. A. *J. Am. Chem. Soc.* **1956**, *78*, 2790. Marks, T. J.; Seyam, A. M. *J. Organomet. Chem.* **1974**, *67*, 61.

(32) Sigurdson, E. R.; Wilkinson, G. *Dalton Trans.* **1977**, 812.

(33) Piers, W. E.; Emslie, D. J. H. *Coord. Chem. Rev.* **2002**, *233*, 131.

(34) Ciliberto, E.; Condorelli, G.; Fagan, P. J.; Manriquez, J. M.; Fragala, I.; Marks, T. J. *J. Am. Chem. Soc.* **1981**, *103*, 4755.

(35) Lauke, H.; Swepston, P. J.; Marks, T. J. *J. Am. Chem. Soc.* **1984**, *106*, 6841.

(36) Bucaille, A.; Le Borgne, T.; Ephritikhine, M.; Daran, J. C. *Organometallics* **2000**, *19*, 4912.

(37) Fortier, S.; Melot, B. C.; Wu, G.; Hayton, T. W. *J. Am. Chem. Soc.* **2009**, *131*, 15512.

(38) Seaman, L. A.; Walensky, J. R.; Wu, G.; Hayton, T. W. *Inorg. Chem.* **2013**, 3556.

(39) Pedrick, E. A.; Hrobarik, P.; Seaman, L. A.; Wu, G.; Hayton, T. W. *Chem. Commun.* **2016**, *52*, 689.

(40) Cruz, C. A.; Emslie, D. J. H.; Harrington, L. E.; Britten, J. F.; Robertson, C. M. *Organometallics* **2007**, *26*, 692.

(41) Köhler, E.; Brüser, W.; Thiele, K.-H. *J. Organomet. Chem.* **1974**, *76*, 235.

(42) Eisen, M. S.; Marks, T. J. *J. Am. Chem. Soc.* **1992**, *114*, 10358.

(43) Thiele, K.-H.; Opitz, R.; Köhler, E. *Z. Anorg. Allg. Chem.* **1977**, *435*, 45.

(44) Kraft, S. J.; Fanwick, P. E.; Bart, S. C. *J. Am. Chem. Soc.* **2012**, *134*, 6160.

(45) Seaman, L. A.; Pedrick, E. A.; Tsuchiya, T.; Wu, G.; Jakubikova, E.; Hayton, T. W. *Angew. Chem. Int. Ed.* **2013**, *52*, 10589.

(46) Behrle, A. C.; Myers, A. J.; Rungthanaphatsophon, P.; Lukens, W. W.; Barnes, C. L.; Walensky, J. R. *Chem. Commun.* **2016**, *52*, 14373.

(47) Edwards, P. G.; Andersen, R. A.; Zalkin, A. *J. Am. Chem. Soc.* **1981**, *103*, 7792.

(48) Edwards, P. G.; Andersen, R. A.; Zalkin, A. *Organometallics* **1984**, *3*, 293.

(49) Duhović, S.; Khan, S.; Diaconescu, P. L. *Chem. Commun.* **2010**, *46*, 3390.

(50) Vandersluys, W. G.; Burns, C. J.; Sattelberger, A. P. *Organometallics* **1989**, *8*, 855.

(51) Clark, D. L.; Gordon, J. C.; Hay, P. J.; Martin, R. L.; Poli, R. *Organometallics* **2002**, *21*, 5000. Perrin, L.; Maron, L.; Eisenstein, O.; Lappert, M. F. *New J. Chem.* **2003**, *27*, 121.

(52) Zwick, B. D., Sattelberger, A. P., and Avens, L. R., in *Transuranium Elements: A Half Century* (eds. L. R. Morss and J. Fuger), American Chemical Society,Washington, DC, **1992**, 239–46.

(53) Fortier, S.; Walensky, J. R.; Wu, G.; Hayton, T. W. *J. Am. Chem. Soc.* **2011**, *133*, 11732.

(54) Seaman, L. A.; Hrobarik, P.; Schettini, M. F.; Fortier, S.; Kaupp, M.; Hayton, T. W. *Angew. Chem. Int. Ed.* **2013**, *52*, 3259.

(55) Seyam, A. M. *Inorg. Chim. Acta.* **1985**, *110*, 123. Seyam, A. M. *Inorg. Chim. Acta* **1982**, *58*, 71.

(56) G. Wilke; B. Bogdanovic; P. Hardt; P. Heimbach; W. Keim; M. Kroner; W. Oberkirch; K. Tanaka; E. Steinrucke; D. Walter; Zimmermann, H. *Angew. Chem. Int. Ed. Engl.* **1966**, *5*, 151.

(57) Lugli, G.; Marconi, W.; Mazzei, A.; Paladino, N.; Pedretti, U. *Inorg. Chim. Acta* **1969**, *3*, 253. Brunelli, M.; Lugli, G.; Giacometti, G. *J. Magn. Resonance* **1973**, *9*, 247.

(58) Brunelli, M.; Perego, G.; Lugli, G.; Mazzei, A. *Dalton Trans.* **1979**, 861.

(59) Carlson, C. N.; Hanusa, T. P.; Brennessel, W. W. *J. Am. Chem. Soc.* **2004**, *126*, 10550.

(60) Jantunen, K. C.; Haftbaradaran, F.; Katz, M. J.; Batchelor, R. J.; Schatte, G.; Leznoff, D. B. *Dalton Trans.* **2005**, 3083.

(61) Tourneux, J.-C.; Berthet, J.-C.; Thuery, P.; Mezailles, N.; Le Floch, P.; Ephritikhine, M. *Dalton Trans.* **2010**, *39*, 2494.

(62) Webster, C. L.; Langeslay, R. R.; Ziller, J. W.; Evans, W. J. *Organometallics* **2016**, *35*, 520.

(63) Matson, E. M.; Forrest, W. P.; Fanwick, P. E.; Bart, S. C. *Organometallics* **2012**, *31*, 4467.

(64) Cruz, C. A.; Chu, T.; Emslie, D. J. H.; Jenkins, H. A.; Harrington, L. E.; Britten, J. F. *J. Organomet. Chem.* **2010**, *695*, 2798.

(65) Ren, W. S.; Zi, G. F.; Fang, D. C.; Walter, M. D. *Chem. Eur. J.* **2011**, *17*, 12669.

(66) Danopoulos, A. A.; Hankin, D. M.; Cafferkey, S. M.; Hursthouse, M. B. *Dalton Trans.* **2000**, 1613.

(67) Jantunen, K. C.; Batchelor, R. J.; Leznoff, D. B. *Organometallics* **2004**, *23*, 2186.

(68) Webster, C. L.; Bates, J. E.; Fang, M.; Ziller, J. W.; Furche, F.; Evans, W. J. *Inorg. Chem.* **2013**, *52*, 3565.

(69) Evans, W. J.; Nyce, G. W.; Forrestal, K. J.; Ziller, J. W. *Organometallics* **2002**, *21*, 1050.

(70) Van Der Sluys, W. G.; Burns, C. J.; Sattelberger, A. P. *Organometallics* **1989**, *8*, 855.

(71) Evans, W. J.; Kozimor, S. A.; Ziller, J. W.; Kaltsoyannis, N. *J. Am. Chem. Soc.* **2004**, *126*, 14533.

(72) Evans, W. J.; Traina, C. A.; Ziller, J. W. *J. Am. Chem. Soc.* **2009**, *131*, 17473.

(73) Straub, T.; Frank, W.; Reiss, G. J.; Eisen, M. S. *J. Chem. Soc. Dalton Trans.* **1996**, 2541.

(74) Zi, G. F.; Blosch, L. L.; Jia, L.; Andersen, R. A. *Organometallics* **2005**, *24*, 4602.

(75) Behrle, A. C.; Castro, L.; Maron, L.; Walensky, J. R. *J. Am. Chem. Soc.* **2015**, *137*, 14846.

(76) Bruno, J. W.; Marks, T. J.; Morss, L. R. *J. Am. Chem. Soc.* **1983**, *105*, 6824.

(77) Lin, Z. R.; Brock, C. P.; Marks, T. J. *Inorg. Chim. Acta* **1988**, *141*, 145.

(78) Manriquez, J. M.; Fagan, P. J.; Marks, T. J. *J. Am. Chem. Soc.* **1978**, *100*, 3939.

(79) Fagan, P. J.; Manriquez, J. M.; Maatta, E. A.; Seyam, A. M.; Marks, T. J. *J. Am. Chem. Soc.* **1981**, *103*, 6650.

(80) Pagano, J. K.; Dorhout, J. M.; Waterman, R.; Czerwinski, K. R.; Kiplinger, J. L. *Chem. Commun.* **2015**, *51*, 17379. Webster, C. L.; Ziller, J. W.; Evans, W. J. *Organometallics* **2014**, *33*, 433.

(81) Green, J. C.; Watts, O. *J. Organomet. Chem.* **1978**, *153*, C40.

(82) Montalvo, E.; Miller, K. A.; Ziller, J. W.; Evans, W. J. *Organometallics* **2010**, *29*, 4159.

(83) Berthet, J.-C.; Boisson, C.; Lance, M.; Vigner, J.; Nierlich, M.; Ephritikhine, M. *J. Chem. Soc. Dalton Trans.* **1995**, 3027.

(84) Ephritikhine, M. *Organometallics* **2013**, *32*, 2464. Bursten, B. E.; Strittmatter, R. J. *Angew. Chem. Int. Ed. Engl.* **1991**, *30*, 1069. Kanellakopulos, B., Cyclopentadienyl Compounds of the Actinide Elements. In *Organometallics of the f-Elements: Proceedings of the NATO Advanced Study Institute held at Sogesta, Urbino, Italy, September 11–22, 1978*, Marks, T. J.; Fischer, R. D., Eds.; Springer Netherlands: Dordrecht, 1979; p 1. Albrecht-Schmitt, T. E., *Organometallic and Coordination Chemistry of the Actinides*, Springer Berlin Heidelberg: 2008.

(85) Fischer, E. O., Von; Treiber, A. *Z. Naturforschung* **1962**, *17b*, 276. Maier, R.; Kanellakopulos, B.; Apostolidis, C.; Meyer, D.; Rebizant, J. *J. Alloy. Compd.* **1993**, *190*, 269.

(86) Fischer, E. O., Von; Hristidu, Y. *Z. Naturforschung* **1962**, *17b*, 275. Burns, J. H. *J. Am. Chem. Soc.* **973**, *95*, 3815.

(87) Baumgärtner., F.; E. O. Fischer; B. Kanellakopulos; Laubereau, P. *Angew. Chem. Int. Ed. Engl.* **1969**, *8*, 202.

(88) Baumgärtner., F.; E. O. Fischer; B. Kanellakopulos; Laubereau, P. *Angew. Chem. Int. Ed. Engl.* **1968**, *7*, 634.

(89) Clark, D. L., Hecker, S. S., Jarvinen, G. D., Neu, M. P., Plutonium. in *The Chemistry of the Actinide and Transactinide Elements*, 4 ed.; Morss, L. R.; Edelstein, N. M.; Fuger, J.; Springer: Dordrecht, The Netherlands, 2010; Vol. 2, p 813.

(90) J. L. Calderon; F.A. Cotton; B. G. DeBoer; Takats, J. J. *J. Am. Chem. Soc.* **1971**, *93*, 3592. Rogers, R. D.; Bynum, R. V.; Atwood, J. L. *J. Am. Chem. Soc.* **1981**, *103*, 692.

(91) V. I. Kulishov; N. G. Bokii; Struchkov, Y. T. *J. Struct. Chem.* **1970**, *11*, 700.

(92) Rebizant, J.; Spirlet, M. R.; Kanellakopulos, B.; Dornberger, E. *J. Less-Common Met.* **1986**, *122*, 211.

(93) Reynolds, L. T.; Wilkinson, G. J. *Inorg. Nucl. Chem.* **1956**, *2*, 246.

(94) Marks, T. J.; Seyam, A. M.; Kolb, J. R. *J. Am. Chem. Soc.* **1973**, *95*, 5529.

(95) Weydert, M.; Brennan, J. G.; Andersen, R. A.; Bergman, R. G. *Organometallics* **1995**, *14*, 3942.

(96) Gebala, A. E. T., M. *J. Am. Chem. Soc.* **1973**, *95*, 91. Villiers, C.; Ephritikhine, M. *J. Organomet. Chem.* **1990**, *393*, 339. Halstead, G. W.; Baker, E. C.; Raymond, K. N. *J. Am. Chem. Soc.* **1975**, *97*, 3049.

(97) Berthet, J.-C.; Lemarechal, J. F.; Lance, M.; Nierlich, M.; Vigner, J.; Ephritikhine, M. *J. Chem. Soc. Dalton Trans.* **1992**, 1573.

(98) Leverd, P. C.; Ephritikhine, M.; Lance, M.; Vigner, J.; Nierlich, M. *J. Organomet. Chem.* **1996**, *507*, 229.

(99) Zanella, P.; Ossola, F.; Porchia, M.; Rossetto, G.; Villa, A. C.; Guastini, C. *J. Organomet. Chem.* **1987**, *323*, 295. Porchia, M.; Brianese, N.; Ossola, F.; Rossetto, G.; Zanella, P. *J. Chem. Soc. Dalton Trans.* **1987**, 691.

(100) Ossola, F.; Brianese, N.; Porchia, M.; Rossetto, G.; Zanella, P. *J. Organomet. Chem.* **1986**, *310*, C1.

(101) Porchia, M.; Brianese, N.; Casellato, U.; Ossola, F.; Rossetto, G.; Zanella, P.; Graziani, R. *J. Chem. Soc. Dalton Trans.* **1989**, 677. Porchia, M.; Ossola, F.; Rossetto, G.; Zanella, P.; Brianese, N. *J. Chem. Soc. Chem. Commun.* **1987**, 550. Porchia, M.; Casellato, U.; Ossola, F.; Rossetto, G.; Zanella, P.; Graziani, R. *J. Chem. Soc. Chem. Commun.* **1986**, 1034.

(102) Ossola, F.; Brianese, N.; Porchia, M.; Rossetto, G.; Zanella, P. *Inorg. Synth.* **1992**, *29*, 234.

(103) Paolucci, G.; Rossetto, G.; Zanella, P.; Fischer, R. D. *J. Organomet. Chem.* **1985**, *284*, 213.

(104) Ossola, F.; Rossetto, G.; Zanella, P.; Paolucci, G.; Fischer, R. D. *J. Organomet. Chem.* **1986**, *309*, 55.

(105) Tourneux, J.-C., Thuery, P., Berthet, J.-C., Ephritikhine, M. 2016, private communication to the Cambridge Structural Database, deposition number CCDC 958748.

(106) Bagnall, K. W.; Payne, G. F.; Alcock, N. W.; Flanders, D. J.; Brown, D. *J. Chem. Soc. Dalton Trans.* **1986**, 783.

(107) Mintz, E. A.; Moloy, K. G.; Marks, T. J.; Day, V. W. *J. Am. Chem. Soc.* **1982**, *104*, 4692.

(108) Cymbaluk, T. H.; Ernst, R. D.; Day, V. W. *Organometallics* **1983**, *2*, 963.

(109) Marks, T. J.; Day, V. W., Actinide Hydrocarbyl and Hydride Chemistry. In *Fundamental and Technological Aspects of Organo-f-Element Chemistry*, Nato Science Series C: *Vol. 155*, Marks, T. J.; Fragalà, I. L., Eds.; D. Reidel Publishing Company: Dordrecht, 1985; p 115.

(110) Butcher, R. J.; Clark, D. L.; Grumbine, S. K.; Scott, B. L.; Watkin, J. G. *Organometallics* **1996**, *15*, 1488.

(111) Johnson, S. A.; Bart, S. C. *Dalton Trans.* **2015**, *44*, 7710.

(112) Ernst, R. D.; Kennelly, W. J.; Day, C. S.; Day, V. W.; Marks, T. J. *J. Am. Chem. Soc.* **1979**, *101*, 2656.

(113) Zalkin, A.; Brennan, J. G.; Andersen, R. A. *Acta Crystallogr. C* **1987**, *43*, 418. Zalkin, A.; Brennan, J. G.; Andersen, R. A. *Acta Crystallogr. C* **1987**, *43*, 421.

(114) Webster, C. L.; Ziller, J. W.; Evans, W. J. *Organometallics* **2012**, *31*, 7191.

(115) Lukens, W. W.; Beshouri, S. M.; Blosch, L. L.; Stuart, A. L.; Andersen, R. A. *Organometallics* **1999**, *18*, 1235. Ren, W.; Zhao, N.; Chen, L.; Zi, G. *Inorg. Chem. Commun.* **2013**, *30*, 26. Schelter, E. J.; Veauthier, J. M.; Graves, C. R.; John, K. D.; Scott, B. L.; Thompson, J. D.; Pool-Davis-Tournear, J. A.; Morris, D. E.; Kiplinger, J. L. *Chem. Eur. J.* **2008**, *14*, 7782.

(116) Zi, G. F.; Jia, L.; Werkema, E. L.; Walter, M. D.; Gottfriedsen, J. P.; Andersen, R. A. *Organometallics* **2005**, *24*, 4251.

(117) Bruno, J. W.; Smith, G. M.; Marks, T. J.; Fair, C. K.; Schultz, A. J.; Williams, J. M. *J. Am. Chem. Soc.* **1986**, *108*, 40.

(118) Fendrick, C. M.; Schertz, L. D.; Day, V. W.; Marks, T. J. *Organometallics* **1988**, *7*, 1828.

(119) Schnabel, R. C.; Scott, B. L.; Smith, W. H.; Burns, C. J. *J. Organomet. Chem.* **1999**, *591*, 14.

(120) Dash, A. K.; Gourevich, I.; Wang, J. Q.; Wang, J.; Kapon, M.; Eisen, M. S. *Organometallics* **2001**, *20*, 5084.

(121) Stubbert, B. D.; Stern, C. L.; Marks, T. J. *Organometallics* **2003**, *22*, 4836.

(122) Wobser, S. D.; Marks, T. J. *Organometallics* **2013**, *32*, 2517.

(123) Maynadié, J.; Berthet, J.-C.; Thuéry, P.; Ephritikhine, M. *J. Am. Chem. Soc.* **2006**, *128*, 1082. Berthet, J.-C.; Maynadie, J.; Thuery, P.; Ephritikhine, M. *Dalton Trans.* **2010**, *39*, 6801.

(124) Maynadie, J.; Berthet, J. C.; Thuery, P.; Ephritikhine, M. *Organometallics* **2007**, *26*, 4585.

(125) Jantunen, K. C.; Burns, C. J.; Castro-Rodriguez, I.; Da Re, R. E.; Golden, J. T.; Morris, D. E.; Scott, B. L.; Taw, F. L.; Kiplinger, J. L. *Organometallics* **2004**, *23*, 4682.

(126) Evans, W. J.; Siladke, N. A.; Ziller, J. W. *Chem. Eur. J.* **2010**, *16*, 796.

(127) Manriquez, J. M.; Fagan, P. J.; Marks, T. J.; Day, C. S.; Day, V. W. *J. Am. Chem. Soc.* **1978**, *100*, 7112.

(128) Pool, J. A.; Scott, B. L.; Kiplinger, J. L. *J. Am. Chem. Soc.* **2005**, *127*, 1338.

(129) Fendrick, C. M.; Marks, T. J. *J. Am. Chem. Soc.* **1986**, *108*, 425.

(130) Braunschweig, H.; Gackstatter, A.; Kupfer, T.; Radacki, K.; Franke, S.; Meyer, K.; Fucke, K.; Lemee-Cailleau, M. H. *Inorg. Chem.* **2015**, *54*, 8022.

(131) Streitwieser, A., Jr.; Müller-Westerhoff, U. *J. Am. Chem. Soc.* **1968**, *90*, 7364.

(132) Zalkin, A.; Raymond, K. N. *J. Am. Chem. Soc.* **1969**, *91*, 5667.

(133) Kerridge, A.; Kaltsoyannis, N. *J. Phys. Chem. A* **2009**, *113*, 8737.

(134) Streitwieser, A.; Yoshida, N. *J. Am. Chem. Soc.* **1969**, *91*, 7528.

(135) Karraker, D. G.; Stone, J. A.; Jones, E. R., Jr.; Edelstein, N. *J. Am. Chem. Soc.* **1970**, *92*, 4841.

(136) Burns, C. J.; Eisen, M. S., Organoactinide Chemistry: Synthesis and Characterization. In *The Chemistry of the Transactinide Elements*, 3 ed.; Morss, L. R.; Edelstein, N. M.; Fuger, J., Eds.; Springer: Dordrecht, The Netherlands, 2006; Vol. 5, p 2799.

(137) A. Streitwieser, J.; Barros, M. T.; Wang, H.-K.; Boussie, T. R. *Organometallics* **1993**, *12*, 5023.

(138) Braunschweig, H.; Celik, M. A.; Dìck, K.; Hupp, F.; Krummenacher, I. *Chem. Eur. J.* **2015**, *21*, 9339

(139) Burton, N. C.; Cloke, F. G. N.; Hitchcock, P. B.; Delemos, H. C.; Sameh, A. A. *J. Chem. Soc. Chem. Commun.* **1989**, 1462.

(140) Kilimann, U.; Herbst-Irmer, R.; Stalke, D.; Edelmann, F. T. *Angew. Chem. Int. Ed. Engl.* **1994**, *33*, 1618. Apostolidis, C.; Edelmann, F. T.; Kanellakopulos, B.; Reißmann, U. *Z. Naturforsch. B* **1999**, *54*, 960.

(141) Summerscales, O. T.; Cloke, F. G. N.; Hitchcock, P. B.; Green, J. C.; Hazari, N. *Science* **2006**, *311*, 829.

(142) Lorenz, V.; Schmiege, B. M.; Hrib, C. G.; Ziller, J. W.; Edelmann, A.; Blaurock, S.; Evans, W. J.; Edelmann, F. T. *J. Am. Chem. Soc.* **2011**, *133*, 1257.

(143) Lyttle, M. H.; Streitwieser, A.; Miller, M. J. *J. Org. Chem.* **1989**, *54*, 2331.

(144) Seyferth, D. *Organometallics* **2004**, *23*, 3562.

(145) Cendrowski-Guillaume, S. M.; Nierlich, M.; Ephritikhine, M. *Eur. J. Inorg. Chem.* **2001**, 1495.

(146) Boussie, T. R.; Moore, R. M.; Streitwieser, A.; Zalkin, A.; Brennan, J.; Smith, K. A. *Organometallics* **1990**, *9*, 2010.

(147) Boisson, C.; Berthet, J.-C.; Lance, M.; Vigner, J.; Nierlich, M.; Ephritikhine, M. *J. Chem. Soc. Dalton Trans.* **1996**, 947.

(148) Boisson, C.; Berthet, J.-C.; Ephritikhine, M.; Lance, M.; Nierlich, M. *J. Organomet. Chem.* **1996**, *522*, 249.

(149) Berthet, J.-C.; Lemarechal, J. F.; Ephritikhine, M. *J. Organomet. Chem.* **1994**, *480*, 155.

(150) Gilbert, T. M.; Ryan, R. R.; Sattelberger, A. P. *Organometallics* **1989**, *8*, 857.

(151) Evans, W. J.; Kozimor, S. A.; Ziller, J. W. *Polyhedron* **2006**, *25*, 484.

(152) Evans, W. J.; Takase, M. K.; Ziller, J. W.; Rheingold, A. L. *Organometallics* **2009**, *28*, 5802.

(153) Takase, M. K.; Siladke, N. A.; Ziller, J. W.; Evans, W. J. *Organometallics* **2011**, *30*, 458.

(154) Evans, W. J.; Nyce, G. W.; Ziller, J. W. *Angew. Chem. Int. Ed.* **2000**, *39*, 240. Evans, W. J.; Takase, M. K.; Ziller, J. W.; DiPasquale, A. G.; Rheingold, A. L. *Organometallics* **2009**, *28*, 236.

(155) Higgins, J. A.; Cloke, F. G. N.; Roe, S. M. *Organometallics* **2013**, *32*, 5244.

(156) Button, Z. E.; Higgins, J. A.; Suvova, M.; Cloke, F. G. N.; Roe, S. M. *Dalton Trans.* **2015**, *44*, 2588.

(157) Summerscales, O. T.; Cloke, F. G. N.; Hitchcock, P. B.; Green, J. C.; Hazari, N. *J. Am. Chem. Soc.* **2006**, *126*, 9602.

(158) Turner, H. W.; Andersen, R. A.; Zalkin, A.; Templeton, D. H. *Icarus* **1979**, *18*, 1221. Simpson, S. J.; Turner, H. W.; Andersen, R. A. *J. Am. Chem. Soc.* **1979**, *101*, 7728. Simpson, S. J.; Andersen, R. A. *J. Am. Chem. Soc.* **1981**, *103*, 4063. Baudry, D.; Dormond, A.; Hafid, A. *J. Organomet. Chem.* **1995**, *494*, C22.

(159) Diaconescu, P. L.; Odom, A. L.; Agapie, T.; Cummins, C. C. *Organometallics* **2001**, *20*, 4993.

(160) Stewart, J. L.; Andersen, R. A. *J. Chem. Soc. Chem. Commun.* **1987**, 1846.

(161) Baudin, C.; Ephritikhine, M. *J. Organomet. Chem.* **1989**, *364*, C1. Baudin, C.; Baudry, D.; Ephritikhine, M.; Lance, M.; Navaza, A.; Nierlich, M.; Vigner, J. *J. Organomet. Chem.* **1991**, *415*, 59.

(162) Clark, D. L.; Grumbine, S. K.; Scott, B. L.; Watkin, J. G. *Organometallics* **1996**, *15*, 949.

(163) Beshouri, S. M.; Fanwick, P. E.; Rothwell, I. P.; Huffman, J. C. *Organometallics* **1987**, *6*, 2498.

(164) Wedler, M.; Knösel, F.; Edelmann, F. T.; Behrens, U. *Chem. Ber.* **1992**, *125*, 1313.

(165) Antunes, M. A.; Domingos, Â.; dos Santos, I. C.; Marques, N.; Takats, J. *Polyhedron* **2005**, *24*, 3038. Silva, M.; Domingos, Â.; de Matos, A. P.; Marques, N.; Trofimenko, S. *Dalton Trans.* **2000**, 4628. Silva, M.; Marques, N.; de Matos, A. P. *J. Organomet. Chem.* **1995**, *493*, 129. Campello, M. P. C.; Domingos, Â.; Galvao, A.; de Matos, A. P.; Santos, I. *J. Organomet. Chem.* **1999**, *579*, 5. Campello, M. P. C.; Calhorda, M. J.; Domingos, Â.; Galvão, A.; Leal, J. P.; de Matos, A. P.; Santos, I. *J. Organomet. Chem.* **1997**, *538*, 223. Domingos, Â.; Marques, N.; de Matos, A. P.; Santos, I.; Silva, M. *Organometallics* **1994**, *13*, 654.

(166) Roussel, P.; Boaretto, R.; Kingsley, A. J.; Alcock, N. W.; Scott, P. *Dalton Trans.* **2002**, 1423. Boaretto, R.; Roussel, P.; Kingsley, A. J.; Munslow, I. J.; Sanders, C. J.; Alcock, N. W.; Scott, P. *Chem. Commun.* **1999**, 1701.

(167) Matson, E. M.; Kiernicki, J. J.; Fanwick, P. E.; Bart, S. C. *Eur. J. Inorg. Chem.* **2016**, 2527. Matson, E. M.; Crestani, M. G.; Fanwick, P. E.; Bart, S. C. *Dalton Trans.* **2012**, *41*, 7952.

(168) Matson, E. M.; Forrest, W. P.; Fanwick, P. E.; Bart, S. C. *Organometallics* **2013**, *32*, 1484.

(169) Matson, E. M.; Forrest, W. P.; Fanwick, P. E.; Bart, S. C. *J. Am. Chem. Soc.* **2011**, *133*, 4948.

(170) Gardner, B. M.; Lewis, W.; Blake, A. J.; Liddle, S. T. *Organometallics* **2015**, *34*, 2386.

(171) Gardner, B. M.; Cleaves, P. A.; Kefalidis, C. E.; Fang, J.; Maron, L.; Lewis, W.; Blake, A. J.; Liddle, S. T. *Chem. Sci.* **2014**, *5*, 2489.

(172) Gardner, B. M.; McMaster, J.; Lewis, W.; Blake, A. J.; Liddle, S. T. *J. Am. Chem. Soc.* **2009**, *131*, 10388.

(173) Lu, E. L.; Cooper, O. J.; McMaster, J.; Tuna, F.; McInnes, E. J. L.; Lewis, W.; Blake, A. J.; Liddle, S. T. *Angew. Chem. Int. Ed.* **2014**, *53*, 6696.

(174) Hayes, C. E.; Leznoff, D. B. *Organometallics* **2010**, *29*, 767.

(175) Hayes, C. E.; Platel, R. H.; Schafer, L. L.; Leznoff, D. B. *Organometallics* **2012**, *31*, 6732.

(176) Hayes, C. E.; Gill, D. E.; Brown, M. L.; Leznoff, D. B. *Eur. J. Inorg. Chem.* **2014**, 3690. Hayes, C. E.; Leznoff, D. B. *Coord. Chem. Rev.* **2014**, *266*, 155.

(177) Andreychuk, N. R.; Ilango, S.; Vidjayacoumar, B.; Emslie, D. J. H.; Jenkins, H. A. *Organometallics* **2013**, *32*, 1466.

(178) Cruz, C. A.; Emslie, D. J. H.; Jenkins, H. A.; Britten, J. F. *Dalton Trans.* **2010**, *39*, 6626.

(179) Cruz, C. A.; Emslie, D. J. H.; Robertson, C. M.; Harrington, L. E.; Jenkins, H. A.; Britten, J. F. *Organometallics* **2009**, *28*, 1891.

(180) Cruz, C. A.; Emslie, D. J. H.; Harrington, L. E.; Britten, J. F. *Organometallics* **2008**, *27*, 15.

(181) Monreal, M. J.; Diaconescu, P. L. *J. Am. Chem. Soc.* **2010**, *132*, 7676. Duhovic, S.; Monreal, M. J.; Diaconescu, P. L. *J. Organomet. Chem.* **2010**, *695*, 2822. Monreal, M. J.; Khan, S.; Diaconescu, P. L. *Angew. Chem. Int. Ed.* **2009**, *48*, 8352.

(182) Diaconescu, P. L. *Acc. Chem. Res.* **2010**, *43*, 1352.

(183) Monreal, M. J.; Diaconescu, P. L. *Organometallics* **2008**, *27*, 1702.

(184) Matson, E. M.; Franke, S. M.; Anderson, N. H.; Cook, T. D.; Fanwick, P. E.; Bart, S. C. *Organometallics* **2014**, *33*, 1964.

(185) Mora, E.; Maria, L.; Biswas, B.; Camp, C.; Santos, I. C.; Pecaut, J.; Cruz, A.; Carretas, J. M.; Marcalo, J.; Mazzanti, M. *Organometallics* **2013**, *32*, 1409.

(186) Hayes, C. E.; Leznoff, D. B. *Coord. Chem. Rev*. **2014**, *266–267*, 155 and references therein.

(187) Vidjayacoumar, B.; Ilango, S.; Ray, M. J.; Chu, T.; Kolpin, K. B.; Andreychuk, N. R.; Cruz, C. A.; Emslie, D. J. H.; Jenkins, H. A.; Britten, J. F. *Dalton Trans.* **2012**, *41*, 8175.

(188) Wilson, D. J.; Sebastian, A.; Cloke, F. G. N.; Avent, A. G.; Hitchcock, P. B. *Inorg. Chim. Acta* **2003**, *345*, 89.

(189) Kiernicki, J. J.; Staun, S. L.; Zeller, M.; Bart, S. C. *Organometallics* **2017**, *36*, 665.

(190) Bénaud, O.; Berthet, J.-C.; Thuéry, P.; Ephritikhine, M. *Inorg. Chem.* **2011**, *50*, 12204.

(191) Korobkov, I.; Gorelsky, S.; Gambarotta, S. *J. Am. Chem. Soc.* **2009**, *131*, 10406.

(192) Athimoolam, A.; Gambarotta, S.; Korobkov, I. *Can. J. Chem.* **2005**, *83*, 832. Batrice, R. J.; Fridman, N.; Eisen, M. S. *Inorg. Chem.* **2016**, *55*, 2998. Swartz, D. L.; Spencer, L. P.; Scott, B. L.; Odom, A. L.; Boncella, J. M. *Dalton Trans.* **2010**, *39*, 6841. Korobkov, I.; Vidjayacoumar, B.; Gorelsky, S. I.; Billone, P.; Gambarotta, S. *Organometallics* **2010**, *29*, 692.

(193) Arnold, P. L.; Farnaby, J. H.; Gardiner, M. G.; Love, J. B. *Organometallics* **2015**, *34*, 2114.

(194) Miller, K. L.; Williams, B. N.; Benitez, D.; Carver, C. T.; Ogilby, K. R.; Tkatchouk, E.; Goddard, W. A., III; Diaconescu, P. L. *J. Am. Chem. Soc.* **2010**, *132*, 342.

(195) Jia, L.; Yang, X.; Stern, C. L.; Marks, T. J. *Organometallics* **1997**, *16*, 842.

(196) Chen, Y.-X.; Stern, C. L.; Yang, S.; Marks, T. J. *J. Am. Chem. Soc.* **1996**, *118*, 12451.

(197) Jia, L.; Yang, X.; Stern, C.; Marks, T. J. *Organometallics* **1994**, *13*, 3755.

(198) Yang, X.; King, W. A.; Sabat, M.; Marks, T. J. *Organometallics* **1993**, *12*, 4254.

(199) Yang, X.; Stern, C. L.; Marks, T. J. *Organometallics* **1991**, *10*, 840.

(200) Lin, Z.; Le Marechal, J.-F.; Sabat, M.; Marks, T. J. *J. Am. Chem. Soc.* **1987**, *109*, 4127.

(201) Chen, Y. X.; Metz, M. V.; Li, L. T.; Stern, C. L.; Marks, T. J. *J. Am. Chem. Soc.* **1998**, *120*, 6287.

(202) Evans, W. J.; Kozimor, S. A.; Ziller, J. W. *Organometallics* **2005**, *24*, 3407.

(203) Dietrich, H. M.; Ziller, J. W.; Anwander, R.; Evans, W. J. *Organometallics* **2009**, *28*, 1173.

(204) Dash, A. K.; Wang, J. X.; Berthet, J.-C.; Ephritikhine, M.; Eisen, M. S. *J. Organomet. Chem.* **2000**, *604*, 83.

(205) Cendrowski-Guillaume, S. M.; Lance, M.; Nierlich, M.; Ephritikhine, M. *Organometallics* **2000**, *19*, 3257.

(206) Moisan, L.; Le Borgne, T.; Villiers, C.; Thuery, P.; Ephritikhine, M. *C. R. Chim.* **2007**, *10*, 883.

(207) *Chem. Eng. News* **1978**, *56*, 24.

(208) Bowman, R. G.; Nakamura, R.; Fagan, P. J.; Burwell, R. L.; Marks, T. J. *J. Chem. Soc. Chem. Commun.* **1981**, 257.

(209) He, M.-Y.; Xiong, G.; Toscano, P. J.; Burwell, R. L., Jr.; Marks, T. J. *J. Am. Chem. Soc.* **1985**, *107*, 641. Toscano, P. J.; Marks, T. J. *J. Am. Chem. Soc.* **1985**, *107*, 653. Finch, W. C.; Gillespie, R. D.; Hedden, D.; Marks, T. J. *J. Am. Chem. Soc.* **1990**, *112*, 6221. Hedden, D.; Marks, T. J. *J. Am. Chem. Soc.* **1988**, *110*, 1647. Marks, T. J., *Acc. Chem. Res.* **1992**, *25*, 57.

(210) Marks, T. J., Ja, L., Yang, X. U.S. Patent 5,477,895, 1995; Marks, T. J., Chen, Y.-X. U.S. Patent 6,229,034 B1, 2001; Marks, T. J., Chen, Y.-X. U.S. Patent 6,274,752 B1, 2001; Marks, T. J., Chen, Y.-X. U.S. Patent 6,403,732 B2, 2002; Marks, T. J., Chen, Y.-X. U.S. Patent 6,388,114 B1, 2002.

(211) Campbell, R. E., Jr. (The Dow Chemical Company) U.S. Patent 4,665,046, 1987.

(212) Evans, W. J.; Forrestal, K. J.; Ziller, J. W. *Angew. Chem. Int. Ed.* **1997**, *36*, 774.

(213) Domeshek, E.; Batrice, R. J.; Aharonovich, S.; Tumanskii, B.; Botoshansky, M.; Eisen, M. S. *Dalton Trans.* **2013**, *42*, 9069.

(214) Porter, R. M.; Danopoulos, A. A. *Polyhedron* **2006**, *25*, 859.

(215) Nowick, J. S.; Ballester, P.; Ebmeyer, F.; Julius Rebek, J. *J. Am. Chem. Soc.* **1990**, *112*, 8902.

(216) Korobkov, I.; Gambarotta, S.; Yap, G. P. A. *Angew. Chem. Int. Ed.* **2003**, *42*, 4958.

(217) A. Zaeni, F. T. Edelmann, T. Kaehler and F. Olbrich, 2003, private communication to the Cambridge Structural Database, deposition number CCDC 178656.

(218) Kawaguchi, H.; Matsuo, T. *J. Organomet. Chem.* **2005**, *690*, 5333.

(219) Reynolds, J. G.; Zalkin, A.; Templeton, D. H.; Edelstein, N. M. *Inorg. Chem.* **1977**, *16*, 1090.

(220) Silva, M.; Antunes, M. A.; Dias, M.; Domingos, Â.; dos Santos, I. C.; Marcalo, J.; Marques, N. *Dalton Trans.* **2005**, 3353.

(221) Cramer, R. E.; Engelhardt, U.; Higa, K. T.; Gilje, J. W. *Organometallics* **1987**, *6*, 41.

(222) Cantat, T.; Scott, B. L.; Morris, D. E.; Kiplinger, J. L. *Inorg. Chem.* **2009**, *48*, 2114.

(223) Old, J.; Danopoulos, A. A.; Winston, S. *New J. Chem.* **2003**, *27*, 672. Salmon, L.; Thuéry, P.; Asfari, Z.; Ephritikhine, M. *Dalton Trans.* **2006**, 3006.

(224) For advantages of the $[NBu_4][B(C_6F_5)_4]$ anion as the base electrolyte in transition metal electrochemistry, see: (a) Ohrenberg, N. C., Paradee, L. M., DeWitte, R. J., Chong, D. S., Geiger,W. E. *Organometallics*, **2010**, *29*, 3179; (b) Swarts,J. C., Nafady, A., Roudebush, J. H., Trupia, S., Geiger, W. E. *Inorg. Chem.*, **2009**, *48*, 2156; (c) Chong, D. S. Slote J., Geiger, W. E. *J. Electroanal. Chem.*, **2009**, *630*, 28; (d) Nafady, A., Geiger, W. E., *Organometallics*, **2008**, *27*, 5624; (e) Chong, D., Laws, D. R., Nafady, A., Costa, P. J., Rheingold, A. L., Calhorda, M. J., Geiger, W. E. *J. Am. Chem. Soc.*, **2008**, *130*, 2692; (f) Nafady, A., Chin, T. T., Geiger, W. E. *Organometallics*, **2006**, *25*, 1654; (g) Barriere, F., Kirss, R. U., Geiger, W. E. *Organometallics*, **2005**, *24*, 48; (h) Camire, N., Nafady, A., Geiger, W. E. *J. Am. Chem. Soc.*, **2002**, *124*, 7260; (i) Camire, N., Mueller-Westerhoff, U. T., Geiger, W. E. *J. Organomet. Chem.*, **2001**, *637*, 823; (j) LeSuer, R. J., Buttolph, C., Geiger, W. E. *Anal. Chem.*, **2004**, *76*, 6395; (k) Barriere, F., Geiger, W. E. *J. Am. Chem. Soc.*, **2006**, *128*, 3980. For examples of the use of the $[NR_4][B(C_6F_5)_4]$ (R = $^n$Bu or $^i$Pr) base electrolytes in actinide electrochemistry,

see: (a) Thomson, R. K., Scott, B. L., Morris D. E., Kiplinger, J. L., *C. R. Chim.*, **2010**, *13*, 790 and references therein; (b) Schelter, E. J., Wu, R. L., Scott, B. L., Thompson, J. D., Cantat, T., John, K. D., Batista, E. R. Morris, D. E., Kiplinger, J. L., *Inorg. Chem.*, **2010**, *49*, 924; (c) Cantat, T., Scott, B. L., Morris, D. E., Kiplinger, J. L., *Inorg. Chem*., **2009**, *48*, 2114; (d) Morris, D. E., Da Re, R. E., Jantunen, K. C., Castro-Rodriguez, I., Kiplinger, J. L., *Organometallics*, **2004**, *23*, 5142; (e) Schelter, E. K., Yang, P., Scott, B. L.,Thompson, J. D., Martin, R. L., Hay, P. J., Morris, D. E., Kiplinger, J. L. *Inorg. Chem.*, **2007**, *46*, 7477.

(225) Morris, D. E.; Da Re, R. E.; Jantunen, K. C.; Castro-Rodriguez, I.; Kiplinger, J. L. *Organometallics* **2004**, *23*, 5142.

(226) Korobkov, I.; Gambarotta, S.; Yap, G. P. A. *Organometallics* **2001**, *20*, 2552.

(227) Brennan, J.; Shinomoto, R.; Zalkin, A.; Edelstein, N. *Inorg. Chem.* **1984**, *23*, 4143.

(228) Roger, M.; Arliguie, T.; Thuery, P.; Ephritikhine, M. *Inorg. Chem.* **2008**, *47*, 3863.

(229) For examples of considerably shifted $^{1}$H NMR resonances arising from the α-protons of paramagnetic uranium alkyl complexes, see: (a) Evans, W. J.; Walensky, J. R.; Ziller, J. W.; Rheingold, A. L. *Organometallics* **2009**, *28*, 3350; (b) Jantunen, K. C.; Batchelor, R. J.; Leznoff, D. B. *Organometallics* **2004,** *23*, 2186; (c) Evans, W. J.; Kozimor, S. A.; Ziller, J. W. *Organometallics* **2005**, *24*, 3407; (d) Evans, W. J.; Montalvo, E.; Ziller, J. W.; DiPasquale, A. G.; Rheingold, A. L. *Inorg. Chem.* **2010**, *49*, 222; (e) Marks, T. J.; Seyam, A. M. *J. Am. Chem. Soc.* **1972**, *94*, 6545; (f) Jantunen, K. C.; Haftbaradaran, F.; Katz, M. J.; Batchelor, R. J.; Schatte, G.; Leznoff, D. B. *Dalton Trans*. **2005**, 3083.

(230) Wetzel, D. M.; Brauman, J. I. *J. Am. Chem. Soc.* **1988**, *110*, 8333. Damrauer, R.; Kass, S. R.; Depuy, C. H. *Organometallics* **1988**, *7*, 637.

(231) Kiplinger, J. L.; Scott, B. L.; Burns, C. J. *Inorg. Chim. Acta* **2005**, *358*, 2813.

(232) Montalvo, E.; Ziller, J. W.; DiPasquale, A. G.; Rheingold, A. L.; Evans, W. J. *Organometallics* **2010**, *29*, 2104.

(233) Duhović, S.; Oria, J. V.; Odoh, S. O.; Schreckenbach, G.; Batista, E. R.; Diaconescu, P. L. *Organometallics* **2013**, *32*, 6012.

(234) Several groups have observed that organothorium species are invariably less soluble than the analogous organouranium complexes; [$Cp^*_2AnR_2$] systems, see: (a) Fagan, P. J.; Manriquez, J. M.; Maatta, E. A.; Seyam, A. M.; Marks, T. J. *J. Am. Chem. Soc*. **1981**, *103*, 6650; [$Cp_3AnR$] systems, see: (b) Marks, T. J.; Wachter, W. A. *J. Am. Chem. Soc.* **1976**, *98*, 703; [$(COT)_2An$] systems, see: (c) Streitwieser, A.; Yoshida, N. J. Am. Chem. Soc. **1969**, *91*, 7528; (d) Streitwieser, A.; Mueller-Westerhoff, U. *J. Am. Chem. Soc*. **1968**, *90*, 7364; [$Cp_4An$] systems, see: (e) Edelmann, F. T.; Herrmann, W. A., *Synthetic Methods of Organometallic and Inorganic Chemistry*, Volume 6, 1997: Volume 6: Lanthanides and Actinides, Thieme: 2014; p 176.

(235) Evans, W. J.; Kozimor, S. A.; Ziller, J. W. *Organometallics* **2005**, *24*, 3407.

(236) *Intraligand* uranium–arene interactions have been observed in bulky aryloxide species and in complexes featuring multidentate ligands with arene units in the ligand backbone. Selected examples include: (a) Franke, S. M.; Tran, B. L.; Heinemann, F. W.; Hieringer, W.; Mindiola, D. J.; Meyer, K. *Inorg. Chem*. **2013,** *52*, 10552; (b) Arnold, P. A.; Farnaby, J. H; Gardiner, M. G; Love, J. B. *Organometallics* **2015**, *34*, 2114; (c) Halter, D. P.; La Pierre, H. S.; Heinemann, F. W.; Meyer, K. *Inorg. Chem*. **2014**, *53*, 8418. Additionally, a family of uranium complexes bearing *reduced* arene ligands have also been reported. Selected examples include: (d) Diaconescu, P. L.; Arnold, P. L.; Baker, T. A.; Mindiola, D. J.; Cummins, C. C. *J. Am. Chem. Soc*. **2000**, *122*, 6108; (e) Arnold, P. L.; Mansell, S. M.; Maron, L.; McKay, D. *Nat. Chem*. **2012**, *4*, 668; (f) Mills, D. P.; Moro, F.; McMaster, J.; van Slageren, J.; Lewis, W.; Blake, A. J.; Liddle, S. T. *Nat. Chem*. **2011**, *3*, 454; (g) Evans, W. J.; Traina, C. A.; Ziller, J. W. *J. Am. Chem. Soc.* **2009**, *131*, 17473; (h) Mougel, V.; Camp, C.; Pecaut, J.; Coperet, C.; Maron, L.; Kefalidis, C. E.; Mazzanti, M. *Angew. Chem. Int. Ed*. **2012**, *51*, 12280.

(237) Cotton, F. A.; Schwotzer, W. *Organometallics* **1985**, *4*, 942. Campbell, G. C.; Cotton, F. A.; Haw, J. F.; Schwotzer, W. *Organometallics* **1986**, *5*, 274.

(238) Hayes, P. G.; Piers, W. E.; Parvez, M. *Chem. Eur. J.* **2007**, *13*, 2632.

(239) Bouwkamp, M. W.; de Wolf, J.; Morales, I. D.; Gercama, J.; Meetsma, A.; Troyanov, S. I.; Hessen, B.; Teuben, J. H. *J. Am. Chem. Soc.* **2002**, *124*, 12956.

(240) Hayes, P. G.; Piers, W. E.; Parvez, M. *J. Am. Chem. Soc.* **2003**, *125*, 5622.

(241) Hayes, P. G.; Piers, W. E.; McDonald, R. *J. Am. Chem. Soc.* **2002**, *124*, 2132.

(242) Gillis, D. J.; Tudoret, M.-J.; Baird, M. C. *J. Am. Chem. Soc.* **1993**, *115*, 2543. Wang, Q.; Quyoum, R.; Gillis, D. J.; Tudoret, M.-J.; Jeremic, D.; Hunter, B. K.; Baird, M. C. *Organometallics* **1996**, *15*, 693. Gillis, D. J.; Quyoum, R.; Tudoret, M.-J.; Wang, Q.; Jeremic, D.; Roszak, A. W.; Baird, M. C. *Organometallics* **1996**, *15*, 3600.

(243) Lancaster, S. J.; Robinson, O. B.; Bochmann, M.; Coles, S. J.; Hursthouse, M. B. *Organometallics* **1995**, *14*, 2456.

(244) Scollard, J. D.; McConville, D. H.; Payne, N. C.; Vittal, J. J. *Macromolecules* **1996**, *29*, 5241.

(245) Scollard, J. D.; McConville, D. H. *J. Am. Chem. Soc.* **1996**, *118*, 10008.

(246) Chen, Y.-X.; Marks, T. J. *Organometallics* **1997**, *16*, 3649.

(247) Schrock, R. R.; Bonitatebus, P. J.; Schrodi, Y. *Organometallics* **2001**, *20*, 1056.

(248) Kenward, A. L.; Piers, W. E.; Parvez, M. *Organometallics* **2009**, *28*, 3012.

(249) Kenward, A. L.; Ross, J. A.; Piers, W. E.; Parvez, M. *Organometallics* **2009**, *28*, 3625.

(250) Hayes, P. G.; Piers, W. E.; Parvez, M. *Organometallics* **2005**, *24*, 1173.

(251) Li, X.; Nishiura, M.; Mori, K.; Mashiko, T.; Hou, Z. *Chem. Commun.* **2007**, 4137.

(252) Based on the scale of merit outlined by Gibson *et. al*., polymerization activities less than 1000 g(PE)•mol$^{-1}$•h$^{-1}$•atm$^{-1}$ are considered "very low". See: Britovsek, G. J. P.; Gibson, V. C.; Wass, D. F. *Angew. Chem. Int. Ed.* **1999**, *38*, 428.

(253) Gibson, V. C.; Kimberley, B. S.; White, A. J. P.; Williams, D. J.; Howard, P. *Chem. Commun.* **1998**, 313.

(254) Renfrew, A. K.; Phillips, A. D.; Tapavicza, E.; Scopelliti, R.; Rothlisberger, U.; Dyson, P. J. *Organometallics* **2009**, *28*, 5061.

(255) Chaplin, A. B.; Hooper, J. F.; Weller, A. S.; Willis, M. C. *J. Am. Chem. Soc.* **2012**, *134*, 4885.

(256) Pauling, L., *The Nature of the Chemical Bond*, 3rd ed.; Cornell University Press: New York, 1960. Mantina, M.; Chamberlin, A. C.; Valero, R.; Cramer, C. J.; Truhlar, D. G. *J. Phys. Chem. A* **2009**, *113*, 5806.

(257) Pike, S. D.; Pernik, I.; Theron, R.; McIndoe, J. S.; Weller, A. S. *J. Organomet. Chem.* **2015**, *784*, 75. Palacios, M. D.; Puerta, M. C.; Valerga, P.; Lledós, A.; Veilly, E. *Inorg. Chem.* **2007**, *46*, 6958.

(258) Ramirez-Contreras, R.; Ozerov, O. V. *Dalton Trans.* **2012**, *41*, 7842.

(259) Slattery, J. M.; Higelin, A.; Bayer, T.; Krossing, I. *Angew. Chem. Int. Ed.* **2010**, *49*, 3228.

(260) Bouwkamp, M. W.; Budzelaar, P. H. M.; Gercama, J.; Del Hierro Morales, I.; de Wolf, J. M., A.; Troyanov, S. I.; Teuben, J. H.; Hessen, B. *J. Am. Chem. Soc.* **2005**, *127*, 14310.

(261) Basuli, F.; Aneetha, H.; Huffman, J. C.; Mindiola, D. J. *J. Am. Chem. Soc.* **2005**, *127*, 17992.

(262) Schaverien, C. J. *Organometallics* **1992**, *11*, 3476.

(263) Calderazzo, F.; Pampaloni, G.; Rocchi, L.; Englert, U. *Organometallics* **1994**, *13*, 2592.

(264) Simões, J. A. M.; Beauchamp, J. L. *Chem. Rev.* **1990**, *90*, 629.

(265) Liu, B.; Liu, X. L.; Cui, D. M.; Liu, L. *Organometallics* **2009**, *28*, 1453.

(266) Klimpel, M. G.; Eppinger, J.; Sirsch, P.; Scherer, W.; Anwander, R. *Organometallics* **2002**, *21*, 4021.

(267) Mani, G.; Gabbai, F. P. *Angew. Chem. Int. Ed.* **2004**, *43*, 2263.

(268) Samsel, E. G; Eisenberg, D. C. (Ethyl Corporation, USA), US Patent 5,276,220, 1994. Kretschmer, W. P.; Bauer, T.; Hessen, B.; Kempe, R. *Dalton Trans.* **2010**, *39*, 6847. Kretschmer, W. P.; Meetsma, A.; Hessen, B.; Schmalz, T.; Qayyum, S.;

Kempe, R. *Chem. Eur. J.* **2006**, *12*, 8969. Hey, T. W.; Wass, D. F. *Organometallics* **2010**, *29*, 3676.

(269) Ni Bhriain, N.; Brintzinger, H. H.; Ruchatz, D.; Fink, G. *Macromolecules* **2005**, *38*, 2056.

(270) Wei, J.; Zhang, W.; Sita, L. R. *Angew. Chem. Int. Ed.* **2010**, *49*, 1768.

(271) Lin, W. T.; Niu, H.; Chung, T. C. M.; Dong, J. Y. *J. Polym. Sci. Pol. Chem.* **2010**, *48*, 3534.

(272) Arriola, D. J.; Carnahan, E. M.; Hustad, P. D.; Kuhlman, R. L.; Wenzel, T. T. *Science* **2006**, *312*, 714.

(273) Pelletier, J. F.; Mortreux, A.; Olonde, X.; Bujadoux, K. *Angew. Chem. Int. Ed. Engl.* **1996**, *35*, 1854.

(274) Hartwig, J. F., *Organotransition Metal Chemistry: From Bonding to Catalysis*, University Science Books: Sausalito, California, 2010. Crabtree, R. H., *The Organometallic Chemistry of the Transition Metals*, 3rd ed.; John Wiley & Sons: Toronto, 2001.

(275) Schlenk, W.; Holtz, J. *Chem. Ber.* **1917**, 262. Zieger, H.; Perri, C.; Bharucha, K. *Tetrahedron Lett.* **1987**, *28*, 5989.

(276) Alvarez, C. S.; Boss, S. R.; Burley, J. C.; Humphry, S. M.; Layfield, R. A.; Kowenicki, R. A.; McPartlin, M.; Rawson, J. M.; Wheatley, A. E. H.; Wood, P. T.; Wright, D. S. *Dalton Trans.* **2004**, 3481.

(277) Brinkmann, C.; Garcia, F.; Morey, J. V.; McPartlin, M.; Singh, S.; Wheatley, A. E. H.; Wright, D. S. *Dalton Trans.* **2007**, 1570.

(278) Fernandez-Cortabitarte, C.; Garcia, F.; Morey, J. V.; McPartlin, M.; Singh, S.; Wheatley, A. E. H.; Wright, D. S. *Angew. Chem. Int. Ed.* **2007**, *46*, 5425.

(279) Haywood, J.; Stokes, F. A.; Less, R. J.; McPartlin, M.; Wheatley, A. E. H.; Wright, D. S. *Chem. Commun.* **2011**, *47*, 4120.

(280) Lu, E.; Tuna, F.; Lewis, W.; Kaltsoyannis, N.; Liddle, S. T. *Chem. Eur. J.* **2016**, *22*, 11554.

(281) For examples where the $^{1}H$ resonance of the uranium-bound methyl group is not located, see: (a) Evans, W. J.; Walensky, J. R.; Ziller, J. W.; Rheingold, A. L. *Organometallics* **2009**, *28*, 3350; (b) Diaconescu, P. L.; Odom, A. L.; Agapie, T.; Cummins, C. C. *Organometallics* **2001**, *20*, 4993.

(282) Turner, H. W.; Andersen, R. A.; Zalkin, A.; Templeton, D. H. *Inorg. Chem.* **1979**, *18*, 1221. Lewis, A. J.; Carroll, P. J.; Schelter, E. J. *J. Am. Chem. Soc.* **2013**, *135*, 13185.

(283) Newell, B. S.; Schwaab, T. C.; Shores, M. P. *Inorg. Chem.* **2011**, *50*, 12108.

(284) For examples of *early transition metal* complexes featuring activation of an *N*-2,6-$^{i}Pr_2C_6H_3$ group at the isopropyl *methyl* moiety, see: (a) Otten, E.; Dijkstra, P.; Visser, C.; Meetsma, A.; Hessen, B. *Organometallics* **2005**, *24*, 4374; (b) Knight, L. K.; Piers, W. E.; Fleurat-Lessard, P.; Parvez, M.; McDonald, R. *Organometallics* **2004**, *23*, 2087; (c) Basuli, F.; Bailey, B. C.; Huffman, J. C.; Mindiola, D. J. *Organometallics* **2005**, *24*, 3321.

(285) For examples of *f-element* complexes featuring activation of a 2,6-$^{i}Pr_2C_6H_3$ group at the isopropyl *methyl* moiety, see: (a) Athimoolam, A.; Gambarotta, S.; Korobkov, I. *Organometallics* **2005**, *24*, 1996; (b) Behrle, A. C.; Castro, L.; Maron, L.; Walensky, J. R. *J. Am. Chem. Soc*. **2015**, *137*, 14846.

(286) Zimmermann, M.; Estler, F.; Herdtweck, E.; Törnroos, K. W.; Anwander, R. *Organometallics* **2007**, *26*, 6029.

(287) Basuli, F.; Bailey, B. C.; Watson, L. A.; Tomaszewski, J.; Huffman, J. C.; Mindiola, D. J. *Organometallics* **2005**, *24*, 1886. Basuli, F.; Bailey, B. C.; Huffman, J. C.; Mindiola, D. J. *Organometallics* **2005**, *24*, 3321.

(288) Ossig, G.; Meller, A.; Freitag, S.; Herbst-lrmer, R. *J. Chem. Soc., Chem. Commun*, **1993**, 497.

(289) Gianetti, T. L.; Bergman, R. G.; Arnold, J. *J. Am. Chem. Soc.* **2013**, *135*, 8145.

(290) Schädle, D.; Schädle, C.; Schneider, D.; Maichle-Mössmer, C.; Anwander, R. *Organometallics* **2015**, *34*, 4994.

(291) Eichler, B. E.; Powell, D. R.; West, R. *Organometallics* **1999**, *18*, 540.

(292) Bruno, J. W.; Marks, T. J.; Day, V. W. *J. Am. Chem. Soc.* **1982**, *104*, 7357.

(293) Lu, E.; Li, Y.; Chen, Y. *Chem. Commun.* **2010**, *46*, 4469.

(294) Che, C.-M.; Ho, C.-M.; Huang, J.-S. *Coord. Chem. Rev.* **2007**, *251*, 2145. Schrock, R. R. *Chem. Rev.* **2009**, *109*, 3211. Öfele, K.; Tosh, E.; Taubmann, C.; Herrmann, W. A. *Chem. Rev.* **2009**, *109*, 3408.

(295) Herndon, J. W. *Coord. Chem. Rev.* **2000**, *206–207*, 237.

(296) Doyle, M. P. *Chem. Rev.* **1986**, *86*, 919.

(297) Ephritikhine, M. *C. R. Chim.* **2013**, *16*, 391.

(298) Gregson, M.; Wooles, A. J.; Cooper, O. J.; Liddle, S. T. *Comments Inorganic Chem.* **2015**, *35*, 262.

(299) Solola, L. A.; Zabula, A. V.; Dorfner, W. L.; Manor, B. C.; Carroll, P. J.; Schelter, E. J. *J. Am. Chem. Soc.* **2016**, *138*, 6928.

(300) Cramer, R. E.; Maynard, R. B.; Paw, J. C.; Gilje, J. W. *J. Am. Chem. Soc.* **1981**, *103*, 3589. Cramer, R. E.; Maynard, R. B.; Paw, J. C.; Gilje, J. W. *Organometallics* **1983**, *2*, 1336. Stevens, R. C.; Bau, R.; Cramer, R. E.; Afzal, D.; Gilje, J. W.; Koetzle, T. F. *Organometallics* **1990**, *9*, 694. Cramer, R. E.; Bruck, M. A.; Edelmann, F.; Afzal, D.; Gilje, J. W.; Schmidbaur, H. *Chem. Ber.* **1988**, *121*, 417.

(301) Fortier, S.; Walensky, J. R.; Wu, G.; Hayton, T. W. *J. Am. Chem. Soc.* **2011**, *133*, 6894.

(302) Cantat, T.; Arliguie, T.; Noel, A.; Thuery, P.; Ephritikhine, M.; Le Floch, P.; Mezailles, N. *J. Am. Chem. Soc.* **2009**, *131*, 963.

(303) Cooper, O. J.; McMaster, J.; Lewis, W.; Blake, A. J.; Liddle, S. T. *Dalton Trans.* **2010**, *39*, 5074.

(304) Pool, J. A.; Scott, B. L.; Kiplinger, J. L. *J. Alloy. Compd.* **2006**, *418*, 178.

(305) Kiplinger, J. L.; Scott, B. L.; Schelter, E. J.; Tournear, J. *J. Alloy. Compd.* **2007**, *444*, 477.

(306) Lu, E.; Cooper, O. J.; Tuna, F.; Wooles, A. J.; Kaltsoyannis, N.; Liddle, S. T. *Chem. Eur. J.* **2016**, *22*, 11559.

(307) Zhang, L.; Fang, B.; Hou, G.; Ai, L.; Ding, W.; Walter, M. D.; Zi, G. *Dalton Trans.* **2016**, *45*, 16441.

(308) Dormond, A.; El Bouadili, A. A.; Moise, C. *J. Chem. Soc., Chem. Commun.* **1985**, 914.

(309) Boaretto, R.; Roussel, P.; Alcock, N. W.; Kingsley, A. J.; Munslow, I. J.; Sanders, C. J.; Scott, P. *J. Organomet. Chem.* **1999**, *591*, 174.

(310) Duhovic, S.; Monreal, M. J.; Diaconescu, P. L. *Inorg. Chem.* **2010**, *49*, 7165.

(311) Fang, B.; Zhang, L.; Hou, G. H.; Zi, G. F.; Fang, D. C.; Walter, M. D. *Chem. Sci.* **2015**, *6*, 4897.

(312) Arnold, P. L.; McMullon, M. W.; Rieb, J.; Kühn, F. E. *Angew. Chem. Int. Ed.* **2015**, *54*, 82.

(313) McGovern, G. P.; Hung-Low, F.; Tye, J. W.; Bradley, C. A. *Organometallics* **2012**, *31*, 3865.

(314) Tandon, R.; Unzner, T.; Nigst, T. A.; De Rycke, N.; Mayer, P.; Wendt, B.; David, O. R. P.; Zipse, H. *Chem. Eur. J.* **2013**, *19*, 6435.

(315) Wong, K.-T.; Ku, S.-Y.; Yen, F.-W. *Tetrahedron Lett.* **2007**, *48*, 5051.

(316) Rivard, E.; Power, P. P. *Inorg. Chem.* **2007**, *46*, 10047. Ni, C.; Power, P. P., Transition Metal Complexes Stabilized by Bulky Terphenyl Ligands: Application to Metal–Metal Bonded Compounds. In *Metal-Metal Bonding*, Parkin, G., Ed.; Springer Berlin Heidelberg: Berlin, Heidelberg, 2010; p 59. Kays, D. L. *Dalton Trans.* **2011**, *40*, 769. Kays, D. L. *Chem. Soc. Rev.* **2016**, *45*, 1004.

(317) Andreychuk, N. R.; Emslie, D. J. H. *Angew. Chem. Int. Ed.* **2013**, *52*, 1696.

(318) Johnson, K. R. D.; Hayes, P. G. *Organometallics* **2009**, *28*, 6352.

(319) Saednya, A.; Hart, H. *Synthesis* **1996**, *12*, 1455. Dory, Y. L.; Zhao, Y. *Chem. Eur. J.* **2009**, *15*, 4428. Gavenonis, J.; Tilley, T. D. *Organometallics* **2002**, *21*, 5549.

(320) Hinz, A.; Schulz, A.; Villinger, A. *Chem. Commun.* **2015**, *51*, 11437.

(321) Piesik, D. F. J.; Haack, P.; Harder, S.; Limberg, C. *Inorg. Chem.* **2009**, *48*, 11259.

(322) Turculet, L.; McDonald, R. *Organometallics* **2007**, *26*, 6821.

(323) Kotlyar, S. A.; Zubatyuk, R. I.; Shishkin, O. V.; Chuprin, G. N.; Kiriyak, A. V.; Kamalov, G. L. *Acta Crystallogr., Sect. E: Struct. Rep. Online* **2005**, *61*, m2163.

(324) Arndtsen, B. A.; Bergman, R. G.; Mobley, T. A.; Peterson, T. H. *Acc. Chem. Res.* **1995**, *28*, 154. Labinger, J. A.; Bercaw, J. E. *Nature* **2002**, *417*, 507. Crabtree, R. H. *J. Chem. Soc. Dalton Trans.* **2001**, 2437.

(325) Ferrari, A. M.; Neyman, K. M.; Huber, S.; Knozinger, H.; Rosch, N. *Langmuir* **1998**, *14*, 5559. Calero, S.; Dubbeldam, D.; Krishna, R.; Smit, B.; Vlugt, T. J. H.; Denayer, J. F. M.; Martens, J. A.; Maesen, T. L. M. *J. Am. Chem. Soc.* **2004**, *126*, 11377. Liu, B.; Smit, B. *Phys. Chem. Chem. Phys.* **2006**, *8*, 1852.

(326) Young, R. D. *Chem. Eur. J.* **2014**, *20*, 12704.

(327) Geftakis, S.; Ball, G. E. *J. Am. Chem. Soc.* **1998**, *120*, 9953. Calladine, J. A.; Torres, O.; Anstey, M.; Ball, G. E.; Bergman, R. G.; Curley, J.; Duckett, S. B.; George, M. W.; Gilson, A. I.; Lawes, D. J.; Perutz, R. N.; Sun, X. Z.; Vollhardt, K. P. C. *Chem. Sci.* **2010**, *1*, 622.

(328) Ball, G. E.; Brookes, C. M.; Cowan, A. J.; Darwish, T. A.; George, M. W.; Kawanami, H. K.; Portius, P.; Rourke, J. P. *Proc. Natl. Acad. Sci. U. S. A.* **2007**, *104*, 6927.

(329) Torres, O.; Calladine, J. A.; Duckett, S. B.; George, M. W.; Perutz, R. N. *Chem. Sci.* **2015**, *6*, 418.

(330) Duckett, S. B.; George, M. W.; Jina, O. S.; Matthews, S. L.; Perutz, R. N.; Sun, X. Z.; Vuong, K. Q. *Chem. Commun.* **2009**, 1401.

(331) Bernskoetter, W. H.; Schauer, C. K.; Goldberg, K. I.; Brookhart, M. *Science* **2009**, *326*, 553.

(332) Young, R. D.; Lawes, D. J.; Hill, A. F.; Ball, G. E. *J. Am. Chem. Soc.* **2012**, *134*, 8294.

(333) Yau, H. M.; McKay, A. I.; Hesse, H.; Xu, R.; He, M.; Holt, C. E.; Ball, G. E. *J. Am. Chem. Soc.* **2016**, *138*, 281.

(334) The binding of ethane and propane to iron centers in an extended metal-organic framework was recently characterized by neutron diffraction: Bloch, E. D.;

Queen, W. L.; Krishna, R. ; Zadrozny, J. M.; Brown, C. M.; Long, J. R. *Science* **2012**, *335*, 1606.

(335) Evans, D. R.; Drovetskaya, T.; Bau, R.; Reed, C. A.; Boyd, P. D. W. *J. Am. Chem. Soc.* **1997**, *119*, 3633.

(336) Castro-Rodriguez, I.; Nakai, H.; Gantzel, P.; Zakharov, L. N.; Rheingold, A. L.; Meyer, K. *J. Am. Chem. Soc.* **2003**, *125*, 15734.

(337) Pike, S. D.; Thompson, A. L.; Algarra, A. G.; Apperley, D. C.; Macgregor, S. A.; Weller, A. S. *Science* **2012**, *337*, 1648. McKay, A. I.; Krämer, T.; Rees, N. H.; Thompson, A. L.; Christensen, K. E.; Macgregor, S. A.; Weller, A. S. *Organometallics* **2017**, *36*, 22. Chadwick, F. M.; Rees, N. H.; Weller, A. S.; Krämer, T.; Iannuzzi, M.; Macgregor, S. A. *Angew. Chem. Int. Ed.* **2016**, *55*, 3677. Pike, S. D.; Chadwick, F. M.; Rees, N. H.; Scott, M. P.; Weller, A. S.; Krämer, T.; Macgregor, S. A. *J. Am. Chem. Soc.* **2015**, *137*, 820.

(338) Hao, J.; Song, H.; Cui, C. *Organometallics* **2009**, *28*, 3100. Niemeyer, M. *Inorg. Chem.* **2006**, *45*, 9085. Hitchcock, P. B.; Lappert, M. F.; Sablong, R. *Dalton Trans.* **2006**, 4146. Evans, W. J.; Rego, D. B.; Ziller, J. W. *Inorg. Chem.* **2006**, *45*, 3437. Forbes, G. C.; Kennedy, A. R.; Mulvey, R. E.; Roberts, B. A.; Rowlings, R. B. *Organometallics* **2002**, *21*, 5115. Bai, G.; Roesky, H. W.; Noltemeyer, M.; Schmidt, H.-G. *J. Chem. Soc. Dalton Trans.* **2002**, 2437. Schaverien, C. J.; Vanmechelen, J. B. *Organometallics* **1991**, *10*, 1704. Fuentes, G. R.; Coan, P. S.; Streib, W. E.; Caulton, K. G. *Polyhedron* **1991**, *10*, 2371.

(339) Klinkhammer, K. W. *Chem. Eur. J.* **1997**, *3*, 1418.

(340) Eaborn, C.; Hitchcock, P. B.; Izod, K.; Jaggar, A. J.; Smith, J. D. *Organometallics* **1994**, *13*, 753.

(341) Bowman, L. J.; Izod, K.; Clegg, W.; Harrington, R. W.; Smith, J. D.; Eaborn, C. *Dalton Trans.* **2006**, 502.

(342) Anslyn, E. V.; Dougherty, D. A., *Modern physical organic chemistry*, University Science Books: Sausalito, California, 2006. Ehlers, A. W.; de Koster, C. G.; Meier, R. J.; Lammertsma, K. *J. Phys. Chem. A* **2001**, *105*, 8691.

(343) Hayes, C. E.; Sarazin, Y.; Katz, M. J.; Carpentier, J.-F.; Leznoff, D. B. *Organometallics* **2013**, *32*, 1183.

(344) Stubbert, B. D.; Marks, T. J. *J. Am. Chem. Soc.* **2007**, *129*, 6149.

(345) Bruno, J. W.; Marks, T. J.; Day, V. W. *J. Organomet. Chem.* **1983**, *250*, 237.

(346) Cruz, C. A.; Emslie, D. J. H.; Harrington, L. E.; Britten, J. F.; Robertson, C. M. *Organometallics* **2007**, *26*, 692. and references therein.

(347) Hayes, P. G.; Welch, G. C.; Emslie, D. J. H.; Noack, C. L.; Piers, W. E.; Parvez, M. *Organometallics* **2003**, *22*, 1577.

(348) Wright, W. R. H.; Batsanov, A. S.; Howard, J. A. K.; Tooze, R. P.; Hanton, M. J.; Dyer, P. W. *Dalton Trans.* **2010**, *39*, 7038.

(349) Lorber, C.; Choukroun, R.; Vendier, L. *Organometallics* **2008**, *27*, 5017.

(350) Chen, E. Y.-X.; Marks, T. J. *Chem. Rev.* **2000**, *100*, 1391.

(351) Wilke, G.; Bogdanović, B.; Hardt, P.; Heimbach, P.; Keim, W.; Kröner, M.; Oberkirch, W.; Tanaka, K.; Steinrücke, E.; Walter, D.; Zimmermann, H. *Angew. Chem. Int. Ed. Engl.* **1966**, *5*, 151.

(352) Marks, T. J.; Wachter, W. A. *J. Am. Chem. Soc.* **1976**, *98*, 703.

(353) Langeslay, R. R.; Walensky, J. R.; Ziller, J. W.; Evans, W. J. *Inorg. Chem.* **2014**, *53*, 8455.

(354) White, R. E.; Carlson, C. N.; Veauthier, J. M.; Simpson, C. K.; Thompson, J. D.; Scott, B. L.; Hanusa, T. P.; John, K. D. *Inorg. Chem.* **2006**, *45*, 7004.

(355) Richards, S. A.; Hollerton, J. C., In *Essential Practical NMR for Organic Chemistry*, John Wiley & Sons, Ltd: 2010; p 41.

(356) Hitchcock, P. B.; Lappert, M. F.; Liu, D.-S. *J. Organomet. Chem.* **1995**, *488*, 241.

(357) Diaconescu, P. L.; Arnold, P. L.; Baker, T. A.; Mindiola, D. J.; Cummins, C. C. *J. Am. Chem. Soc.* **2000**, *122*, 6108.

(358) Monreal, M. J.; Khan, S. I.; Kiplinger, J. L.; Diaconescu, P. L. *Chem. Commun.* **2011**, *47*, 9119.

(359) Arnold, P. L.; Mansell, S. M.; Maron, L.; McKay, D. *Nat. Chem.* **2012**, *4*, 668.

(360) Mougel, V.; Camp, C.; Pecaut, J.; Coperet, C.; Maron, L.; Kefalidis, C. E.; Mazzanti, M. *Angew. Chem. Int. Ed.* **2012**, *51*, 12280.

(361) Mills, D. P.; Moro, F.; McMaster, J.; van Slageren, J.; Lewis, W.; Blake, A. J.; Liddle, S. T. *Nat. Chem.* **2011**, *3*, 454.

(362) Patel, D.; Moro, F.; McMaster, J.; Lewis, W.; Blake, A. J.; Liddle, S. T. *Angew. Chem. Int. Ed.* **2011**, *50*, 10388.

(363) Stasch, A.; Jones, C. *Dalton Trans.* **2011**, *40*, 5659.

(364) Robert, D.; Abinet, E.; Spaniol, T. P.; Okuda, J. *Chem. Eur. J.* **2009**, *15*, 11937.

(365) Huang, L.; Arndt, M.; Gooßen, K.; Heydt, H.; Gooßen, L. J. *Chem. Rev.* **2015**, *115*, 2596. Bytschkov, I.; Doye, S. *Eur. J. Org. Chem.* **2003**, *2003*, 935.

(366) Hong, S.; Marks, T. J. *Acc. Chem. Res.* **2004**, *37*, 673.

(367) Karmel, I.; Batrice, R.; Eisen, M. *Inorganics* **2015**, *3*, 392.

(368) Burger, B. J.; Bercaw, J. E., Vacuum Line Techniques for Handling Air-Sensitive Organometallic Compounds. In *Experimental Organometallic Chemistry - A Practicum in Synthesis and Characterization*, American Chemical Society: Washington D.C., 1987; Vol. 357, p 79.

(369) Burchat, A. F.; Chong, J. M.; Nielsen, N. *J. Organomet. Chem.* **1997**, *542*, 281.

(370) Ghosh, A. K.; Bischoff, A.; Cappiello, J. *Eur. J. Org. Chem.* **2003**, 821.

(371) Emslie, D. J. H.; Blackwell, J. M.; Britten, J. F.; Harrington, L. E. *Organometallics* **2006**, *25*, 2412.

(372) Schrock, R. R.; Fellmann, J. D. *J. Am. Chem. Soc.* **1978**, *100*, 3359.

(373) Bailey, P. L.; Coxall, R. A.; Dick, C. M.; Fabre, S.; Henderson, L. C.; Herber, C.; Liddle, S. T.; Lorono-Gonzalez, D.; Parkin, A.; Parsons, S. *Chem. Eur. J.* **2003**, *9*, 4820.

(374) Alberti, D.; Pörschke, K.-R. *Organometallics* **2004**, *23*, 1459.

(375) Hong, S. W.; Tian, S.; Metz, M. V.; Marks, T. J. *J. Am. Chem. Soc.* **2003**, *125*, 14768.

(376) LeSuer, R. J.; Buttolph, C.; Geiger, W. E. *Anal. Chem.* **2004**, *76*, 6395.

(377) Tyburn, J.-M., Bruker Variable Temperature Unit User Manual. In Wissembourg, France, 1998; Vol. 001, p 35.

(378) Barriere, F.; Geiger, W. E. *J. Am. Chem. Soc.* **2006**, *128*, 3980.

## Appendix 1

Gel Permeation Chromatography (GPC) data for polyethylene produced using cation **12**:

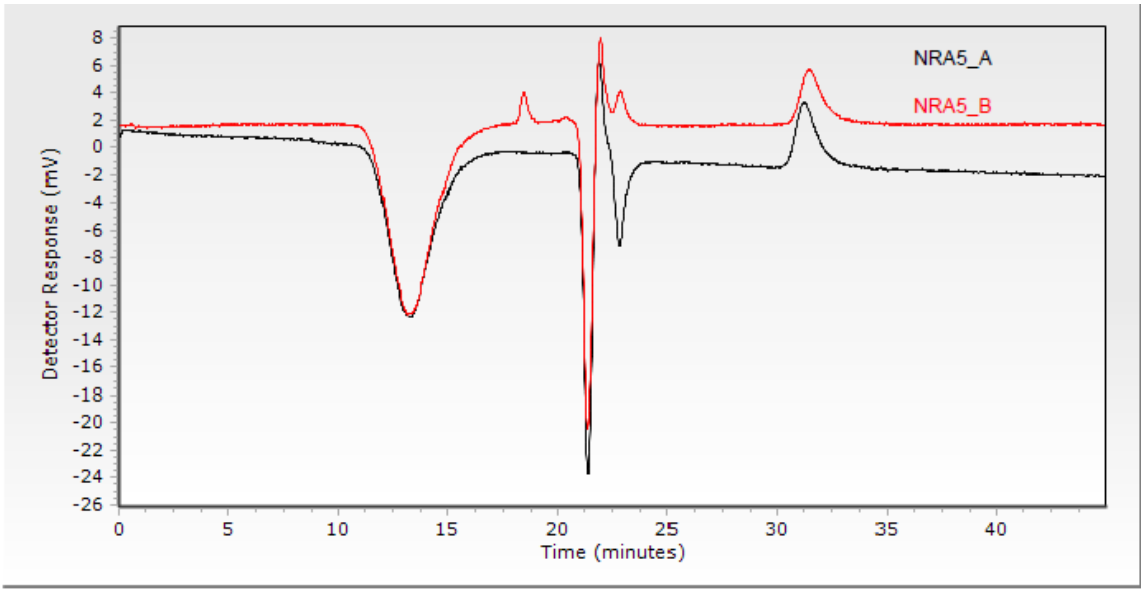


**Appendix Figure 1** – DRi chromatograms of NRA5 duplicates.

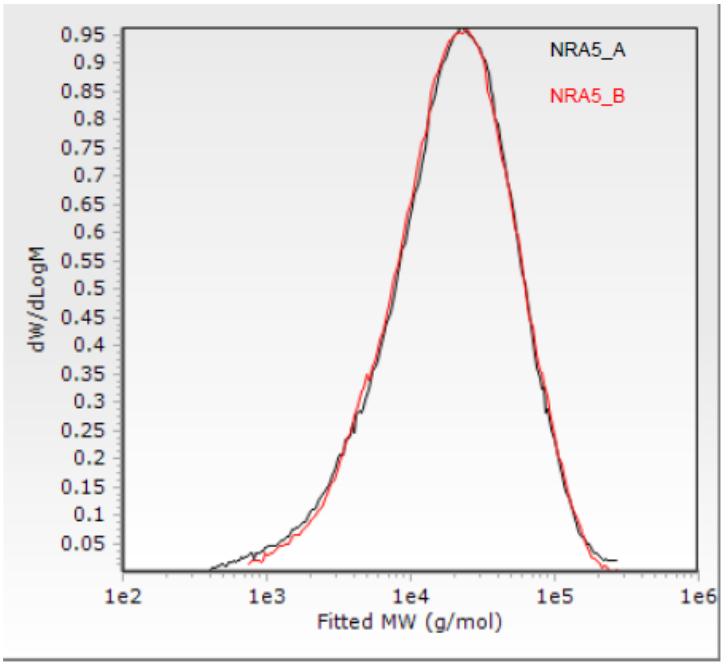


**Appendix Figure 2** – Molecular weight distribution plot of NRA5 duplicates.